University of Southampton

Faculty of Engineering and Physical Sciences

Chemistry

Coordination Chemistry of High Valent Early Transition Metals with Neutral Donor Ligands: Towards Precursors for the Electrodeposition and LPCVD of Molybdenum and Tungsten Dichalcogenides

by

Danielle Emily Smith

Thesis for the degree of Doctor of Philosophy

October 2020

University of Southampton

Abstract

Faculty of Engineering and Physical Sciences

Chemistry

Thesis for the degree of Doctor of Philosophy

Coordination Chemistry of High Valent Early Transition Metals with Neutral Donor Ligands: Towards Precursors for the Electrodeposition and LPCVD of Molybdenum and Tungsten Dichalcogenides

by

Danielle Emily Smith

The work in this thesis concerns the development of several new series of high valent Group VI (Mo, W) complexes and explores their application for the deposition of molybdenum and tungsten dichalcogenide thin films *via* electrodeposition and low-pressure chemical vapour deposition.

A review of the relevant background literature is presented in Chapter 1, while Chapter 2 presents an investigation to explore the chemistry of tungsten(VI) and develop the first systematic series of tungsten oxytetrachloride and thiotetrachloride coordination complexes, six-coordinate $[WECl_4(L)]$ or $[(WECl_4)_2(\mu\text{-L-L})]$ (E = O or S) or seven-coordinate $[WECl_4(L\text{-}L)]$ and to explore their properties. The ligands used include phosphine oxides ($dppeO_2$, $dppmO_2$, $OPPh_3$ and $OPMe_3$) and N-heterocycles (2,2'-bipy, 1,10-phen and py).

Unusual seven-coordinate pentagonal bipyramidal tungsten(VI) oxo- and thio-tetrachloride complexes with a series of phosphine and arsine ligands to give complexes of the form $[WECl_4(L\text{-}L)]$ (E = O or S), are reported in Chapter 3, together with investigation of monodentate ligands. The ligands used include *o*-$C_6H_4(E'Me_2)_2$ (E' = P or As), $Me_2P(CH_2)_2PMe_2$, PMe_3, $AsEt_3$ and *o*-$C_6H_4(PPh_2)_2$.

The coordination chemistry of a series of $WSCl_4$ complexes with thioethers and comparative $WOCl_4$ complexes are described in Chapter 4. Softer selenium donor ligands are also investigated and the properties of hard metal-soft ligand interactions explored. Potential precursors for low pressure chemical vapour deposition are identified on the basis of certain criteria i.e. butyl substituent ligands and M:E ratio.

Reported in Chapter 5, $[(WSCl_4)_2(^iPrS(CH_2)_2S^iPr)]$, $[WSCl_3(^iPrS(CH_2)_2S^iPr)]$ and $[WSCl_4(S^nBu_2)]$ were tested as single source LPCVD precursors. $[(WSCl_4)_2(^iPrS(CH_2)_2S^iPr)]$ and $[WSCl_4(S^nBu_2)]$ deposit 4H-WS_2 thin films, the two W(VI) precursors deposited continuous films with a W:S ratio of 1:2.2 consistent with WS_2. These are the first examples of single source LPCVD precursors to deposit WS_2 thin films and the films have been characterised by Raman spectroscopy, grazing incidence XRD and in-plane XRD, EDX, WDX, XPS and SEM.

Presented in Chapter 6, a family of $MoOCl_3$ complexes with a range of neutral donor ligands, with a particular emphasis on thio-, seleno- and telluro-ether ligands, allowing comparisons to be drawn to the coordination complexes of $WECl_4$ (E = O or S). The reaction of $MoOCl_4$ with various ligands is investigated and compared to the $MoOCl_3$ coordination complexes.

The development and synthesis of a series of potential precursors suitable for the electrodeposition of ME_2 (M = Mo or W; E = S or Se) thin films using non-aqueous solvents is discussed in Chapter 7, particularly including the synthesis of precursors for the electrodeposition of MoS_2 and WS_2 and their respective electrochemical studies. Deposited films have been characterised by Raman spectroscopy, grazing incidence XRD, EDX, WDX and SEM analysis.

Where possible, new complexes have been characterised by IR, Raman, multinuclear NMR (^1H, $^{31}P\{^1H\}$, $^{77}Se\{^1H\}$ and ^{95}Mo where appropriate), UV-Vis spectroscopy, magnetic measurements, elemental analysis and single crystal X-ray structures.

Table of Contents

Table of Tables

Table of Figures

List of Accompanying Materials

DOI containing the Crystallographic Information Files (cifs) for the X-ray diffraction studies reported throughout this thesis and any non-published data: 10.5258/SOTON/D1591.

Research Thesis: Declaration of Authorship

Print name: Danielle Emily Smith

Title of thesis: Coordination Chemistry of High Valent Early Transition Metals with Neutral Donor Ligands: Towards Precursors for the Electrodeposition and LPCVD of Molybdenum and Tungsten Dichalcogenides

I declare that this thesis and the work presented in it are my own and has been generated by me as the result of my own original research.

I confirm that:

1. This work was done wholly or mainly while in candidature for a research degree at this University;
2. Where any part of this thesis has previously been submitted for a degree or any other qualification at this University or any other institution, this has been clearly stated;
3. Where I have consulted the published work of others, this is always clearly attributed;
4. Where I have quoted from the work of others, the source is always given. With the exception of such quotations, this thesis is entirely my own work;
5. I have acknowledged all main sources of help;
6. Where the thesis is based on work done by myself jointly with others, I have made clear exactly what was done by others and what I have contributed myself;
7. Parts of this work have been published as:-

"Complexes of $WOCl_4$ and $WSCl_4$ with N- and O- donor ligands: Synthesis, spectroscopy and structures", Victoria K. Greenacre, Andrew L. Hector, William Levason, Gillian Reid, Danielle E. Smith, Laura Sutcliffe, *Polyhedron,* 2019, **162**, 14-19.

"*Pentagonal bipyramidal complexes of $WOCl_4$ and $WSCl_4$ with diphosphine and diarsine ligands*", William Levason, Gillian Reid, Danielle E. Smith, Wenjian Zhang, *Polyhedron*, 2020, **179**, 114372

"*Thioether complexes of $WSCl_4$, $WOCl_4$ and $WSCl_3$ and evaluation of thiochloride complexes as CVD precursors for WS_2 thin films."*, Danielle E. Smith, Victoria K. Greenacre, Andrew L. Hector, Roumeng Huang, William Levason, Gillian Reid, Fred Robinson, Shibin Thomas, *Dalton Trans.* 2020, **49**, 2496-2504.

"*Electrodeposition of MoS_2 from Dichloromethane*", Shibin Thomas, Danielle E. Smith, Victoria K. Greenacre, Yasir J. Noori, Andrew L. Hector, C. H. (Kees) de Groot, Gillian Reid, Philip N. Bartlett, *J. Electrochem. Soc.* 2020, **167**, 106511

Signature: Date:

Acknowledgements

During my Ph.D. I have been incredibly fortunate with the help I have received. I would firstly like to thank my supervisors Prof. Gill Reid and Prof. Andrew Hector for their time, patience and constant support. I would like to extend my thanks to Prof. Bill Levason for inexhaustible knowledge, enthusiasm and willingness to provide help.

Many thanks to Dr Victoria Greenacre who was always my willing second pair of hands in the laboratory and always provided new ideas when syntheses were not working. Also, from the Reid Group, Fred Robinson, whose experience and assistance in CVD experiments and endless help in characterisation of materials was invaluable. Also, Dr Robert Bannister for the limitless help in solving X-ray crystal structures and answering all of my never-ending questions. As well as the NCS staff, Dr Graham Tizzard and Dr Peter Horton, for their help and guidance for running single crystal experiments. From Electrochemistry I would like to thank Dr Shibin Thomas for completing all the electrochemistry experiments and Dr Roumeng Huang from ECS for his help with materials characterisation.

I would like to thank Laura Sutcliffe who started initial investigations into $WOCl_4$ complexes when working on her final year project in the Reid laboratory. My thanks also go to my project student James Powell who developed work on $MoOCl_4$ complexes and the initial investigation on $MoOCl_3$ complexes described herein.

Thank you to the Reid Group, both past and present, who have made my time at the University an incredible experience. I hope you all enjoy your time at the University and continue the tradition of cake Thursday.

I would like to thank the EPSRC for funding this work and the University of Southampton for providing wonderful facilities and support systems, it has been an amazing experience to study here.

Finally, I would like to thank my family for their continued support throughout my studies as I would not be here today without it. I am unbelievably grateful for Thomas who has provided all the support I would need and listened to me constantly talking about Chemistry, as well as completing the extortionate amount of proof-reading.

Definitions and Abbreviations

δ	Chemical Shift (ppm)
AACVD	Aerosol Assisted Chemical Vapour Deposition
APCVD	Ambient Pressure Chemical Vapour Deposition
^{n}Bu	n-butyl
CV	Cyclic Voltammogram
CVD	Chemical Vapour Deposition
dee	1,2-diethoxyethane
DFT	Density-Functional Theory
dme	1,2-dimethoxyethane
dmpe	1,2-bis(dimethylphosphino)ethane
dmso	Dimethyl Sulfoxide
dppe	1,2-bis(diphenylphosphino)ethane
dppm	1,2-bis(diphenylphosphino)methane
E	O, S or Se
EDX	Energy-Dispersive X-ray Spectroscopy
[EMIM][TFSI]	1-ethyl-3-methylimidazolium bis(trifluoromethanesulfonyl) imide
EQCM	Electrochemical Quartz Crystal Microbalance
ER_2	Chalcogenoether (E = S, Se or Te)
Et	Ethyl
Fac	Facial
GIXRD	Grazing Incidence X-ray Diffraction
HMPA	Hexamethylphosphoramide
IPXRD	In-Plane X-ray Diffraction
IR	Infrared
L	General Ligand Group

L-L	Bidentate Ligand
LPCVD	Low-Pressure Chemical Vapour Deposition
Me	Methyl
Mer	Meridional
NMR	Nuclear Magnetic Resonance
o-	Ortho-
Oxt	1,4-dioxane
Ph	Phenyl
PP_{13}-TFSI	N-methyl-N-propyl-piperidinium bis(trifluoromethanesulfonyl) imide
ppm	Parts Per Million
^{i}Pr	Isopropyl
PVD	Physical Vapour Deposition
PXRD	Powder X-ray Diffraction
Py	Pyridine
SEM	Scanning Electronic Microscopy
THF	Tetrahydrofuran
Thiox	1,4-thioxane
THP	Tetrahydropyran
tht	Tetrahydrothiophene
TMDC	Transition Metal Dichalcogenide
tmeda	Tetramethylethylenediamine
WDX	Wavelength Dispersive X-ray Spectroscopy
X	Halide Ion
XPS	X-ray Photoelectron Spectroscopy
1,10-phen	1,10-phenanthroline
2,2'-bipy	2,2'-bipyridine

Introduction

The work in this thesis is concerned with the development of new coordination chemistry of the hard high valent Group VI metals. Including, W(VI) oxo- and thio-halides with hard phosphine oxide and imine ligands (Chapter 2), soft phosphine and arsine ligands (Chapter 3), soft chalcogenoethers (Chapter 4) and of Mo(V) oxohalides (Chapter 6). The work also reports the investigation of precursors for the deposition of MoS_2 and WS_2 thin films *via* CVD (Chapter 5) and electrodeposition (Chapter 7). This introduction is provided to give a general background to some of the main aspects of the chemistry and techniques for the work described herein. A more specific review of background literature is presented at the start of each respective chapter and may refer to chemistry in this chapter where appropriate.

1.1 Hard Soft Acids and Bases

The hard soft acid base (HSAB) theory is one of the fundamental principles of inorganic and coordination chemistry. It categorises chemical elements and species into one of two types, hard or soft, depending on a number of criteria and states. Hard acids prefer to bond to hard bases and soft acids to soft bases.[1] The Lewis definition of acids and bases is used in HSAB theory, a Lewis acid is any substance which can accept a pair of non-bonding electrons (known as an acceptor) and a Lewis base is any substance which can donate a pair of non-bonding electrons (known as a donor).[2]

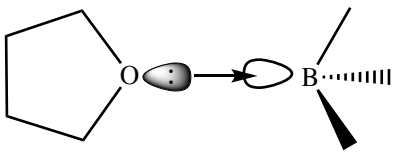

Figure 1.1: A simplified Lewis acid and Lewis base using an electron poor acid (BH_3) and an electron rich base (THF), to form a simple adduct.[3]

Hard acids and bases have a relatively small atomic or ionic radii, are high valent species which are not particularly polarisable and show a preference for electrostatic bonding. High valent early transition metals are hard Lewis acids as well as *f* and *s* block metals, conversely, hard Lewis bases include fluoride ions, water and ethers.[1,2] The strong interactions between Lewis acids and Lewis bases can often improve the stability of high valent metal centres and their subsequent complexes.[4]

Soft Lewis acids and bases have larger atomic or covalent radii, tend to be low valent or neutral, prefer covalent bonding and are highly polarisable. Soft acids include late transition metals (gold(I), silver(I) and platinum(II)) and soft bases include chalcogenoethers, phosphines and arsines.[5,6] The hard and soft descriptions are independent of the relative strength of the acid or base; hard and soft acids and bases can be either weak or strong respective acids and bases. The HSAB theory is not a conclusive explanation of bonding as there are many examples of bonding between soft Lewis base donors and hard Lewis acid acceptors.[7-11] However, bonding between a hard Lewis

acid (high valent transition metals) and a softer Lewis base (sulfur and phosphorus) can make compounds unstable and particularly sensitive to moisture.[12,13] The study of hard Lewis acids and soft Lewis bases has become an area of interest, with literature investigating the characteristics of bonds and the limits of this type of bonding.

This work will investigate the behaviour of the Lewis acidic high valent early transition metals, W(VI), Mo(VI) and Mo(V), with both hard Lewis bases (phosphine oxides and imines) and softer Lewis bases (phosphines and chalcogenoethers). The weak nature of these interactions can result in soft Lewis bases being out-competed by hard donor solvents and subsequently being displaced. Therefore, reactions need to be performed under rigorously dry and inert conditions, in weakly coordinating solvents, such as CH_2Cl_2 or toluene.

1.2 High Valent Complexes of Tungsten and Molybdenum

Molybdenum and tungsten's chemical behaviour is not significantly different from each other due to similar atomic radii, Mo (1.54 Å) and W (1.62 Å), as a result of the lanthanide contraction.[14,15] Both metals exhibit a range of formal oxidation states -II to +VI, and when Group VI metals are in the +VI oxidation state they are highly reactive or strongly oxidising.[16] Tungsten(VI) is more readily available compared to molybdenum(VI), which can be unstable and is more easily reduced; however tungsten(VI) compounds are still susceptible to reduction.[17]

The coordination chemistry of molybdenum has attracted attention over the years as molybdenum is an important constituent in biological species, including metalloenzymes and molybdenum nitrogenase.[18,19] Molybdenum species such as $[MoS_4]^{2-}$ are used for the regulation of copper in cattle.[20] Both tungsten and molybdenum coordination compounds merit considerable interest due to their role in oxido-transfer reagents, metathesis catalysis precursors and in ring-opening catalysis.[18,21-23] The coordination chemistry of Group VI metals largely revolves around the metal halides and their derivatives due to commercial availability or metal carbonyls, $M^0(CO)_n$. The hexahalides are known for WX_6 (X = F, Cl or Br) and MoX_6 (X = F or Cl) although $MoCl_6$ is only known at low temperature.[24] MX_6 are formed *via* direct reaction of the metal and halogens and form octahedral monomers, whereas WX_5 (X = Cl or Br) and $MoCl_5$ form dimeric structures and MF_5 (M = W or Mo) form tetramers (Figure 1.2).[17] MX_5 are isostructural to NbX_5 and TaX_5 metal halides and their chemistries are similar.[25]

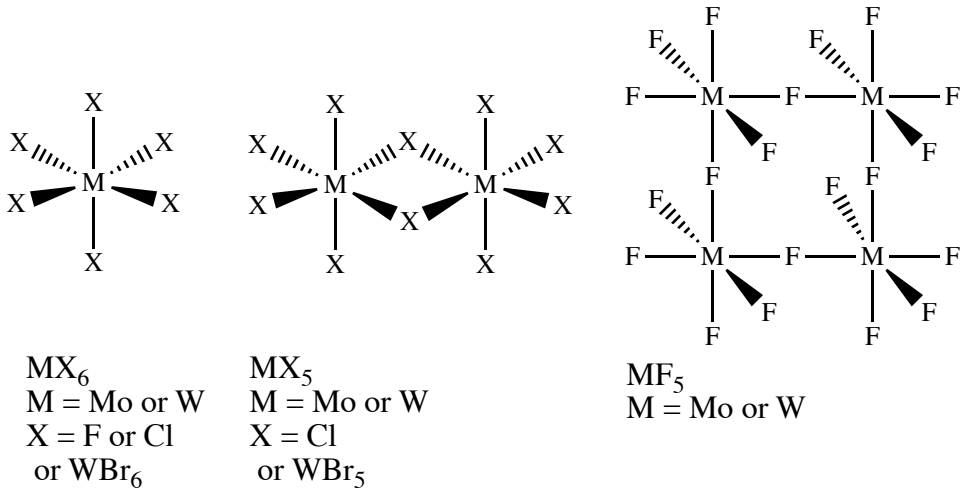

Figure 1.2: Illustration of the solid-state structure of MX_6 and MX_5 metal halides.

All the metal halides react readily with moisture commonly forming MO_3 or other oxohalide derivatives, MOX_4 or MO_2Cl_2, or reduce to lower oxidation states. The metal halides are often the starting reagents for metal oxo- and thio-halides, MEX_n (E = O, S or Se; n = 3 or 4) especially in the formation of MOX_n compounds, which have been shown to form readily with oxygen donor ligands.[26-28] The traditional route for the synthesis of metal thiohalides is *via* solid-state methods, typically mixing MCl_n with a sulfur-containing compound, (elemental sulfur, Sb_2S_3 or B_2S_3) in an evacuated sealed tube and heating (further details in Chapter 2).[29-31]

The polymeric units found in MX_5 are readily broken up upon the addition of a variety of ligands although $MoCl_5$ is shown to readily reduce or abstract oxygen from oxygen-donor ligands.[26,32,33] The metal fluorides are stronger Lewis acids than the chloro- and bromo- analogues, resulting in more stable complexes (with stronger Lewis bases) but limited stability with softer Lewis bases such as chalcogenoethers.[34-36]

1.3 Ligand Types

1.3.1 Neutral Phosphine and Arsine Ligands

Like their lighter congeners (NR_3), neutral phosphines (PR_3) and arsines (AsR_3) are versatile ligands that can be finely sterically and electronically tuned by the choice of substituents (R groups), allowing the properties of the donor-acceptor complex to be modified.[37] Phosphines, PR_3, utilise a lone pair and can be used with a range of alkyl or aryl substituents. Tertiary alkyl phosphines are more readily oxidised than aryl phosphines making them more difficult to handle, although they are stronger σ-donors.[38] Tertiary phosphines exist as pyramidal structures and can undergo pyramidal inversion like NR_3, however it is a much higher energy process and so is rarely observed.[39] Phosphines readily form multidentate species, such as *o*-*bis*(dimethylphosphino)benzene or 1,2-*bis*(dimethylphosphino)ethane which allows further tuning

of properties of the Lewis base. Using a bidentate ligand means the chelate effect aids the formation and stability of coordination complexes.

Phosphine ligands are classed as soft Lewis bases and therefore prefer coordinating to soft Lewis acids, however since many are strong σ-donors there are examples of phosphines forming bonds with hard Lewis acids.[36,40-42] For complexes involving phosphine ligands, $^{31}P\{^{1}H\}$ NMR spectroscopy provides a highly convenient probe at the site of coordination, from the atom bonded directly to the Lewis acid.

Phosphine and arsine donor ligands follow the *σ*-donor *π*-acceptor model when bonding to *d* block transition metals and as the group descends, the energy separation between *s* and *p* orbitals increases.[8] This increases *s* character on the lone pair making them less available, and coupled with increased orbital diffusivity, results in arsine ligands being weaker *σ*-donors than phosphines.[39,43] The *σ*-donation power of Group XV ligands can be improved with electron donating substituents, thus alkyl ligands are better *σ*-donors than aryl ligands.[38] This strong *σ*-donation allows a variety of complexes of hard metal acceptors with phosphine or arsine donor ligands to be stabilised.[4,42,44,45] Only certain Group XV ligands will produce stable complexes as the orbital overlap can become too poor.[42] Strong *σ*-donation from an alkyl phosphine ligand allows coordination to high valent metal centres, but in some conditions phosphines can reduce transition metals in a competing reaction.[46,47] Softer Group VX ligands (arsines or stibines) with poor orbital overlap with the metal's *d* orbitals increase the likelihood of halogenating the ligands and reducing the metal centres.

The three R groups on tertiary phosphines play an important role in the electronic and steric properties of the ligand. Large and bulky R groups (aryls) can cause steric clash and prevent coordination, the method used to quantify the steric properties of phosphines is by its 'cone angle'.

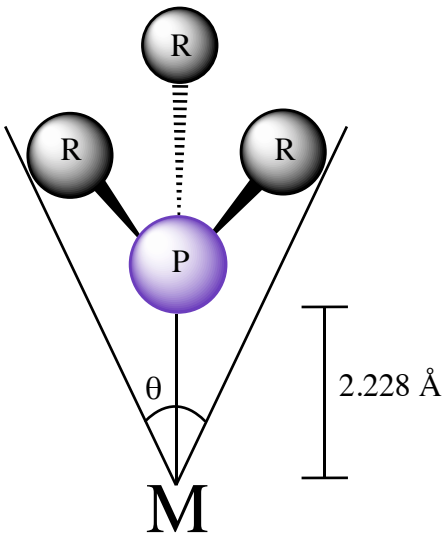

Figure 1.3: Tolman's cone angle (θ) model.[48]

The Tolman's cone angle can easily be measured from crystallographic studies however it can also be calculated, to a reasonable degree of accuracy, when no crystallographic data is available. The cone angle is defined as the apex of a cylindrical cone formed by a point 2.228 Å (representing an idealised M-P bond length) away from the phosphorus atom and just touching the Van der Waals radii of the outermost atoms of the R group when folded up (Figure 1.3).[48] Wider cone angles indicate greater steric bulk (e.g. PMe_3 θ = 118º and PPh_3 θ = 145º)[48,49] whereas for bidentate ligands the cone angle is calculated from the outer non-bridging substituents and the bisector of the P-M-P angle ($Me_2P(CH_2)_2PMe_2$ θ = 107º).[50] The Tolman's cone angle model has been extended to include arsine and stibine ligands showing the cone angle decreasing as Group XV descends.[11]

The model does have some limitations when compared to actual crystallographic data, it is shown to generally underestimate the steric demands of the phosphine ligands, and it is suggested to underestimate these demands by 15 to 25º, with increased differences in bidentate ligands.[51] Tolman's cone angle model is now considered outdated with significant advancements in modelling steric bulk computationally. DFT optimised models have been used to calculate new cone angles with methodologies including AARON[52] and Solid-G[53,54] or alternatively mapping average local ionization energy of ligands.[55]

Chelating diphosphines and diarsines have bite angles (E-M-E) which are important when choosing ligands. The bite angle is determined by constraints imposed by the backbone of the ligand, steric repulsion between substituents and the steric and electronic requirements of the Lewis acid (and any other ligands coordinated). Bidentate phosphines and arsines tend to form the most stable complexes when a five-membered ring is formed because the bite angle is close to 90º, which is beneficial to octahedral and square planar complexes.[56] The *d*(M-E) bond length also strongly influences the observed bite angle.[57]

It is shown for monodentate phosphines that the change in chemical shift upon coordination, Δ, compared to uncoordinated ligand in solution, δ, are directly related to Equation 1.1. Using this equation the predicted chemical shift can be determined with high accuracy, provided there is enough analogous data.[58]

$$\Delta = A\delta + \mathrm{B}$$

Equation 1.1: The prediction of chemical shift of a monodentate phosphine ligand upon coordination in ^{31}P NMR spectroscopy. A and B are constants derived from the individual ligand.[58,59]

This prediction is extremely useful to help determine the structure of a species; however, it cannot be applied to bidentate phosphines. This is due to a ring contribution, Δ_R, which is defined as the difference between the coordination chemical shift, Δ, of a *cis*-disubstituted phosphine complex and the coordination chemical shift of the analogous phosphorus in a chelate complex. Table 1.1 shows an example of the contribution of the ring to the chemical shift of a number of bidentate phosphine and monodentate phosphine ligands.[59]

Complex	Chelate Ring Size	Δ	Δ_R
$[Me_2Pt(PPh_2Me)_2]$	0	+34.4	-
$[Me_2Pt(Ph_2P(CH_2)PPh_2)]$	4	-17.4	-51.9
$[Me_2Pt(Ph_2P(CH_2)_2PPh_2)]$	5	+67.7	+33.3
$[Me_2Pt(Ph_2P(CH_2)_3PPh_2)]$	6	-20.5	-14.0

Table 1.1: An example of the ring contribution of three different phosphine ligands of varying ring size.[59]

Complexes which have five-membered chelate rings show a large positive ring contribution and, as such, resonances are found much further downfield than four- and six-member ring analogues.[60] The exact origin of this ring contribution is unclear but the existence and subsequent downfield shift, particularly for the five-member ring systems, is a widely observed phenomena.[36,61,62]

Many monodentate and bidentate phosphines and arsines are now commercially available, a small number still have to be synthesised in-house, such as the methyl substituted *o*-phenylene backbone ligands *o*-$C_6H_4(EMe_2)_2$, whereas *o*-$C_6H_4(PPh_2)_2$ can be purchased. The one common method is the reduction of a phosphine oxide, however given the strength of the P=O bond, powerful non-selective reagents are required, $LiAlH_4$, $HSiCl_3$ or Si_2Cl_6.[63]

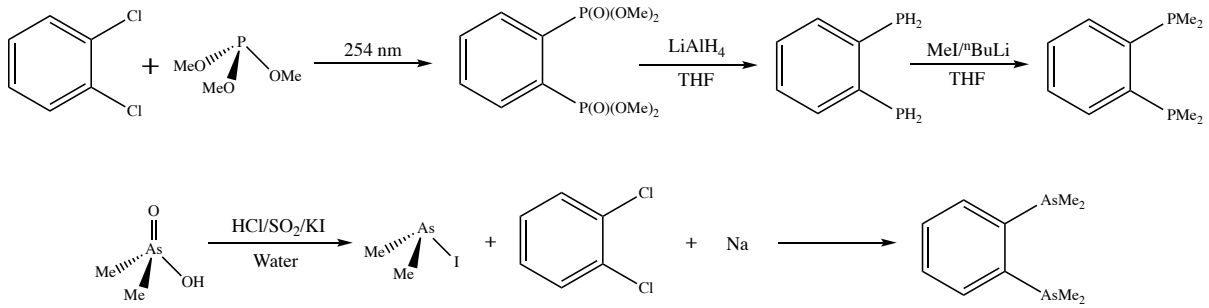

Figure 1.4: Scheme showing the synthesis of o-$C_6H_4(PMe_2)_2$ and o-$C_6H_4(AsMe_2)_2$ in THF.[64,65]

1.3.2 Neutral Phosphine Oxide Ligands

Phosphine oxide (OPR_3) ligands are an important class of neutral ligands which are usually significantly easier to handle than their phosphine counterparts. The P=O bond is very stable (589 kJ/mol),[66] resulting in phosphine oxides being very robust molecules and can be obtained from phosphines with a variety of oxidising agents; conversely the reverse reaction requires strong reducing agents (Figure 1.4).[63] The behaviour of phosphine oxides is strikingly different to phosphines owing to the hard nature of the bonded oxygen, classing them as hard Lewis bases. Unlike amine oxides which are easily reduced, phosphine oxides are often unwanted side products from reactions with phosphines.

Phosphine oxides are in their own right a versatile and useful series of ligands, allowing the ability to change substituents. In bidentate ligands, the length of the backbone which provides greater control over the electronic and steric requirements of the ligand. Due to the extensive range of P=O

containing ligands this work will focus primarily on tertiary phosphine oxides and for monodentate phosphine oxide all substituents will be the same (to remove the possibility of chiral centres).

The nature of the phosphorus-oxygen bond has been the subject of much debate, it was first suggested as a dative bond, with the lone pair of electrons on the phosphorus filling the 'octet' of electrons on the oxygen. It was subsequently described as a formal double bond owing to the vacant *d*-orbitals on the phosphorus allowing π-back bonding from a pair of electrons on the oxygen.[67] However, P=O bonds behave very differently to other double bonds, C=C or C=O and a theoretical study showed the *d*-orbitals had no role in bonding.[68] Alternatively, the bond is described as a σ-bond which causes a strong ionic charge on each atom; this ionic component strengthens and subsequently shortens the bond. It also includes π-back bonding from the lone pairs on the oxygen and acceptor antibonding orbitals in the PR_3 moiety.[69] It is still unclear the precise nature of the bond, however in most literature it is referred to as P=O with a caveat that the bonding is not fully understood. The P=O bond exhibits a large dipole moment and readily forms complexes with hard Lewis acids unlike soft neutral phosphines.[12,70,71]

Phosphine oxides have smaller steric requirements around the metal centre compared to phosphine ligands but no longer possess the ability to form a five-member chelate ring. An ethylene backbone ligand would lead to a seven-member chelate ring, which can result in the formation of bridging complexes between two or more metals instead of chelation.[72]

Phosphine oxides are commonly prepared from their respective phosphines, traditionally aqueous H_2O_2 was used as an oxidising agent to form aryl-phosphine oxides.[73,74] The co-crystallisation of H_2O_2 with the phosphine oxide however can result in the violent detonation of the peroxide.[75] Transition metals have been shown to promote the oxidation of aryl-phosphines, likely through metal-dioxygen intermediates. Reaction of aryl phosphines, SnI_4 and dry O_2 has been shown to cleanly catalytically convert phosphines to phosphine oxides.[75]

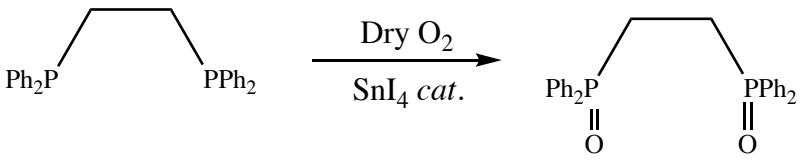

Figure 1.5: Scheme showing the synthesis of bis-(diphenylphosphino)ethane dioxide by dry oxidation catalysed by SnI_4.[75]

1.3.3 Chalcogenoether Ligands

Coordination chemistry of chalcogenoethers (ER_2, where E = S, Se or Te; R = alkyl or aryl) to transition metals has gained a considerable amount of interest in recent years. High oxidation state transition metals with neutral chalcogenoethers however are still relatively scarce.[76,77] Thioethers are soft Lewis bases and the ligands get softer as the chalcogen gets heavier. While steric effects play a vital role in the coordination of Group XV ligands including phosphine and arsine ligands

(as described by Tolman's cone angle), this is not the case for Group XVI ligands; as the chalcogen only has two substituents. Therefore, the electronic factors play a more substantial role than in phosphine and arsine ligands. In neutral chalcogenoether ligands, ER_2, the chalcogen has two available lone pairs for bonding, in most cases a single σ-bond is formed to a metal centre (σ-acceptor). Occasionally, the second set of paired electrons can contribute to a σ-bond to a second metal centre forming a bridged dimer as described by, $[(WCl_3)_2(\mu\text{-}SEt_2)_3]$ or $[(NbCl_2(SMe_2))_2(\mu\text{-}SMe_2)(\mu\text{-}Cl)_2]$ (Figure 1.6).[78,79]

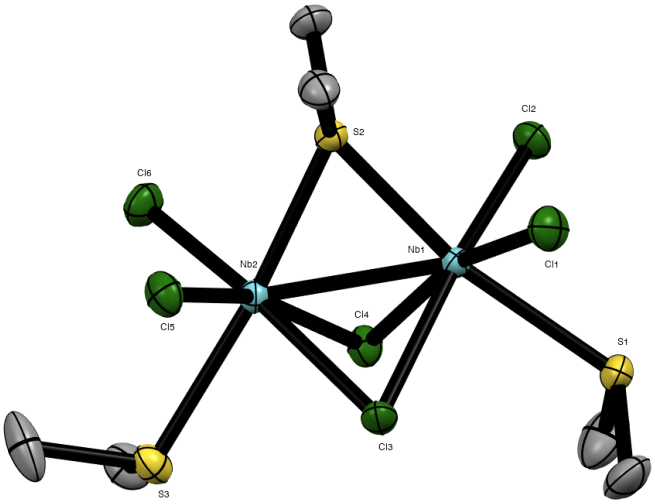

Figure 1.6: The structure of $[(NbCl_2(SMe_2))_2(\mu\text{-}SMe_2)(\mu\text{-}Cl)_2]$ showing an example of a bridging thioether. Hydrogen atoms omitted for clarity.[79]

As Group XVI is descended there is increased shielding from the nucleus meaning the valence electrons of tellurium are more diffuse than the valence electrons on sulfur, resulting in tellurium being much softer. Tellurium orbitals have poor overlap with the valence shells of carbon resulting in many tellurium ligands being unstable and Te-C cleavage is common.[34,80] The diffuse orbitals also interact poorly with contracted orbitals of high valent early transition metals, tellurium ligands (especially telluroethers) with high valent metals are therefore extremely rare.[34,80]

Chalcogenoethers can have two different R groups which are not always the same, this can give rise to chirality upon coordination. The monodentate chalcogenoethers used in this project had the same R groups to prevent the formation of chiral centres on the chalcogen atoms. Bidentate chalcogenoethers, for example $MeS(CH_2)_2SMe$, have two different alkyl groups (terminal methyl and an ethylene linker) on the chalcogen atom. Upon coordination, this gives a *meso* form (an achiral compound with optically inactive stereocentres) and a pair of *DL* enantiomers (Figure 1.7). Conversion between diastereoisomers can occur within an NMR spectroscopy time scale by pyramidal inversion.[34,81,82] A bidentate chalcogenoether such as $MeSe(CH_2)_3SeMe$ can either chelate to a metal centre or act as a bridging ligand shown in $[NbCl_4(MeSe(CH_2)_3SeMe)]$ or $[(TaCl_5)_2(o\text{-}C_6H_4(CH_2SEt)_2)]$ (Figure 1.8).[44,83]

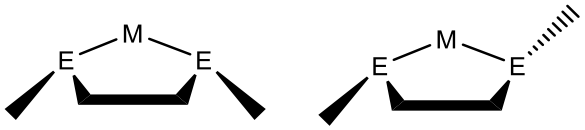

Figure 1.7: Illustration of meso (left) and DL isomers (right).

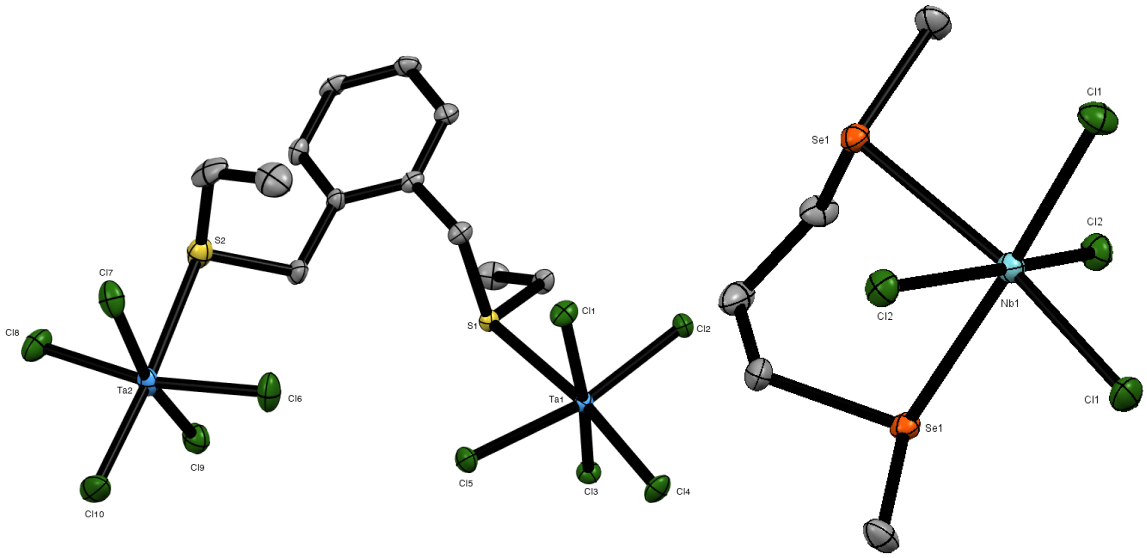

Figure 1.8: Crystal structures of [$(TaCl_5)_2$(o-$C_6H_4(CH_2SEt)_2$)] (left) an example of a bridging thioether and a meso chelated thioether, [$NbCl_4(MeSe(CH_2)_3SeMe)$] (right).Hydrogen atoms omitted for clarity.[84,85]

In this research, the monodentate chalcogenoethers ER_2 (E = S, Se or Te; R = Me, ^{n}Bu or Ph) were used. The Me-substituted ligands were chosen as the simplest chalcogenoethers and to encourage crystal growth, whereas ^{n}Bu terminal groups were used to investigate the suitability of the products for the potential use in CVD applications. Ph substituents were selected when evidence of reduction was observed, these ligands are poorer σ-donors but less readily oxidized or chlorinated, making reduction of the metal centre less favourable. Bidentate chalcogenoethers, $RE(CH_2)_nER$ (E = S, Se; R = Me, Ph or ^{i}Pr; n = 2 or 3) and *o*-$C_6H_4(EMe_2)_2$ (E = Se or Te), were used to attempt to form either chalcogenoether bridged dinuclear complexes or mononuclear chelate complexes.

Many simple chalcogenoethers are now commercially available (SMe_2, SPh_2, $SeMe_2$, S^nBu_2, *etc.*), but given their volatility and niche use, dichalcogenoethers and tellurium ligands still need to be made in the laboratory. The bidentate thioethers with aliphatic backbones are typically prepared from thiols, 1,2-ethanedithiol, sodium and haloalkanes (RX) are used to prepare $RS(CH_2)_2SR$ (Figure 1.9).[74]

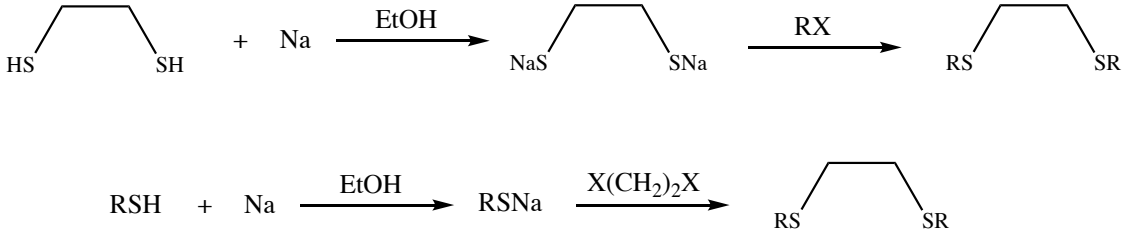

Figure 1.9: Scheme of the synthesis of $RS(CH_2)_2SR$ from thiols.[74,86]

Alternatively, bidentate thioethers can be prepared from RSNa and $X(CH_2)_nX$ (X = Cl, Br or I) (Figure 1.9) to form $RS(CH_2)_nSR$.[86,87] Most aliphatic backbone bidentate thioether ligands can be prepared with analogous starting materials, both routes use commercially available reagents and produce good yields.

Synthesis of *o*-phenylene backbone thioethers are slightly more complicated, initial methods used copper thiolate with *o*-dihalobenzene in pyridine.[87] This avoided the use of high temperatures and highly reactive reagents however yields were variable and copper reagents are challenging to handle.[88,89] An alternative method uses *o*-dihalobenzene and ^{i}PrSNa to form *o*-$C_6H_4(S^{i}Pr)_2$, subsequent reaction with MeI results in the formation of *o*-$C_6H_4(SMe_2)_2$ (Figure 1.10).[90] Direct reaction of RSNa and halobenzenes requires careful stoichiometric control and certain conditions as excess RSNa produces aromatic thiols.[91]

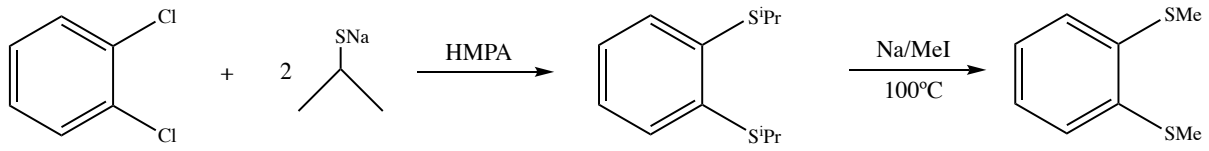

Figure 1.10: Synthesis of o-$C_6H_4(SMe_2)_2$ in HMPA via a o-$C_6H_4(S^{i}Pr)_2$ intermediate.[90]

Selenols, RSeH, are not commercially available as they are not particularly stable; therefore RSeLi reagents tend to be made *in-situ*. Reaction of elemental selenium and an alkyllithium in frozen THF prepares RSeLi which is subsequently reacted with a dihaloalkane in THF forming $RSe(CH_2)_nSeR$ (Figure 1.11).[92]

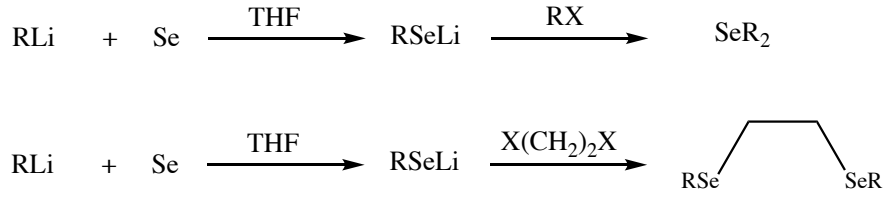

Figure 1.11: Synthesis of mono- and bi-dentate selenoethers from the addition of RLi and selenium with haloalkanes.[77,92]

Although simple monodentate selenoethers are commercially available, those with less common R groups can be prepared in the same way as the bidentate selenoethers (Figure 1.11).[77] The preparation of the *o*-phenylene backbone selenoethers are significantly more complicated than their aliphatic counterparts. The RSe^- ions are not sufficiently nucleophilic to react directly with *o*-dihalobenzene, therefore *o*-$C_6H_4(SeMe)_2$ can be prepared from reaction of Me_2Se_2 and benzyne in

o-dichlorobenzene (Figure 1.12).[92] However, this synthesis can be problematic as the intermediates are highly reactive and can be explosive when dried.

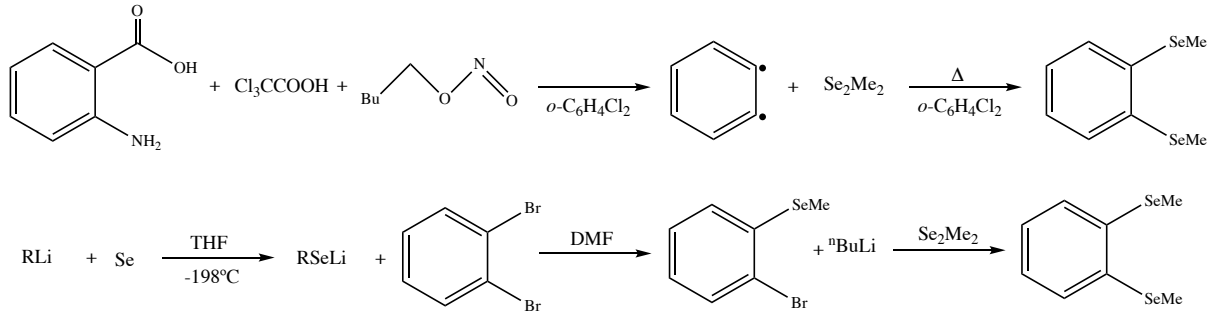

Figure 1.12: Synthesis of o-$C_6H_4(SeMe)_2$ from o-benzyne and Se_2Me_2 and from RLiSe solution.[80,92]

A second method can be used which utilises RSeLi and *o*-dibromobenzene with a second addition of alkyllithium, which eliminates the need for benzyne (Figure 1.12).[80]

Tellurium ligands have been shown to be much more challenging to synthesise due to poor orbital overlap between tellurium and carbon. In addition, tellurium forms weak bonds with hydrogen meaning the resulting tellurols are poor reagents.[76] Telluroethers are usually air sensitive unlike their seleno- and thio-ether analogues and their malodorous nature means they are not that extensively studied.[10,76]

Dimethyl tellurium can be synthesised from MeLi, elemental tellurium and MeI to isolate $[TeMe_3]I$ followed by reduction with PPh_3.[93] The synthesis of bidentate telluroethers, $RTe(CH_2)_nTeR$, are significantly more difficult than their lighter counterparts and only n = 1 or 3 backbone ligands have been successfully synthesised (Figure 1.13). They proceed through a similar reaction as their seleno- analogues but the addition of the dihaloalkane has to be completed in frozen THF.[94,95] Attempts to isolate $MeTe(CH_2)_2TeMe$ have been unsuccessful resulting in Te_2Me_2 and olefin and longer backbones produce tellurocycles.[94,96] An alternative method is the cleavage of Te_2R_2 with a base and the addition of a dihaloalkane at low temperature although the Te_2R_2 requires pre-synthesis.[97]

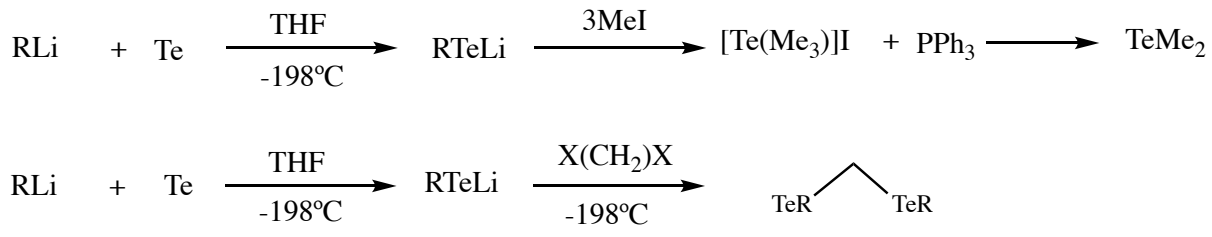

Figure 1.13: Synthesis of $TeMe_2$ and $RTe(CH_2)_nTeR$ (n = 1 or 3) from RLi and tellurium.[93,94,96]

Oddly, the *o*-phenylene backbone ligands are simpler to synthesise than their selenium analogues and follow a similar preparation to the tellurium ligands described above.[80] Additionally, the *o*-xylyl backbone ligand, $o\text{-}C_6H_4(CH_2TeMe)_2$ can also be prepared this way (Figure 1.14).[98]

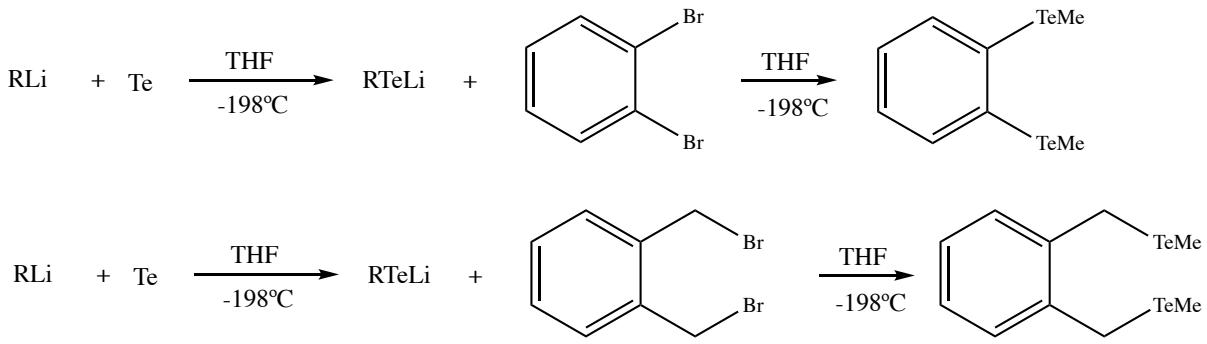

Figure 1.14: Synthesis of the ligands o-$C_6H_4(TeMe)_2$ and o-$C_6H_4(CH_2TeMe)_2$ from RLi and elemental tellurium.[80,98]

1.4 Semiconductors

Semiconductors are of huge importance across science and research, they are present in nearly all electronics and batteries, and have a wide range of properties. A semiconductor is a material which has a filled/mostly filled valence band and an empty conductance band, similar to an insulator. The valance and conductance bands are separated by an energy gap, E_g, (the energy required for an electron to jump from the valence band to the conductance band).[6] In an insulator, this gap is too wide, and the electrons cannot move bands therefore the material cannot conduct (Figure 1.15). In most semiconductors their conductivity depends on temperature, as the closer to absolute zero they get the more they behave like insulators.[99] This ability to regulate the amount of conductance in a material is vital to many applications including lasers and light emitting diodes. There are two types of semiconductors, intrinsic and extrinsic.

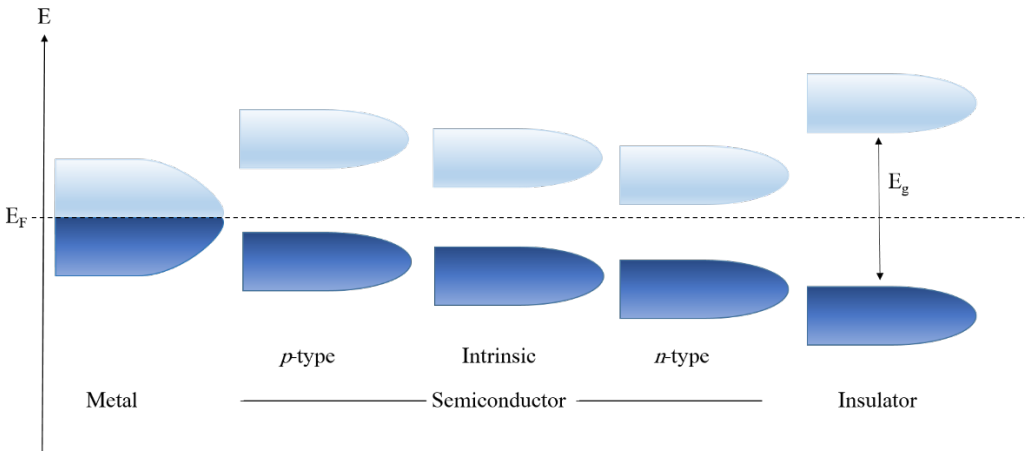

Figure 1.15: Illustration of electronic states where light blue is the conductance band and blue is the valence band.

Intrinsic semiconductors are chemically pure but their conductivity is poor due to equal numbers of electrons and holes and conductance is provided by excited electrons. Extrinsic semiconductors differ from intrinsic semiconductors as the charge carriers are provided from impurities in the material - this can be done deliberately in a process known as doping.[100] Doping allows increased conductivity, depending on the type of impurity, *n*-type and *p*-type semiconductors can be produced. Silicon, for example, is a poor semiconductor in its pure form but if doped with

pentavalent impurities *i.e.* phosphorus or arsenic it produces an *n*-type semiconductor, the impurities are electron donors resulting in additional electrons in the conductance band. Conversely, if doped with trivalent boron which acts as an electron acceptor, the energy level of the impurity is closer to the valence band, so the electrons are excited, leaving the valence band, resulting in holes in the valence band which act as the charge carriers.[101]

The ability of an electron to jump to an excited state is governed by the energy between the valence and the conductance band, E_g, known as the bandgap; the smaller the bandgap, the higher the conductivity. Doped semiconductors have reduced bandgaps due to the impurities moving the energy levels closer to either the valence or the conductance bands. Semiconductors can either have a direct or indirect bandgap, both the valence and conductance band have an assigned *k*-vector for crystal momentum. If these vectors are equal then an excited electron jumps to the conductance band, which allows the formation of an electron-hole pair causing the electron to emit a photon (Figure 1.16). In semiconductors that have indirect bandgap, the maxima energy of the valence band and the minima of the conductance band do not occur at the same momentum. Therefore, they do not have the same *k*-vector and a photon cannot be directly emitted because the electron must undertake a significant change of direction to produce an electron-hole pair. As a result direct bandgap semiconductors are used to make optical devices whereas indirect bandgap materials are not suitable.[102]

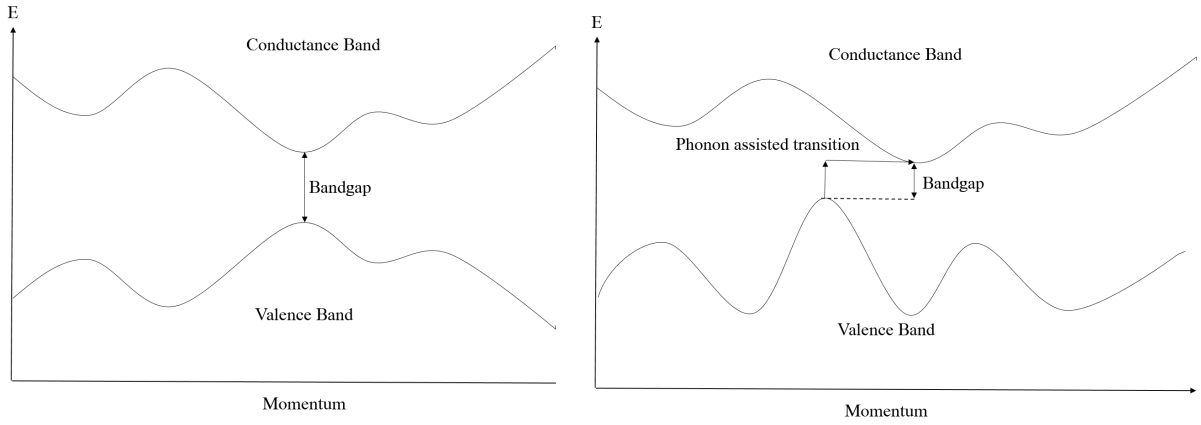

Figure 1.16: Illustration depicting direct band gap (left) and indirect bandgap (right) showing the excitation of an electron into the conductance band.

1.5 Thin Film Transition Metal Dichalcogenides

The production of layered transition metal dichalcogenide thin films is attracting huge interest due to the ability to tune various properties (importantly bandgap) and their structural relationship to graphene. These two-dimensional transition metal dichalcogenides (TMDC) have a general formula of ME_2 where M is a transition metal and E is a chalcogen (S, Se or Te). M–E bonds are mainly covalent, but the individual layers are held together by van der Waals forces, allowing easy cleavage between the layers, similar to graphene. Having been studied since the 1960s, 2D TMDCs

have regained scientific interest since the characterization of graphene.[103] In bulk, TMDC have a large range of properties, such as, semiconductors (MoS_2), semimetals (WTe_2) and insulators (HfS_2). Producing these materials as two dimensional films not only retains many of their original properties from bulk but can lead to additional desirable properties and characteristics (including direct bandgaps and increased conductivity).[104]

Each layer of the material consists of a transition metal sandwiched between two chalcogens; since the chalcogens are saturated, this results in the material being relatively inert due to the lone pair electrons on the chalcogen terminating on the surface, forming a protective layer.[105] These sandwich layers form hexagonal planes of M-E-M, these planes can then stack in different orders giving rise to different polymorphs (Figure 1.18).[106] This sandwiching also confines the charge carriers in the *x* and *y* directions, differing their properties from their bulk counterparts.[107] These differing properties makes their potential for a wide range of applications very attractive, such as electro catalysis, photovoltaics and microelectronics.[104,108]

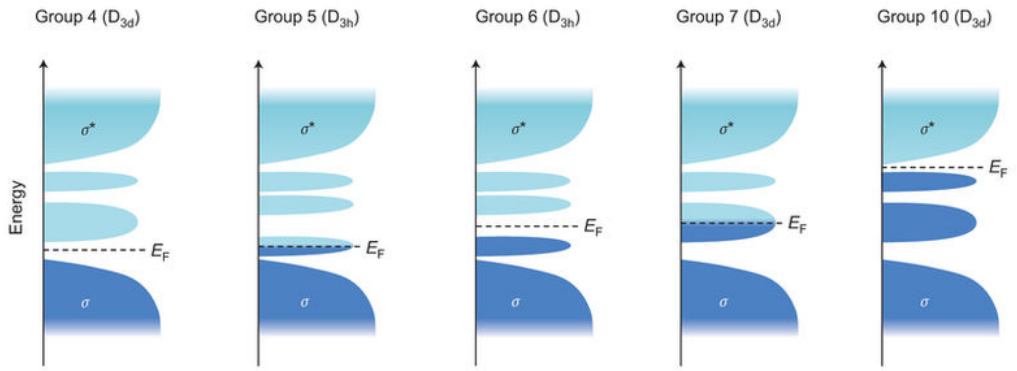

Figure 1.17: Illustration showing the filling of d orbitals and the effect on the bonding and anti-bonding states, for groups 4-7, 10 and their associated point group, assuming ideal coordination.[107]

Thin ME_2 films which only contain a few layers can be in one of three phases, the most common polymorphs are 1T, 2H and 3R, where T, H and R, are tetragonal, hexagonal and rhombohedral respectively and the number refers to the number of layers in the stacking sequence.[104] Monolayer TMDC only show two polymorphs; trigonal prismatic and an octahedral phase, D_{3h} and O_h point group, respectively.[104] MoS_2 and WS_2 both exhibit 1T and 2H phases. Studies show that the two phases show lattice matching, forming domains between the phases.[109] In MoS_2, the 2H phase is considered semiconducting and the 1T phase is considered metallic.[110] The majority of the electronic properties of a TMDC arise from the chalcogen, S > Se > Te (bandgap decreases with heavier chalcogens) the metal atom's *d* orbitals still have a small effect on the bandgap (Figure 1.17).[111]

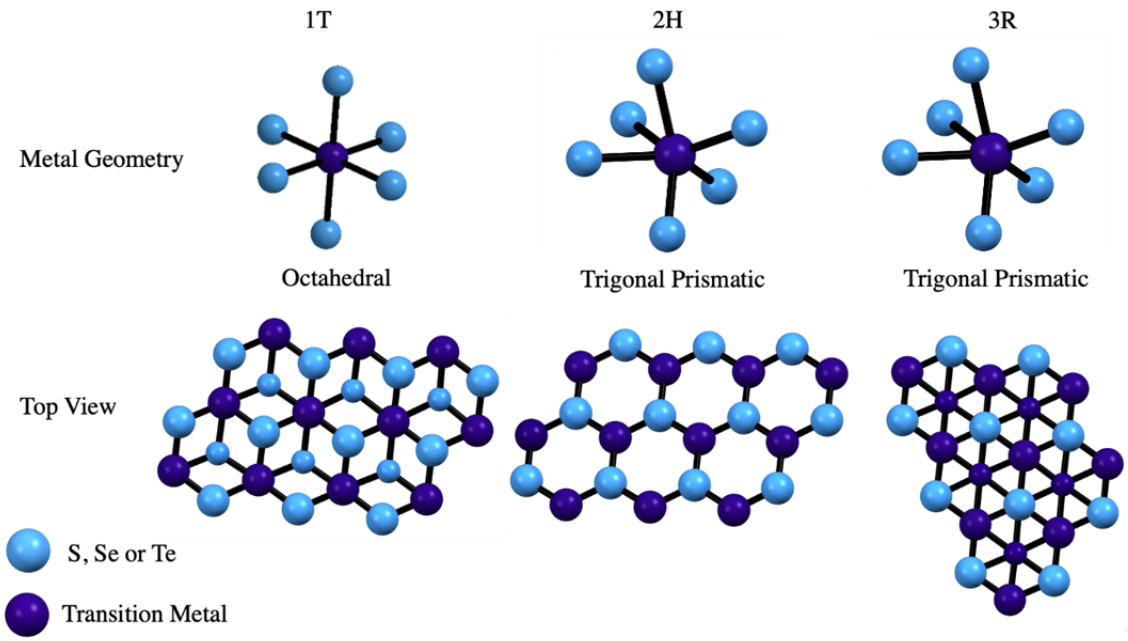

Figure 1.18: Illustration of bonding and layer stacking in transition metal dichalcogenides for the 1T, 2H and 3R phases.

When the thickness of Group VI TMDCs are reduced, the bandgap becomes larger and moves from indirect to direct band gap, which causes enhanced photoluminescence;[112] these properties in the 2D are desirable for thin film optoelectronics.[113] These properties can be desirable for specific applications, this has allowed significant developments in the TMDC field in recent years as interest has grown, shown in the range of methods and materials reported.

1.6 Chemical Vapour Deposition

Chemical vapour deposition is a technique used to coat usually an insulating substrate with a desired material, in this instance layered transition metal dichalcogenides, ME_2 (M = Ti, Hf, Nb, Ta, Mo or W; E = S, Se or Te). CVD is a thermally driven technique that utilises the formation of a stable solid product, as either a powder or thin film. A precursor(s) is heated (or activated with light or plasma) and decomposes onto a substrate, products are formed under a homogenous phase (e.g. vapour).

CVD allows deposition of very thin crystalline films and in some examples, selective deposition onto nano-patterned substrates has been reported.[114,115] The method utilised in the project is low pressure chemical vapour deposition (LPCVD) where depositions are performed under vacuum and precursors are decomposed with heat, an example set up is shown below (Figure 1.19).

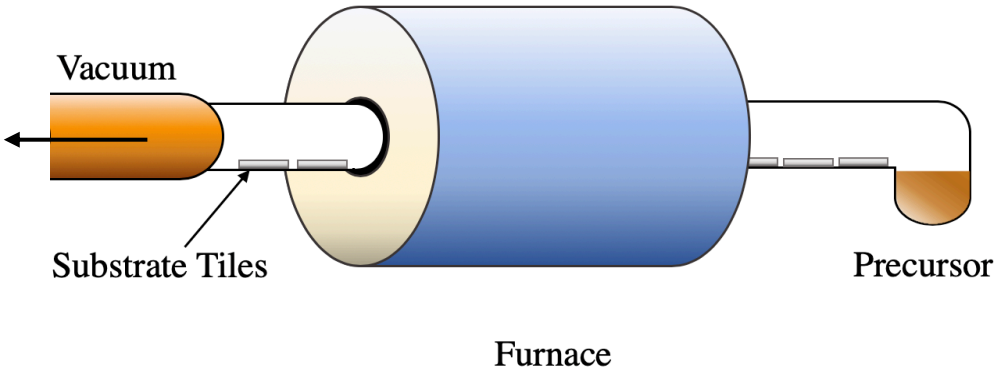

Figure 1.19: A typical set up for LPCVD experiments. The precursor is loaded into the tube on the right hand side bulb. Substrate tiles are place across the length of the tube, the arrow representing an active vacuum.

Chemical vapour deposition experiments can be performed using either a single source or dual source precursor (Figure 1.21). Single source precursors provide the ability to control more variables and therefore more influence over the films produced. Predetermining the stoichiometry of the metal and the chalcogen and the molecular weight allows greater control over the deposition conditions and subsequent film characteristics. In contrast, dual source or multisource precursors consist of separate molecules each providing one of the target elements.

As single source precursors have all the required elements, they tend to have higher molecular weights than dual source precursors. This results in greater stability but reduced volatility, especially when the target material contains heavy atoms (tungsten or tellurium for example). The reduced volatility means higher temperatures are required but precursors must also be stable at these higher temperatures.

The criteria of single source precursors mean they are tailored for each material and generally have to be synthesised as they are not commercially available. However, this allows the precursors to be individually tailored, depending on the material to be deposited. A drawback is some complexes are unstable, there are no examples of single source deposition of MTe_2 (M= Ti, Zr, Hf, V, Nb, Ta, Mo or W) films, as Te-C bonds are prone to cleavage.

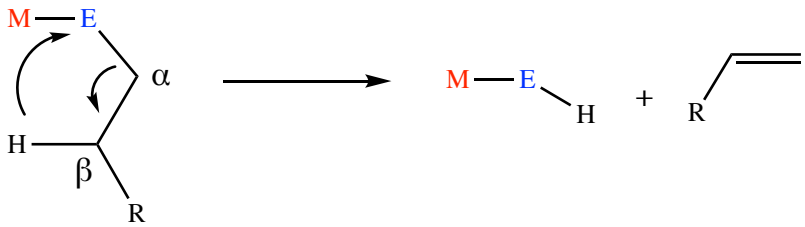

Figure 1.20: A diagram showing ß-hydride elimination pathway.

To minimise impurities in the films, precursors are designed to have a facile decomposition pathway; forming volatile by-products (Figure 1.20). Terminal alkyl chains are often employed to stabilise precursors and provide a low energy decomposition pathway *via* ß-hydride

elimination.[116,117] Precursors which can undergo ß-hydride elimination can facilitate the removal of gaseous by-products such as ethene or butene (Figure 1.21).

Dual source precursors tend to be commercially available with lower molecular weights, common reagents include metal halides, metal oxides and chalcogen sources tend to include elemental chalcogen, chalcogen containing oxides or thiols.[118-121] The high ratio of oxygen can result in MO_2 or MO_3 incorporated into the deposited films and affect the film's properties.[122]

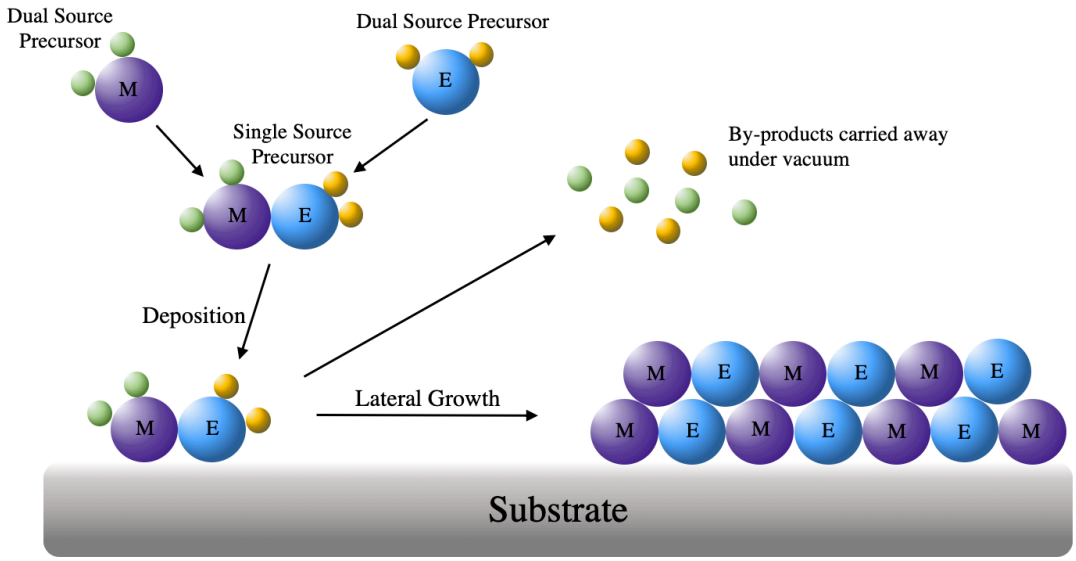

Figure 1.21: Illustration of deposition of a thin film of a desired material onto a substrate via single or dual source deposition.[123,124]

1.7 Electrochemical Deposition

The possibility of being able to electrochemically deposit materials onto surfaces was first discovered in the late 1830s. However, the only application for electrodeposition at this time was likely to be electroforming, involving simple copper salts. The deposition of various metals in thin, dense coatings is linked to the development of cyanide plating baths, enabling the deposition of silver by John Wright in 1840. Following this, a number of examples for the deposition of gold, copper, lead and other metals from cyanide baths were causing new interest in the development of thin film materials which has continued to today.[125]

Electrodeposition is an electrochemical process that usually involves the reduction of a metal species at an electrode from an electrolyte solution. The applied electrical current allows the formation of a desired material at the electrode, it then subsequently deposits onto a conductive substrate (electrode). This process is controlled mainly by the diffusion of the metal species to the surface of the electrode. The diffusion of the metal species is dependent on the size of the species and the electrolyte chosen for the solution *i.e.* how viscous it is.[126] The potential used in the system can be just as important as the size and charge of the metal species, if the potential is less negative than the equilibrium potential, deposition occurs prior to equilibrium, resulting in non-favourable

deposition, a process known as under-potential deposition. However a larger potential can lead to little or no deposition at all, known as over-potential.[127]

Traditionally, electrodeposition has been conducted using aqueous solutions as this allows the ability to control the pH of the bath and influence the chemistry of the metal ions and therefore the potential product. However there are some drawbacks of using aqueous solutions; it can promote hydrogen liberation, small electrical windows (~2V), low thermal stability and is not always suitable for some transition metals.[128] Therefore, alternative electrochemical baths are required; organic solvents, molten salts and ionic liquids have all shown to be suitable baths for some depositions.[128-130]

Typically, electrochemical solutions contain a solvent (i.e. water) containing a solvated salt, whose ions conduct electricity. Traditional salts can be melted down to form a molten solution that can conduct electricity. These salts have a relatively good heat capacity and can be heated to relatively high temperatures (>700 ºC). The most commonly used salts are LiCl-KCl and NaCl-KCl,[128] however they can be highly corrosive.[131] A subset of molten salts are room temperature ionic liquids (RTIL), viscous liquids at room temperature, where the cations are typically tetraalkylammonium, $[R_4N]^+$, or cyclic amines.[128] First generation ionic liquids were air and moisture sensitive until 1-ethyl-3-methylimidazolium (EMIM) and tetrafluoroborate were used as air and moisture stable electrolytes.[132] These ionic liquids are usually non-volatile, non-flammable and have a wide electrical window however, due to their high viscosity and high density, ionic liquids can have high conductivity but the diffusion of the metal species can be limited.

The use of conventional organic solvents is also common place in electrodeposition, which allows techniques that are easy to control, are cost effective and are proven to effectively deposit metals and compounds such as Lu-Ni alloys from dimethyl sulfoxide (dmso).[133,134] Organic solvents do have some challenges such as evaporation of the solvent and flammability, however they do allow better solubility of electrolytes and materials, but compared to ionic liquids they have been given relatively little attention.

Electrodeposition offers some advantages that other methods do not, most notably control of the end product (thickness and deposition area). Material will only form if there is an electrical contact using relatively mild reaction conditions, allowing materials that would not be stable under harsh conditions to deposit. Processes like CVD require high temperatures in which to vaporise the precursors in contrast, electrodeposition is typically carried out at much lower temperatures (r.t. to ~150 ºC).[128] These lower temperatures, and the ability to control the potential of the system (and therefore the rate of deposition), in principle allows greater control of the deposits than other thin film techniques. Also, electrodeposition is a bottom up technique allowing a high density material to be formed and therefore offers efficient volume filling with fewer defects. Electrodeposition has many potential applications and is already used in industry,[135] for integrated copper circuits known as the Damascene process[136] and magnetic recording devices.[137]

1.8 Analytical Techniques

A number of analytical techniques have been used to characterise compounds that have been synthesised in this work. Solid state techniques, such as IR spectroscopy, X-ray diffraction and UV-vis spectroscopy, and solution techniques, including multinuclear NMR spectroscopy ^{1}H, $^{31}P\{^{1}H\}$, $^{77}Se\{^{1}H\}$, ^{95}Mo, ^{183}W were used to fully characterise the complexes in solid and in solution. An important caveat to NMR spectroscopy is that it may not be representative of the compound in solid state (e.g. due to poor solubility or dissociation of the ligand and the metal centre owing to high lability of donor-acceptor interactions) making solid state analysis vital. Elemental analysis (C, H and N) has also been undertaken to confirm the chemical composition and verify purity of the bulk products. Analysis of thin films has also been completed using Raman spectroscopy, EDX/WDX, grazing incidence X-ray diffraction and XPS.

1.8.1 Infrared Spectroscopy

Infrared spectroscopy was performed, as Nujol mulls over the range 4000-200 cm^{-1}, to identify the bonds or functional groups within a compound, with an emphasis on M-X and M=E bands due to their characteristic stretching frequencies. Every bond has a vibrational energy and a number of vibrational transitions. When a compound is irradiated with energy that matches the vibrational transition, the energy is absorbed by the compound; these vibrational transitions must cause a change in a permanent dipole for the bond to be IR active.[138] This absorption can be measured against a pre-recorded background resulting in the characteristic IR spectrum.

Key vibration bands lie in the 'fingerprint' region (1500-200 cm^{-1}). IR spectroscopy is particularly useful for coordination chemistry as functional groups such as P=O and P=S have well defined absorptions (P=O ~1100 cm^{-1}) that shift significantly upon coordination to a metal centre. It can also be useful in showing the absence of particular solvents, especially water which has a strong broad absorption at (3500-3300 cm^{-1}) and a bending mode (~1650 cm^{-1}). The presence of W=S (600-500 cm^{-1}), W=O (900-1000 cm^{-1}) and Mo=O (900-1000 cm^{-1}) stretches are important for showing the incorporation of a terminal bond and all show a shift upon coordination to neutral ligands (due to increased coordination number).

Group theory can be used to determine the molecular symmetry of a complex from the number of stretches observed for a particular bond.[138] Typically, ν(M–X) (M = metals; X = halides) of transition metal halide complexes lie between 600-200 cm^{-1}, providing information on the oxidation state of the metal centre and the geometry of these complexes.[4,70,138] However, group theory assumes the compound is a molecular species and does not take into account solid state effects such as intermolecular interactions. This can cause broadening of peaks and fewer bands being observed due to reduced symmetry; peak splitting can also occur. IR spectroscopy also provides an insight into oxidation state and coordination number if a series of compounds can be compared.

1.8.2 Multinuclear NMR Spectroscopy

Nuclear magnetic resonance (NMR) spectroscopy is an analytical technique that exploits the magnetic properties of atomic nuclei, typically in the solution state. It can give information regarding structure and chemical environments, providing the molecule contains NMR active nuclei. It provides data on chemical shifts, multiplicities, coupling constants and coordination shifts, which are vital to identifying compounds and their behaviour in solution.

NMR Nucleus	Nuclear Spin (I)	Natural Abundance (%)	Quadrupole Moment (10^{-28} m^2) (Q)	Resonance Frequency (at 2.35 T)	Reference Standard
^{1}H	1/2	99.9	-	100	Residual solvent protons
^{31}P	1/2	100	-	40.5	H_3PO_4, 85% aq
^{77}Se	1/2	7.63	-	19.1	Me_2Se
^{95}Mo	5/2	9.55	0.12	6.7	2M Na_2MoO_4 aq
^{183}W	1/2	14.31	-	4.2	1M Na_2WO_2 aq

Table 1.2: Selected properties of NMR nuclei utilised in this work.[139]

All reported parameters in Table 1.2 affect what is observed in an NMR spectrum. In a molecule or complex there is an electric field gradient (efg) at each nucleus, caused by asymmetry in the local charge distribution (from electrons of nearby nuclei). The nucleus always tries to orient itself to be in the lowest energy state, if a nucleus has I = 1/2 then the nucleus can remain in the lowest energy state. If a nucleus has I > 1/2 then it cannot be in the lowest energy state and it is constantly trying to orient to the lowest possible energy level. The electric field gradient couples with the quadrupole moment from the nucleus to provide an efficient relaxation pathway (quadrupolar relaxation). Quadrupolar relaxation is normally more dominant than other relaxation pathways which can result in line broadening. In some cases, the broadening is so significant that the resonance cannot be determined; it can also broaden nearby nuclei as a result of interactions with the quadrupolar nucleus. In some quadrupolar nuclei, NMR spectra can only be observed in highly symmetric molecules. Symmetrical molecules have a lower electric field gradient and therefore a slower relaxation time, which results in sharper resonances, sometimes couplings can be observed, but only over one bond.[139]

The favourable nuclear properties of the ^{31}P NMR nucleus (I = 1/2) make it vital for characterising complexes involving phosphine or phosphine oxide ligands. The ^{75}As nucleus has a spin of I = 3/2 and a natural abundance of 100%, however it has a large quadrupole moment (Q = 0.29 x 10^{-28} m^2) that leads to severe broadening and cannot be studied except in highly symmetrical environments.

1.8.2.1 Selenium NMR Spectroscopy

There are six naturally occurring isotopes of selenium, but only one, ^{77}Se, has a nuclear spin of I = 1/2, selected properties can be found in Table 1.2. The chemical shift range for ^{77}Se is

approximately 3000 ppm (2000 to -1000 ppm).[139] In the NMR spectra of nuclei bonded to selenium, ^{77}Se satellites are easily recognisable with a simple coupling pattern. In similar ways to ^{1}H NMR spectra, a chemical shift can be observed upon coordination, which is indicative of the coordination of selenoether ligands.

1.8.2.2 Molybdenum NMR Spectroscopy

There are seven naturally occurring isotopes of molybdenum, two of which are NMR active nuclei, ^{95}Mo and ^{97}Mo; both are quadrupolar (I = 5/2). The ^{95}Mo nucleus has higher sensitivity than ^{97}Mo, ^{97}Mo has a larger quadrupole moment (1.1 Q) resulting in large line broadening.[140] The chemical shift range for ^{95}Mo is approximately 4300 ppm (2300 to -2000 ppm). With such large chemical shift values, solvent choice, concentration and temperature can have a major effect on the resonance, solvent can shift the resonances by ~100 ppm as seen in $[MoS_4]^{2-}$ (2252 ppm in D_2O and 2176 ppm in Me_2SO).[141]

1.8.2.3 Tungsten NMR Spectroscopy

There is only one NMR active nucleus of tungsten, ^{183}W, which is very insensitive, with I = ½. It shows large coupling constants to other nuclei (e.g. J_{SeW} ~50 Hz in $[Et_4N]_2[WSe_4]$).[142] Once again, the chemical shift range for ^{183}W is very large, approximately 6700 ppm (2050 to -4650 ppm) with large chemical window solvents can have a significant effect on the resonance value. Due to the inherent insensitivity and low resonance frequency, ^{183}W NMR spectroscopy has been of limited use however ^{183}W satellites are observed on other nuclei (^{31}P and ^{77}Se).

As previously stated, ^{31}P, ^{77}Se, ^{95}Mo and ^{183}W have large chemical shift ranges, donor ligands, coordination geometry, temperature and solvent can all influence the resonance, this allows information regarding coordination around the metal centre to be obtained. While NMR spectroscopy provides a large array of information for complexes in solution, this relies on complexes being soluble and therefore NMR spectroscopy may not be representative of the bulk solid. Some complexes are dynamic in solution or have labile ligands which can cause line broadening, particularly in ^{1}H NMR spectroscopy, this can be reduced in some instances by cooling the solution therefore increasing the relaxation time. However, complexes with unpaired electrons cannot be studied by NMR, as they are paramagnetic and therefore spectra cannot be interpreted due to interference with the magnetic field.

1.8.3 Single Crystal X-ray Diffraction

Single crystal X-ray diffraction is an extremely powerful technique, once obtained, a structure can be determined by locating the position of atoms or ions in a crystalline solid. A single crystal is required to use this technique and it must be of suitable size and quality. Suitable crystals may be

obtained from slow evaporation of a saturated solution or by vapour diffusion. A crystal can be thought of as identical repeating units of the same structure, this can be atoms, ions or molecules. The extended crystal lattice is a pattern formed by points that represent repeating structural elements, one repeat of the pattern is called a unit cell; this is an imaginary volume from which a whole crystal can be recreated through a series of translations in the *x*-, *y*- or *z*-axes.

System	Unit Cell Parameters
Triclinic	$a \neq b \neq c$; $\alpha \neq \beta \neq \gamma \neq 90°$
Monoclinic	$a \neq b \neq c$; $\alpha = \gamma = 90°$, $\beta \neq 90°$
Orthorhombic	$a \neq b \neq c$; $\alpha = \beta = \gamma = 90°$
Rhombohedral	$a = b = c$; $\alpha = \beta = \gamma \neq 90°$
Tetragonal	$a = b \neq c$; $\alpha = \beta = \gamma = 90°$
Hexagonal	$a = b \neq c$; $\alpha = \beta = 90°$, $\gamma \neq 90°$
Cubic	$a = b = c$; $\alpha = \beta = \gamma = 90°$

Table 1.3: Crystal systems.[143]

The unit cell is a parallelepiped and has a number of parameters; three sides (*a*, *b* and *c*) and three angles (α, β and γ) that define the unit cell, and this gives rise to seven crystal systems (Table 1.3).

The asymmetric unit of a crystal is a section of the unit cell that contains the structural and symmetry information. The asymmetric unit can consist of one molecule or part of a molecule this basic unit can have symmetry operations applied, upon which the unit cell can be obtained, and space group discovered. Translational operations can then be applied to the unit cell to determine the packing of the extended crystal system.

In a single crystal X-ray experiment, X-rays hit a crystal at the angle of incidence, θ_i, and diffracts at the angle of reflection, θ_r, where θ_i is equal to θ_r (Figure 1.22). If Bragg's law is satisfied, then a spot is observed by the detector. Bragg's law is satisfied when the atoms are a certain distance apart that the X-rays diffract between them, in a single crystal these diffracted X-rays are constructive and therefore observed by the detector.

$$n\lambda = 2d_{hkl} \sin \theta$$

Equation 1.2: Bragg's law, n = integer, λ = wavelength, θ = angle of incidence.

Where λ is the wavelength of the X-ray beam, d is the distance between Miller planes, *hlk* are three integer numbers which define the direction of the symmetry planes with respect to the sides of the unit cell, and θ is the angle between the plane and the outgoing beam. The conditions in Bragg's law will only be satisfied by a few reflections in a randomly orientated crystal, hence the crystal must be rotated to obtain all the reflections which appear as a spot on the detector. Every crystal has different sets of Miller planes resulting in different spots and different atoms give rise to spots of varying intensity.

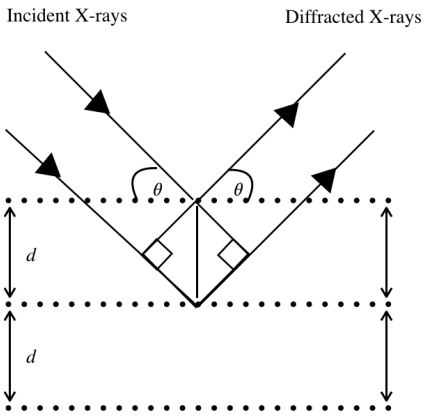

Figure 1.22: Illustration showing Braggs law.

Once all these images have been generated the pattern can be collated and undergoes data reduction. Since the intenisity of the X-ray beam, I(*hkl*), is proportional to the square of the wave amplitude, $|F_o|^2$, a number of corrections can be appiled to obtain the 'observed structure amplitudes'. Geometric corrections (known as Lorenz-polarization factors) are instrument dependent and therefore are well known and easily corrected for. Corrections are also made for variations in the incidence X-ray beam and scattering power of the crystal. Sometimes when there is significant absorption effects a correction is made, either by using the size and shape of the crystal or comparing symmetry equivalent reflections. Data reduction includes the merging and the averaging of repeated and symmtery equivalent measurments to produce a unique and scaled set of data.

To generate an electron density distribution map through the unit cell is a challenge because of what is known as the phase problem. Each wave has a phase, Φ, which cannot be measured and is therefore unknown, so direct calculation of electron density is impossible. There are a number of methods to solve a structure, the one used in this work is 'heavy atom methods' or Patterson Methods. The Fourier transform of the squared amplitudes, $|F_o|^2$, (where all phases are set to zero) produces what is known as a Patterson Synthesis. The map shows peaks of positive density for pairs of atoms, the peaks show where the atoms lie relative to each other. The Patterson peaks are proportional in size to the atomic numbers of the atoms concerned. Every pair of atoms has n^2 vectors which converge at the origin making this the largest peak and as the vectors between pairs are equal, the map will always have an inversion centre. Patterson peaks are broad and therefore there can be considerable peak overlap with no identifiable maxima. If a structure contains a few heavy atoms there will be a small number of peaks above the background level which are easily identified.

Once these heavy atoms are identified this gives a 'trial structure', using the forward Fourier transform equation a calculated diffraction pattern is produced and the calculated structure factors, F_c, can be compared to F_o. If the model is approximately correct there will be some resemblance between F_c and F_o. Using the calculated phases, Φ_c, as the observed phases are unknown, a new

model can be produced with more atoms. The new $|F_c|$ values are used in the next Fourier transform which gives improved Φ_c, this can be repeated until no further improvement in the model is observed. This repeated process is called a bootstrap procedure. Once all the atoms have been found the model is refined, which involves varying the numerical parameters to give the best agreement between $|F_c|$ and $|F_o|$. These parameters are known as the anisotropic displacement parameters (ADP) and are represented as thermal ellipsoids. Crystals are mounted on a support and the experiment is run at 100 K, this is to minimise thermal motion within the crystal and reduces the possibility of the crystal decomposing during collection. The thermal motion of the atoms in the structure is quantified graphically using an Oak Ridge Thermal Ellipsoid Plot (ORTEP) image.

From this technique, information about type and position of atoms, bond lengths and angles as well as intra and inter-molecular interaction may be obtained. The crystal is one or a few out of a bulk sample so may not be representative of the whole solid or the species in solution; also, multiple structures may be obtained from one attempt of growing crystals.

Disorder within crystals can make structural solution more difficult and even disorded solvent within the lattice can lead to inaccuracies in bond lengths and angles of the complex. Dynamic disorder is where bonds vibrate, bend and stretch (thermal motion) and is overcome by running experiments at low temperatures. Static disorder is caused by the random deviation of atom positions from the perfect single crystal, which results in partially occupied atom sites. In this project, the most prevalent disorder is S/Cl disorder, where M=S and M-Cl bond lengths are similar and difficult to distinguish from each other in the X-ray scattering pattern. It is common for $[MECl_3(L\text{-}L)]$ complexes to exhibit this disorder as the chalcogen is usually *trans* to ligand, therefore it is equally likely to be in one of two positions (Figure 1.23). Complexes are modelled by making E/Cl free then using split atoms sites to ascertain the atom's respective occupancies. The atoms are then fixed at these occupancies and refined. In some instances, the bond lengths are indistinguishable and can falsely increase the symmetry in the unit cell which can result in the space group being misidentified.

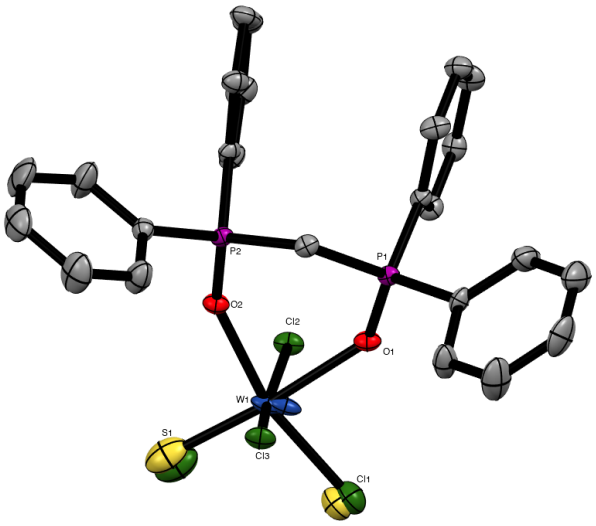

Figure 1.23: Crystal structure of [$WSCl_3(dppmO_2)$] showing the atom numbering scheme, an example of S/Cl across two different sites. Ellipsoids shown at 50% probability, hydrogen atoms omitted for clarity.

In high valent metal complexes, Cl^- and S^{2-} bridged dimers can be common, but Cl^- and S^{2-} ligands are isoelectronic and very difficult to distinguish by X-ray crystallography without further spectroscopic data making structural refinement inaccurate.[144] However, differences in bond lengths between the metal and Cl/S can help differentiate the atoms by comparing them to literature values. Another common cause of disorder is the presence of disordered solvent which has crystallised in the lattice. In cases where the solvent is disordered over a large number of sites unfortunately it can be impossible to model accurately, in some instances the use of a solvent mask is vital.

1.9 UV-Visible Spectroscopy

Ultraviolet-visible spectroscopy is a simple method for observing the absorption of the electromagnetic radiation in the UV and visible regions. It is a quick and non-destructive technique and can be performed on gas, solution and solids. During an experiment, a beam is split into two, one passes through a sample and the other passes through a reference. The resulting beams are compared at a detector and the absorption displayed as function of wavelength. The intensity of absorption is measured as the absorbance and can be related to the molar concentration of the absorbing species using the Beer Lambert Law, Equation 1.3.[6]

$$A = -\log\left(\frac{I}{I_0}\right) = \varepsilon l c$$

Equation 1.3: Beer Lambert Law. A = absorbance, ε = molar absorptivity, l = path length and c =concentration.

UV-Vis spectroscopy is often used to probe ligand-ligand, metal-metal and charge transfer transitions. Ligand-ligand transitions are most common in organic ligands containing π systems. Metal transitions occur mostly in transition metals with partially filled *d* orbitals, in octahedral species *d*-orbitals split into t_{2g} and e_g orbitals. Excitation of an electron would promote it from the

t_{2g} orbital to the e_g orbital; this *d-d* transition is spin forbidden by the Laporte Rule (g→u) and often $\Delta I = \pm 1$ selection rule. Due to this, they are usually weak transitions but can be observed due to vibronic coupling, especially in distorted octahedral environments. Transition metals also benefit from charge transfer bands, either metal to ligand or ligand to metal and are often intense bands (depending on symmetry and selection rules) and can be observed in either the UV or visible range and give rise to intense colours.

Diffuse reflectance UV-Vis spectroscopy on solids is the main technique used in this work. In low symmetry complexes (which causes splitting of the *d* orbital energy levels) it can be challenging to definitively assign LMCT bands, but tentative assignments can be made using Equation 1.4.

$$v'_{CT} = 30{,}000\,[\chi_{opt}(M) - \chi_{opt}(X)]$$

Equation 1.4: UV-Vis LMCT bands using optical electronegativity. χ_{opt} = optical electronegativity of specific atoms or compounds.

Equation 1.4 suggests the lowest energy for each ligand-metal charge transfer band, which can be applied to each individual spectrum. Although, when comparing a series of complexes more confident assignments can be made, but with the caveat that there are many charge transfer bands for the same transfers and they can overlap each other with different intensities.

1.10 Materials Characterisation

1.10.1 Grazing Incidence X-ray Diffraction

GIXRD follows the same principles as single crystal XRD but collects a 2D X-ray spectrum, compared to single crystal XRD which produces 3D electron density maps. While the incidence angle of the X-ray beam changes in a typical PXRD or single crystal XRD, it remains fixed in GIXRD (1° or lower) to minimise scattering and therefore suppress the effects of substrates on the pattern when examining thin films.[145] During the experiment the detector moves across the sample at the angle of 2θ. The analysis of the diffraction pattern usually involves comparison to previously reported PXRD data. Crystalline thin films usually have a preferred orientation which can result in inconsistent intensities when comparing to powder diffraction patterns.

In-plane XRD can further suppress the reflections from the substrate by offsetting the angle of the detector by $2\theta_\chi$. This means the detector only collects scattered electrons rather than direct diffraction making the signal strength much weaker and collection times significantly longer.[145]

It is possible to calculate the crystallite size from an XRD pattern using the Scherrer equation for calculating crystallite size from line broadening (Equation 1.5).[146]

$$t = \frac{K\lambda}{\beta cos\theta}$$

Equation 1.5: The Scherrer equation. t = is the crystallite size, λ the X-ray wavelength, θ the Bragg angle, K the shape factor, β the line broadening (FWHM).

The Williamson-Hall method uses the Scherrer equation and the equation for strain broadening to give Equation 1.6, where β (FWHM of peaks) can be plotted to give size and strain of the material.

$$\beta = C_\varepsilon \, tan\theta \qquad\qquad \beta_{tot} \, cos\theta = \, C_\varepsilon \, sin\theta + \frac{K\lambda}{L}$$

Equation 1.6: The strain broadening equation (left) and the equation used in the Williamson-Hall method (right). θ the Bragg angle, C_ε the strain component, β the line broadening (FWHM,). K the shape factor, , λ the X-ray wavelength.

1.10.2 Raman Spectroscopy

Raman spectroscopy is very similar to IR spectroscopy in that they both probe vibrational modes; IR spectra shows the absorption of light whereas Raman spectra show scattering. Normally Raman spectroscopy is complementary to IR spectroscopy, but Raman spectroscopy offers some benefits for characterising materials, since it is a surface technique. It is used extensively for characterising thin film materials produced, for example, from electrodeposition or CVD. In some cases, it even allows the determination of the film thickness as there are small shifts in peaks proportional to thickness, it is a very sensitive technique that can even detect monolayer films, e.g. in MoS_2.[147] The detector is usually set at a 90 º angle to avoid picking up signal from the beam source.[148,149] It also uses excitation wavelength to avoid generating fluorescence, if fluorescence is produced the only way to minimise this is to change excitation length (e.g. change the laser).

1.10.3 Scanning Electron Microscopy

In scanning electron microscopy a narrow beam of electrons are accelerated down a column through a lens and apertures to generate a focused electron beam which hits the surface of the sample. The electrons then interact with the surface producing backscattered electrons and secondary electrons. Secondary electrons show the topography of the surface and backscattered electrons show the spatial distribution of elements in the first few microns of the sample. Secondary and backscattered electrons are the main signals detected in SEM and these signals are transformed into images; both sets of electrons are emitted from the surface of the sample.[150] To obtain an image, the sample must be metallic or a conducting material, insulators and semiconductors can cause irregular release of electrons, thus reducing the resolution of the image.

1.10.4 Energy-Dispersive X-ray and Wavelength Dispersive X-ray Spectroscopy

Often EDX is coupled with SEM in one system when the accelerated electrons strike an atom; some of the energy is transferred into the atom. This allows an electron within the atom to 'jump' to a higher energy shell or leave, ionising the sample. If this process occurs a hole is left behind. Due to this positive charge, a negatively charged electron from a higher energy shell drops down to fill the hole and the energy difference is emitted in the form of an X-ray. If an electron drops from an L shell to a K shell, it is known as K_α, if the electron drops from an M shell to an L shell, it is known as L_α. Each element has unique K_α and L_α energies which allows the elements to be distinguished from one another. These peaks can also be quantified to get a percentage composition of the sample.[149,150] Lighter elements like Na can be qualitatively identified but cannot be quantified due to a low fluorescence yield and their K_α peaks overlapping with heavier elements.[149,150] If peaks overlap it can be difficult to distinguish between the two elements, for example, the energy of Mo L_α (2.293 eV) is similar to the energy of S K_α (2.306 eV), thus making it difficult to determine the stoichiometry of a molybdenum sulfide material.[151]

Wavelength dispersive X-ray (WDX) spectroscopy collects the same data as EDX but is more similar to X-ray diffraction. Electrons are accelerated at a sample, generating X-rays, these X-rays are then passed through a known crystal with certain lattice spacings. The sample generated X-rays encounter the known crystal at a specific angle, θ, only those that satisfy Bragg's law are reflected and passed to the detector.[152] The wavelength the detector received can be changed by moving the known crystal, consequently only X-rays from one element at a time may be measured whereas EDX collects all signals at once. WDX can identify lighter elements that EDX cannot detect, (all apart from H, He and Li), also WDX has greater resolution increasing peak separation allowing easier identification and quantification.

1.10.5 X-ray Photoelectron Spectroscopy

XPS is a surface technique used for identifying composition, chemical and electronic states of the elements present within a material. XPS is a cross between EDX and WDX, X-rays are fired at a solid sample and measure the kinetic energy of the photoelectrons that are subsequently emitted. A spectrum is recorded by counting the photoelectrons at a range of energies, the characteristic energies can be assigned to particular elements; all assignable apart from hydrogen.

$$KE = h\nu - BE - \Phi$$

Equation 1.7: Photoelectric effect. KE = kinetic energy, hν = energy of the photon, BE = binding energy of the atomic orbital, Φ = spectrometer work function.

The binding energies are unique to each atomic orbital and can be regarded as the difference between the initial and final states after the photoelectron has left, (Equation 1.7).[153] Because of the variety of final states there are different kinetic energies of the electrons and different probabilities

of each state. For emission from *p, d* and *f* orbitals two peaks (or energies) are observed, the separation is caused by spin orbital splitting and can be defined as $j = l \pm s$ the differences in energy is small but it can aid elemental determination.

1.10.6 Electrical Measurements

The sheet resistance of a thin film can be investigated using the Hall and van der Pauw method. This method uses a four-point probe and applies a current across the sample. The four probes are placed linearly and equally spaced and a current is induced through the two probes on the outside of the sample. The voltage is then measured between the two inner probes. Measuring the thickness of the samples (usual by cross-sectional SEM), allows for calculation of the resistivity of the sample.[154,155]

Application of a magnetic field perpendicular to the flow of electrons, results in the electrons experiencing a Lorentz force (F_L). This is proportional to the magnetic field strength (B) and the travelling velocity (v), see Equation 1.8.[156]

$$F_L = qvB$$

Equation 1.8: Lorentz force equation. F_L is Lorentz force, B is magnetic field strength, v is travelling velocity and q is the particle charge.

The Lorentz force (F_L) can be expressed in terms of current (I) and therefore Equation 1.9 can be used to quantify the carrier denisty of the sample.

$$F_L = \frac{IB}{\eta_m A}$$

Equation 1.9: Lorentz force equation for carrier density. F_L is Lorentz force, B is magnetic field strength, I is current and A is the area.

Subsquently, once carrier density and resistivity are known, the carrier mobility (μ_m) can be calculated using Equation 1.10. A low carrier density and high carrier mobilty are an indication of high purity semiconductors. Materials with a high carrier density (i.e. more conductive) behave more like conductors or semi-metals and can be an indication of a high volume of defects in a semi-conductor.

$$\rho = \frac{1}{q\eta_m\mu_m}$$

Equation 1.10: Equation for resistivity. ρ is resistivity, η_m is carrier density, μ_m is carrier mobility.

1.11 Cyclic Voltammetry

One of the aims of this work was to design suitable precursors for non-aqueous electrodeposition of molybdenum and tungsten dichalcogenide thin films. Therefore, the electrochemical behaviour of the new precursors was initially studied by cyclic voltammetry. This technique was used as it

provides fast and efficient insight into the electrochemical behaviour of a precursor, including information on oxidation and reduction potentials, hence the compound deposition potential (E_{pe}) and the electrochemical window of the system.[157]

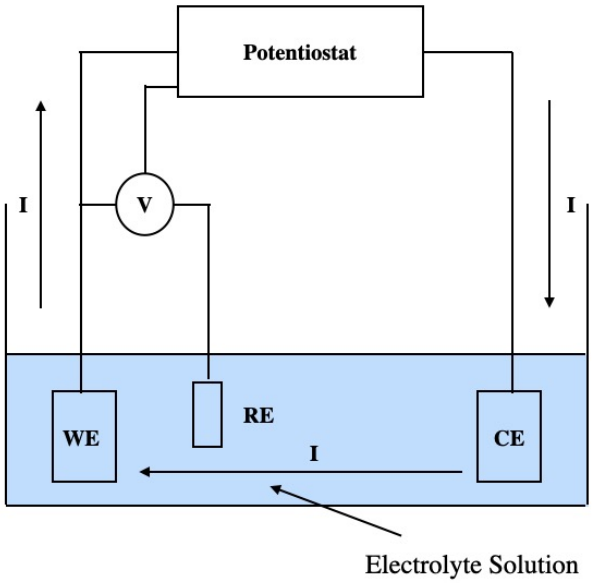

Figure 1.24: Illustration of a standard three electrode electrochemical cell. Where the working electrode (WE), counter electrode (CE) and reference electrode (RE) are immersed in an electrolyte solution.

To study electrochemical properties, a three electrode system (working, reference and counter) (Figure 1.24) is immersed in an electrolyte solution containing the electroactive species that is to be studied. The potential of the working electrode is controlled against a reference electrode, the current (I) flows between the counter and working electrodes. The working electrode is normally composed of a strongly conducting material, such as platinum, gold or glassy carbon, which is not reactive under the potential window and conditions used. If reduction occurs at the working electrode, then oxidation occurs at the counter electrode or *vice versa* to complete the circuit. Platinum is often used as the counter electrode to provide an electrochemically inert material; the reference electrode maintains a constant potential throughout the experiment. For the experiments in CH_2Cl_2, an Ag/AgCl reference electrode was submersed in 100 mM $[^nNBu_4]Cl$ in CH_2Cl_2 (i.e. the same concentration of supporting electrolyte).

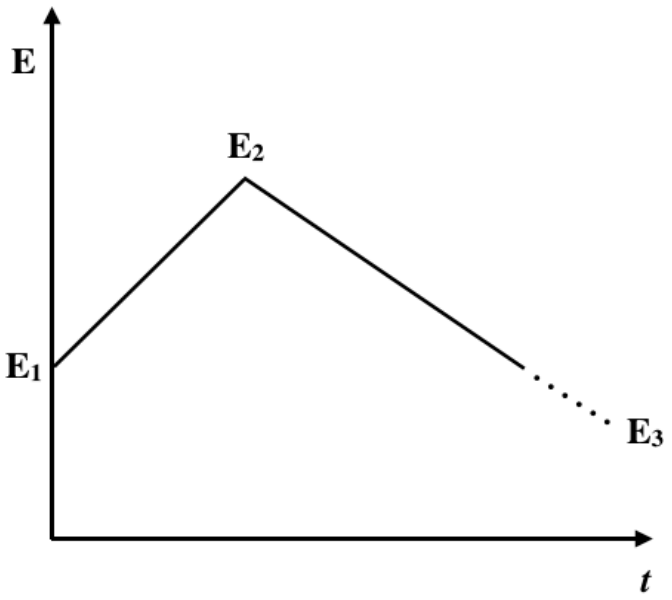

Figure 1.25: The potential-time profile employed in cyclic voltammetry.

When taking a cyclic voltammogram, the potential of the working electrode is varied with time, from the initial potential (E_1) by a fixed value known as the scan rate. Once it reaches the chosen potential, (E_2) the potential is then scanned back to E_1 or *via* a different chosen potential E_3 before returning to E_1 to complete the cycle. The current (I) is measured as a function of potential and the response is plotted as current *vs*. potential, which is known as the cyclic voltammogram. Typically, the open circuit potential (where the net current is zero) is chosen to be E_1 and the potential can be scanned either positively first or negatively first to study oxidation or reduction, respectively.

Cyclic voltammetry allows information on the precursor to be gained to help choose the parameters to use for electrodeposition including deposition potential. In electrodeposition, metal ions in solution are reduced to neutral species, whereby they form a new solid phase on the electrode surface. Potentiostatic electrodeposition involves applying and holding a constant potential, where the potential of the working electrode is stepped from a potential where no reaction is occurring to the desired deposition potential. The resulting current is monitored as a function of time, which can be plotted as a chronoamperogram.[158] The deposition potentials and times can be tailored in order to obtain films of a desired thickness (typically a 1 to 2 μm thickness is sufficient for EDX and XRD analysis).

1.12 Project Aims

The objectives of this project are to investigate new coordination complexes of W(VI) oxo- and thio-halides and develop a systematic series of complexes with a range of hard donor ligands (Chapter 2) and softer phosphine and arsine donor ligands (Chapter 3) to form six-coordinate $[WECl_4(L)]$, $[(WSCl_4)_2(\mu\text{-L-L})]$ or the unusual seven-coordinate $[WSCl_4(L\text{-L})]$ systems. This will be followed by the chemistry of W(VI) oxo- and thio-halides with the softer moderate donors,

thioethers, (Chapter 4) and work to investigate their suitability as low pressure chemical vapour deposition precursors for the deposition of WS_2 thin films (Chapter 5) and their subsequent electrical measurements.

Further aims include synthesising a family of Mo(V) oxohalide complexes with thio-, seleno- and telluro-ethers, in the form $[MoOCl_3(L\text{-}L)]$ and $[(MoOCl_2L)_2(\mu\text{-}Cl)_2]$. In addition a range of known $[MoOCl_3(L\text{-}L)]$ complexes will subsequently be synthesised. These complexes will be used as comparators, for the products from reactions with $MoOCl_4$ and a variety of ligands to attempt to form Mo(VI) oxohalide complexes (Chapter 6).

In Chapter 7, I will look at the initial development of a series of tailored single source precursors for the electrodeposition of MoS_2 and WS_2 thin films including electrochemical studies. In addition metal-selenium containing salts will be synthesised for initial investigations of MSe_2 electrodeposition from non-aqueous media and subsequent material characterised (Chapter 7).

The compounds synthesised in this project will be fully characterised where appropriate by IR, ^{1}H, ^{31}P, $^{77}Se\{^{1}H\}$, ^{95}Mo NMR spectroscopy, elemental analysis, UV-vis spectroscopy, magnetic moment and X-ray crystal structures. Deposited thin films of ME_2 will be characterised by Raman spectroscopy, X-ray diffraction (grazing incidence or in-plane), XPS, SEM and EDX/WDX.

1.13 References

(1) Pearson, R. G. *J. Am. Chem. Soc.,* **1963,** *85*, 3533-39
(2) Lewis, G. N. *Valence and the Structure of Atoms and Molecules*; Chemical Catalog Company: New York, 1923.
(3) Pearson, R. G. *J. Chem. Educ.,* **1968,** *45*,
(4) Greenacre, V. K.; Hector, A. L.; Levason, W.; Reid, G.; Smith, D. E.; Sutcliffe, L. *Polyhedron,* **2019,** *162*, 14-19
(5) Miessler, G. L.; Fischer, P. J.; Tarr, D. A. *Inorganic Chemistry*; Pearson: London, 2014.
(6) Atkins, P.; Overton, T. *Shriver and Atkins' Inorganic Chemistry*; OUP Oxford, 2003.
(7) Levason, W.; Monzittu, F. M.; Reid, G. *Coord. Chem. Rev.,* **2019,** *391*, 90-130
(8) Burt, J.; Levason, W.; Reid, G. *Coord. Chem. Rev.,* **2014,** *260*, 65-115
(9) Benjamin, S. L.; Levason, W.; Reid, G. *Chem. Soc. Rev.,* **2013,** *42*, 1460-99
(10) Levason, W.; Orchard, S. D.; Reid, G. *Coord. Chem. Rev.,* **2002,** *225*, 159-99
(11) Levason, W.; Reid, G. *Coord. Chem. Rev.,* **2006,** *250*, 2565-94
(12) Bannister, R. D.; Levason, W.; Light, M. E.; Reid, G.; Zhang, W. *Polyhedron,* **2019,** *167*, 1-10
(13) Davis, M. F.; Levason, W.; Light, M. E.; Ratnani, R.; Reid, G.; Saraswat, K.; Webster, M. *Eur. J. Inorg. Chem.,* **2007,** *13*, 1903-10
(14) McCleverty, J. A. In *Molybdenum: Inorganic & Coordination Chemistry*, Eds.; John Wiley and Sons, 2006.
(15) McCleverty, J. A. In *Tungsten: Inorganic & Coordination Chemistry*, Eds.; John Wiley and Sons, 2006.
(16) Dori, Z. *Comprehensive Coordination Chemistry I,* **1987,** *3*, 973-1022
(17) Greenwood, N. N.; Earnshaw, A. In *23. Chromium, Molybdenum and Tungsten*, Eds.; Butterworth-Heinemann: Oxford, 1997.
(18) Tunney, J. M.; McMaster, J.; Garner, C. D. *Comprehensive Coordination Chemistry II,* **2004,** *8*, 359-477
(19) Boyd, E. S.; Costas, A. M. G.; Hamilton, T. L.; Mus, F.; Peters, J. W.; Metcalf, W. W. *J. Bacteriol.,* **2015,** *197*, 1690-99
(20) Laurie, S. H. *Eur. J. Inorg. Chem.,* **2000**, 2443-50
(21) Holm, R. H. *Chem. Rev.,* **1987,** *87*, 1401-49
(22) Okamura, T.; Ueyama, N. *Comprehensive Coordination Chemistry II,* **2004,** *4*, 529-73
(23) Young, C. G. *Comprehensive Coordination Chemistry II,* **2004,** *4*, 415-527
(24) Tamadon, F.; Seppelt, K. *Angew. Chem. Int. Ed.,* **2013,** *52*, 767-69
(25) Greenwood, N. N.; Earnshaw, A. In *22. Vanadium, Niobium and Tantalum* Eds.; Butterworth-Heinemann: Oxford, 1997; Vol. 108.
(26) Levason, W.; McAuliffe, C. A.; Sayle, B. J. *J. Chem. Soc., Dalton Trans.,* **1976**, 1177-81
(27) Bortoluzzi, M.; Marchetti, F.; Pampaloni, G.; Zacchini, S. *Eur. J. Inorg. Chem.,* **2016**, 3169-77
(28) Marchetti, F.; Pampaloni, G.; Zacchini, S. *Eur. J. Inorg. Chem.,* **2008**, 453-62
(29) Baghlaf, A. O.; Thompson, A. *J. Less Common Met.,* **1977,** *53*, 291-93
(30) Britnell, D.; Fowles, G. W. A.; Rice, D. A. *J. Chem. Soc., Dalton Trans.,* **1974**, 2191-94
(31) Page, E. M.; Rice, D. A.; Hagen, K.; Hedberg, L.; Hedberg, K. *Inorg. Chem.,* **1982,** *21*, 3280-83
(32) Chang, Y. P.; Hector, A. L.; Levason, W.; Reid, G.; Whittam, J. *Dalton Trans.,* **2018,** *47*, 2406-14
(33) Levason, W.; McAuliffe, C. A.; McCullough, F. P. *Inorg. Chim. Acta,* **1977,** *24*, L13-L14
(34) Benjamin, S. L.; Hyslop, A.; Levason, W.; Reid, G. *J. Fluorine. Chem.,* **2012,** *137*, 77-84
(35) Levason, W.; Reid, G.; Trayer, J.; Zhang, W. *Dalton Trans.,* **2014,** *43*, 3649-59
(36) Levason, W.; Reid, G.; Zhang, W. *J. Fluorine. Chem.,* **2015,** *172*, 62-67
(37) Bessac, F.; Frenking, G. *Inorg. Chem.,* **2006,** *45*, 6956-64
(38) Kendall, A. J.; Tyler, D. R. *Dalton Trans.,* **2015,** *44*, 12473-83
(39) McAuliffe, C. A. *Comprehensive Coordination Chemistry I,* **1987,** *2*, 989-1066
(40) Carravetta, M.; Concistre, M.; Levason, W.; Reid, G.; Zhang, W. *Chem. Commun.,* **2015,** *51*, 9555-58
(41) Carravetta, M.; Concistre, M.; Levason, W.; Reid, G.; Zhang, W. *Inorg. Chem.,* **2016,** *55*, 12890-96
(42) Levason, W.; Monzittu, F. M.; Reid, G.; Zhang, W. *Chem. Commun.,* **2018,** *54*, 11681-84

(43) Davis, M. F.; Levason, W.; Reid, G.; Webster, M. *Polyhedron,* **2006,** *25*, 930-36
(44) Arnaudet, L.; Bougon, R.; Ban, B.; Charpin, P.; Isabey, J.; Lance, M.; Nierlich, M.; Vigner, J. *Can. J. Chem.,* **1990,** *68*, 507-12
(45) Arnaudet, L.; Bougon, R.; Buu, B.; Lance, M.; Nierlich, M.; Thuéry, P.; Vigner, J. *J. Fluorine. Chem.,* **1995,** *71*, 123-29
(46) Crans, D. C.; Smee, J. J. *Comprehensive Coordination Chemistry II,* **2004,** *4*, 175-239
(47) Rice, D. A. *Coord. Chem. Rev.,* **1982,** *45*, 87-103
(48) Tolman, C. A. *Chem. Rev.,* **1977,** *77*, 313-48
(49) Dias, P. B.; de Piedade, M. E. M.; Simões, J. A. M. *Coord. Chem. Rev.,* **1994,** *135-136*, 737-807
(50) Tolman, C. A.; Seidel, W. C.; Gosser, L. W. *J. Am. Chem. Soc.,* **1974,** *96*, 53-60
(51) Bilbrey, J. A.; Kazez, A. H.; Locklin, J.; Allen, W. D. *J. Comput. Chem.,* **2013,** *34*, 1189-97
(52) Guan, Y.; Ingman, V. M.; Rooks, B. J.; Wheeler, S. E. *J. Chem. Theory Comput.,* **2018,** *14*, 5249-61
(53) Niemeyer, Z. L.; Milo, A.; Hickey, D. P.; Sigman, M. S. *Nat. Chem.,* **2016,** *8*, 610-7
(54) Smith, J. M.; Coville, N. J. *Organomet.,* **2001,** *20*, 1210-15
(55) Coll, D. S.; Vidal, A. B.; Rodríguez, J. A.; Ocando-Mavárez, E.; Añez, R.; Sierraalta, A. *Inorg. Chim. Acta,* **2015,** *436*, 163-68
(56) van Leeuwen, P. W.; Kamer, P. C.; Reek, J. N.; Dierkes, P. *Chem. Rev.,* **2000,** *100*, 2741-70
(57) Dierkes, P.; van Leeuwen, P. W. N. M. *J. Chem. Soc. Dalton Trans.,* **1999**, 1519-30
(58) Mann, B. E.; Masters, C.; Shaw, B. L. *J. Chem. Soc. A,* **1971**, 1104-06
(59) Garrou, P. E. *Chem. Rev.,* **1981,** *81*, 229-66
(60) Hietkamp, S.; Stufkens, D. J.; Vrieze, K. *J. Organomet. Chem.,* **1976,** *122*, 419-28
(61) Kapoor, P. N.; Kapoor, R. N.; Pathak, D. D.; Gaur, G. *Inorg. Chim. Acta,* **1986,** *112*, 153-57
(62) Emsley, J. W.; Levason, W.; Reid, G.; Zhang, W.; De Luca, G. *J. Fluorine. Chem.,* **2017,** *197*, 74-79
(63) Quinn, L. D. *A Guide to Organophosphorus Chemistry*; John Wiley & Sons: New York, 2000.
(64) Feltham, R. D.; Kasenally, A.; Nyholm, R. S. *J. Organomet. Chem.,* **1967,** *7*, 285-88
(65) Kyba, E. P.; Liu, S. T.; Harris, R. L. *Organomet.,* **1983,** *2*, 1877-79
(66) Luo, Y. R. *Comprehensive Handbook of Chemical Bond Energies*; Taylor & Francis Group: Boca Raton, 2007.
(67) Schmidt, M. W.; Yabushita, S.; Gordon, M. S. *J. Phys. Chem.,* **1984,** *88*, 382-89
(68) Gilheany, D. G. *Chem. Rev.,* **1994,** *94*, 1339-74
(69) Kutzelnigg, W. *Angew. Chem. Int. Ed.,* **1984,** *23*, 272-95
(70) Davis, M. F.; Levason, W.; Ratnani, R.; Reid, G.; Rose, T.; Webster, M. *Eur. J. Inorg. Chem.,* **2007**, 306-13
(71) Davis, M. F.; Levason, W.; Paterson, J.; Reid, G.; Webster, M. *Eur. J. Inorg. Chem.,* **2008**, 802-11
(72) Spichal, Z.; Necas, M.; Pinkas, J. *Inorg. Chem.,* **2005,** *44*, 2074-80
(73) Petersson, M. J.; Loughlin, W. A.; Jenkins, I. D. *Chem. Commun.,* **2008**, 4493-94
(74) Schevenels, F. T.; Shen, M.; Snyder, S. A. *J. Am. Chem. Soc.,* **2017,** *139*, 6329-37
(75) Levason, W.; Patel, R.; Reid, G. *J. Organomet. Chem.,* **2003,** *688*, 280-82
(76) Chang, Y. P.; Levason, W.; Reid, G. *Dalton Trans.,* **2016,** *45*, 18393-416
(77) Levason, W.; Reid, G. *Comprehensive Coordination Chemistry II,* **2003,** *1*, 391-98
(78) Boorman, P. M.; Gao, X.; Freeman, G. K. W.; Fait, J. F. *J. Chem. Soc., Dalton Trans.,* **1991**, 115-20
(79) Kakeya, M.; Fujihara, T.; Nagasawa, A. *Acta Cryst. E,* **2006,** *62*, m553-m54
(80) Kemmitt, T.; Levason, W. *Organomet.,* **1989,** *8*, 1303-08
(81) Hart, R.; Levason, W.; Patel, B.; Reid, G. *J. Chem. Soc., Dalton Trans.,* **2002**, 3153-59
(82) Jura, M.; Levason, W.; Ratnani, R.; Reid, G.; Webster, M. *Dalton Trans.,* **2010,** *39*, 883-91
(83) Britnell, D.; Drew, M. G. B.; Fowles, G. W. A.; Rice, D. A. *Inorg. Nucl. Chem. Lett.,* **1973,** *9*, 501-04
(84) Benjamin, S. L.; Chang, Y. P.; Gurnani, C.; Hector, A. L.; Huggon, M.; Levason, W.; Reid, G. *Dalton Trans.,* **2014,** *43*, 16640-48

(85) Chang, Y. P.; Levason, W.; Light, M. E.; Reid, G. *Dalton Trans.,* **2016,** *45*, 16262-74
(86) Brown, E. D.; Iqbal, S. M.; Owen, L. N. *J. Chem. Soc. C,* **1966**, 415-19
(87) Hartley, F. R.; Murray, S. G.; Levason, W.; Soutter, H. E.; McAuliffe, C. A. *Inorg. Chim. Acta,* **1979,** *35*, 265-77
(88) Baleja, J. D. *Synth. Commun.,* **2006,** *14*, 215-18
(89) Oae, S.; Shinhama, K. i.; Kim, Y. H. *Bull. Chem. Soc. Jpn.,* **1980,** *53*, 2023-26
(90) Maiolo, F.; Testaferri, L.; Tiecco, M.; Tingoli, M. *J. Org. Chem.,* **1981,** *46*, 3070-73
(91) Testaferri, L.; Tingoli, M.; Tiecco, M. *J. Org. Chem.,* **1980,** *45*, 4376-80
(92) Gulliver, D. J.; Hope, E. G.; Levason, W.; Murray, S. G.; Potter, D. M.; Marshall, G. L. *J. Chem. Soc., Perkin Trans. II,* **1984,** *2*, 429-34
(93) Kuhn, N.; Faupel, P.; Zauder, E. *J. Organomet. Chem.,* **1986,** *302*, C4-C6
(94) Hope, E. G.; Kemmitt, T.; Levason, W. *Organomet.,* **1988,** *7*, 78-83
(95) Selvakumar, D.; Singh, R.; Nasim, M.; Mathjr, G. N. *Phosphorus, Sulfur, Silicon and related Elements,* **2001,** *172*, 247-59
(96) Hope, E. G.; Kemmitt, T.; Levason, W. *Organomet.,* **1987,** *6*, 206-07
(97) Irgolic, K. J. *The Organic Chemistry of Tellurium*; Gordon and Breach: New York, 1974.
(98) Levason, W.; Patel, B.; Reid, G.; Ward, A. J. *J. Organomet. Chem.,* **2001,** *619*, 218-25
(99) Housecroft, C. E.; Sharpe, A. G. *Inorganic Chemistry*; Pearson: London, 2005.
(100) Grahn, H. T. *Introduction to Semiconductor Physics*; World Scientific: Berlin, 1999.
(101) Diffenderfer, R. *Electronic Devices: Systems and Applications*; Cengage Learning: New York, 2005.
(102) Takahashi, K.; Yoshikawa, A.; Sandhu, A. *Wide Bandgap Semiconductors: Fundermentals Properties and Modern Photonic and Elctronic Devices*; Springer Science & Business Media: Berlin, 2007.
(103) Neto, A. H. C.; Novoselov, K. *Mater. Express,* **2011,** *1*, 10-17
(104) Chhowalla, M.; Shin, H. S.; Eda, G.; Li, L. J.; Loh, K. P.; Zhang, H. *Nat. Chem.,* **2013,** *5*, 263-75
(105) Heine, T. *Acc. Chem. Res.,* **2015,** *48*, 65-72
(106) Wang, Q. H.; Kalantar-Zadeh, K.; Kis, A.; Coleman, J. N.; Strano, M. S. *Nat. Nanotechnol.,* **2012,** *7*, 699-712
(107) Chhowalla, M.; Liu, Z.; Zhang, H. *Chem. Soc. Rev.,* **2015,** *44*, 2584-86
(108) Jaramillo, T. F.; Jorgensen, K. P.; Bonde, J.; Nielsen, J. H.; Horch, S.; Chorkendorff, I. *Science,* **2007,** *317*, 100-02
(109) Eda, G.; Fujita, T.; Yamaguchi, H.; Voiry, D.; Chen, M.; Chhowalla, M. *ACS Nano,* **2012,** *6*, 7311-17
(110) Eda, G.; Yamaguchi, H.; Voiry, D.; Fujita, T.; Chen, M.; Chhowalla, M. *Nano Lett.,* **2011,** *11*, 5111-16
(111) Wilson, J. A.; Yoffe, A. D. *Adv. Phys.,* **1969,** *18*, 193-335
(112) Splendiani, A.; Sun, L.; Zhang, Y.; Li, T.; Kim, J.; Chim, C. Y.; Galli, G.; Wang, F. *Nano Lett.,* **2010,** *10*, 1271-75
(113) Pu, J.; Yomogida, Y.; Liu, K. K.; Li, L. J.; Iwasa, Y.; Takenobu, T. *Nano Lett.,* **2012,** *12*, 4013-17
(114) Benjamin, S. L.; de Groot, C. H.; Gurnani, C.; Hawken, S. L.; Hector, A. L.; Huang, R.; Jura, M.; Levason, W.; Reid, E.; Reid, G.; Richards, S. P.; Stenning, G. B. G. *J. Mater. Chem. C,* **2018,** *6*, 7734-39
(115) de Groot, C. H.; Gurnani, C.; Hector, A. L.; Huang, R.; Jura, M.; Levason, W.; Reid, G. *Chem. Mater.,* **2012,** *24*, 4442-49
(116) Reid, S. D.; Hector, A. L.; Levason, W.; Reid, G.; Waller, B. J.; Webster, M. *Dalton Trans.,* **2007**, 4769-77
(117) Hector, A. L.; Jura, M.; Levason, W.; Reid, S. D.; Reid, G. *New J. Chem.,* **2009,** *33*, 641-45
(118) Zhao, S.; Hotta, T.; Koretsune, T.; Watanabe, K.; Taniguchi, T.; Sugawara, K.; Takahashi, T.; Shinohara, H.; Kitaura, R. *2D Mater.,* **2016,** *3*, 025027
(119) Yanase, T.; Watanabe, S.; Weng, M.; Wakeshima, M.; Hinatsu, Y.; Nagahama, T.; Shimada, T. *Cryst. Growth Des.,* **2016,** *16*, 4467-72
(120) Ge, W.; Kawahara, K.; Tsuji, M.; Ago, H. *Nanoscale,* **2013,** *5*, 5773-78
(121) Carmalt, C. J.; Peters, E. S.; Parkin, I. P.; Manning, T. D.; Hector, A. L. *Eur. J. Inorg. Chem.,* **2004**, 4470-76

(122) Boscher, N. D.; Blackman, C. S.; Carmalt, C. J.; Parkin, I. P.; Prieto, A. G. *Appl. Surf. Sci.,* **2007,** *253*, 6041-46
(123) Jones, A. C.; L., H. M. *Chemical Vapour Deposition*; Royal Society of Chemistry: Cambridge, 2009.
(124) Choy, K. *Prog. Mater. Sci.,* **2003,** *48*, 57-170
(125) Brenner, A. In *History and Literature of the Electrodeposition of Alloys*, Eds.; Academic Press: Washington, 1963.
(126) Bard, A. J.; Faulkner, L. R. *Electrochemical Methods, Fundamentals and Applications*; 2 ed.; Wiley Global Education: New York, 2001.
(127) Sudha, V.; Sangaranarayanan, M. V. *J. Phys. Chem. B,* **2002,** *106*, 2699-707
(128) Simka, W.; Puszczyk, D.; Nawrat, G. *Electrochim. Acta,* **2009,** *54*, 5307-19
(129) Bartlett, P. N.; Cook, D.; de Groot, C. H.; Hector, A. L.; Huang, R.; Jolleys, A.; Kissling, G. P.; Levason, W.; Pearce, S. J.; Reid, G. *RSC Adv.,* **2013,** *3*, 15645-54
(130) Meng, L.; Cicvarić, K.; Hector, A. L.; de Groot, C. H.; Bartlett, P. N. *J. Electroanal. Chem.,* **2019,** *839*, 134-40
(131) Endres, F. *ChemPhysChem,* **2002,** *3*, 145-54
(132) Wilkes, J. S.; Zaworotko, M. J. *J. Chem. Soc., Chem. Commun.,* **1992**, 965-67
(133) Li, G.; Tong, Y.; Liu, G. *J. Electroanal. Chem.,* **2004,** *562*, 223-29
(134) Li, G.; Tong, Y.; Wang, Y.; Liu, G. *Electrochim. Acta,* **2003,** *48*, 4061-67
(135) Karatutlu, A.; Barhoum, A.; Sapelkin, A. In *Liquid-phase synthesis of nanoparticles and nanostructured materials*, Eds.; Elsevier: Amsterdam, 2018.
(136) Andricacos, P. C.; Uzoh, C.; Dukovic, J. O.; Horkans, J.; Deligianni, H. *IBM J. Res. Dev.,* **1998,** *42*, 567-74
(137) Andricacos, P. C.; Romankiw, L. T. *Adv. Electrochem. Sci. Eng.,* **1993**, 227-321
(138) Nakamoto, K. *Infrared and Raman Spectra of Inorganic and Coordination Compounds*; 4th ed.; Wiley-Interscience: New York, 1986.
(139) Mason, J. *Multinuclear NMR*; Plenum Press: New York, 1987.
(140) Narath, A.; Alderman, D. W. *Phys. Rev.,* **1966,** *143*, 328-34
(141) Gheller, S. F.; Hambley, T. W.; Rodgers, J. R.; Brownlee, R. T. C.; O'Connor, M. J.; Snow, M. R.; Wedd, A. G. *Inorg. Chem.,* **1984,** *23*, 2519-28
(142) Wardle, R. W. M.; Mahler, C. H.; Chau, C. N.; Ibers, J. A. *Inorg. Chem.,* **1988,** *27*, 2790-95
(143) Bennett, D. W. *Understanding Single-Crystal X-Ray Crystallography*; John Wiley & Sons: New York, 2010.
(144) Babaian-Kibala, E.; Cotton, F. A.; Kibala, P. A. *Inorg. Chem.,* **1990,** *29*, 4002-05
(145) Kobayashi, S. *The Rigaku J.,* **2010,** *26*, 3-6
(146) Suryanarayana, C.; Norton, M. G. *X-Ray Diffraction: A Practical Approach*; Springer Science: New York, 1998.
(147) Li, H.; Zhang, Q.; Yap, C. C. R.; Tay, B. K.; Edwin, T. H. T.; Olivier, A.; Baillargeat, D. *Adv. Funct. Mater.,* **2012,** *22*, 1385-90
(148) Marchetti, F.; Pampaloni, G.; Zacchini, S. *J. Fluorine. Chem.,* **2010,** *131*, 21-28
(149) Skoog, D. A.; Holler, F. J.; Crouch, S. R. *Principles of Instrumental Analysis*; Thomson Brooks/Cole: Belmont, CA, 2007.
(150) Goldstein, J. I. *Scanning Electron Microscopy and X-ray Microanalysis*; Plenum Press: New York, 2003.
(151) Thompson, A. C.; Vaughan, D. *X-ray data booklet*; Lawrence Berkeley National Laboratory, University of California: Berkely, CA, 2001.
(152) Russ, J. C. *Fundermentals of Energy Dispersive X-Ray Analysis*; Butterworth-Hinemann, 2013.
(153) Moulder, J. F.; Stickle, W. F.; Sobol, P. E.; Bomben, K. D. *Handbook of X-ray Photoelectron Spectroscopy*; Perkin-Elmer Corporation: Minnesota, 1992.
(154) Van der Pauw, L. J. *Phillps Tech. Rev.,* **1958,** *20*, 220-24
(155) Van der Pauw, L. J. *Phillps Res. Rep.,* **1958,** *13*, 1-9
(156) Gaj, J. A. *Comprehensice Semiconductir Science and Technology*; Elsevier Science: Amsterdam, 2011.
(157) Elgrishi, N.; Rountree, K. J.; McCarthy, B. D.; Rountree, E. S.; Eisenhart, T. T.; Dempsey, J. L. *J. Chem. Educ.,* **2017,** *95*, 197-206

(158) Pletcher, D. *A First Course in Electrode Processes*; 2nd ed.; RSC Publishing: Cambridge, 2009.

Complexes of $WOCl_4$ and $WSCl_4$ with Neutral Nitrogen and Oxygen Donor Ligands

2.1 Introduction

Published literature on neutral complexes of tungsten in its highest oxidation state are rare, with a significant proportion of the reported compounds not fully characterised. Work on neutral $WOCl_4$ and $WSCl_4$ complexes is scarce due to the complexes being unstable and readily hydrolysed by trace moisture, often resulting in the reduction of the metal centre. This chapter details the synthesis and characterisation of a series of $WOCl_4$ complexes with hard donor ligands, including phosphine oxides and N-heterocyclic ligands, as well as comparisons with their $WSCl_4$ analogues and (unsuccessful) attempts to form neutral WCl_6 complexes.

2.2 Tungsten(VI) and Molybdenum(VI) Coordination Chemistry

Tungsten, in terms of coordination chemistry, is relatively underdeveloped compared to its 3*d* and 4*d* counterparts (Cr or Mo). Being in the third row means there is a wider range of oxidation states that are readily available; in tungsten's case W^{II-} to W^{VI}, allowing complexes to form with a wide variety of ligands and coordination numbers.[1] Tungsten(VI) is a hard acceptor, therefore more receptive to hard ligands (e.g. nitrogen and oxygen donor ligands), forming relatively stable complexes. Tungsten(VI) is more readily available compared to molybdenum(VI), which can be highly unstable and more easily reduced; however tungsten(VI) compounds are still highly reactive.[2] Owing to their similar chemistries, tungsten and molybdenum are often compared in literature; however, due to the inherent instability of molybdenum(VI), this can be challenging and comparisons limited. While the compound $MoOCl_4$ exists,[3] it has no comparator coordination chemistry literature available and $MoSCl_4$ has not been reported.

The coordination chemistry of molybdenum has attracted attention over the years as it is an important constituent in biological species, including metalloenzymes.[4] Both tungsten and molybdenum(VI) coordination compounds also merit considerable interest due to their role as oxido-transfer reagents, metathesis catalysis precursors and ring-opening catalysts.[4-7]

Known oxohalides of molybdenum(VI) and tungsten(VI)			
$MoOF_4$	MoO_2F_2	WOF_4	WO_2F_2
$MoOCl_4$	MoO_2Cl_2	$WOCl_4$	WO_2Cl_2
	MoO_2Br_2	$WOBr_4$	WO_2Br_2
			WO_2I_2

Table 2.1: Table of known oxohalides of molybdenum(VI) and tungsten(VI).[1,8]

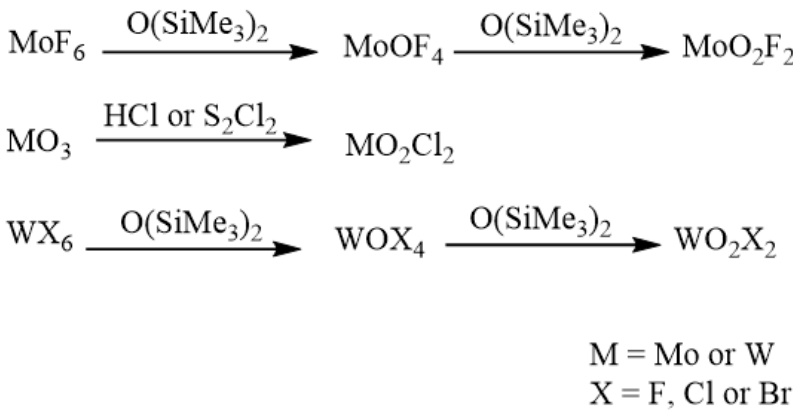

Figure 2.1: Some examples of syntheses for the formation of MO_2X_2 and MOX_4.

The dioxo-dihalide compounds MoO_2X_2 and WO_2X_2 (X = F, Cl or Br) provide sufficient electron density to the metal centre to stabilise the +VI oxidation state, allowing coordination complexes to form. These compounds can be synthesised *via* both solution-based routes and using solid state methods.

Most compounds can be formed from their respective metal hexahalide, MX_6, by reacting with two equivalents of $O(SiMe_3)_2$. MoO_2Cl_2 and MoO_2Br_2 cannot be formed this way as $MoCl_6$ is unstable at room temperature[9] and $MoBr_6$ is completely unknown. These reactions pass through an intermediate compound of MOX_4.

$MoOF_4$ is a stable compound, but rather unreactive due to its polymeric structure. A useful intermediate is $[MoOF_4(MeCN)]$, where a soluble monomer is stabilised by an MeCN ligand.[10] An alternate method to produce MO_2X_2 is to use a chlorinating agent such as HCl or Cl_2 gas to chlorinate a metal oxide.[11]

Many of the parent metal oxohalides are polymeric with M=O-M bridges, which results in limited reactivity and solubility, but increases stability. Therefore, to get sufficient reactivity with ligands, compounds generally have to be made *in-situ* to prevent polymerisation. Alternatively, the reactions can be completed in coordinating solvents to block the polymerisation (i.e. THF, py or MeCN), followed by ligand metathesis.[12]

2.2.1 Synthesis of $[MO_2X_2(L)_2]$ or $[MO_2X_2(L\text{-}L)]$

High oxidation state early transition metals are hard Lewis acids, meaning that they favour bonding with hard Lewis bases; a substance with a pair of non-bonding electrons and relatively small covalent or ionic radii, for example, oxygen and nitrogen donor ligands (see Section 1.1).[13,14] These strong interactions between a Lewis acid and a Lewis base can often improve the stability of high oxidation state metal centres.[15] Conversely, bonding between a hard Lewis acid and softer Lewis

base (e.g. sulfur and phosphorus donor ligands) is typically much less favourable, making complexes unstable and particularly sensitive to moisture.[16,17] In the case of $[MO_2X_2(L)_2]$ or $[MO_2X_2(L\text{-}L)]$, on contact with moisture, these complexes readily decompose releasing HX; therefore handling in inert conditions is paramount.

Relatively recent work on $[MO_2X_2(L)_2]$ or $[MO_2X_2(L\text{-}L)]$ coordination complexes has been completed, some examples are shown in Figure 2.2; all complexes reported have a coordination number of six.

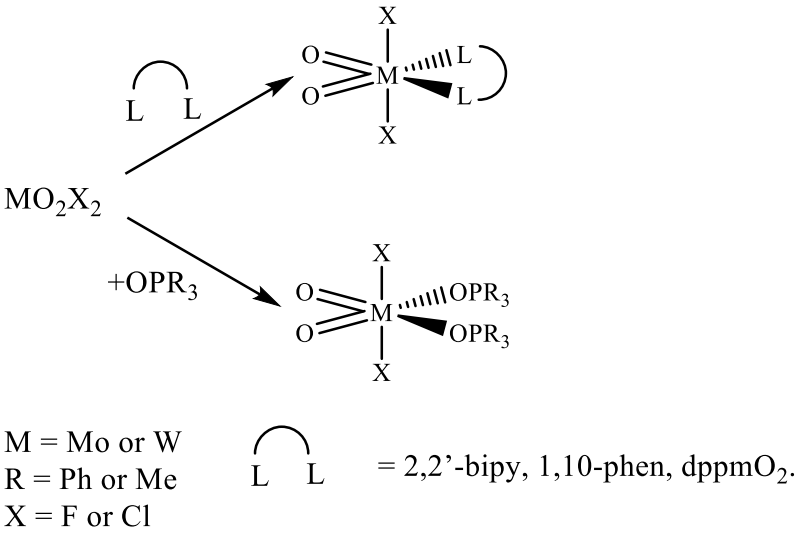

Figure 2.2: Some examples of $[MO_2X_2(L)_2]$ and $[MO_2X_2(L\text{-}L)]$ coordination complexes from the literature.[10,12,18-23]

MO_2X_2 (where M = Mo or W; X = F, Cl or Br) reacts readily with 1:2 equivalents of OPR_3, as demonstrated by a number of structural determinations,[10,12,18,19,21,24-26] differences in M-O_P bond lengths are small and erratic across similar complexes. With N-heterocycles, $[MO_2Cl_2(L\text{-}L)]$ (L-L = 2,2'-bipy or 1,10-phen) there are more obvious differences in M-N bond lengths. In the tungsten(VI) analogues $[WO_2X_2(L\text{-}L)]$, the W-N bond lengths are shorter than in the molybdenum structures, suggesting stronger bonding.[12,20,27,28] In the $[MoO_2X_2(2,2'\text{-bipy})]$ complexes the Mo-N bond lengths increase as the halogen gets heavier. Both molybdenum(VI) and tungsten(VI) are hard Lewis acids, therefore the fluoride analogue would be expected to be a better acceptor than the bromide analogue towards hard donor ligands, resulting in shorter M-N bonds.[20,22,27,29]

The compounds described in this chapter will allow for comparison between them and the $[MO_2X_2(L\text{-}L)]$ complexes. Also, since literature has established that $WOCl_4$ is an intermediate for the synthesis of WO_2Cl_2, steps must be taken to ensure that $[WO_2Cl_2(L\text{-}L)]$ complexes are not formed as side products.

2.2.2 Tungsten Oxytetrachloride and Thiotetrachloride

The compounds $WECl_4$ (E = O or S) are more sensitive and less readily available than their MO_2Cl_2 (M = Mo or W) counterparts, a likely reason as to why there is less coordination chemistry

reported in literature. $MoSCl_4$ as a neutral monomer has yet to be reported; $MoOCl_4$ can be isolated, but is highly reactive and often reduces to molybdenum(V), see Chapter 6. As described above, $WOCl_4$ can be an intermediate in the synthesis of WO_2Cl_2 and strictly anhydrous conditions and controlled stoichiometry are required for isolating $[WOCl_4(L)]$ complexes.

Tungsten(VI) oxytetrachloride forms readily through the hydrolysis of WCl_6 when exposed to trace moisture. Further hydrolysis can form WO_2Cl_2. $WOCl_4$ can also be formed in a controlled manner by refluxing WO_3 or tungstic acid in thionyl chloride, releasing SO_2 gas.[30,31] A more convenient method is to react WCl_6 with non-metal oxides, for example, using Cl/O exchange with siloxanes, $O(SiMe_3)_2$.[32] In its solid form, $WOCl_4$ exists in the tetragonal space group I4, oxygen/chlorine corner shared octahedra are distorted around each tungsten atom and are linked by bridged W=O-W chains. The $WOCl_4$ fragment has a molecular symmetry of C_{4v}.[33,34] Neutral ligand complexes of $WOCl_4$ are mostly prepared by the direct *in-situ* reaction of $WOCl_4$ with the ligands, but there are some examples of their formation *via* oxygen abstraction from ligands when reacting with WCl_6.[1,6,35,36] For example, WCl_6 has been shown to ring-open THF to abstract the oxygen and form $[WOCl_4(THF)]$ and $MeO(CH_2)_2OH$ reacts with WCl_6 to form $[(WOCl_4)_2(\mu\text{-}\kappa^2\text{-}1,4\text{-dioxane})]$.[37] Extensive work by Marchetti and co-workers has shown that the formation of $[WOCl_4(L)]$ from WCl_6 is highly dependent on the ligand in question and the reaction conditions, with examples of WCl_5, $WOCl_3$ complexes and mixed ligand fragments (Figure 2.3).[38-41]

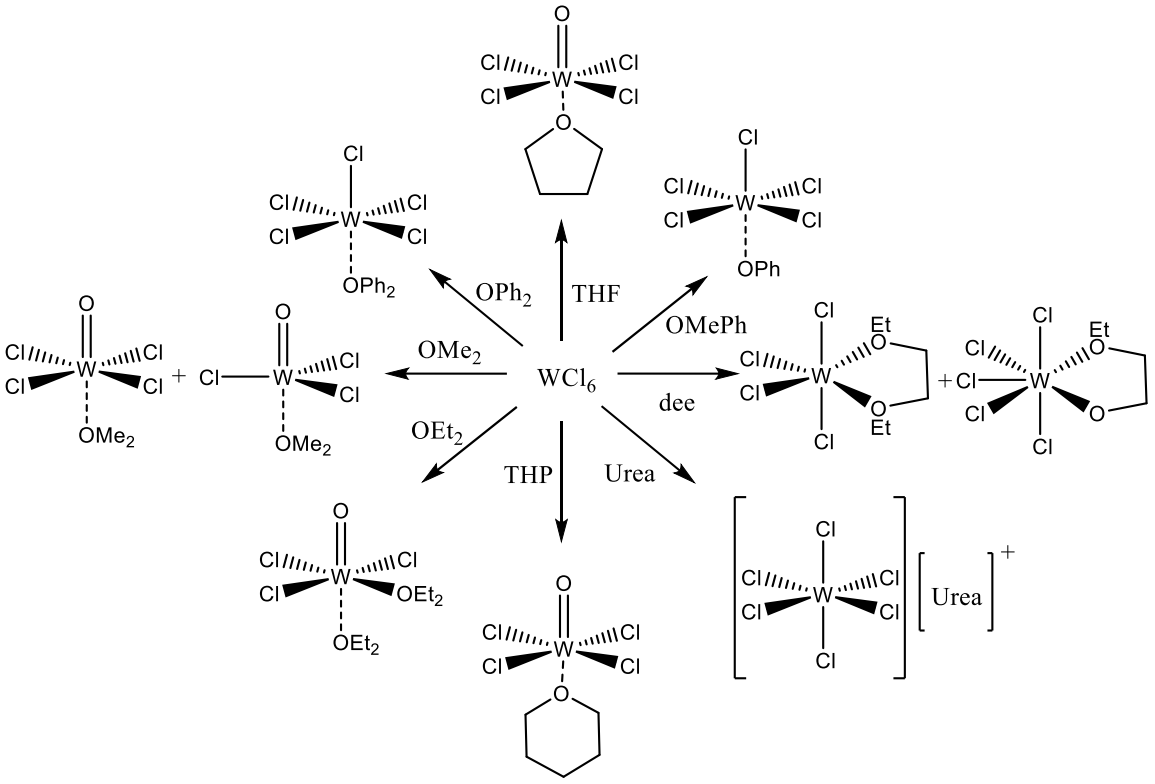

Figure 2.3: Some examples of reactions with WCl_6 and oxygen donor ligands and their products.[38,40-42]

There are a few reported complexes of $WOCl_4$ with neutral ligands made by direct reaction of $WOCl_4$ with the ligand; Funk and co-workers reported complexes with acetonitrile, diethyl ether,

pyridine and 1,4-dioxane, but with little structural or robust spectroscopic information.[43,44] This was added to by Frost and co-workers with the report of a 2,2'-bipy adduct, [$WOCl_3$(2,2'-bipy)], but they suggest the tungsten centre has been reduced, although the reason for this is unclear.[45] There are some examples of $WOCl_4$ with phosphines and phosphine oxides, [$WOCl_4$(L)] (L = PPh_3, PPh_2Et, $OPPh_3$) and [$WOCl_4(L_2)$] (L = PPh_3, PEt_3, P $^nPr_3$ or $OPPh_3$); the seven coordinate monodentate phosphine and phosphine oxide complexes seem questionable, as the ligands would need to be strong enough σ-donors to force this reaction, especially since the phosphines are soft donor ligands.[46]

There are a small number of reports of coordination complexes with $WOBr_4$; Frost and Fowles have reported complexes of $WOBr_4$ with THF, THP, 1,4-dioxane and 2,2'-bipy.[45,47] The limited number of complexes of $WOBr_4$ is likely to do with WBr_6 not being as readily available as WCl_6 commercially and being a poorer acceptor and hence more easily reduced.[48] Work on the fluoride analogues has mainly been undertaken by the Reid Group. [$MoOF_4$(L)] (L = MeCN, THF, OPR_3, 2,2'-bipy, dmf and dmso) compounds are scarce and limited to hard donor ligands, with only a few simple examples.[21] Complexes of WOF_4 have been studied in more detail than the molybdenum analogues; six coordinate complexes [WOF_4(L)] (L = MeCN, THF, OPR_3, py, PR_3 and dmso) have been described.[10,49-51] For further examples with softer donor ligands see Section 3.2.1.

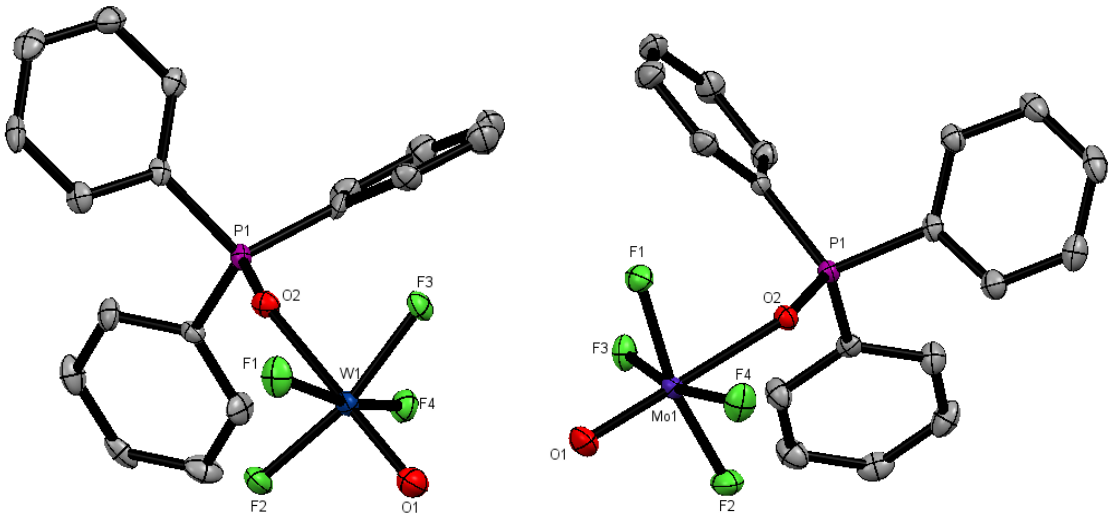

Figure 2.4: Crystal structures of [$WOF_4(OPPh_3)$] and [$MoOF_4(OPPh_3)$]. Hydrogen atoms omitted for clarity.[10,21]

[$MoOF_4(OPPh_3)$] is the only structurally characterised neutral $MoOF_4$ complex; it is isostructural with [$WOF_4(OPPh_3)$], see Figure 2.4. Interestingly, a small selection of seven coordinate systems have also been shown to exist, [WOF_4(L-L)] (L = 2,2'-bipy, *o*-$C_6H_4(PMe_2)_2$ and $Me_2P(CH_2)_2PMe_2$).[49,51] The metal oxofluorides are harder Lewis acids than the oxochlorides, therefore the complexes have a lower affinity for bonding with softer or moderate donors, limiting the range of WOF_4 complexes reported.

In its solid form $WSCl_4$ has two polymorphs. The triclinic polymorph with a space group of $P\bar{1}$, where the tungsten can be considered as a five-coordinate (square pyramidal) monomer linked

together to form a six-coordinate (distorted octahedral) dimer.[52] The second polymorph is monoclinic with the space group $P2_1/n$. Unlike $WOCl_4$ and $WOBr_4$, which form W=O-W bridges, $WSCl_4$ forms dimeric units *via* weak W-Cl-W bridges in both polymorphs.[53] In the triclinic form there are two chlorine bridges to form a dimer, $[SCl_3W(\mu\text{-}Cl)_2WCl_3S]$, whereas in the monoclinic structure the dimer core is linked by single chlorine bridges to two other $WSCl_4$ units.

$WSCl_4$ is slightly more challenging to synthesise than $WOCl_4$, and an analogous route using $S(SiMe_3)_2$ is reported, similar to the synthesis of $WOCl_4$.[32,54] It has been suggested there is a solvent-assisted dismutation, see Equation 2.1, resulting in a brown solid forming (WS_3); therefore a sublimation step is required to obtain pure $WSCl_4$.[55]

$$WSCl_4 \rightarrow WS_3 + WCl_6$$

Equation 2.1: Suggested solvent-assisted dismutation of $WSCl_4$.

This regenerated WCl_6 can lead to the formation of $WOCl_4$ upon contact with trace water, contaminating the compound. The traditional route for compounds of this nature is a solid-state method, typically mixing WCl_6 with a sulfur-containing compound, (elemental sulfur, Sb_2S_3 or B_2S_3) in an evacuated sealed tube and heating. This method can prove temperamental and challenging to isolate clean products and specialised equipment is often required.[32,56-59] Most synthetic routes start from WCl_6, although Fedorov and co-workers report reacting $W(CO)_6$ and sulfur monochloride in chlorinated solvents, to form $WSCl_4$.[60]

As previously mentioned, $[WOCl_4(THF)]$ can be formed *via* reaction of WCl_6 and THF, however $[WSCl_4(tht)]$ cannot be formed in the same way. Reaction of WCl_6 and tht gives $[WCl_6(tht)_2]$, which is suggested to behave as an ionic salt $[WCl_5(tht)_2]Cl$.[61] At elevated temperatures the reaction yields a variety of products, including salts and dimers, but no $WSCl_4$ derivatives.[62] Investigations into the formation of the molybdenum(V) species, $[MoSCl_3(tht)_2]$, *via* DFT calculations concluded that tht does not provide the ring opening mechanism that THF does.[63]

The majority of literature on coordination complexes of $WSCl_4$ are direct *in-situ* reactions with a limited selection of hard ligands, $[WSCl_4(L)]$ (L = THF, py, RCN, $OPPh_3$) and $[(WSCl_4)_2(\mu\text{-}1,4\text{-dioxane})]$ have been prepared, but appear to be less stable than comparator complexes of $WOCl_4$.[1,36,64] There are very limited examples of $WSBr_4$, $WSeCl_4$ and $WSeBr_4$ complexes with a small selection of neutral coordinating solvents, (py, THF, MeCN, 1,4-dioxane).[64] Additional complexes of $WSeCl_4$ are reported, $[WSeCl_4(1,4\text{-oxathiane})]$ and a bridged complex $[(WSeCl_4)_2(MeO(CH_2)_2OMe)]$, which the ligand has been shown to abstract an oxygen and reduce the tungsten to form an alkoxide over a longer period of time.[64,65] Complexes of WSF_4 are very scarce, with only $[WSF_4(L)]$ (L = py and MeCN) being reported, but both being structurally characterised.[55,66,67]

2.2.3 Aims

The aim of this chapter was to explore the chemistry of tungsten(VI), develop the first systematic series of tungsten oxytetrachloride and thiotetrachloride coordination complexes of the form, $[WECl_4(L)]$ or $[WECl_4(L\text{-}L)]$ (E = O or S) and to explore their properties. The ligands used include neutral O–donor phosphine oxide ligands ($dppeO_2$, $dppmO_2$, $OPPh_3$ and $OPMe_3$) and N-heterocycles (2,2'-bipy, 1,10-phen and py). Complexes have been characterised by IR spectroscopy, ^1H NMR spectroscopy, $^{31}P\{^1H\}$ spectroscopy, elemental analysis and X-ray crystal structure analyses.

2.3 Results and Discussion

2.3.1 Complexes of $WOCl_4$

The compound $WOCl_4$ has been prepared from WCl_6 following the reported method.[32] The IR data for $WOCl_4$ shows absorptions at 889 cm^{-1} and 875 cm^{-1} which indicates W=O-W bridging units, as a terminal W=O absorption would be much higher, ~970 cm^{-1}.[35] The W=O-W bridges are asymmetric causing the two W=O stretches observed.[33] Two bands are expected for W-Cl bonds (A_1 and E), shown as a broad peak at 381 cm^{-1} (combination of A_1 at 399 cm^{-1} and the E stretch at 379 cm^{-1}), and 327 cm^{-1} is assigned to the E δ(O-W-Cl) mode.[35] Stretches around 845 cm^{-1} (indicative of a W=O stretch from WO_2Cl_2) were not present in the spectrum.

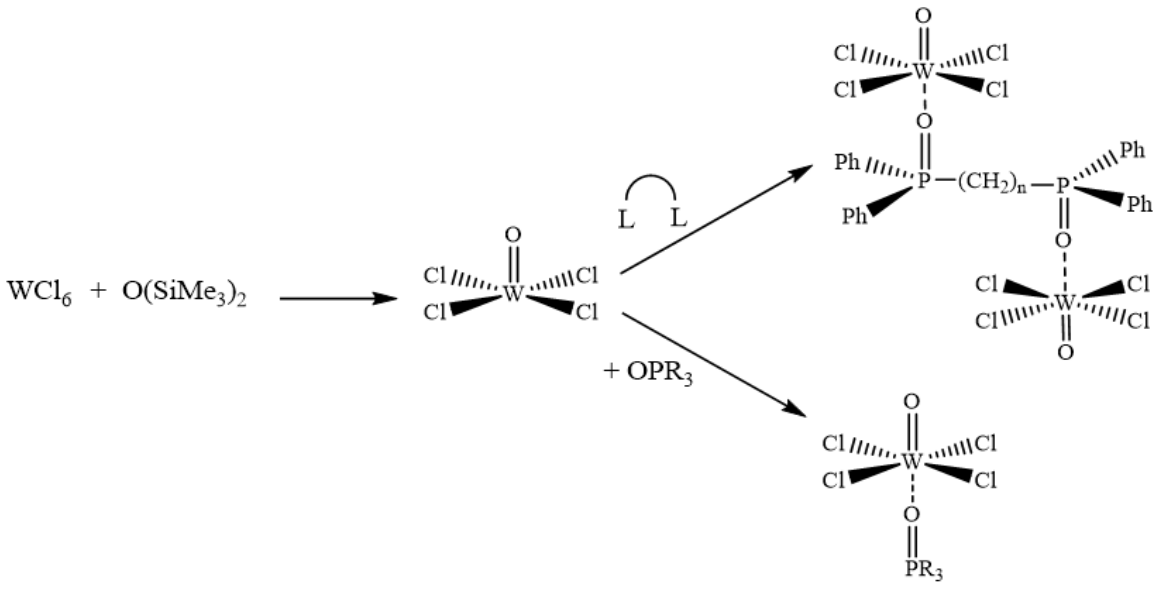

Figure 2.5: A reaction scheme showing the synthesis of $[WOCl_4(OPR_3)]$ and $[(WOCl_4)_2(\mu\text{-}L\text{-}L)]$ (R = Ph or Me; L-L = $dppmO_2$ or $dppeO_2$).

2.3.2 Complexes of $WOCl_4$ with Phosphine Oxide Ligands

The complexes $[WOCl_4(L)]$ or $[(WOCl_4)_2(\mu\text{-}L\text{-}L)]$ (L = $OPPh_3$ or $OPMe_3$; L-L = $dppmO_2$ or $dppeO_2$) were obtained as moisture sensitive yellow or orange powders in moderate to good yields

(30-83%). The compounds were synthesised by direct stoichiometric reactions of pre-formed $WOCl_4$ and the ligands in an appropriate solvent (CH_2Cl_2 or toluene). *In-situ* reactions with WCl_6, $O(SiMe_3)_2$ and the ligand resulted in impure products.

The complex $[WOCl_4(OPPh_3)]$ has been re-prepared and characterised by IR spectroscopy (see Table 2.2); uncoordinated $OPPh_3$ exhibits a P=O stretch at 1195 cm^{-1}, which should shift to a lower frequency once coordinated, as the oxygen from the ligand is donating its electrons to the metal centre. The IR spectrum shows a shift in wavenumber from 1195 cm^{-1} to 1135 cm^{-1}, which conflicts with one of the literature values of 1163 cm^{-1}.[68] Additionally, the W-Cl stretch at 338 cm^{-1} corresponds with both literature values (340 cm^{-1}) and the W=O stretch at 981 cm^{-1} matches the reported value. The point group of this molecule is C_{4v}, therefore there are two W-Cl IR active bands (A_1 and E) expected, however in this instance only one is seen. The W-Cl band observed (338 cm^{-1}) is the E band as the A_1 band would be considerably weaker. The $^{31}P\{^1H\}$ NMR spectrum shows a sharp singlet at +46.2 ppm, which is not free ligand (expected at +24.9 ppm); this also does not correspond to the $[WO_2Cl_2(OPPh_3)_2]$ analogue, which could form upon trace hydrolysis.[12] In conclusion, the spectroscopic data obtained in this work matches the reported literature by Behzadi *et al.*

Assigned Stretch	This Work	Behzadi *et al.*[68]	Agh-Atabay *et al.*[46]
ν(P=O)	1135 cm^{-1}	1130 cm^{-1}	1163 cm^{-1}
ν(W=O)	981 cm^{-1}	984 cm^{-1}	983 cm^{-1}
ν(W-Cl)	338 cm^{-1}	340 cm^{-1}	340 cm^{-1}
$^{31}P\{^1H\}$ NMR	+46.2 ppm	-	+24.2 ppm

Table 2.2: Comparison of literature values for $[WOCl_4(OPPh_3)]$ against this study.

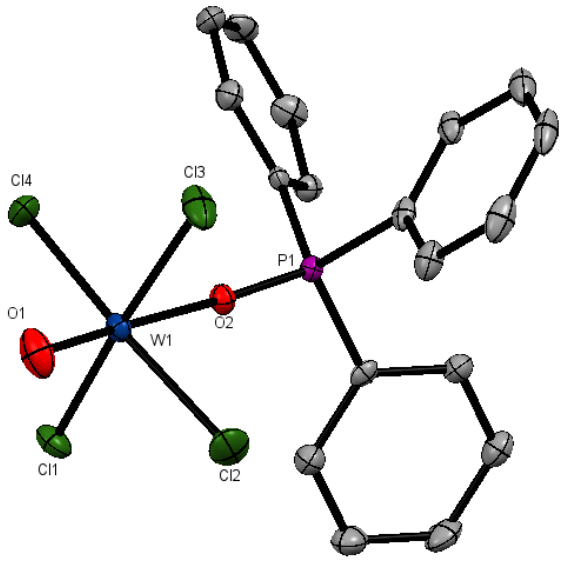

Figure 2.6: The structure of $[WOCl_4(OPPh_3)]$ showing the atom numbering scheme. Ellipsoids shown at 50% probability, H atoms are omitted for clarity. Two independent molecules are present in the asymmetric unit, only one is shown for clarity.

$[WOCl_4(OPPh_3)]$			
Bond Lengths/ Å		Bond Angles/ °	
W1-Cl1	2.3460(5)	Cl1-W1-Cl2	87.77(2)
W1-Cl2	2.3015(6)	Cl1-W1-Cl3	169.82(2)
W1-Cl3	2.2936(6)	Cl2-W1-Cl4	167.79(2)
W1-Cl4	2.3151(6)	Cl2-W1-Cl3	92.65(2)
W1-O1	1.6839(16)	Cl1-W1-Cl4	86.60(2)
W1-O2	2.1047(14)	O1-W1-O2	178.33(8)

Table 2.3: Selected bond lengths and angles for $[WOCl_4(OPPh_3)]$.

Red crystals grown from chloroform solution by slow evaporation (Figure 2.6), show the structure of $[WOCl_4(OPPh_3)]$, which is remarkably similar to that of $[WOF_4(OPPh_3)]$,[10] with the phosphine oxide ligand *trans* to the W=O bond and perpendicular to the WCl_4 plane; typical of this type of complex. The bond distances between W1-O1 are not significantly different to the fluoride analogue, 1.6839(16) Å in this complex and 1.682(5) Å in the fluoride complex. The W1-O1 and W1-O2 bond distances are very different, with W1-O1 being much shorter due to double bond character, compared with 2.1047(14) Å for the W1-O2 single bond. Due to higher electron density on O1, the chlorine atoms are distorted away from the W=O bond and out of the equatorial plane, shown by O=W-Cl angles >90°.

$[WOCl_4(OPMe_3)]$ has also been synthesised as a yellow powder. There is no reported literature for this compound, but similarities can be drawn from $[WOCl_4(OPPh_3)]$. The data can be found in Table 2.9, showing all the same spectroscopic characteristics as $[WOCl_4(OPPh_3)]$.

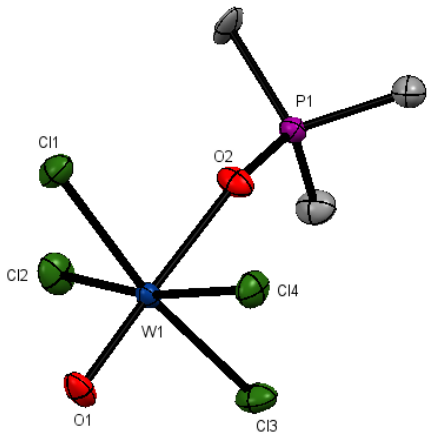

Figure 2.7: The structure of $[WOCl_4(OPMe_3)]$ showing the atom numbering scheme. Ellipsoids shown at 50% probability, H atoms are omitted for clarity.

[$WOCl_4(OPMe_3)$]			
Bond Lengths/ Å		Bond Angles/ °	
W1-Cl1	2.3460(5)	Cl-W1-Cl2	88.23(17)
W1-Cl2	2.3015(6)	Cl1-W1-Cl3	169.39(17)
W1-Cl3	2.2936(6)	Cl1-W1-Cl4	90.69(18)
W1-Cl4	2.3151(6)	O1-W1-Cl	93.4(2) - 96.2(2)
W1-O1	1.6839(16)	O1-W1-O2	178.3(7)
W1-O2	2.1047(14)		

Table 2.4: Selected bond lengths and angles for [$WOCl_4(OPMe_3)$].

Bright yellow crystals of [$WOCl_4(OPMe_3)$] (Figure 2.7) were isolated from chloroform and the structure is very similar to [$WOCl_4(OPPh_3)$] described above. The W1-O1 distance is slightly longer in this structure compared to [$WOCl_4(OPPh_3)$], 1.700(14) Å and 1.6839(16) Å, respectively. A small number of pale yellow decomposition crystals were also isolated and shown to be [$WO_2Cl_2(OPMe_3)_2$], which has been reported previously.[12]

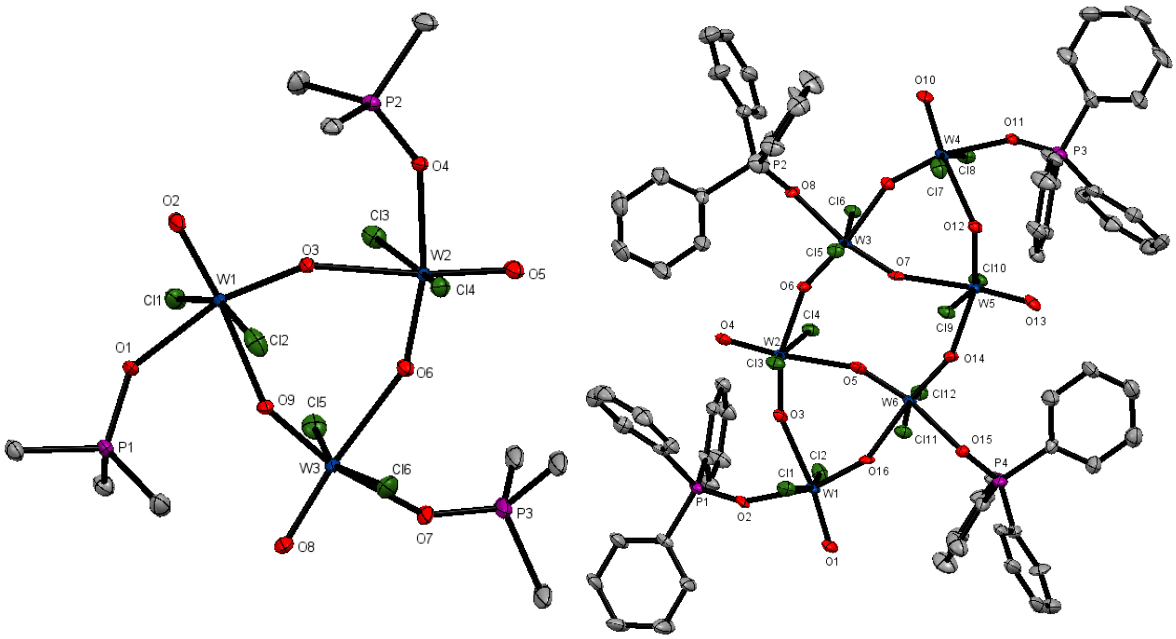

Figure 2.8: The structure of [$W_3O_3(\mu\text{-}O)_3Cl_6(OPMe_3)_3$]•$2CH_2Cl_2$ (left) and [$W_6O_6(\mu\text{-}O)_6Cl_{12}(OPPh_3)_4$] (right) showing the atom numbering scheme. Ellipsoids shown at 50% probability, H atoms and the solvent molecules are omitted for clarity. The Me groups on P3 show disorder over two sites, only one is shown.

$[W_3O_3(\mu\text{-}O)_3Cl_6(OPMe_3)_3]\cdot 2CH_2Cl_2$			
Bond Lengths/ Å			
W1-Cl2	2.3491(8)	W2-O6	1.7669(19)
W1-Cl1	2.3397(8)	W2-O3	2.301(18)
W1-O9	2.2211(18)	W2-O5	1.7167(19)
W1-O1	2.0817(18)	W3-Cl5	2.3522(8)
W1-O3	1.7651(18)	W3-Cl6	2.3549(8)
W1-O2	1.710(2)	W3-O9	1.7539(18)
W2-Cl4	2.3528(7)	W3-O7	2.0681(19)
W2-Cl3	2.3522(8)	W3-O8	1.715(2)
W2-O4	2.0715(18)		
Bond Angles/ °			
W-O_h-W	152.97(11)	O_h-W-O_h	86.07(8)
W-O_h-W	154.90(11)	O_h-W-O_h	85.01(8)
W-O_h-W	154.52(11)	O_h-W-O_h	86.07(8)

Table 2.5: Selected bond lengths and angles for $[W_3O_3(\mu\text{-}O)_3Cl_6(OPMe_3)_3]\cdot 2CH_2Cl_2$.

Decomposition of some $WOCl_4$ complexes can occur, resulting in the formation of $[WO_2Cl_2(L)_2]$ complexes, as revealed by crystallographically. However, under more harsh conditions reduction to tungsten(V) species can occur.[36,45,64]

During attempts to grow crystals of $[WOCl_4(OPPh_3)]$ and $[WOCl_4(OPMe_3)]$ by slow evaporation from chloroform, a small amount of colourless crystals were collected, which were discovered to be cyclic $\{W_n(\mu\text{-}O)_n\}$ species. The compound grown from $[WOCl_4(OPMe_3)]$ solution shows tungsten(VI) in a distorted octahedral environment consisting of three $\{WO_2Cl_2(OPMe_3)\}$ units linked by asymmetric oxido-bridges to form a six-membered ring. In this system the W=O bonds are *trans* to the bridging oxygen, not the oxygen from the $OPMe_3$ ligand, as seen in mononuclear phosphine oxide complexes.[10,12,21] The W=O bond (W1-O3) is 1.7651(18) Å, comparable to terminal W=O bonds in other tungsten(VI) complexes; this oxygen then forms a weak oxido bridge to another tungsten(VI), W2-O3 = 2.2301(18) Å. A similar trimetric structure has been reported in 2016 by Bortoluzzi *et al.* using trimethylurea as a ligand,[39] the only other similar complex is a tetramer with coordinated THF on each tungsten centre (Figure 2.9).[69]

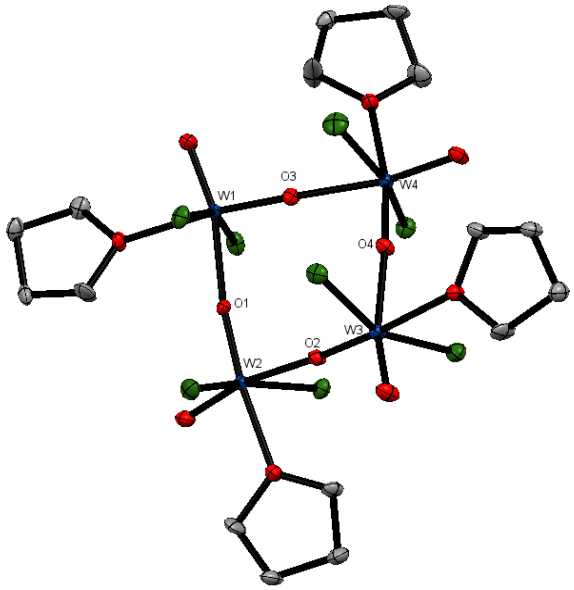

Figure 2.9: Showing $[W_4O_4(\mu\text{-}O)_4Cl_8(THF)_4]\bullet 2CH_2Cl_2$ crystal structure redrawn from literature.[69]

A crystal grown from $[WOCl_4(OPPh_3)]$ solution formed a similar cyclic ring (shown in Figure 2.8), but due to the steric bulk of the phenyl rings, it has forced the structure to adopt a larger ring. Like the trimeric structure, there are asymmetric oxido bridges around the outer ring and across the structure (due to the quality of the data bond lengths cannot be compared). Like the trimer, the W=O bonds are *trans* to the bridging oxygens and *cis* to the chlorine atoms. Attempts to synthesise these complexes in bulk *in situ* directly from WO_2Cl_2 and from $WOCl_4$ by varying the conditions were unsuccessful, resulting in different impure products. These degradation compounds seem to require trace water/oxygen to form, but there appears to be no obvious way to control their formation.

The synthesis of the complex $[WOCl_4(dppmO_2)]$ using 2:1 metal centre to ligand was tried, resulting in the formation of a six-coordinate bridged complex, $[(WOCl_4)_2(dppmO_2)]$, presumably this complex is more favourable than a seven-coordinate monomer (which had no evidence of formation). The IR spectrum for the bridged complex shows the P=O stretch at 1076 cm^{-1}, shifted from 1183 cm^{-1}.[70] The single W=O stretch is observed at 981 cm^{-1} and is close to the W=O stretch from $[WOCl_4(OPPh_3)]$ at 983 cm^{-1}. Finally, the W-Cl stretch is observed at 338 cm^{-1}. The ^1H NMR data shows multiplets from the phenyl rings and a sharp triplet for the methylene linker at 4.62 ppm, which shows a large shift from free ligand (2.41 ppm).[70] The $^{31}P\{^1H\}$ NMR spectrum shows a sharp singlet at +44.6 ppm, which is also similar to $[WOCl_4(OPPh_3)]$ and bulk composition confirmed by elemental analysis.

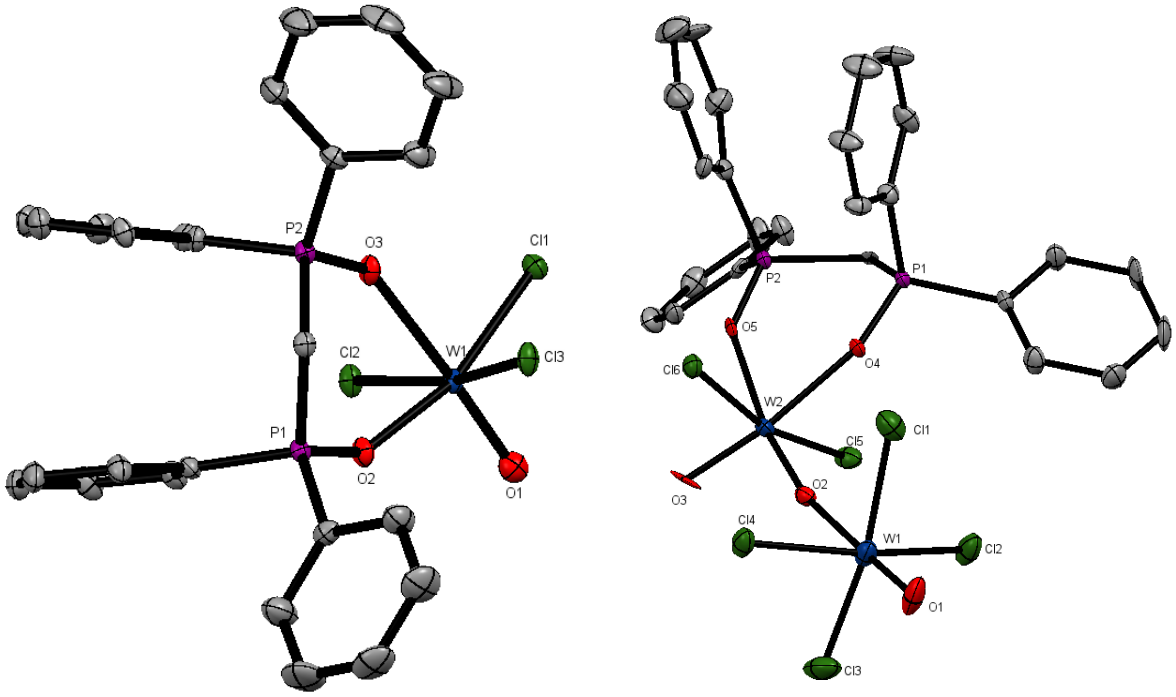

Figure 2.10: The structure of [$WOCl_3(dppmO_2)$] (left) and [$WOCl_2(dppmO_2)((\mu\text{-}O)(WOCl_4))$] (right) showing the atom numbering scheme. Ellipsoids shown at 50% probability, H atoms and solvent are omitted for clarity. Note that the O/Cl in [$WOCl_3(dppmO_2)$] exhibited disorder, which was modelled with split atom sites and refined to occupancies of 0.39:0.61. Only the major form is shown.

[$WOCl_3(dppmO_2)$]			
Bond Lengths/ Å		Bond Angles/ °	
W1-Cl	2.343(3) - 2.395(1)	Cl1-W1-O1	98.4(3)
W1-O1	1.69(1)	Cl2-W1-O1	95.00(3)
W1-O2	2.022(2)	Cl3-W1-O1	82.67(6)
W2-O3	2.234(2)		
[$WOCl_2(dppmO_2)((\mu\text{-}O)(WOCl_4))$]			
Bond Lengths/ Å		Bond Angles/ °	
W1-Cl(1-4)	2.297(2) - 2.315(2)	O1–W1–Cl	95.5(2)-98.3(2)
W1-O1	1.675(5)	O2–W2–Cl	93.5(1) – 95.6(1)
W1-O2	2.207(5)		
W2-Cl(5-6)	2.348(2) – 2.364(2)		

Table 2.6: Selected bond lengths and angles for [$WOCl_3(dppeO_2)$] and [$WOCl_2(dppmO_2)((\mu\text{-}O)(WOCl_4))$].

A few crystals, of a number of decomposition structures, have been obtained from a solution of [$(WOCl_4)_2(dppmO_2)$] in CH_2Cl_2. A large number of orange crystals, of [$(WOCl_4)_2(dppmO_2)$] were collected, confirming the formation of a bridged dimer (Figure 2.11). The W=O and W-Cl bond lengths in this complex and [$WOCl_4(OPPh_3)$] are not dissimilar. The W-O_p in this complex is longer than in [$WOCl_4(OPPh_3)$], however W1-O2 and W2-O3 in the dimer structure distances are surprisingly not equal, a possible explanation is due to some effect of crystal packing.

The first decomposition structure obtained, $[WOCl_2(dppmO_2)((\mu\text{-}O)(WOCl_4))]$, is a minor hydrolysis product (Figure 2.10), showing the formation of an asymmetric oxido bridge and the loss of chlorine from one of the metal centres. The structure shows one $\{WOCl_4\}$ unit and one $\{WO_2Cl_2\}$ unit. A second hydrolysis structure of $[WO_2Cl_2(dppmO_2)]$ has also been isolated as a further minor decomposition product, which has previously been identified.[71]

In addition to these two decomposition structures, a reduction product was also obtained after crystallisation over an extended period, $[WOCl_3(dppmO_2)]$ (Figure 2.10); despite the considerable amount of work on neutral hard donor $WOCl_3$ complexes,[72] this compound has not been reported previously. Due to the loss of one chloride, the $dppmO_2$ ligand has chelated to the tungsten(V) centre reducing the molecular symmetry (to C_s). This structure has O/Cl disorder *trans* to ligand, which is not uncommon for complexes of this type, the W=O bond length is not considerably different to the W=O bonds in other tungsten complexes.

The complex $[(WOCl_4)_2(dppeO_2)]$ also formed as a bridged complex, similar to $[(WOCl_4)_2(dppmO_2)]$ (Figure 2.11). The IR spectrum is almost identical to that of $[(WOCl_4)_2(dppmO_2)]$ - see data in Table 2.9, while the $^{31}P\{^1H\}$ NMR spectrum shows a singlet at +53.2 ppm, which again has shifted from uncoordinated ligand at +33.2 ppm. The structure of $[(WOCl_4)_2(dppeO_2)]$ shows a centrosymmetric crystal, in the space group $P\bar{1}$. Once again, the neutral ligand is lying *trans* to the oxygen with the chlorines slightly out of the equatorial plane, as shown in Figure 2.11.

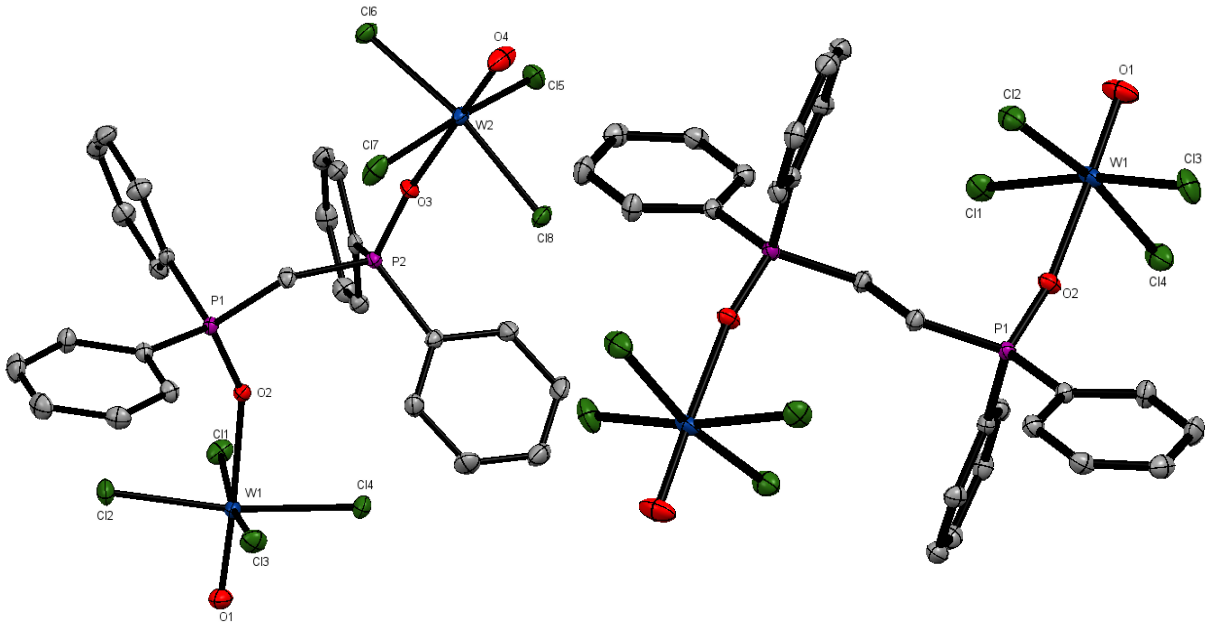

Figure 2.11: The structure of $[(WOCl_4)_2(dppmO_2)]$ (left) and $[(WOCl_4)_2(dppeO_2)]$ (right), showing the atom numbering scheme. Ellipsoids shown at 50% probability, H atoms are omitted for clarity.

$[(WOCl_4)_2(dppmO_2)]$			
Bond Lengths/ Å		Bond Angles/ °	
W1-Cl	2.3092(5) - 2.3190(5)	Cl-W1-Cl (*cis*)	88.129(18) – 90.672(19)
W1-O1	1.6861(14)	O_P–W–Cl	83.60(4) - 87.35(4)
W1-O2	2.1886(12)	O–W–Cl	93.36(5) – 96.94(6)
W2-O3	2.1224(13)	O1–W1–O2	176.96(6)
W2-O4	1.6846(14)	O4–W2–O3	179.31(7)
W2-Cl	2.3119(5) – 2.3198(5)		
$[(WOCl_4)_2(dppeO_2)]$			
Bond Lengths/ Å		Bond Angles/ °	
W1-Cl	2.304(1) - 2.343(1)	O_P–W–Cl	83.72(9) - 85.51(9)
W1-O1	1.693(4)	O–W–Cl	93.9(1) – 96.8(1)
W1-O2	2.115(3)		
W2-O3	2.1224(13)		

Table 2.7: Selected bond lengths and angles for $[(WOCl_4)_2(dppmO_2)]$ and $[(WOCl_4)_2(dppeO_2)]$.

2.3.3 Complexes of $WOCl_4$ with Nitrogen Donor Ligands

Precision over the ratio of metal centre to nitrogen donor ligand and the use of rigorously dried solvent is imperative for the successful formation of these compounds. The imine complexes are readily hydrolysed in solution with formation of protonated imine, which was commonly observed as a minor species during NMR analysis.

The seven-coordinate complex, $[WOCl_4(2,2'\text{-bipy})]$, has been synthesised. This compound has a point group of C_s, the IR spectrum shows a W=O stretch at 954 cm^{-1}, comparable to $[WOF_4(2,2'\text{-bipy})]$ at 968 cm^{-1}. It is expected the W=O stretch will be lower in frequency than the other six-coordinate complexes due to the higher coordination number;[73] this is consistent with our findings. There are two expected IR active stretching modes for W-Cl (A', A''), and in practise a broad peak is observed at 329 cm^{-1}, which is likely the unresolved overlapping vibrations. The ^1H NMR spectrum shows four unique proton environments, meaning the ligand is symmetrically coordinated – also shown by four equal integrals. There is also a shift of +0.4 ppm in all peaks compared to 'free' ligand, confirming there is coordination through both nitrogen atoms. If only one nitrogen was coordinated there would be eight environments as the symmetry in the ligand would be lost. There is a very small amount of protonated 2,2'-bipy present in the NMR spectrum, probably due to trace water in the NMR solvent.

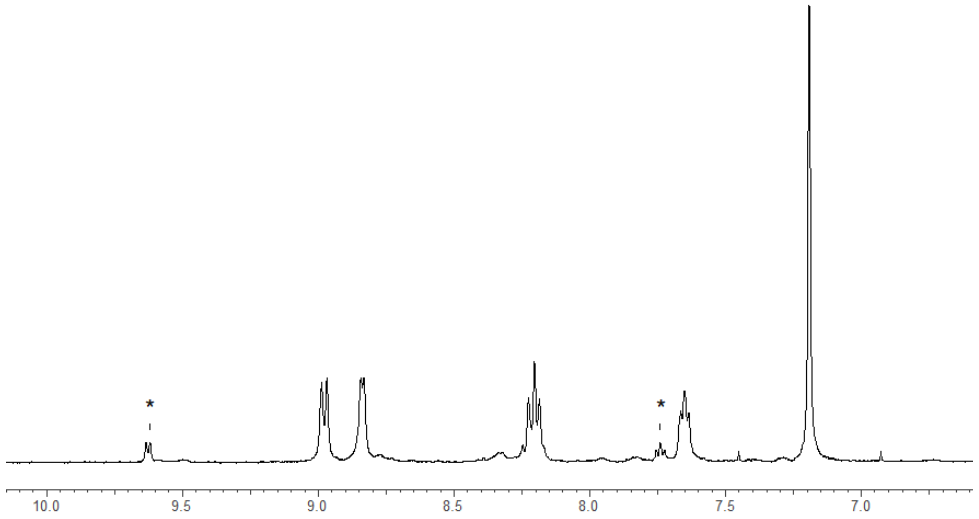

*Figure 2.12: ^{1}H NMR spectrum of [$WOCl_4$(2,2'-bipy)]. Showing four equal proton environments consistent with coordination through both nitrogen atoms. In addition, there is a small shift in ppm showing coordination to the metal centre. * = protonated 2,2-bipy.*

Fowles and co-workers reported that the complex [$WOCl_3$(2,2'bipy)] formed upon reaction of $WOCl_4$ and excess 2,2'-bipy in benzene and propionitrile,[45] however this investigation shows no evidence of this compound forming under the conditions used here.

The synthesis of [$WOCl_4$(1,10-phen)] has been attempted, but no clean complex was isolated. The IR spectrum of the product does not correspond with that of [WO_2Cl_2(1,10-phen)], which has been previously reported.[12] In the ^{1}H NMR spectrum, there is a shift in ppm compared to free ligand implying the ligand has coordinated. However, only part of the bulk product is soluble in dichloromethane, leaving behind a reasonable amount of brown solid, therefore the ^{1}H NMR spectrum may not be representative of the bulk. All attempts to obtain crystals for X-ray structure analysis resulted in formation of [WO_2Cl_2(1,10-phen)]. It should be noted that the fluorine analogue [WOF_4(1,10-phen)] could not be isolated and the major product was [WO_2F_2(1,10-phen)].[10]

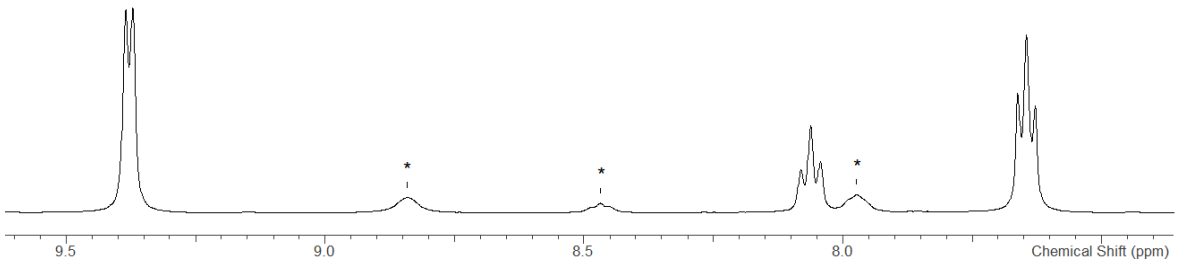

*Figure 2.13: ^{1}H NMR spectrum of [$WOCl_4(C_5H_5N)$]. Showing major 3 proton environments in a 2:1:2 integration, representing pyridine's 5 hydrogen atoms. In addition, there is a small shift in ppm showing coordination to the metal centre through the nitrogen atom. * Trace [$WO_2Cl_2(py)_2$)].*

The last nitrogen-donor complex is [$WOCl_4(C_5H_5N)$]. Unlike [$WOCl_4$(2,2'-bipy)] this complex is six-coordinate. This complex has the point group C_{4v}, the same as the monodentate phosphine oxide complexes. The IR spectrum shows a W=O stretch at 987 cm^{-1}. There are two expected W-Cl

stretches (A_1 and E), a strong absorption at 338 cm^{-1} and then a smaller shoulder. There is no observed W-N stretch in $[WOCl_4(C_5H_5N)]$; it is suggested to be expected at 375 cm^{-1}, [74] but could be hidden in this complex under the W-Cl stretch. The ^1H NMR spectrum, as seen in Figure 2.13, shows three proton environments consistent with pyridine with the correct integrals.

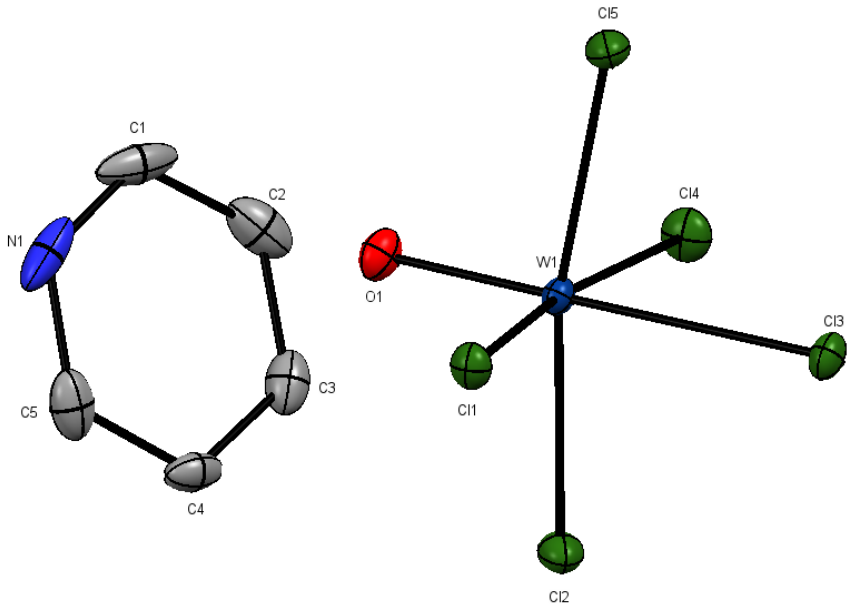

Figure 2.14: The structure of $[C_5H_5NH][WOCl_5]$ showing the atom numbering scheme. Ellipsoids are shown at 50% probability, H atoms are omitted for clarity.

$[(C_5H_5NH)][WOCl_5]$			
Bond Lengths/ Å		Bond Angles/ °	
W1-Cl1	2.3172(6)	Cl1-W1-Cl2	90.46(2)
W1-Cl2	2.3144(5)	Cl1-W1-Cl3	84.67(2)
W1-Cl3	2.5704(6)	Cl1-W1-Cl5	89.71(2)
W1-Cl4	2.3182(6)	O1–W1–Cl1	94.12(5)
W1-Cl5	2.3182(6)		
W1-O1	1.689(1)		

Table 2.8: Selected bond lengths and angles for $[C_5H_5NH][WOCl_5]$.

Attempts to crystallise this complex have been unsuccessful, but a protonated decomposition compound $[C_5H_5NH][WOCl_5]$ has been isolated on extended standing (Figure 2.14). The protonation of pyridine results in the formation of the $[WOCl_5]^-$ anion, the addition of a chloride to the metal centre has shortened the W-Cl bonds compared to neutral $WOCl_4$ complexes. The fifth W-Cl bond *trans* to oxygen is longer than typical, but not unexpected in complexes of this nature, see $[Et_4N][WOCl_5]$ in Chapter 6.[75,76]

Compound	IR			$^{31}P\{^{1}H\}$ NMR / ppm
	ν(P=O)	ν(W=E)	ν(W-Cl)	
$WSCl_4$	-	555 cm^{-1}	370/346 cm^{-1}	-
$[WSCl_4(OPPh_3)]$	1136 cm^{-1}	[a]	329 cm^{-1}	+45.9
$[WSCl_4(OPMe_3)]$	1075 cm^{-1}	522 cm^{-1}	322 cm^{-1}	+63.8
[WSCl4(2,2'-bipy)]	-	521 cm^{-1}	316 cm^{-1}	-
$[WSCl_4(C_5H_5N)]$	-	533 cm^{-1}	334 cm^{-1}	-
$[(WSCl_4)_2(dppmO_2)]$	1074 cm^{-1}	530 cm^{-1}	338 cm^{-1}	+45.4
$[(WSCl_4)_2(dppeO_2)]$	1077 cm^{-1}	536 cm^{-1}	330 cm^{-1}	+49.2
$WOCl_4$	-	875 cm^{-1}	381/326 cm^{-1}	-
$[WOCl_4(OPPh_3)]$	1135 cm^{-1}	983 cm^{-1}	343 cm^{-1}	+46.6
$[WOCl_4(OPMe_3)]$	1090 cm^{-1}	957 cm^{-1}	335 cm^{-1}	+64.2
[WOCl4(2,2'-bipy)]	-	970 cm^{-1}	332 cm^{-1}	-
$[WOCl_4(C_5H_5N)]$	-	987 cm^{-1}	338 cm^{-1}	-
$[(WOCl_4)_2(dppmO_2)]$	1076 cm^{-1}	980 cm^{-1}	338 cm^{-1}	+44.6
$[(WOCl_4)_2(dppeO_2)]$	1091 cm^{-1}	985 cm^{-1}	337 cm^{-1}	+53.2

Table 2.9: Selected IR and ^{1}H and $^{31}P\{^{1}H\}$ NMR data for the compounds in this chapter. [a] W=S band not observed, obscured by P-C band. E = O or S.

2.3.4 Complexes of $WSCl_4$

The compound $WSCl_4$ had initially been prepared from WCl_6 and $S(SiMe_3)_2$ in CH_2Cl_2 following the reported method,[32] however this method gave erratic results and low yields due to the formation of some $WOCl_4$, which could not be separated. A second method was tried and gave much more consistent results and yield, by using toluene as the solvent and including a sublimation step.[54] The W=S bond shows a single absorption (due to the C_{4v} symmetry) at 556 cm^{-1} assigned to the A_1 stretch, which corresponds to the literature values.[32,59] Two bands are expected for W-Cl bonds (A_1 and E), bands at 371 cm^{-1} and 346 cm^{-1} are assigned to A_1 and E respectively. $WSCl_4$ and WCl_6 are extremely moisture sensitive, which can lead to the formation of $WOCl_4$ and further hydrolysis products of WO_2Cl_2 and $WOSCl_2$; if this had occurred the IR spectrum would show a strong sharp stretch around 980-990 cm^{-1} for a W=O bond, which is not present in the spectrum of the $WSCl_4$ used in this study.

2.3.5 Complexes of $WSCl_4$ with Phosphine Oxide Ligands

The complex $[WSCl_4(OPPh_3)]$ has been synthesised by direct reaction of $WSCl_4$ and $OPPh_3$ in CH_2Cl_2. In the IR spectrum, the P=O stretch is at 1137 cm^{-1} showing a coordination shift which is

also consistent with the literature value, 1136 cm^{-1}.[77] Additionally, the two W-Cl stretches, (A_1 and E), 329 cm^{-1} and 310 cm^{-1} also correspond with the literature values. However, no W=S stretch is reported, a single W=S stretch is expected but is most likely hidden by the peak at 537 cm^{-1} from the $OPPh_3$. The $^{31}P\{^1H\}$ NMR data also shows a single peak at +45.9 ppm and the composition was confirmed by elemental analysis.

A number of attempts to make the $[WSCl_4(OPPh_3)]$ complex *in-situ* directly from WCl_6 have been unsuccessful, the P=O stretch in the products has shifted to 1157 cm^{-1}, which is reported as the complex $[WSCl_3(OPPh_3)_2]$ by Behzadi and co-workers.[77] The $^{31}P\{^1H\}$ NMR spectrum shows a singlet at +66.4 ppm likely to be PPh_3Cl_2,[78] however if the main compound is tungsten(V), it is paramagnetic and not NMR active.

Red crystals were isolated from a solution of $[WSCl_4(OPPh_3)]$ in CH_2Cl_2 (Figure 2.15), showing the formation of a mononuclear tungsten(VI) complex with $OPPh_3$. This structure is very similar to $[WOCl_4(OPPh_3)]$ but is not isomorphous, the ligand lies *trans* to the W=S bond, as expected.

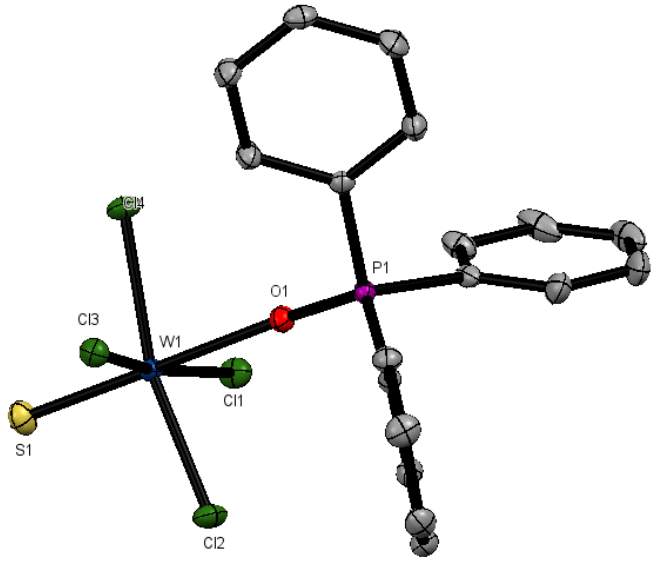

Figure 2.15: The structure of $[WSCl_4(OPPh_3)]$ showing the atom numbering scheme. Ellipsoids shown at 50% probability, H atoms are omitted for clarity.

$[WSCl_4(OPPh_3)]$			
Bond Lengths/ Å		Bond Angles/ °	
W1-Cl1	2.3196(6)	Cl1-W-S	95.21(2)
W1-Cl2	2.3142(6)	Cl2-W-S	97.32(2)
W1-Cl3	2.23488(5)	Cl3-W-S	96.83(2)
W1-Cl4	2.3447(7)	Cl4-W-S	96.88(2)
W1-O1	2.163(2)	O-W-Cl	82.20(4) – 84.46(4)
W1-S1	2.0938(6)		

Table 2.10: Selected bond lengths and angles for $[WSCl_4(OPPh_3)]$.

$[WSCl_4(OPMe_3)]$, like the oxide analogue, has not been reported previously. The compound has a P=O stretch at 1075 cm^{-1} in the IR spectrum, again, lower than the $OPPh_3$ analogue. The W=S stretch is at 522 cm^{-1} and W-Cl stretch at 322 cm^{-1}, consistent with the values observed for $[WOCl_4(OPMe_3)]$ and $[WSCl_4(OPPh_3)]$. The W=S stretching vibration appears in the correct range, so it is assumed that the W=S peak in $[WSCl_4(OPPh_3)]$ is hidden by a P-C band. The $^{31}P\{^1H\}$ NMR spectrum shows a singlet at +63.8 ppm, very similar to $[WOCl_4(OPMe_3)]$ at +64.2 ppm, suggesting the terminal sulfur and oxygen have little effect on the deshielding of the phosphorus on the ligand.

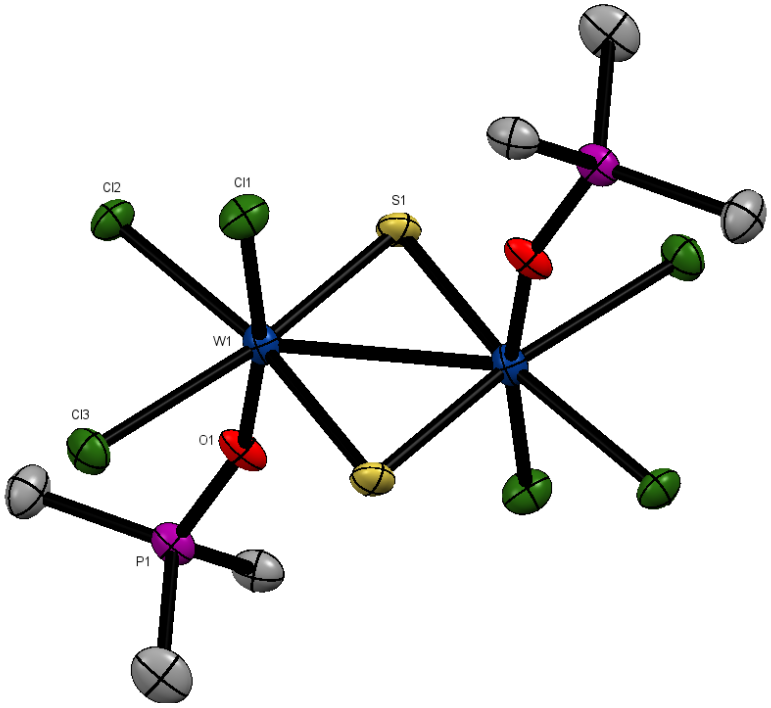

Figure 2.16: The structure of $[(WCl_3)_2(\mu\text{-}S)_2(OPMe_3)_3]\bullet CH_2Cl_2$ showing the atom numbering scheme. Ellipsoids shown at 50% probability, H atoms are omitted for clarity.

A few orange crystals were isolated from a CH_2Cl_2 solution of $[WSCl_4(OPMe_3)]$ and were identified as the neutral tungsten(V) dimer, $[(WCl_3)_2(\mu\text{-}S)_2(OPMe_3)_3]\bullet CH_2Cl_2$ (Figure 2.15). These crystals were isolated after the compound was >6 months old and are likely the result of degradation over time, even in inert conditions. The bridging sulfurs coming from rearrangement from $WSCl_4$ (see Section 3.3.1 and 4.3.1 for other examples).

The bidentate phosphine oxide complexes of $WSCl_4$ behave extremely similarly to the $WOCl_4$ analogues, forming bridging dimers. Neither the mono- nor the bi-dentate phosphine oxides are strong enough donors to force the tungsten centre to go seven-coordinate. Some crystal structures have also been obtained showing a loss of chloride to form W(V) species, for example, $[WECl_3(dppmO_2)]$ compounds, as a degradation route. For these examples, some show the metal thiohalide compounds have also been hydrolysed to form the oxide species. The compounds $[(WSCl_4)_2(dppmO_2)]$ and $[(WSCl_4)_2(dppeO_2)]$ show W=S stretches around ~530 cm^{-1} and W-Cl stretches ~340 cm^{-1} (Table 2.9) with bulk composition confirmed by elemental analysis.

A few orange crystals of the tungsten(V) complex $[WSCl_3(dppmO_2)]$ and red crystals of $[(WSCl_4)_2(dppmO_2)]$ were isolated from CH_2Cl_2 (Figure 2.16), showing similar structures to those of $[WOCl_3(dppmO_2)]$ and $[(WOCl_4)_2(dppmO_2)]$, respectively. These reduction products (which were obtained when compounds were >6 months old) seem to suggest that the tungsten(VI) complexes are not indefinitely stable in solution or solid-state over time.

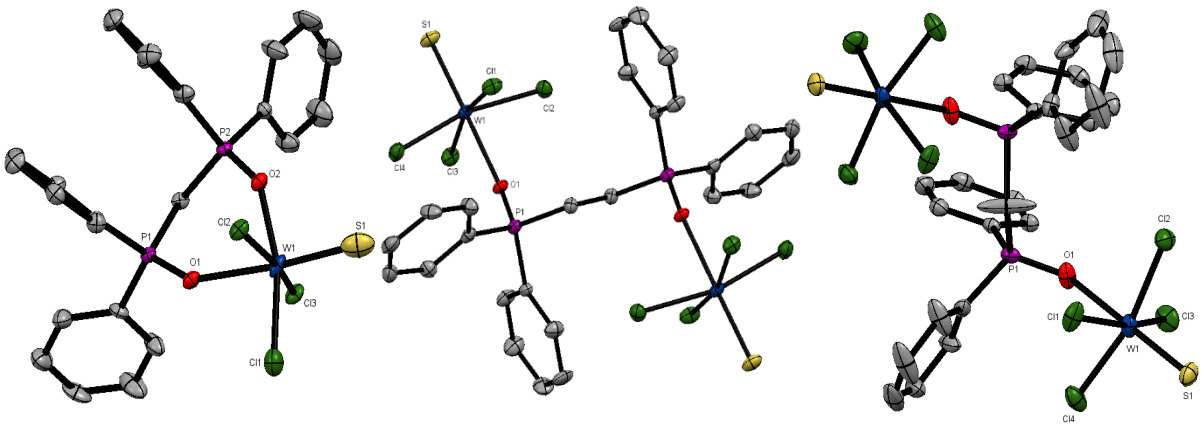

Figure 2.17: The structures of $[WSCl_3(dppmO_2)]$ (left), $[(WSCl_4)_2(dppeO_2)]$ (middle) and $[(WSCl_4)_2(dppmO_2)]$ (right) showing the atom numbering scheme. Ellipsoids shown at 50% probability, H atoms and solvent are omitted for clarity. Note that the axial S/Cl exhibited disorder in the tungsten(V) complex, which was modelled with split atom sites and refined to occupancies of 0.25:0.75. Only the major form is shown.

$[(WSCl_4)_2(dppeO_2)]$			
Bond Lengths/ Å		Bond Angles/ °	
W1-Cl	2.3126(8) - 2.34848(8)	Cl-W-Cl (*cis*)	87.80(3) - 90.29(3)
W1-S1	2.1059(9)	Cl-W-S	95.99(3) - 97.99(3)
W1-O1	2.159(2)	O-W-Cl	82.33(6) - 83.74(6)
$[WSCl_3(dppmO_2)]$			
Bond Lengths/ Å		Bond Angles/ °	
W1-Cl	2.269(4) – 2.386(1)	O1-W1-Cl	83.6(1) – 84.3(2)
W1-O_p	2.076(3) – 2.198(4)	S1-W1-Cl	95.5(2) – 101.1(2)
W1-S1	2.060(7)		
$[(WSCl_4)_2(dppmO_2)]$			
Bond Lengths/ Å		Bond Angles/ °	
W1-Cl	2.291(1)-2.365(1)	Cl-W-Cl (*cis*)	87.14(5) - 91.59(5)
W1-O	2.179(4)	Cl-W-S	96.27(5) - 97.09(5)
W1-S1	2.109(1)	O-W-Cl	81.7(1) - 83.8(1)

Table 2.11: Selected bond lengths and angles for $[(WSCl_4)_2(dppeO_2)]$, $[WSCl_3(dppmO_2)]$ and $[(WSCl_4)_2(dppmO_2)]$.

Orange crystals of $[(WSCl_4)_2(dppeO_2)]$, isolated from a CH_2Cl_2 solution, the structure is again similar to the other similar compounds. The X-ray crystal structure of this complex shows a centrosymmetric dimer with the sulfur lying *trans* to the oxygen from the ligand, similar to the structures of $[(WOCl_4)_2(dppmO_2)]$ and $[WOCl_4(OPPh_3)]$. The tungsten(VI) atoms lie out of the

equatorial WCl_4 plane away from the sulfur, as it does in the complex $[(WOCl_4)_2(dppmO_2)]$, but to a lesser extent (as sulfur is less electronegative).

2.3.6 Complexes of $WSCl_4$ with Nitrogen Donor Ligands

The reaction between $WSCl_4$ and 2,2'-bipy forms the complex $[WSCl_4(2,2'\text{-bipy})]$, which is probably seven-coordinate, as suggested by the ^1H NMR data. The ^1H NMR data shows four different environments with chemical shifts consistent with chelated 2,2'-bipy; this is also indicated in the IR spectrum as there is a shift to a lower frequency of the W=S band at 521 cm^{-1}, compared to its six-coordinate counterparts. Attempts to crystallise this complex have been unsuccessful, but crystals of the previously reported W(V) complex, $[WSCl_3(2,2'\text{-bipy})]$ have been grown (Figure 2.18).[64] This is most likely a degradation product formed by crystallisation over an extended period of time, as the seven-coordinate W(VI) complex is relatively stable compared to the other six-coordinate sulfide complexes, but not very soluble in organic solvents.

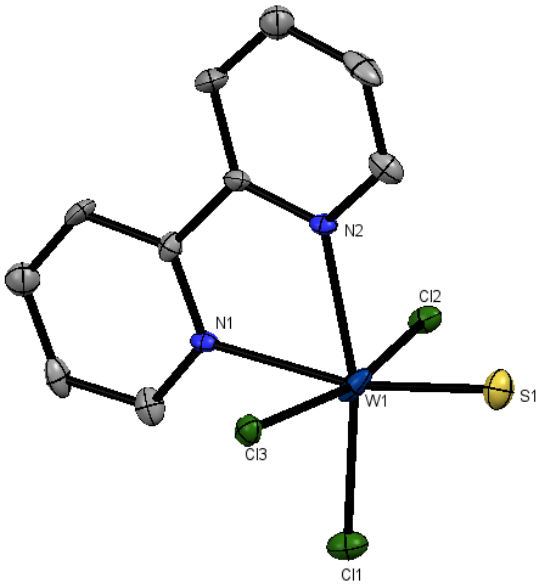

Figure 2.18: The structure of $[WSCl_3(2,2'\text{-bipy})]$ showing the atom numbering scheme. Ellipsoids shown at 50% probability, H atoms are omitted for clarity. Two molecules were present in the asymmetric unit, but only one is shown here for clarity.

$[WSCl_3(2,2'\text{-bipy})]$			
Bond Lengths/ Å		Bond Angles/ °	
W1-Cl1	2.284(4)	Cl2–W1–Cl3	166.21(11)
W1-Cl2	2.356(3)	S1–W1–Cl2	96.40(13)
W1-Cl3	2.3636(3)	S1–W1–N1	166.1(3)
W1-S1	2.206(4)	S1–W1–N2	93.3(3)
W1-N1	2.268(11)	S1–W1–Cl3	95.79(13)
W1-N2	2.215(11)	N1–W1–Cl2	83.5(3)

Table 2.12: Selected bond lengths and angles for $[WSCl_3(2,2'\text{-bipy})]$.

Finally, the compound [$WSCl_4(C_5H_5N)$] has been prepared from a 1:1 metal to ligand ratio at room temperature. There is a report of [$WSCl_4(C_5H_5N)_3$] being synthesised after a 3 week reaction time, but characterisation was extremely limited.[64] All the data collected in the present work indicates a 1:1 ratio, including elemental analysis. A crystal structure has also been obtained (Figure 2.19), although a large amount of residual electron density is present due to unresolved twinning, precluding detailed analysis of the geometric parameters.

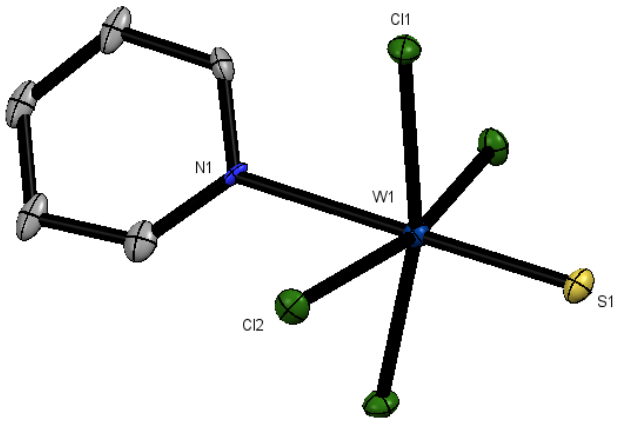

Figure 2.19: The structure of [$WSCl_4(C_5H_5N)$] showing the atom numbering scheme. Ellipsoids shown at 50% probability, H atoms are omitted for clarity. Two molecules were present in the asymmetrical unit cell; one is shown here for clarity.

2.4 WCl_6 Chemistry

The coordination chemistry of WCl_6 is complex as it is highly reactive and moisture sensitive, often resulting in a large number and variety of products (see Section 2.2.2). Following the formation of [$WECl_4$(2,2'-bipy)], efforts to form other seven-coordinate complexes of the type [WCl_6(L)] were attempted. Reports of complexes of this nature are extremely limited, with ligands often causing the reduction of the metal centre to tungsten(V),[38,79,80] although there are also a number of examples of WCl_6 being reduced to [$W^{IV}Cl_4(L)_2$] when using excess ligand over an extended period of time.[81,82] A general consensus is that it is challenging to maintain the +VI oxidation state upon the addition of ligands, with only a few reported examples.

Boorman *et al.* have reported the formation of [$WCl_6(tht)_2$], [$WCl_6(MeS(CH_2)_2SMe)$] and [$WCl_6(SMe_2)$]; these complexes are formed under harsh conditions over extended periods of time.[61] However, it is not clear if these species are neutral mononuclear complexes as neutral 8-coordinate compounds are extremely rare. It has also been reported that under similar conditions, the reduction of WCl_6 to tungsten(V) occurs for nitrogen ligands.[80] Reaction attempts of WCl_6 with NEt_3, PPh_3 or THF are reported to have formed intractable products.[80]

Similar work on coordination complexes of WF_6 has been more successful, fluoride is strongly bound to high oxidation state metal ions, which often results in different behaviour to analogous

compounds with heavier halogens.[83,84] A larger amount of literature has been reported for complexes of WF_6 with nitrogen donors, including some 8-coordinate systems, $[WF_6(py)_2]$.[50,85-89] A limited number of neutral WF_6 complexes with soft ligands ($AsEt_3$ and PMe_3) have been shown, however other arsine or phosphine ligands form rare cationic W(VI) species (further details in Chapter 3).[88,90]

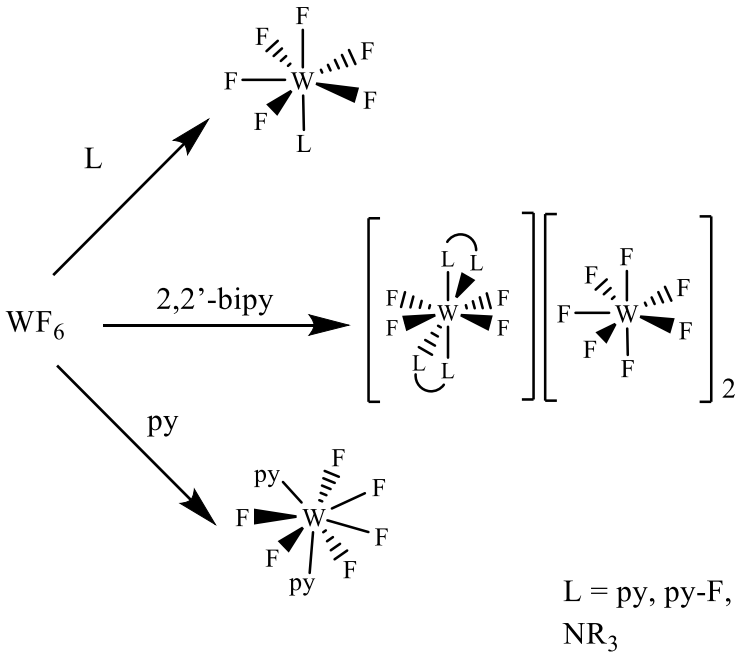

Figure 2.20: Scheme of known complexes of WF_6 with nitrogen donor ligands.

The aim of this work was to replicate known literature and potentially to expand on the WCl_6 coordination chemistry, to create species analogous to known WF_6 complexes. The ligands used include $OPPh_3$, 2,2'-bipy, 1,10-phen, py, tht and SMe_2. Products have been characterised by IR spectroscopy, ^1H NMR spectroscopy, $^{31}P\{^1H\}$ spectroscopy and elemental analysis.

2.4.1 Results and Discussion

Attempts to replicate literature compounds of seven coordinate WCl_6 complexes proved challenging with most compounds being unable to be isolated cleanly. A variety of ligand types and conditions were attempted in efforts to understand the chemistry involved. Due to the nature of the complexes there are limited spectroscopic techniques available compared to the $WECl_4$ complexes. Boorman *et al.* have that shown WCl_6 with a 1:1 equivalent of 2,2'-bipy at room temperature produces the complex $[WCl_5(2,2'\text{-bipy})]$. This was reproduced in the present work, confirmed by IR spectroscopy and elemental analysis.[80] Following this, 1,10-phen was used to see if the analogue could be prepared in the same way, however the spectroscopy did not support this. The IR spectra for both complexes looked similar, both having a W-Cl stretch ~ 316 cm^{-1}, however the NMR spectra were different, $[WCl_5(2,2'\text{-bipy})]$ showed no peaks (indicative of paramagnetism), whereas the 1,10-phen complexes showed at least two 1,10-phen species. It is

likely that one species is protonated ligand, which is common in N- donor ligands; the identity of the other complex is unknown. The products from the reaction with pyridine also produced similar spectra to those with 1,10-phen.

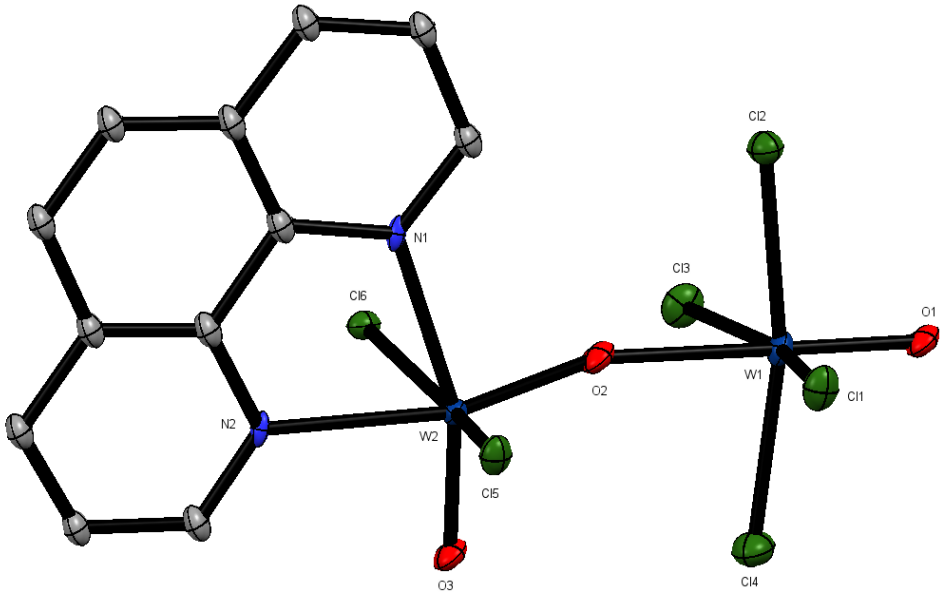

Figure 2.21: The structure of [((WOCl$_2$)(1,10-phen))(μ-O)(WOCl$_4$)] showing the atom numbering scheme. Ellipsoids shown at 50% probability, H atoms are omitted for clarity.

[((WOCl$_2$)(1,10-phen))(μ-O)(WOCl$_4$)]			
Bond Lengths/ Å		Bond Angles/ °	
W1-Cl(1-4)	2.299(4) - 2.325(5)	O1–W1–Cl	95.5(5)-98.3(5)
W1-O1	1.70(1)	O2–W2–Cl	93.6(6) – 97.3(1)
W1-O2	2.219(1)		
W2-Cl(5-6)	2.331(4) – 2.348(4)		

Table 2.13: Selected bond lengths and angles for [((WOCl$_2$)(1,10-phen))(μ-O)(WOCl$_4$)].

A few orange crystals were isolated from a solution of the solid isolated from the reaction between WCl_6 and 1,10-phen, which revealed a tungsten(VI) oxide bridged dimer (Figure 2.21). The structure is similar to [((WOCl$_2$)(dppmO$_2$))(μ-O)(WOCl$_4$)] with both structures being oxide bridged, linking two tungsten(VI) centres. The oxygen present is likely coming from adventitious oxygen or trace water in the atmosphere.

To get an understanding of these systems $OPPh_3$ was also tried as a ligand, the $^{31}P\{^1H\}$ NMR spectrum of the product showed two equal intensity peaks at 66.6 and 47.61 ppm. The peak at 66.6 ppm is indicative of chlorinated phosphine.[78] The second peak is close to the value of [WOCl$_4$(OPPh$_3$)]. This is supported by the evidence of a W=O stretch observed by IR spectrum (978 cm^{-1}), presumably resulting from trace hydrolysis.

Softer sulfur donors were used to try to replicate the reported literature, [WCl$_6$(L)] (L = SMe$_2$ or tht) which have been isolated using a 1:2 metal to ligand ratio. In this work, attempts were made

using a 1:1 ratio, but clean products could not be isolated. NMR spectra either showed no peaks (tht) or many (SMe_2). Due to the limited characterisations and difficulty to produce clean products this work was not continued further.

2.5 Conclusions

The main aim of this chapter was to synthesise a range of neutral complexes of $WOCl_4$ and $WSCl_4$ with phosphine oxides and N-heterocycles under mild reaction conditions. All compounds are hydrolytically unstable and must be handled and stored under anhydrous conditions at all stages. Excluding the 2,2'-bipy complexes, which are seven-coordinate, all other complexes are six-coordinate. Comparison of all the data collected suggests that the sulfide chlorides are slightly less Lewis acidic than the oxide chlorides. The products are characterised by infrared spectroscopy, ^{1}H and $^{31}P\{^{1}H\}$ NMR spectroscopy, elemental analysis and some examples are characterised by X-ray structures. A number of examples of decomposition and degradation products/pathways have also been shown by X-ray crystal structures, but spectroscopic data confirms these degradation products are not the bulk compounds.

A short investigation into complexes of WCl_6 to produce analogues of WF_6 has proven unsuccessful, with data indicating reduction to tungsten(V) complexes (and potentially others). The complex $[WCl_5(2,2'\text{-bipy})]$ was isolated and characterised, but 1,10-phen analogues could not be isolated. Therefore, it can be assumed that complexes of WCl_6 are less stable than their WF_6 analogues and cannot be formed under mild conditions.

2.6 Experimental

Syntheses were performed by using standard Schlenk and glove-box techniques under a dry N_2 atmosphere. Solvents were dried by distillation from CaH_2 (CH_2Cl_2) or Na/benzophenone ketyl (toluene, n-hexane). WCl_6, $O(SiMe_3)_2$, $S(SiMe_3)_2$, SMe_2 and tht were obtained from Sigma-Aldrich and used as received. Ligands (2,2'-bipy, 1,10-phen, $OPPh_3$, $OPMe_3$) were obtained from Sigma-Aldrich and dried by heating *in vacuo*. The diphosphine dioxides, $dppmO_2$ and $dppeO_2$, were made by dry air oxidation of the corresponding diphosphines in CH_2Cl_2 solution, catalysed by SnI_4,[91] and were checked for purity by $^{31}P\{^1H\}$ NMR spectroscopy (δ = 25.1 and 33.1 ppm, respectively). Before use, pyridine was dried over sodium and freshly distilled. For further details regarding the instrumentation see Appendix A.

2.6.1 $WOCl_4$ Species

[$WOCl_4$]

Following a reported literature method,[32] a solution of $O(SiMe_3)_2$ (0.818 g, 5.04 mmol) in dichloromethane (5 mL) was added to a stirred solution of WCl_6 (2.00 g, 5.04 mmol) in dichloromethane (5 mL). The orange solution was stirred for 1 h. then the orange precipitate was filtered and washed with cold hexane (2 x 1 mL). Yield: 1.445 g, 84%. IR data (Nujol, ν / cm^{-1}): 889sh, 875s W=O, 381s, 326s W-Cl.

[$WOCl_4(OPPh_3)$]

A solution of $OPPh_3$ (0.105 g, 0.44 mmol) in dichloromethane (5 mL) was slowly added to a suspension of $WOCl_4$ (0.150 g, 0.44 mmol) in dichloromethane (5 mL). The clear orange solution was then stirred for 1 h., concentrated to ~ 3 mL, filtered, and the orange solid washed with hexane (2 x 1 mL), and dried *in vacuo*. Yield: 0.130 g, 48 %. Required for $C_{18}H_{15}Cl_4O_2PW$ (619.9): C: 34.85, H: 2.44 %. Found: C: 35.01, H: 2.44 %. IR spectrum (Nujol, ν / cm^{-1}): 1135s P=O, 981s W=O, 338s W-Cl. ^1H NMR ($CDCl_3$): δ = 7.88 (m, [2H], aromatic CH), 7.70 (m, [H], aromatic CH), 7.58 (m, [2H], aromatic CH). $^{31}P\{^1H\}$ NMR ($CDCl_3$): δ = +46.6 (s).

[$WOCl_4(OPMe_3)$]

A yellow powder, made in an analogous way to [$WOCl_4(OPPh_3)$]. Yield: 0.140 g, 73%. Required for $C_3H_9Cl_4O_2PW$ (433.7): C: 8.31, H: 2.09 %. Found: C: 8.55, H: 2.02 %. IR spectrum (Nujol, ν / cm^{-1}): 1089s, br P=O, 957s W=O, 337s W-Cl. ^1H NMR ($CDCl_3$): δ = 1.88 (d, J_{HP} 13 Hz, CH_3). $^{31}P\{^1H\}$ NMR ($CDCl_3$): δ = +64.2 (s).

[$(WOCl_4)_2(dppmO_2)$]

A solution of $dppmO_2$ (0.120 g, 0.29 mmol) in dichloromethane (5 mL) was slowly added to an orange suspension of $WOCl_4$ (0.200 g, 0.58 mmol) in dichloromethane (5 mL). The clear

orange/brown solution formed was stirred for 1 h., then concentrated to ~ 5mL, filtered and the orange powder washed with hexane (2 x 1 mL) and dried *in vacuo*. Yield: 0.264 g, 83 %. Required for $C_{25}H_{22}Cl_8O_4P_2W_2$ (1099.7): C: 27.30, H: 2.02 %. Found: C: 27.42, H: 2.14 %. IR spectrum (Nujol, ν / cm^{-1}): 1076m, br P=O, 981s W=O, 338s, br W-Cl. ^{1}H NMR ($CDCl_3$): δ = 7.81(m, [2H], aromatic CH), 7.61 (m, [2H], aromatic CH), 7.43 (m, [4H], aromatic CH), 4.62 (t, [H], J_{HP} 15.5 Hz, CH_2). $^{31}P\{^1H\}$ NMR ($CDCl_3$): δ = +44.6 (s).

[$(WOCl_4)_2(dppeO_2)$]

Was made similarly to [$(WOCl_4)_2(dppmO_2)$] as a yellow powder. Yield 0.100 g, 31 %. Required for $C_{26}H_{24}Cl_8O_4P_2W_2$ (1113.7): C: 28.09, H: 1.99 %. Found: C: 27.96, H: 2.12 %. IR spectrum (Nujol, ν / cm^{-1}): 1091s P=O, 985s W=O, 337s W-Cl. ^{1}H NMR ($CDCl_3$): δ = 7.86 (m, [4H], aromatic CH), 7.70 (m, [H], aromatic CH), 7.59 (m, [2H], aromatic CH), 3.15 (s, [H], CH_2). $^{31}P\{^1H\}$ NMR ($CDCl_3$): δ ppm: +53.2 (s).

[$WOCl_4$(2,2'-bipy)]

2,2'-bipy (0.068 g, 0.44 mmol) in dichloromethane (5 mL) was slowly added to an orange suspension of $WOCl_4$ (0.150 g, 0.44 mmol) in dichloromethane (5 mL). A green solution formed and was stirred for 1 h. at room temperature and then concentrated to ~ 3 mL *in vacuo*. The green solid was isolated by filtration, washed with hexane (2 x 1 mL) and dried *in vacuo.* Yield: 0.067 g, 30 %. Required for $C_{10}H_8Cl_4N_2OW$ (499.85): C: 24.11, H: 1.62, N: 5.63 %. Found: C: 24.33, H: 1.73, N: 5.84 %. IR spectrum (Nujol, ν / cm^{-1}): 970s W=O, 329s, br W-Cl. ^{1}H NMR ($CDCl_3$): δ = 8.99 (d, [H], J_{HH} 8.1 Hz, aromatic CH), 8.85 (d, [H], J_{HH} 4.4 Hz, aromatic CH), 8.22 (t, [H], J_{HH} 7.8 Hz, aromatic CH), 7.66 (t, [H], J_{HH} 4.0 Hz, aromatic CH).

[$WOCl_4(C_5H_5N)$]

Pyridine (0.050 g, 0.58 mmol) in toluene (2 mL) was added to a red suspension of $WOCl_4$ (0.20 g, 0.58 mmol). The red solution formed was stirred for 1 h. and then taken to dryness *in vacuo* to obtain a yellow powder. Yield: 0.120 g, 49 %. Required for $C_5H_5Cl_4NOW$ (420.75): C: 14.27, H: 2.20, N: 3.33 %. Found: C: 14.23, H: 2.15, N: 3.31 %. IR spectrum (Nujol, ν / cm^{-1}): 987m W=O, 338s W-Cl. ^{1}H NMR (CD_2Cl_2): δ = 9.37 (dd, [2H], J_{HH} 6.6, 1.5 Hz, aromatic CH), 8.06 (tt, [H], J_{HH} 7.7, 1.5 Hz, aromatic CH), 7.65 (td, [2H], J_{HH} 6.6, 1.2 Hz, aromatic CH).

2.6.2 $WSCl_4$ Species

[$WSCl_4$]

Following the literature method,[54] tungsten hexachloride (2.5 g, 6.3 mmol) in toluene (5 mL) was chilled to 0°C, hexamethyldisilathiane (1.35 g, 6.3 mmol) in toluene (2 mL) was added dropwise over 15 minutes. The red/brown solution was stirred for 30 minutes and taken to dryness *in vacuo*

collecting a brown powder. The brown powder was sublimed *in vacuo* (*ca.* 100 °C, 0.01 mmHg) collecting a red powder from the finger. Yield: 1.742 g, 78 %. IR data (Nujol, ν / cm^{1}): 556m W=S, 372s, 344s W-Cl.

[$WSCl_4(OPPh_3)$]

$OPPh_3$ (0.078 g, 0.28 mmol) in dichloromethane (2 mL) was slowly added to a red solution of $WSCl_4$ (0.100 g, 0.28 mmol) in dichloromethane (5 mL). The solution was then stirred for 1 h., concentrated *in vacuo* to ~ 4 mL. The brown solid was filtered, washed with hexane (2 x 1 mL) and dried *in vacuo*. Yield: 0.120 g, 69 %. Required for $C_{18}H_{15}Cl_4OPSW$ (636.0): C: 33.99, H: 2.38 %. Found: C: 34.14, H: 2.45 %. IR spectrum (Nujol, ν / cm^{-1}): 1137m P=O, 329s, 310sh W-Cl. ^{1}H NMR (CD_2Cl_2): δ = 7.81 (m, [2H], aromatic CH), 7.68 (t, [H], aromatic CH), 7.55 (m, [2H], aromatic CH). $^{31}P\{^{1}H\}$ NMR (CD_2Cl_2): δ = +45.9 (s).

[$WSCl_4(OPMe_3)$]

A brown powder, made in an analogous way to [$WSCl_4(OPPh_3)$]. Yield: 0.080 g, 43 %. Required for $C_3H_9Cl_4OPSW$ (449.8): C: 8.01, H: 2.00 %. Found: C: 8.14, H: 2.14 %. IR spectrum (Nujol, ν / cm^{-1}): 1075s, br P=O, 522m W=S, 322s, br W-Cl. ^{1}H NMR (CD_2Cl_2): δ = 1.81 (d, J_{PH} = 13 Hz, CH_3). $^{31}P\{^{1}H\}$ NMR (CD_2Cl_2): δ = +63.8 (s).

[$(WSCl_4)_2(dppmO_2)$]

A solution of $dppmO_2$ (0.086 g, 0.21 mmol) in dichloromethane (5 mL) was slowly added to a red suspension of $WSCl_4$ (0.150 g, 0.42 mmol) in dichloromethane (5 mL). The resulting brown solution was then stirred for 1 h., concentrated in *vacuo* and the brown solid filtered off and rinsed with hexane (2 x 1 mL), and dried *in vacuo*. Yield: 0.115 g, 48 %. Required for $C_{25}H_{22}Cl_8O_2P_2S_2W_2$ (1131.8): C: 26.53, H: 1.96 %. Found: C: 26.52, H: 2.06 %. IR spectrum (Nujol, ν / cm^{-1}): 1074m P=O, 530m W=S, 338sh, 327s W-Cl. ^{1}H NMR (CD_2Cl_2): δ = 7.76 (br [4H], aromatic CH), 7.56 (br [2H], aromatic CH), 7.43 (br [4H], aromatic CH), 3.82 (br [H], CH_2). $^{31}P\{^{1}H\}$ NMR (CD_2Cl_2): δ = +45.4 (s).

[$(WSCl_4)_2(dppeO_2)$]

A solution of $dppeO_2$ (0.090 g, 0.21 mmol) in dichloromethane (5 mL) was slowly added to a red suspension of $WSCl_4$ (0.150 g, 0.42 mmol) in dichloromethane (5 mL), where a brown solution was formed. After 1 h. the solution was concentrated in *vacuo*, the brown solid filtered off and washed with hexane (2 x 1 mL). Yield: 0.190 g, 79 %. Required for $C_{26}H_{24}Cl_8O_2P_2S_2W_2$ (1145.85): C: 27.25, H: 2.11 %. Found: C: 27.00, H: 2.02 %. IR spectrum (Nujol, ν / cm^{-1}): 1077s P=O, 536s W=S, 330s W-Cl. ^{1}H NMR (CD_2Cl_2): δ = 7.93 (br, [2H], aromatic CH), 7.66 (br, [H], aromatic CH), 7.59 (br, [2H], aromatic CH), 2.78 (s, [H], CH_2). $^{31}P\{^{1}H\}$ NMR (CD_2Cl_2): δ = +49.2 (s).

[$WSCl_4$(2,2'-bipy)]

2,2'-bipy (0.065 g, 0.42 mmol) in dichloromethane (5 mL) was slowly added to a red suspension of $WSCl_4$ (0.150 g, 0.42 mmol) in dichloromethane (5 mL). The purple/red solution was stirred for 1 h. concentrated to ~3 mL and the red-pink powder filtered off, washed with hexane (2 x 1 mL), and dried *in vacuo,* collecting a red/pink powder. Yield: 0.165 g, 76 %. Required for $C_{10}H_8Cl_4N_2SW$ (513.9): C: 23.37, H: 1.57, N: 5.45 %. Found: C: 23.36, H: 1.59, N: 5.50 %. IR spectrum (Nujol, ν / cm^{-1}): 521s W=S, 316s W=Cl. ^1H NMR (CD_2Cl_2): δ = 8.97 (d, [H], J_{HH} 8.3 Hz, aromatic CH), 8.89 (d, [H], J_{HH} 5.1 Hz, aromatic CH), 8.27 (t, [H], J_{HH} 7.6 Hz, aromatic CH), 7.73 (t, [H], J_{HH} 7.6 Hz, aromatic CH).

[$WSCl_4(C_5H_5N)$]

Pyridine (0.050 g, 0.58 mmol) in toluene (2 mL) was added to a dark red solution of $WSCl_4$ (0.200 g, 0.58 mmol). The brown solution formed was stirred for 1 h. and then taken to dryness *in vacuo* to yield a brown/grey powder. Yield: 0.160 g, 87 %. Required for $C_5H_5Cl_4NSW$ (436.8): C: 13.75, H: 1.15, N: 3.21 %. Found: C: 14.06, H: 1.20, N: 3.29 %. IR spectrum (Nujol, ν / cm^{-1}): 533s W=S, 334s, br W-Cl. ^1H NMR (CD_2Cl_2): δ = 8.78 (br, [2H], aromatic CH), 8.56 (br, [H], aromatic CH), 8.11 (br, [2H], aromatic CH).

2.6.3 WCl_6 Species

The products isolated from the WCl_6 reactions were not satisfactorily characterised (see above) but are reported for completeness of work.

Reaction of WCl_6 and $OPPh_3$

$OPPh_3$ (0.140 g, 0.504 mmol) in dichloromethane (2 mL) was slowly added to a dark red solution of WCl_6 (0.200 g, 0.504 mmol) in dichloromethane (5 mL). The solution was then stirred overnight, the light orange solution was layered in hexane (4 mL). A sticky orange oil was isolated *via* filtration and dried *in vacuo.* IR spectrum (Nujol, ν / cm^{-1}): 978s W=O, 322s W-Cl. ^1H NMR (CD_2Cl_2): δ = 8.10-7.55 (m). $^{31}P\{^1H\}$ NMR (CD_2Cl_2): δ = +66.6 (s, PPh_3Cl_2), 47.6 (s).

[WCl_5(2,2'-bipy)]

2,2-bipy (0.079 g, 0.504 mmol) in dichloromethane (2 mL) was slowly added to a red solution of WCl_6 (0.200 g, 0.504 mmol) in dichloromethane (5 mL). The solution was left to stir for 2 h., a green precipitate had formed, which was isolated *via* filtration and dried *in vacuo.* Yield: 0.197 g, 76 %. Required for $C_{10}H_8Cl_5N_2W$ (517.29): C: 23.22, H: 1.56, N: 5.42 %. Found: C: 22.91, H: 1.58, N: 4.75 %. IR spectrum (Nujol, ν / cm^{-1}): 315s, br W-Cl.

Reaction of WCl_6 and 1,10-phen

1,10-phen (0.091 g, 0.504 mmol) in dichloromethane (2 mL) was slowly added to a red solution of WCl_6 (0.200 g, 0.504 mmol) in dichloromethane (5 mL). The solution was left to stir for 2 h., a beige precipitate had formed which was isolated *via* filtration and dried *in vacuo.* IR spectrum (Nujol, ν / cm^{-1}): 320s, br W-Cl. ^1H NMR (CD_2Cl_2): δ = 8.10-7.55 (m).

Reaction of WCl_6 and pyridine

Pyridine (0.040 g, 0.504 mmol) in dichloromethane (2 mL) was slowly added to a red solution of WCl_6 (0.200 g, 0.504 mmol) in dichloromethane (5 mL). The solution was left to stir for 2 h., a green precipitate had formed which was isolated *via* filtration and dried *in vacuo.* IR spectrum (Nujol, ν / cm^{-1}): 322s, br W-Cl. ^1H NMR (CD_2Cl_2): δ = 10.95 (m), 9.37 (dd), 7.55 (m, J_{HH} 1.47, 6.60 Hz), 8.79 (d, J_{HH} 4.40 Hz), 8.38 (t, J_{HH} 7.70 Hz), 7.94 (t, J_{HH} 6.72 Hz), 7.65 (m).

Reaction of WCl_6 and SMe_2

SMe_2 (0.031 g, 0.504 mmol) in dichloromethane (2 mL) was slowly added to a red solution of WCl_6 (0.200 g, 0.504 mmol) in dichloromethane (5 mL). The solution was left to stir for 2 h.: a green precipitate had formed which was isolated *via* filtration and dried *in vacuo.* IR spectrum (Nujol, ν / cm^{-1}): 310s, br W-Cl. ^1H NMR (CD_2Cl_2): δ = 2.56 (s br, CH_3).

2.6.4 Crystallographic Tables

Compound	$[WOCl_4(OPPh_3)]$	$[WOCl_4(OPMe_3)]$	$[W_3O_3Cl_6(\mu\text{-}O)_3(OPMe_3)_3]\cdot 2CH_2Cl_2$	$[W_6O_6Cl_{12}(\mu\text{-}O)_6(OPPh_3)_4]\cdot 4CHCl_3$
Formula	$C_{18}H_{15}Cl_4O_2PW$	$C_3H_9Cl_4O_2PW$	$C_{11}H_{31}Cl_{10}O_9P_3W_3$	$C_{76}H_{64}Cl_{24}O_{16}P_4W_6$
M	1239.84	433.73	1306.32	6144.62
Crystal system	Triclinic	Monoclinic	Monoclinic	Triclinic
Space group (n°)	$P\bar{1}$ (2)	$P2_1/c$ (14)	$P2_1/c$ (14)	$P\bar{1}$ (2)
a /Å	9.36630(10)	11.0381(5)	19.1399(5)	17.2594(4)
b /Å	15.4398(2)	8.5387(3)	11.2360(2)	22.0524(5)
c /Å	16.0484(2)	11.8399(4)	18.2845(5)	27.0009(5)
α /°	109.4180(10)	90	90	106.738(2)
β /°	97.1570(10)	92.1275(3)	116.616(3)	93.940(2)
γ /°	105.4190(10)	90	90	107.216(2)
U /Å^3	2051.31(5)	1111.12(7)	3515.49(17)	9266.4(4)
Z	2	4	4	2
μ(Mo-K_α) /mm^{-1}	6.241	11.417	10.724	8.066
F(000)	1184.0	800.0	2424.0	5776.0
Total number reflns	53470	12618	37791	133745
R_{int}	0.0239	0.0758	0.0297	0.0418
Unique reflns	8081	2575	6842	47595
No. of params, restraints	469/0	103/0	336/0	2119/0
GOF	1.035	1.032	1.028	1.133
R_1, wR_2 [I > 2σ(I)][b]	0.0141, 0.0326	0.0441, 0.0938	0.0159, 0.0297	0.0667, 0.1381
R_1, wR_2 (all data)[b]	0.0158, 0.0331	0.0529, 0.0965	0.0195, 0.0304	0.1037, 0.1588

Table 2.14: X-ray crystallography table. a: common data: wavelength (Mo-K_α) = 0.71073 Å; θ(max) = 27.5°; [b] $R_1 = \Sigma||Fo|-|Fc||/\Sigma|Fo|$; $wR_2=[\Sigma w(Fo^2-Fc^2)^2/\Sigma wFo^4]^{1/2}$

Compound	$[(WOCl_4)_2(dppmO_2)]$	$[WOCl_2(dppmO_2)(\mu\text{-}O)(WOCl_4)]$	$[C_5H_5NH][WOCl_5]$	$[(WSCl_4)_2(dppeO_2)]$
Formula	$C_{25}H_{22}Cl_8O_4P_2W_2$	$C_{26}H_{24}Cl_6O_5P_2W_2$	$C_5H_6Cl_5NOW$	$C_{26}H_{24}Cl_8O_2P_2S_2W_2$
M	1099.66	1145.69	457.21	572.91
Crystal system	Triclinic	Monoclinic	Orthorhombic	Triclinic
Space group (n°)	$P\bar{1}$ (2)	$P2_1/n$ (14)	Pbca (61)	$P\bar{1}$ (2)
a /Å	10.3428(2)	10.6984(5)	12.5650(3)	9.1134(5)
b /Å	11.0799(2)	23.4594(14)	11.1389(3)	9.3623(3)
c /Å	15.3764(2)	15.1239(8)	16.1782(4)	11.7376(4)
α /°	81.7770(10)	90	90	97.087(3)
β /°	70.3800(10)	106.970(6)	90	106.333(4)
γ /°	80.1300(10)	90	90	112.441(4)
U /Å^3	1628.27(5)	3630.5(4)	2264.31(10)	857.70(7)
Z	2	4	8	2
μ(Mo-K$_\alpha$) /mm^{-1}	7.846	7.046	11.342	7.565
F(000)	1036.0	2168.0	1680.0	542.0
Total number reflns	44544	7079	43355	23334
R_{int}	0.0281	0.0516	0.0499	0.0549
Unique reflns	9901	7097	2929	5298
No. of params, restraints	370/0	361/0	122/0	190/0
GOF	1.081	1.031	1.052	1.083
R_1, wR_2 [I > 2σ(I)][b]	0.0173, 0.0355	0.0360, 0.0824	0.0139, 0.0279	0.0263, 0.0629
R_1, wR_2 (all data)[b]	0.0219, 0.0363	0.0460, 0.0849	0.0161, 0.0285	0.0313, 0.0644

Table 2.14: Continued.

Compound	$[(WOCl_4)_2(dppeO_2)]$	$[WSCl_4(OPPh_3)]$	$[WOCl_3(dppmO_2)]\cdot CH_2Cl_2$	$[WSCl_3(dppmO_2)]\cdot CH_2Cl_2$
Formula	$C_{26}H_{24}Cl_8O_4P_2W_2$	$C_{18}H_{15}Cl_4OPSW$	$C_{26}H_{24}Cl_5O_3P_2W$	$C_{26}H_{24}Cl_5O_2P_2SW$
M	1113.69	635.98	807.49	823.55
Crystal system	Triclinic	Monoclinic	Monoclinic	Monoclinic
Space group (n°)	$P\bar{1}$ (2)	$P2_1/n$ (14)	$P2_1/n$ (14)	$P2_1/n$ (14)
a /Å	9.1755(4)	12.48950(10)	16.5408(2)	16.5665(2)
b /Å	9.5095(3)	10.99140(10)	8.38430(10)	8.39180(4)
c /Å	11.2258(4)	15.04610(10)	21.8513(4)	21.9258(4)
α /°	67.129(3)	90	90	90
β /°	83.443(3)	96.1620(10)	105.797(2)	106.089(2)
γ /°	71.395(3)	90	90	90
U /Å^3	855.28(6)	2053.55(3)	2915.95(8)	2928.79(8)
Z	1	4	4	4
μ(Mo-K$_\alpha$) /mm^{-1}	7.470	6.331	4.557	4.605
F(000)	526.0	1216.0	1572.0	1604.0
Total number reflns	23001	76498	61871	95407
R_{int}	0.0377	0.0346	0.0364	0.0461
Unique reflns	5325	6508	9078	9760
No. of params, restraints	190/0	235/0	362/15	343/15
GOF	1.085	1.154	1.170	1.183
R_1, wR_2 $[I>2\sigma(I)]^b$	0.0324, 0.0736	0.0228, 0.0403	0.0340, 0.0608	0.0573, 0.1149
R_1, wR_2 (all data)^b	0.0365, 0.0748	0.0258, 0.0409	0.0436, 0.0627	0.0684, 0.1183

Table 2.14: Continued.

Compound	$[(WSCl_4)_2(dppmO_2)]$	$[WSCl_4(C_5H_6N)]$	$[WSCl_3(2,2'\text{-bipy})]$	$[WOCl_2(1,10\text{-phen})(\mu\text{-O})(WOCl_4)]$
Formula	$C_{25}H_{22}Cl_8O_2P_2S_2W_2$	$C_5H_6Cl_4NSW$	$C_{10}H_8Cl_3N_2SW$	$C_{12}H_8Cl_6N_2O_3W_2$
M	1131.78	436.81	478.44	808.60
Crystal system	Monoclinic	Monoclinic	Triclinic	Triclinic
Space group (n°)	$P2_1/n$ (14)	$P2_1/m$ (11)	P1 (1)	$P\bar{1}$ (2)
a /Å	12.7268(2)	11.9648(2)	6.6843(2)	8.5583(3)
b /Å	10.29240(10)	6.97110(10)	8.1998(2)	8.9998(3)
c /Å	13.0039(2)	12.5550(2)	12.3744(4)	12.8051(3)
α /°	90	90	74.743(2)	88.706(2)
β /°	101.6530(10)	104.643(2)	89.939(2)	76.429(2)
γ /°	90	90	89.988(2)	80.619(2)
U /Å^3	1668.26(4)	1013.17(3)	654.34(3)	945.80(5)
Z	2	4	2	2
μ(Mo-K$_\alpha$) /mm^{-1}	7.777	12.604	9.575	13.015
F(000)	1068.0	800.0	446.0	736.0
Total number reflns	40337	32456	19122	22371
R_{int}	0.0560	0.0508	0.0283	0.0504
Unique reflns	5530	3605	5139	5595
No. of params, restraints	186/0	113/0	278/3	142/0
GOF	1.132	1.252	1.131	1.243
R_1, wR_2 [I > 2σ(I)][b]	0.0416, 0.1041	0.0667, 0.1604	0.0296, 0.0704	0.0673, 0.2123
R_1, wR_2 (all data)[b]	0.0489, 0.1072	0.0691, 0.1611	0.0302, 0.0706	0.0709, 0.2131

Table 2.14: Continued.

2.7 References

(1) Dori, Z. *Comprehensive Coordination Chemistry I,* **1987,** *3*, 973-1022
(2) Greenwood, N. N.; Earnshaw, A. In *23. Chromium, Molybdenum and Tungsten*, Eds.; Butterworth-Heinemann: Oxford, 1997.
(3) Nielson, A. J.; Andersen, R. A. In *Tungsten and Molybdenum Tetrachloride Oxides*, Eds.; McGraw-Hill Book Company, 1990; Vol. 28.
(4) Tunney, J. M.; McMaster, J.; Garner, C. D. *Comprehensive Coordination Chemistry II,* **2004,** *8*, 359-477
(5) Holm, R. H. *Chem. Rev.,* **1987,** *87*, 1401-49
(6) Okamura, T.; Ueyama, N. *Comprehensive Coordination Chemistry II,* **2004,** *4*, 529-73
(7) Young, C. G. *Comprehensive Coordination Chemistry II,* **2004,** *4*, 415-527
(8) Stiefel, E. I. *Prog. Inorg. Chem.,* **1977,** *22*, 1-223
(9) Tamadon, F.; Seppelt, K. *Angew. Chem. Int. Ed.,* **2013,** *52*, 767-69
(10) Levason, W.; Reid, G.; Zhang, W. *J. Fluorine. Chem.,* **2016,** *184*, 50-57
(11) McCullough, L. G.; Schrock, R. R.; Dewan, J. C.; Murdzek, J. C. *J. Am. Chem. Soc.,* **1985,** *107*, 5987-98
(12) Davis, M. F.; Levason, W.; Ratnani, R.; Reid, G.; Rose, T.; Webster, M. *Eur. J. Inorg. Chem.,* **2007**, 306-13
(13) Lewis, G. N. *Valence and the Structure of Atoms and Molecules*; Chemical Catalog Company: New York, 1923.
(14) Pearson, R. G. *J. Am. Chem. Soc.,* **1963,** *85*, 3533-39
(15) Greenacre, V. K.; Hector, A. L.; Levason, W.; Reid, G.; Smith, D. E.; Sutcliffe, L. *Polyhedron,* **2019,** *162*, 14-19
(16) Bannister, R. D.; Levason, W.; Light, M. E.; Reid, G.; Zhang, W. *Polyhedron,* **2019,** *167*, 1-10
(17) Davis, M. F.; Levason, W.; Light, M. E.; Ratnani, R.; Reid, G.; Saraswat, K.; Webster, M. *Eur. J. Inorg. Chem.,* **2007,** *13*, 1903-10
(18) Fronczek, F. R.; Luck, R. L.; Wang, G. *Inorg. Chem. Commun.,* **2002,** *5*, 384-87
(19) Hursthouse, M. B.; Levason, W.; Ratnani, R.; Reid, G. *Polyhedron,* **2004,** *23*, 1915-21
(20) Kühn, F. E.; Groarke, M.; Bencze, É.; Herdtweck, E.; Prazeres, A.; Santos, A. M.; Calhorda, M. J.; Romão, C. C.; Gonçalves, I. S.; Lopes, A. D.; Pillinger, M. *Chem. Eur. J.,* **2002,** *8*, 2370-83
(21) Levason, W.; Monzittu, F. M.; Reid, G.; Zhang, W.; Hope, E. G. *J. Fluorine. Chem.,* **2017,** *200*, 190-97
(22) Sens, I.; Stenger, H.; Mller, U.; Dehnicke, K. *Z. anorg. allg. Chem.,* **1992,** *610*, 117-20
(23) Wang, W.; Zhang, Y.; Jin, X.; Du, X. *Acta Cryst. E,* **2009,** *E65*, m1094-m95
(24) Butcher, R. J.; Penfold, B. R.; Sinn, E. *J. Chem. Soc., Dalton Trans.,* **1979**, 668-75
(25) de Wet, J. F.; Caira, M. R.; Gellatly, B. J. *Acta Cryst. B,* **1978,** *34*, 762-66
(26) Marom, H.; Antonov, S.; Popowski, Y.; Gozin, M. *J. Organomet. Chem.,* **2011,** *76*, 5240-46
(27) Herrmann, W. A.; Thiel, W. R.; Herdtweck, E. *Chem. Ber.,* **1990,** *123*, 271-76
(28) Viossat, B.; Rodier, N. *Acta Cryst. B,* **1979,** *35*, 2715-18
(29) Fenn, R. H. *J. Chem. Soc. A,* **1969**, 1764-69
(30) Crabtree, R. H.; Hlatky, G. G. *Polyhedron,* **1985,** *4*, 521-22
(31) Kovalenko, Y. V.; Abramenko, V. L.; Sergienko, V. S. *Zh. Neorg. Khim.,* **1994,** *39*, 1653-56
(32) Gibson, V. C.; Kee, T. P.; Shaw, A. *Polyhedron,* **1990,** *9*, 2293-98
(33) Gabrusenoks, J. *IOP Conf. Ser.: Mater. Sci. Eng.,* **2015,** *77*, 012032
(34) Hess, H.; Hartung, H. *Z. anorg. allg. Chem.,* **1966,** *344*, 157-66
(35) Adams, D. M.; Churchill, R. G. *J. Chem. Soc. A,* **1968**, 2310-12
(36) Walton, R. A. *Prog. Inorg. Chem.,* **1972,** *16*, 1 -194
(37) Bianchi, S.; Bortoluzzi, M.; Castelvetro, V.; Marchetti, F.; Pampaloni, G.; Pinzino, C.; Zacchini, S. *Polyhedron,* **2016,** *117*, 769-76
(38) Bortoluzzi, M.; Marchetti, F.; Pampaloni, G.; Zacchini, S. *Eur. J. Inorg. Chem.,* **2016**, 3169-77
(39) Bortoluzzi, M.; Marchetti, F.; Pampaloni, G.; Zacchini, S. *New J. Chem.,* **2016,** *40*, 8271-81
(40) Dolci, S.; Marchetti, F.; Pampaloni, G.; Zacchini, S. *Dalton Trans.,* **2013,** *42*, 5635-48

(41) Dolci, S.; Marchetti, F.; Pampaloni, G.; Zacchini, S. *Dalton Trans.,* **2010,** *39*, 5367-76
(42) Bortoluzzi, M.; Evangelisti, C.; Marchetti, F.; Pampaloni, G.; Piccinelli, F.; Zacchini, S. *Dalton Trans.,* **2016,** *45*, 15342-49
(43) Funk, H.; Mohaupt, G. *Z. anorg. allg. Chem.,* **1962,** *315*, 204-12
(44) Funk, H.; Weiss, G.; Mohanraj, K. *Z. anorg. allg. Chem.,* **1960,** *304*, 238-40
(45) Fowles, G. W. A.; Frost, J. L. *J. Chem. Soc. A,* **1967**, 671-75
(46) Agh-Atabay, N.; Ashmawy, F. M.; McAuliffe, C. A.; Hill, W. E. *Inorg. Chim. Acta,* **1985,** *104*, 73-76
(47) Zhang, C.; Schlemper, E. O.; Schrauzer, G. N. *Organomet.,* **1990,** *9*, 1016-20
(48) Ward, B. G.; Stafford, F. E. *Inorg. Chem.,* **1968,** *7*, 2569-73
(49) Arnaudet, L.; Bougon, R.; Ban, B.; Charpin, P.; Isabey, J.; Lance, M.; Nierlich, M.; Vigner, J. *Can. J. Chem.,* **1990,** *68*, 507-12
(50) Arnaudet, L.; Bougon, R.; Ban, B.; Lance, M.; Nierlich, M.; Vigner, J. *Inorg. Chem.,* **1993,** *32*, 1142-46
(51) Emsley, J. W.; Levason, W.; Reid, G.; Zhang, W.; De Luca, G. *J. Fluorine. Chem.,* **2017,** *197*, 74-79
(52) Drew, M. G. B.; Mandyczewsky, R. *J. Chem. Soc. A,* **1970**, 2815-18
(53) Cotton, F. A.; Kibala, P. A.; Sandor, R. B. W. *Inorg. Chem.,* **1989,** *28*, 2485-87
(54) Dietz, S.; Allured, V.; DuBois, M. R. *Inorg. Chem.,* **1993,** *32*, 5418-20
(55) Nieboer, J.; Hillary, W.; Yu, X.; Mercier, H. P. A.; Gerken, M. *Inorg. Chem.,* **2009,** *48*, 11251-58
(56) Baghlaf, A. O.; Thompson, A. *J. Less Common Met.,* **1977,** *53*, 291-93
(57) Britnell, D.; Fowles, G. W. A.; Rice, D. A. *J. Chem. Soc., Dalton Trans.,* **1974**, 2191-94
(58) Gibson, V. C.; Shaw, A.; Williams, D. N. *Polyhedron,* **1989,** *8*, 549-50
(59) Page, E. M.; Rice, D. A.; Hagen, K.; Hedberg, L.; Hedberg, K. *Inorg. Chem.,* **1982,** *21*, 3280-83
(60) Fedorov, V. E.; Fedin, V. P.; Kuz'mina, O. A.; Semyannikov, P. P. *Rus. J. Inorg. Chem.,* **1986,** *31*, 2523-26
(61) Boorman, P. M.; Islip, M.; Reimer, M. M.; Reimer, K. J. *J. Chem. Soc., Dalton Trans.,* **1972**, 890-93
(62) Boorman, P. M.; Chivers, T.; Mahadev, K. N. *Can. J. Chem.,* **1977,** *55*, 869-77
(63) Favero, L.; Marchetti, F.; Pampaloni, G.; Zacchini, S. *Dalton Trans.,* **2014,** *43*, 495-504
(64) Britnell, D.; Fowles, G. W. A.; Rice, D. A. *J. Chem. Soc., Dalton Trans.,* **1975**, 213-15
(65) Britnell, D.; Drew, M. G. B.; Fowles, G. W. A.; Rice, D. A. *Inorg. Nucl. Chem. Lett.,* **1973,** *9*, 501-04
(66) Atherton, M. J.; Holloway, J. H. *J. Chem. Soc., Chem. Commun.,* **1977**, 424-25
(67) Nieboer, J.; Yu, X.; Chaudhary, P.; Mercier, H. P. A.; Gerken, M. *Z. anorg. allg. Chem.,* **2012,** *638*, 520-25
(68) Behzadi, K.; Baghlaf, A. O.; Thompson, A. *J. Less Common Met.,* **1978,** *57*, 103-10
(69) Ma, X.; Yang, Z.; Schulzke, C.; Noltemeyer, M.; Schmidt, H.-G. *Inorg. Chim. Acta,* **2009,** *362*, 5275-77
(70) Boulos, L. S.; Ewies, E. F.; Ibrahim, N. M.; Mohram, M. E. *Phosphorus Sulfur,* **2014,** *189*, 1706-17
(71) Jimtaisong, A.; Luck, R. L. *Inorg. Chem.,* **2006,** *45*, 10391- 402
(72) Levason, W.; McCullough, F. P.; McAuliffe, C. A. *Inorg. Nucl. Chem. Lett.,* **1976,** *12*, 843-47
(73) Sathyanarayana, D. N. *Vibrational Spectroscopy: Theory and Applications*; New Age International (P) Limited: New Delhi, 2004.
(74) Dabas, P.; Rastogi, M. K. *Asian J. Chem.,* **1997,** *9*, 445-52
(75) Bortoluzzi, M.; Guarra, F.; Marchetti, F.; Pampaloni, G.; Zacchini, S. *Polyhedron,* **2015,** *99*, 141-46
(76) Bortoluzzi, M.; Marchetti, F.; Murrali, M. G.; Pampaloni, G.; Zacchini, S. *Dalton Trans.,* **2015,** *44*, 8729-38
(77) Behzadi, K.; Baghlaf, A. O.; Thompson, A. *J. Less Common Met.,* **1987,** *128*, 195-206
(78) Godfrey, S. M.; McAuliffe, C. A.; Pritchard, R. G.; Sheffield, J. M.; Thompson, G. M. *J. Chem. Soc., Dalton Trans.,* **1997**, 4823-28
(79) Boorman, P. M.; Chivers, T.; Mahadev, K. N.; O'Dell, B. D. *Inorg. Chim. Acta,* **1976,** *19*, L35-L37

(80) Boorman, P. M.; Greenwood, N. N.; Hildon, M. A.; Parish, R. V. *J. Chem. Soc. A,* **1968**, 2002-04
(81) Allen, E. A.; Brisdon, B. J.; Edwards, D. A.; Fowles, G. W. A.; Williams, R. G. *J. Chem. Soc.,* **1963**, 4649-57
(82) McCarley, R. E.; Brown, T. M. *Inorg. Chem.,* **1964,** *3*, 1232-36
(83) Benjamin, S. L.; Levason, W.; Reid, G. *Chem. Soc. Rev.,* **2013,** *42*, 1460-99
(84) Levason, W.; Monzittu, F. M.; Reid, G. *Coord. Chem. Rev.,* **2019,** *391*, 90-130
(85) Arnaudet, L.; Bougon, R.; Ban, B.; Lance, M.; Navaza, A.; Nierlich, M.; Vigner, J. *J. Fluorine. Chem.,* **1992,** *59*, 141-52
(86) Arnaudet, L.; Bougon, R.; Ban, B.; Lance, M.; Navaza, A.; Nierlich, M.; Vigner, J. *J. Fluorine. Chem.,* **1994,** *67*, 17-25
(87) Arnaudet, L.; Bougon, R.; Buu, B.; Lance, M.; Nierlich, M.; Thuéry, P.; Vigner, J. *J. Fluorine. Chem.,* **1995,** *71*, 123-29
(88) El-Kurdi, S.; Al-Terkawi, A.-A.; Schmidt, B. M.; Dimitrov, A.; Seppelt, K. *Chem. Eur. J.,* **2010,** *16*, 595-99
(89) Tebbe, F. N.; Muetterties, E. L. *Inorg. Chem.,* **1968,** *7*, 172-74
(90) Levason, W.; Monzittu, F. M.; Reid, G.; Zhang, W. *Chem. Commun.,* **2018,** *54*, 11681-84
(91) Levason, W.; Patel, R.; Reid, G. *J. Organomet. Chem.,* **2003,** *688*, 280-82

Complexes of $WOCl_4$ and $WSCl_4$ with Neutral Phosphine and Arsine Donor Ligands

3.1 Introduction

The behaviour of softer donor ligands is often very different to that of hard donor ligands; high oxidation state early transition metal complexes with soft donor ligands are relatively rare and often unstable. Work with softer ligands with $WECl_4$ is very limited and underdeveloped. The aim of this chapter was to take a systematic approach to synthesise and characterise a series of novel phosphine and arsine tungsten(VI) complexes, in order to draw comparisons to known WOF_4 analogues.

3.2 Tungsten(VI) and Molybdenum(VI) Coordination Chemistry with Phosphine and Arsine Donor Ligands

Phosphine and arsine donor ligands follow the σ-donor π-acceptor model when bonding to *d* block transition metals and on descending Group XV, the energy separation between *s* and *p* orbitals increases, consequently the lone pair on the arsine ligand has more *s* character than lone pairs on phosphine lignds.[1] This increased *s* character means the lone pair is less available and, coupled with increased diffusivity, results in arsine ligands being weaker σ-donors than phosphines.[2,3] The σ-donation power of PR_3 or AsR_3 ligands can be improved with electron donating substituents, thus alkyl ligands are better σ-donors than aryl ligands.[4] This strong σ-donation allows a variety of complexes of high oxidation state early transition metals with phosphine or arsine donor ligands to be stabilised.[5-8] These are rare and interesting systems, only certain ligands will produce stable complexes as the orbital overlap can become too poor; resulting in different behaviour.[8] The strong σ-donation from phosphine ligands allows coordination to high valent metal centres, but in some conditions phosphines can reduce transition metals in a competing reaction.[9,10] The reaction which is favourable is often condition dependent and is directly linked to the metal : ligand ratio.[11]

Comparing other high oxidation state tungsten and molybdenum compounds and their reactions with phosphine and arsine donor ligands will help conclusions to be drawn in this section of work. The previous chapter describes reported hard donor complexes of $[MO_2X_2(L)_2]$ and $[MO_2X_2(L\text{-}L)]$ (M = Mo or W; X = F, Cl or Br), at present there are no reports on these types of neutral complexes with phosphine or arsine donor ligands. Similar complexes with phosphines and arsine ligands will be looked at; the simplest complexes are MX_6 (M = Mo or W; X = F or Cl), but as stated in the previous chapter, WCl_6 chemistry is convoluted and $MoCl_6$ is not stable in ambient conditions. MoF_6 is a moisture sensitive liquid below 35 ºC[12] but no ligand complexes have been reported with neutral MoF_6 maintaining the +VI oxidation state, and MoF_6 is instead often reduced to lower oxidation states.[13]

In contrast, WF_6 is less oxidising than MoF_6 and is known with a variety of neutral ligands, including a small subset of phosphine and arsine ligands.[8,13-15] Reactions of WF_6 with tertiary phosphines (PMe_3 and $PPhMe_2$) produced seven-coordinate neutral complexes, $[WF_6(PR_3)]$,[14] yellow crystals of $[WF_6(PMe_3)]$ were identified showing a capped trigonal prism geometry. Conversely, red crystals of $[WF_6(PPhMe_2)]$[14] show a capped octahedral structure as seen in $Cs[WF_7]$;[16] suggesting little difference in energy between structures. Attempts to isolate similar complexes with PPh_3 and PEt_3 could not be spectroscopically verified, with evidence of PR_3F_2 compounds having formed.[14] Arsine analogues $[WF_6(AsR_3)]$ (R = Me or Et) have been obtained more recently, but readily decompose within a few days at ambient tempertures.[8] They are also very susceptible to trace hydrolysis with some products being identified as $[W_2O_2F_9]^-$ and $[WOF_5]^-$ salts.

Reactions of WF_6 with the strong σ-donor ligands o-$C_6H_4(EMe_2)_2$ (E = P or As) gave orange $[WF_4(o\text{-}C_6H_4(EMe_2)_2)_2][WF_7]_2$ salts, with their crystal structures revealing dodecahedral cations.[8] Similarly, the flexible ligand $Me_2P(CH_2)_2PMe_2$ (dmpe) produced a pale orange solid containing two compounds, $[WF_4(dmpe)_2][WF_7]_2$ and a tentatively assigned bridged dimer $[(WF_6)_2(dmpe)]$ which could not be separated from the reaction mixture.[8] Reactions with WF_6 and the poorer σ-donor $AsPh_3$ or the heavier $SbEt_3$ yielded unidentifiable products.

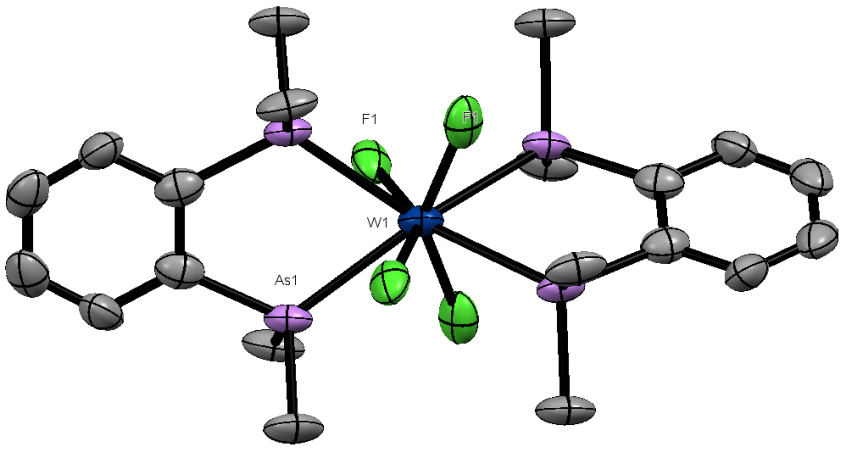

Figure 3.1: $[WF_4((o\text{-}C_6H_4(AsMe_2)_2)_2]^{2+}$ crystal structure obtained from reaction of WF_6 and $o\text{-}C_6H_4(AsMe_2)_2$. Hydrogen and the $[WF_7]$ anions omitted for clarity.[8]

Despite MoF_6 having no known coordination complexes, $MoOF_4$ and MoO_2F_2 both form neutral complexes with hard donor ligands, as shown in Chapter 2.[17] The reaction between $[MoOF_4(MeCN)]$ and neutral ligands ($OPPh_3$, $OPMe_3$, dmso and dmf) gives complexes in the form $[MoOF_4(L)]$. Softer Group XV ligands (PMe_3, dmpe and $AsMe_3$) produce unidentified paramagnetic species indicating reduction of the metal centres.[17] Complexes of $MoOF_4$ have been shown to be highly moisture sensitive with some, upon trace hydrolysis, producing MoO_2F_2 complexes. Hard donor complexes $[MoO_2F_2(L)_2]$ (L = $OPPh_3$, $OPPh_2Me$, $OPMe_3$) are readily made by adding the ligand to a solution of MoO_3 in aqueous HF.[18-24] An alternative method showed Cl/F exchange from $[MoO_2Cl_2(OPPh_3)_2]$ and Me_3SnF in CH_2Cl_2, since MoO_2F_2 does not directly react

with ligands as it is extremely polymeric. There are no reports of Group XV ligands with $MoOF_4$ or MoO_2F_2.[17]

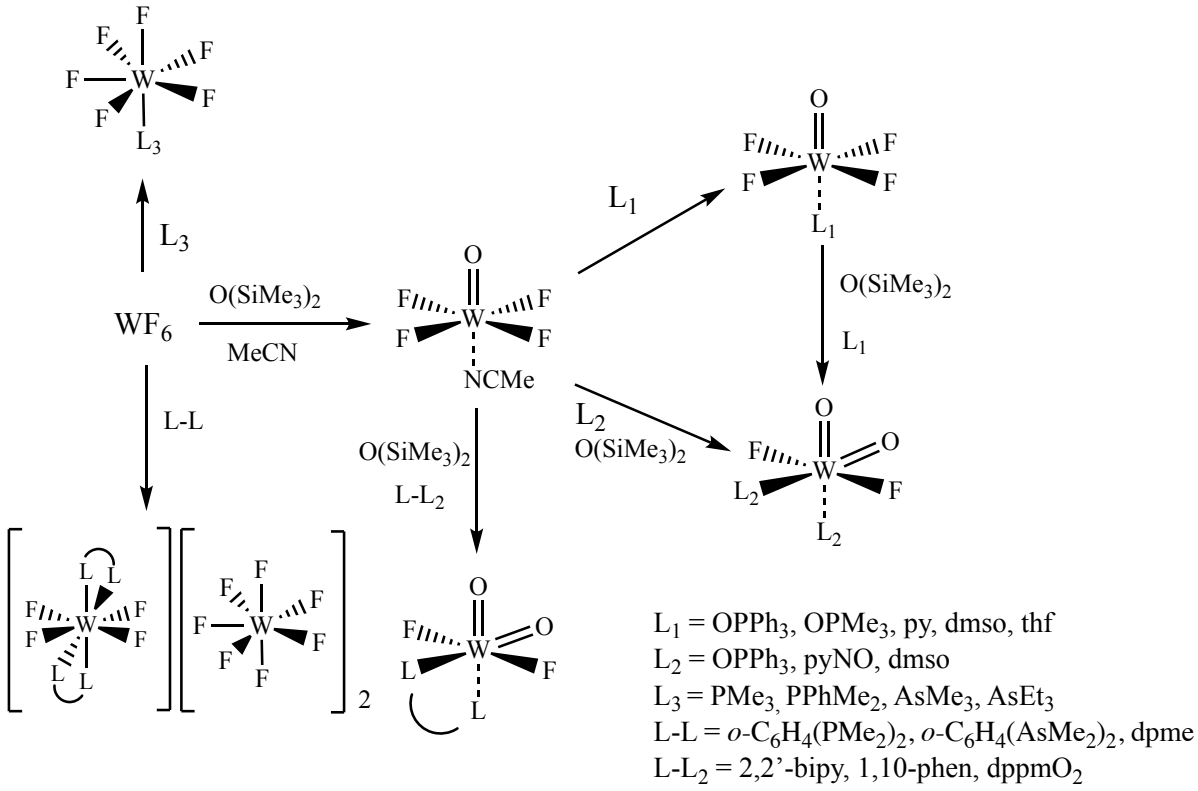

Figure 3.2: Reaction scheme showing complexes of WF_6, WOF_4 and WO_2F_2.[11,24,25]

In contrast to $MoOF_4$ and MoO_2F_2 complexes, WOF_4 and WO_2F_2 have been investigated to a greater extent, as discussed in the previous chapter. The complex $[WOF_4(MeCN)]$ has been shown to react with *o*-$C_6H_4(PMe_2)_2$ and dmpe to form seven-coordinate neutral complexes with their crystal structures showing pentagonal bipyramidal geometry with axial oxygen.[11] Attempts with softer and weaker σ-donors including *o*-$C_6H_4(PPh_2)_2$, *o*-$C_6H_4(AsMe_2)_2$ and *o*-$C_6H_4(SMe)_2$ proved unsuccessful with no evidence of formation. Treating pre-formed $[WOF_4(o\text{-}C_6H_4(PMe_2)_2]$ with an equivalent of $O(SiMe_3)_2$ to try and form $[WO_2F_2(o\text{-}C_6H_4(PMe_2)_2)]$, in a similar way to $[WO_2Cl_2(L)_2]$ complexes, showed no change, potentially suggesting the metal centre is too sterically crowded.[11,26] Therefore, phosphine and arsine ligand complexes of $[WO_2F_2(L\text{-}L)]$ and $[WO_2F_2(L)_2]$ remain unknown but should be relatively stable if they could be accessed.[15]

The limited amount of literature on complexes of tungsten(VI) and molybdenum(VI) oxo-halides with phosphine and arsine ligands has shown a wide variety instability across these compounds. There are no reported complexes of MO_2Cl_2 (M = Mo or W) with phosphine or arsine ligands.[11] WF_6 and WOF_4 both form relatively stable seven-coordinate complexes with phosphines, in contrast to the molybdenum analogues, meaning this chemistry is on the limit of whether the complexes will form and be stable under mild conditions.

3.2.1 Tungsten(V) and Molybdenum(V) Coordination Chemistry with Phosphine and Arsine Ligands

The literature for phosphine and arsine ligand complexes of molybdenum and tungsten in the +VI oxidations state is rather sporadic, whereas extensive work has been carried out on similar complexes in the +V oxidation state. Monodentate and bidentate ligands form a large array of complexes with both $MoOCl_3$ and $WOCl_3$ (see Section 6.2.1), however there are no neutral $MoOF_3$ or WOF_3 complexes known and evidence for the existence of the fluoride parent compounds has not been supplied.[15] Initially $MoOCl_3$ has been shown to form six-coordinate complexes with mono- and bi-dentate Group XV ligands, $[MoOCl_3(PPh_3)_2]$,[27,28] $[MoOCl_3(dppe)]$,[29] $[MoOCl_3(PMe_3)_2]$[30] and $[MoOCl_3(o\text{-}C_6H_4(AsMe_2)_2)]$.[31] Following these early reports, an in-depth study of a series of complexes with bidentate and tridentate ligands has been reported including the use of mixed ligand types.[32,33] The complexes are in the form $[MoOCl_3(L\text{-}L)]$ (L-L see Figure 3.3), all complexes are mildly moisture sensitive and poorly soluble in organic solvents. All these ligands have phenyl rings as their R- groups which results in the ligands being poorer σ-donors and less basic than their methyl substituent counterparts but decreases the chance of reduction. Attempts to isolate complexes with softer antimony containing ligands, ($o\text{-}C_6H_4(SbPh_2)(EPh_2)$, E = P or As), produced intractable black oils.[32] This was also the case for the ligand $Me_2P(CH_2)PMe_2$ likely due to a tight bite angle required for the formation of a four-membered ring due to the shorter methylene backbone.[32,34] The parent complex in this study is $[MoOCl_3(THF)_2]$ so it is possible the complexes would be stable if formed but the ligands cannot displace the THF. In addition, refluxing $[MoOCl_3(L\text{-}L)]$ in methanol reduced the molybdenum and the mixed valent compounds formulated as $[Mo^{IV}OCl(L\text{-}L)_2][Mo^{V}OCl_4]$ formed.[32]

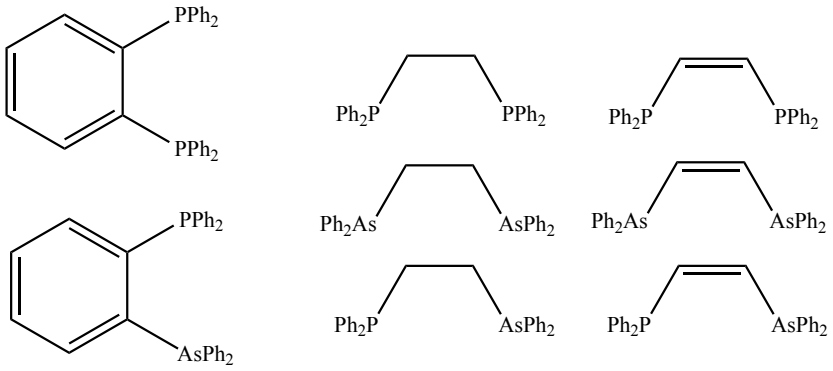

Figure 3.3: Phosphine and arsine ligands reported to form $[MoOCl_3(L\text{-}L)]$ complexes.[32]

There is an example of $[MoOCl_3(THF)_2]$ reacting with the tridentate ligand $PhAs((CH_2)_3AsMe_2)_2$ where the structure is suggested as seven-coordinate species, $[MoOCl_3(PhAs((CH_2)_3AsMe_2)_2]$, with three coordinated arsine donors, however with the absence of a crystal structure this is unclear.[33]

There are examples of neutral complexes of $MoOBr_3$ with hard donors, but no examples with phosphine or arsine ligands.[35,36] $MoOBr_3$ is more likely to be reduced by phosphines than the chloride analogues and is more challenging to synthesise.

The tungsten(V) analogue, $WOCl_3$, has also been extensively investigated and behaves in a similar fashion to $MoOCl_3$. A limited selection of monodentate ligands were tested, PPh_2Me, $PPhMe_2$ and EPh_3 (E = P, As or Sb) to form $[WOCl_3(ER_3)_2]$; only the PPh_2Me and the PPh_3 complex were isolated, however the ligands are quite poor donors and have high steric demands, hence once again, if the ligands did not need to displace the THF they may form stable complexes.[37] Bidentate ligands have increased affinity to form complexes due to the chelate effect increasing stability, shown by a larger range on ligand types forming stable compounds. Reactions of $[WOCl_3(THF)_2]$ and bidentate phosphines (see Figure 3.4) produced grey or green moisture sensitive powders that exhibit a W=O stretch in their IR spectra ~955 cm^{-1}.[37]

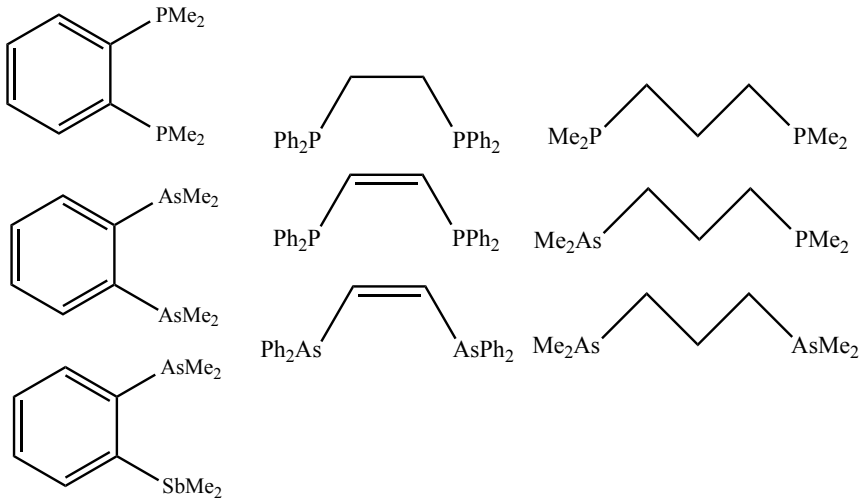

Figure 3.4: Phosphine, arsine and antimony ligands reported to form $[WOCl_3(L\text{-}L)]$ complexes.[37]

A range of arsine ligands have been shown to coordinate as well as an unusual mixed arsine/antinomy ligand, *o*-$C_6H_4(AsMe_2)(SbMe_2)$, which is extremely rare, however the affinity for phenyl substituted ligands is significantly less as many Ph- substituted ligands failed to coordinate. The tungsten complexes are reported to be harder to cleanly isolate and in solution are more moisture sensitive than the molybdenum analogues.[37]

3.2.2 Tungsten Oxotetrachloride and Thiotetrachloride with Phosphine and Arsine donors

There is a small amount of work on $WOCl_4$ complexes with phosphines, although it is rather complicated and there are some conflicting reports. The complex $[WOCl_4(PPh_3)]$[38] has been reported, suggested to form when $WOCl_4$ and PPh_3 were reacted in a 1:1 ratio. However, if the ligand is added in excess it seems to reduce the metal centre ($AsPh_3$ also reduces the metal centre).[39] Some seven-coordinate complexes have been proposed, $[WOCl_4(L)_2]$ (L = PPh_3, PEt_3 or P^nPr_3) formed with stoichiometric 1:2 metal to ligand ratios and long reaction times at low temperature.[38] Similar reactions between $WECl_4$ (E = O, S or Se) and a five-fold excess of PPh_3 yields $[W^{IV}Cl_4(EPPh_3)(PPh_3)]$,[40] clearly indicating the products are highly dependent on the reaction conditions or some are incorrectly characterised. The complex $[WOCl_4(o\text{-}C_6H_4(AsMe_2)_2)]$[31,41] has been isolated and structurally characterised showing a pentagonal

bipyramid geometry, the complex [$WOCl_4$(*o*-$C_6H_4(AsPh_2)_2$)][38] is also suggested to exist, but with little supporting spectroscopic data.

In summary, there are sporadic reports for tungsten and molybdenum complexes in high oxidation states with neutral phosphine and arsine ligands, many have limited spectroscopic characterisation and there are conflicting reports for some complexes. The literature suggests a high tendency for the ligands to reduce the metal centre and the R- substituents play a significant role in affecting the coordination and stability of complexes.

3.2.3 Aims

The aim of this chapter was to continue the chemistry of tungsten(VI) oxo- and thio-tetrachlorides and develop a systematic series of phosphine and arsine complexes. To synthesise complexes in the form [$WECl_4$(L-L)] (E = O or S), together with some monodentate ligand complexes of the form [$WECl_4(L)_2$] or [$WECl_4$(L)] and to investigate their properties. The ligands used include *o*-$C_6H_4(E'Me_2)_2$ (E' = P or As), $Me_2P(CH_2)_2PMe_2$, PMe_3, $AsEt_3$ and *o*-$C_6H_4(PPh_2)_2$. Complexes have been characterised by IR, ^{1}H NMR and ^{31}P{^{1}H} NMR spectroscopy, elemental analysis and by single crystal X-ray diffraction.

3.3 Results and Discussion

3.3.1 Complexes of $WOCl_4$ and $WSCl_4$ with o-$C_6H_4(ER_2)_2$

The seven-coordinate complexes [$WOCl_4$(*o*-$C_6H_4(EMe_2)_2$)] and [$WSCl_4$(*o*-$C_6H_4(EMe_2)_2$] (E = P or As) were isolated as green or brown solids in moderate yields, 49-74%. The complexes were synthesised by direct stoichiometric reaction of pre-formed $WOCl_4$ or $WSCl_4$ with *o*-$C_6H_4(EMe_2)_2$ (E = P or As) in an appropriate solvent (CH_2Cl_2 or toluene) (Figure 3.5).

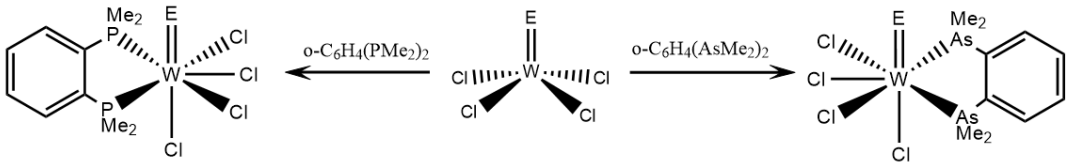

Figure 3.5: Reaction scheme for the synthesis of [$WOCl_4$(o-$C_6H_4(EMe_2)_2$)] and [$WSCl_4$(o-$C_6H_4(EMe_2)_2$)] (E = P or As).

The first compound isolated was [$WOCl_4$(*o*-$C_6H_4(AsMe_2)_2$)], which has been reported previously.[31,41] This complex was re-prepared and the data are consistent with the reported literature. The IR spectrum showed a W=O and W-Cl stretch at 555 and 332 cm^{-1}, respectively. The ^{1}H NMR data show two methyl resonances at 2.46 and 2.51 ppm, compared to a singlet at 1.2 ppm in the 'free' ligand. This is due to the methyl protons being in different environments (above and below the WAs_2Cl_2 plane) in the coordinated complex. Green crystals were isolated from a solution

of CH_2Cl_2, the structure of which confirmed the pentagonal bipyramidal geometry determined from the solution NMR data (Figure 3.6).

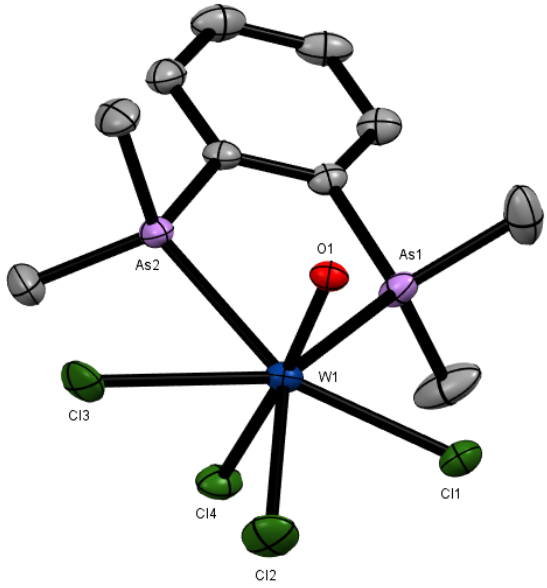

Figure 3.6: The structure of [$WOCl_4$(o-C_6H_4($AsMe_2$)$_2$)] showing the atom numbering scheme. Ellipsoids shown at 50% probability, H atoms are omitted for clarity. Note that the axial O/Cl were disordered, this was modelled using split site occupancies which refined to 0.23 : 0.77. Only the major form is shown.

[$WOCl_4$(*o*-C_6H_4($AsMe_2$)$_2$)]			
Bond Lengths/ Å		**Bond Angles/ °**	
W1-Cl	2.38184 – 2.5809	Cl2-W1-O1	107.5(5)
W1-O1	1.706(5)	Cl3-W1-O1	101.(2)
W1-As1	2.679(8)	Cl1-W1-O1	93.63(4)
W1-As2	2.708(2)	Cl4-W1-O1	164.3(4)

Table 3.1: Selected bond lengths and angles for [$WOCl_4$(o-C_6H_4($AsMe_2$)$_2$)].

This structure has been previously reported,[41] but a more precise structure has been obtained in this work (due to improvement in diffractometer capability in the intervening period). The original report did not identify any axial disorder, however, the reported W=O (1.89 Å) and W-Cl_{ax} (2.26 Å) bond lengths differ considerably from those reported in this work (1.706(5) Å and 2.445(3) Å, respectively), but there is good agreement with W-As and W-Cl bond lengths. The axial units are bent away from linearity (O1-W1-Cl4 = 164.3(4)°), not uncommon in pentagonal bipyramidal structures.

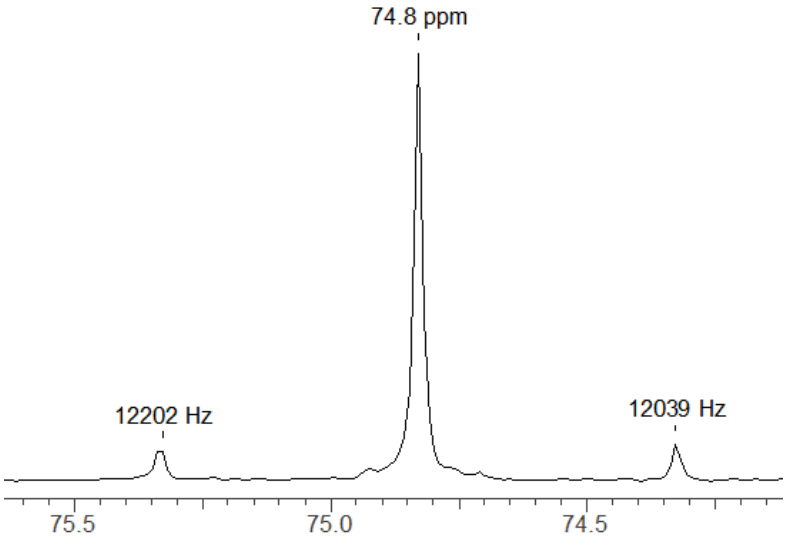

Figure 3.7: $^{31}P\{^{1}H\}$ NMR spectrum of $[WOCl_4(o\text{-}C_6H_4(PMe_2)_2)]$ in CD_2Cl_2.

The phosphine analogue, $[WOCl_4(o\text{-}C_6H_4(PMe_2)_2)]$, was synthesised in a similar way to $[WOCl_4(o\text{-}C_6H_4(AsMe_2)_2)]$ in CH_2Cl_2 and revealed an almost identical IR spectrum. The ^{1}H NMR spectrum shows two sets of triplets, caused by two proton environments (*syn* and *anti* to the W=O) on the methyls and secondary splitting from the NMR active phosphorus nuclei. The $^{31}P\{^{1}H\}$ NMR spectrum shows a single resonance at +74.8 ppm, a very large coordination shift ($\Delta \sim +130$ ppm), Figure 3.7, but not dissimilar to related compounds, ($[WOF_4(o\text{-}C_6H_4(PMe_2)_2)]$ and $[WF_4(o\text{-}C_6H_4(PMe_2)_2)_2]^{2+}$).[8,17] The $^{31}P\{^{1}H\}$ NMR spectrum has satellite resonances from ^{183}W nuclei, the $^{1}J_{W\text{-}P}$ coupling constant is large, 173 Hz, but categorically proves coordination between the tungsten and phosphorus atoms.

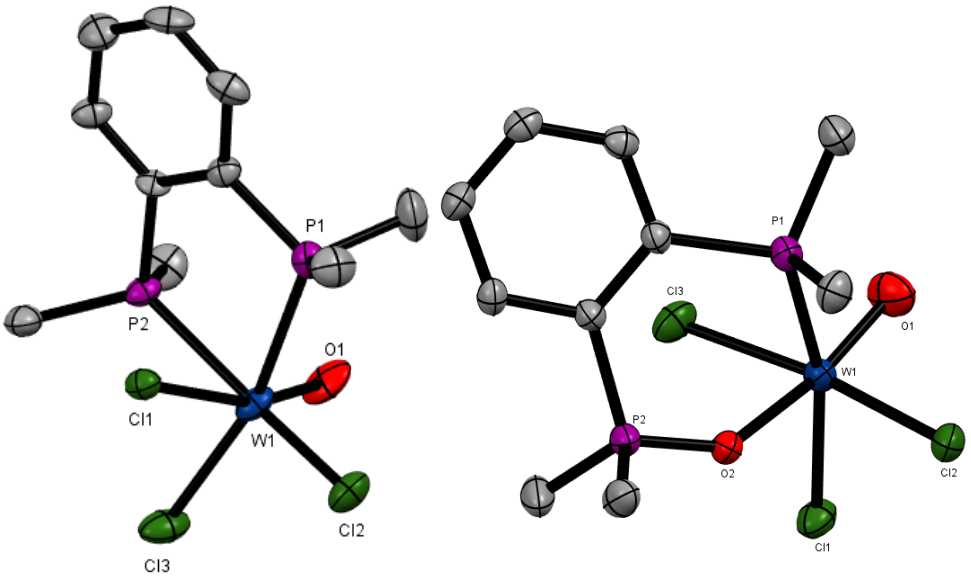

Figure 3.8: The structure of $[WOCl_3(o\text{-}C_6H_4(PMe_2)_2)]$ (left) and $[WOCl_3(o\text{-}C_6H_4(PMe_2)(P(O)Me_2))]\bullet 0.5CH_2Cl_2$ (right) showing the atom numbering scheme. Note that the axial O/Cl were disordered in $[WOCl_3(o\text{-}C_6H_4(PMe_2)_2)]$ and only the major form is shown. Ellipsoids shown at 50% probability, H atoms and solvent molecule are omitted for clarity.

$[WOCl_3(o\text{-}C_6H_4(PMe_2)_2)]$			
Bond Lengths/ Å		**Bond Angles/ °**	
W1-Cl	2.369(4) - 2.510(3)	Cl1-W1-O1	162.9(4)
W1-O1	1.72(1)	Cl2-W1-O1	101.8(4)
W1-P1	2.513(4)	Cl3-W1-O1	103.1(4)
W1-P2	2.509(4)		
$[WOCl_3(o\text{-}C_6H_4(PMe_2)(P(O)Me_2))]\cdot 0.5CH_2Cl_2$			
Bond Lengths/ Å		**Bond Angles/ °**	
W1-Cl	2.367(2) - 2.378(2)	Cl1-W1-O1	106.1(2)
W1-O1	1.702(6)	Cl2-W1-O1	95.1(2)
W1-P1	2.562(2)	Cl3-W1-O1	94.2(2)
W1-O_p	2.145(4)		

Table 3.2: Selected bond lengths and angles for $[WOCl_3(o\text{-}C_6H_4(PMe_2)_2)]$ and $[WOCl_3(o\text{-}C_6H_4(PMe_2)(P(O)Me_2))]\cdot 0.5CH_2Cl_2$.

Attempts to grow crystals of the green seven-coordinate complex, $[WOCl_4(o\text{-}C_6H_4(PMe_2)_2)]$, were unsuccessful due to poor solubility in organic solvents, however a few different crystals of previously unknown decomposition structures have been isolated. A yellow crystal was isolated and was identified as the tungsten(V) complex, $[WOCl_3(o\text{-}C_6H_4(PMe_2)_2)]$, which has previously been reported, but not structurally characterised (Figure 3.8).[37] The six-coordinate tungsten sits in a distorted octahedral environment with the ligand *trans* chlorine and with axial O/Cl disorder, modelled and refined with occupancies 0.17:0.83. In Chapter 2, a crystal of $[WOCl_3(dppmO_2)]$ was reported where the W=O bond was *trans* to the neutral ligand, the W=O bond lengths ($[WOCl_3(o\text{-}C_6H_4(PMe_2)_2]$ 1.72(1) Å, $[WOCl_3(dppmO_2)]$ 1.69(1) Å) are not significantly different.

A second, deep blue crystal was also isolated from a $[WOCl_4(o\text{-}C_6H_4(PMe_2)_2)]$ solution, this was also a tungsten(V) complex, $[WOCl_3(o\text{-}C_6H_4(PMe_2)(P(O)Me_2))]$ (Figure 3.8). The diphosphine monoxide ligand has not previously been identified, however the diphosphine dioxide *o*-$C_6H_4(P(O)Me_2)_2$ is known.[2,42] The oxygen is likely a result of trace hydrolysis or atmospheric O_2. The structure again shows the tungsten in a distorted octahedral geometry with *mer* chlorines, the W=O bond is *trans* to the phosphoryl oxygen as seen in $[WOCl_3(dppmO_2)]$. In $[WOCl_3(dppmO_2)]$ the W-O_p bond lengths are asymmetrical (2.022(2) Å and 2.323(2) Å) and are *trans* O/Cl, the W-O_p bond in $[WOCl_3(o\text{-}C_6H_4(PMe_2)(P(O)Me_2))]$ is 2.145(4) Å in between the W-O_p bond lengths for $[WOCl_3(dppmO_2)]$.

As previously stated, $[WOCl_4(o\text{-}C_6H_4(AsMe_2)_2)]$ is known, including structural characterisation.[31,41] The complex, $[WOCl_4(o\text{-}C_6H_4(AsPh_2)_2)]$ has also been reported, but with little characterisation.[38] In the present work, attempts to isolate $[WOCl_4(o\text{-}C_6H_4(PPh_2)_2)]$ with the weaker σ-phosphine ligand were unsuccessul.[32,37] The green solid isolated was clearly impure, shown by IR spectroscopy which revealed a large number of W-Cl stretches, while the $^{31}P\{^1H\}$ NMR spectrum

showed no resonances, suggesting the products may be paramagnetic (tungsten(V) or tungsten(IV)). The IR spectrum showed a single W=O stretch at 968 cm^{-1}, consistent with the W=O stretch for $[WOCl_3(o\text{-}C_6H_4(PPh_2)_2)]$ (965 cm^{-1})[37] and number of broad W-Cl stretches, suggesting multiple complexes present. Green crystals were isolated from a toluene solution and were identified as $[WCl_4(o\text{-}C_6H_4(PPh_2)_2)_2][WCl_6]\cdot 2.5C_7H_8$ (Figure 3.9), which could be one of the species in the original solid. The cation contains a tungsten(V) species and a $[W^VCl_6]^-$ anion.

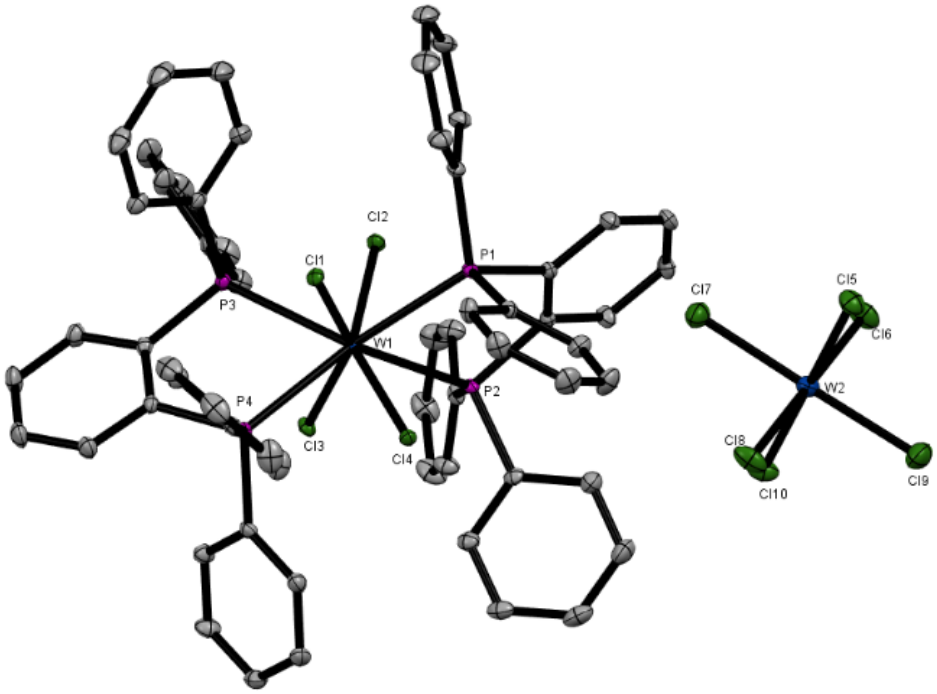

Figure 3.9: The structure of $[WCl_4(o\text{-}C_6H_4(PPh_2)_2)_2][WCl_6]\cdot 2.5(C_7H_8)$, showing the atom numbering scheme. Ellipsoids shown at 50% probability, the toluene solvent and H atoms omitted for clarity.

$[WCl_4(o\text{-}C_6H_4(PPh_2)_2)_2][WCl_6]\cdot 2.5(C_7H_8)$			
Bond Lengths/ Å		**Bond Angles/ °**	
W1-Cl_{Cation}	2.3877(6) – 2.4156(6)	Cl1-W1-Cl2	101.02(2)
W1-P	2.6424(5) – 2.6607(7)	Cl1-W1-Cl3	88.11(2)
W2-Cl_{Anion}	2.3162(5) – 2.3299(5)	Cl7-W1-Cl_{Axial}	89.81(2) – 90.24(2)

Table 3.3: Selected bond lengths and angles for $[WCl_4(o\text{-}C_6H_4(PPh_2)_2)_2][WCl_6]\cdot 2.5(C_7H_8)$.

The crystal structure of the cation is very similar to the $[WF_4(o\text{-}C_6H_4(AsMe_2)_2)_2]^{2+}$ cation with two chelating ligands and in the chloride system the monocationic charge indicates reduction of the tungsten(VI) to tungsten(V). Both species have a dodecahedral cation and $[WCl_4(o\text{-}C_6H_4(PPh_2)_2)_2][WCl_6]\cdot 2.5(C_7H_6)$ has an octahedral W(V) anion.

It appears there is quite different affinity for Me-substituted ligands *verses* the Ph-substituted analogues; the methyl ligands form more stable complexes and are less likely to reduce the tungsten centre due to the pre-defined chelation and its stronger σ-donor capacity. As well as being

poorer donors, the Ph-substituted ligands also increase the steric bulk around the metal centre. This trend also suggests the reported [$WOCl_4$(*o*-$C_6H_4(AsPh_2)_2$)][38] complex likely does not form and potentially could be a lower oxidation state species, especially as there is no NMR data reported.

The complexes [$WSCl_4$(*o*-$C_6H_4(EMe_2)_2$)] (E = P or As) were made in an analogous way to the oxido complexes using toluene. Attempts in CH_2Cl_2 produced impure products, apparently encouraging chlorination of the ligands, particularly with *o*-$C_6H_4(AsMe_2)_2$, and therefore potentially reduction of the tungsten. Both sulfide-chloride complexes are significantly less stable, especially in solution, than their oxido counterparts, [$WSCl_4$(*o*-$C_6H_4(AsMe_2)_2$)] considerably so.

All data collected for [$WSCl_4$(*o*-$C_6H_4(EMe_2)_2$)] were consistent with seven-coordinate tungsten(VI) complexes, including elemental analysis. The IR spectra showed W=S stretches at ~550 cm^{-1}, lower than in six-coordinate analogues (Chapter 2 and 4), suggesting a higher coordination number. The $^{31}P\{^1H\}$ NMR spectrum for [$WSCl_4$(*o*-$C_6H_4(PMe_2)_2$)] shows a single resonance at +74.8 ppm, the same shift as [$WOCl_4$(*o*-$C_6H_4(PMe_2)_2$)], suggesting the chalcogen has little effect on the deshielding on the ^{31}P nuclei, not surprising as the chalcogen is axial to the pnictine ligand.

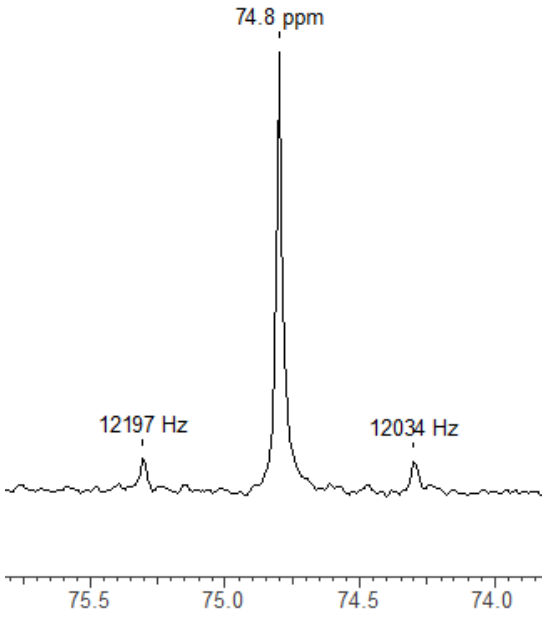

Figure 3.10: $^{31}P\{^1H\}$ NMR spectrum of [$WSCl_4$(o-$C_6H_4(PMe_2)_2$)] in CD_2Cl_2.

Once again, a large coordination shift is observed, this is exaggerated by the formation of a five-membered ring upon coordination.[43] Coupling between ^{31}P and ^{183}W is seen with a similar large coupling constant to that in the oxido-complex, 168 Hz, confirming coordination between $WSCl_4$ and the phosphine ligand. Red crystals were isolated from a toluene solution and identified as [$WSCl_4$(*o*-$C_6H_4(PMe_2)_2$)] (Figure 3.11), showing a pentagonal bipyramidal geometry as seen in [$WOCl_4$(*o*-$C_6H_4(AsMe_2)_2$)].

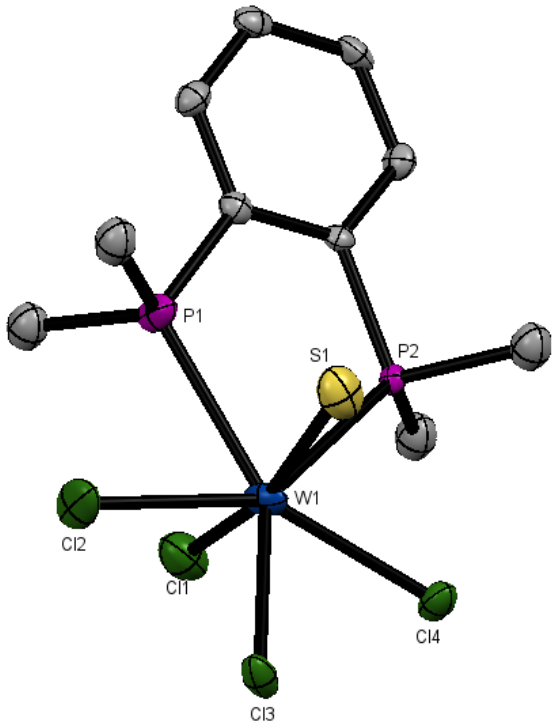

Figure 3.11: The structure of [$WSCl_4(o\text{-}C_6H_4(PMe_2)_2)$] showing the atom numbering scheme. Ellipsoids shown at 50% probability, H atoms are omitted for clarity. Note that the axial S/Cl were disordered, which was modelled as split sites and refined to occupancies of 0.29 : 0.71. Only the major form is shown.

[$WSCl_4(o\text{-}C_6H_4(PMe_2)_2)$]			
Bond Lengths/ Å		**Bond Angles/ °**	
W1-Cl	2.36(1) – 2.439(6)	Cl2-W1-S1	107.9(3)
W1-S1	2.12(1)	Cl3-W1-S1	100.4(3)
W1-P1	2.614(6)	Cl1-W1-S1	87.6(3)
W1-P2	2.595(6)		

Table 3.4: Selected bond lengths and angles for [$WSCl_4(o\text{-}C_6H_4(PMe_2)_2)$].

The complexes, [$WSCl_4(o\text{-}C_6H_4(PMe_2)_2)$] and [$WOCl_4(o\text{-}C_6H_4(AsMe_2)_2)$], are isomorphous and both exhibit axial disorder, which is also seen in [$WOF_4(o\text{-}C_6H_4(PMe_2)_2)$].[11] During multiple attempts to grow crystals, a small number of some tungsten(V) crystals were also isolated, including, [$WCl_4(o\text{-}C_6H_4(PMe_2)_2)_2$][$WS_{0.5}O_{0.5}Cl_4$] - there is some O/S disorder in the anion, but the structure of the cation is robust and not in doubt.

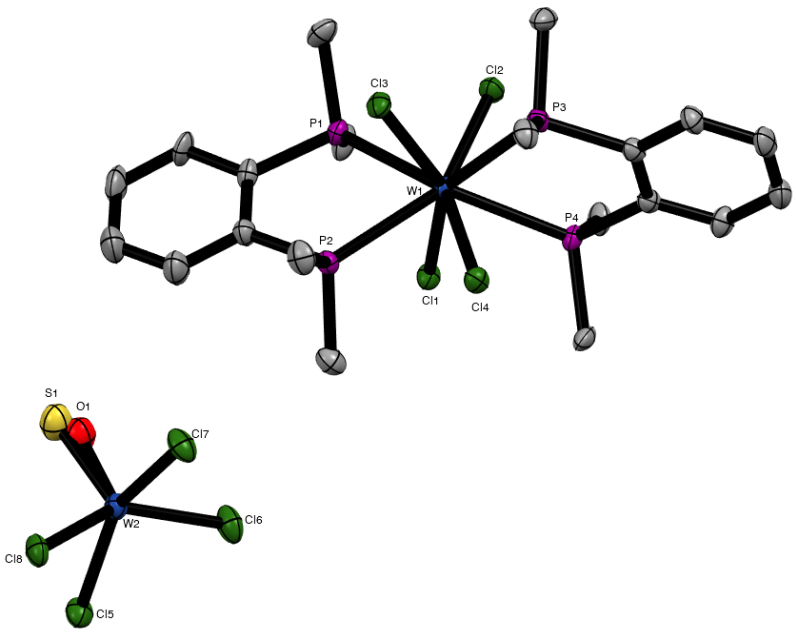

Figure 3.12: The structure of $[WCl_4(o\text{-}C_6H_4(PMe_2)_2)_2][WS_{0.5}O_{0.5}Cl_4]$ showing the atom numbering scheme. Ellipsoids shown at 50% probability, H atoms are omitted for clarity. Note that the S/O on the anion were disordered which was modelled as split sites and refined to occupancies of 0.5 : 0.5. Both forms are shown.

$[WCl_4(o\text{-}C_6H_4(PMe_2)_2)_2][WS_{0.5}O_{0.5}Cl_4]$			
Bond Lengths/ Å		**Bond Angles/ °**	
W1-Cl_{Cation}	2.428(2) – 2.439(3)	Cl-W1-Cl2	94.33(8)
W1-P1	2.593(3)	Cl1-W1-Cl3	144.34(9)
W1-P2	2.589(2)	Cl1-W1-Cl4	95.49(8)

Table 3.5: Selected bond lengths and angles for $[WCl_4(o\text{-}C_6H_4(PMe_2)_2)_2][WS_{0.5}O_{0.5}Cl_4]$.

This structure is similar to that of $[WCl_4(o\text{-}C_6H_4(PPh_2)_2)_2][WCl_6]\cdot 2.5(C_7H_8)$ showing a dodecahedral cation and a singly charged anion. There is little difference in W-Cl_{Cation} bond lengths between the structures. The W-P bond lengths are slightly shorter in the methyl-diphosphine complex (~2.59 Å) compared to that of the phenyl-substituted ligand (~2.65 Å) probably due to the phenyl ligand (o-$C_6H_4(PPh_2)_2$) being more sterically demanding and a poorer σ-donor. In the fluoride analogue, $[WF_4(o\text{-}C_6H_4(PMe_2)_2)_2][WOF_5]$, the W-P bonds are ~2.58 Å, slightly shorter than in the chloro analogue (although the fluoro species is in the W(VI) oxidation state), but both are significantly shorter than in $[WF_4(o\text{-}C_6H_4(PPh_2)_2)_2]^+$.[8]

The complex, $[WSCl_4(o\text{-}C_6H_4(AsMe_2)_2)]$, behaves in a very similar fashion to the other compounds in this series, but is the most unstable in solution. Spectroscopic data suggest the ligand readily chlorinates or most readily reduces the metal centre and the complex was the most difficult to isolate cleanly. Attempts to grow crystals of $[WSCl_4(o\text{-}C_6H_4(AsMe_2)_2)]$ failed as the compound was only slightly soluble and its longevity is poor in solution. However, some orange crystals were collected which showed a tungsten(V) species, which showed the cation $[WCl_4(o\text{-}C_6H_4(AsMe_2)_2)_2]^+$, a number of crystals were isolated and they all showed a large amount of disorder in the anion, so a definitive assignment could not be made. The cation structure is not in

doubt and has been repeatedly identified, although bond lengths cannot be compared due to the rather poor-quality data. The structure of the cation is very similar to the fluoro analogue, $[WF_4(o\text{-}C_6H_4(AsMe_2)_2)_2]^{2+}$, although the latter contains tungsten(VI).

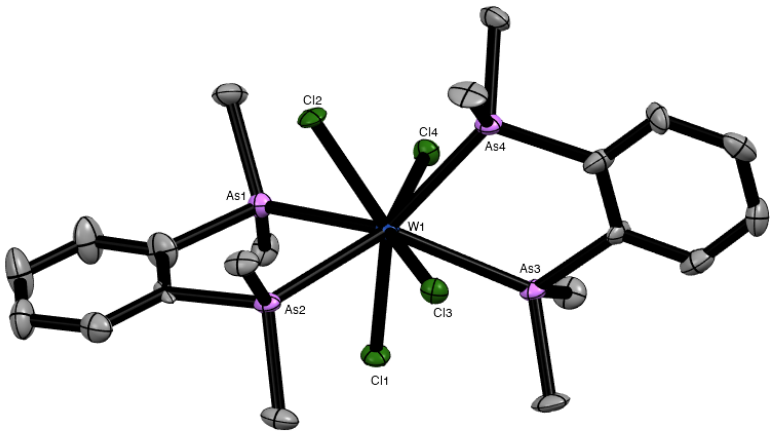

Figure 3.13: The structure of $[WCl_4(o\text{-}C_6H_4(AsMe_2)_2)_2]^+$ showing the atom numbering scheme. Ellipsoids shown at 50% probability, H atoms and disordered anion are omitted for clarity.

During the repeated attempts to isolate crystals of $[WSCl_4(o\text{-}C_6H_4(AsMe_2)_2)]$ a few crystals of an ionic bridged species were isolated. The bridging atoms are most likely S^{2-}, rearrangement from $WSCl_4$, however they could also be Cl^- ions. The anion is likely $[WSCl_5]^{2-}$ or $[WCl_6]^{2-}$ therefore the cation is either sulfur bridged and both the cation and anion would be tungsten(V). Alternatively, the dimer could be chloride bridged making the cation tungsten(IV) and mixed valance which is less likely. A similar structure, $[(WCl_2)_2(\mu\text{-}E)_2(^iPrS(CH_2)_2S^iPr)][WSCl_5]\bullet CH_2Cl_2$ has been reported in Chapter 4, there is no ambiguity that the anion is $[WSCl_5]^{2-}$ and it is highly likely that this is the anion here. Unfortunately, due to similar W-Cl and W=S bond lengths they cannot be distinguished from each other in this structure due to high symmetry.

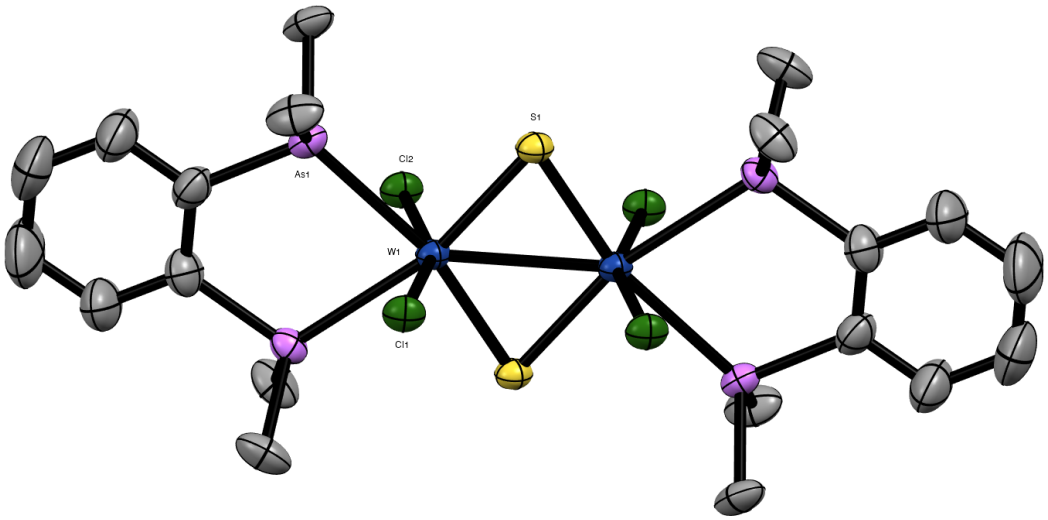

Figure 3.14: The structure of $[(WCl_2)_2(\mu\text{-}S)_2(o\text{-}C_6H_4(AsMe_2)_2)_2][WCl_6]\bullet CH_2Cl_2$ showing the atom numbering scheme. Ellipsoids shown at 50% probability, H atoms and anion are omitted for clarity.

3.3.2 Reactions with Other Phosphine and Arsine Donors

Following the successful isolation of [$WOCl_4$(*o*-$C_6H_4(EMe_2)_2$)] and [$WSCl_4$(*o*-$C_6H_4(EMe_2)_2$)] (E = P or As), other tertiary phosphine and arsine ligands were attempted (PMe_3, $AsEt_3$ and dmpe). The flexible ligand dmpe was used to try and isolate [$WOCl_4$(dmpe)] or [$(WOCl_4)_2$(dmpe)], but no clean products could be isolated. There was no evidence of the formation of the bridged dimer when using 1:2 metal to ligand.

A short investigation into tertiary alkyl substituted phosphine and arsine ligands was undertaken, all reactions were carried out with a 1:1 metal to ligand ratio to attempt to isolate [$WECl_4(E'R_3)$] (E' = P or As, E = O or S and R = Me or Et). Spectroscopic data for $WECl_4$ and PMe_3 attempts does not support this conclusion. Attempts with both $WOCl_4$ and $WSCl_4$ show a sharp resonance in the $^{31}P\{^1H\}$ NMR spectra at ~+92 ppm, this could be attributed to Me_3PCl_2 and is much higher than expected resonance, ([$WOF_4(PMe_3)$], ∂ = +44.8 ppm).[11,44]

The attempts to isolate [$WECl_4(AsEt_3)$] were equally unsuccessful, both showed evidence of Et_3AsCl_2 in the ^1H NMR spectra.[45] The reaction with $WOCl_4$ seemed to show a mixture of products, there is a strong stretch at 857 cm^{-1} which can be tentatively assigned to a coordinated As=O stretch suggesting chalcogen abstraction or a tungsten-oxide bridge.[46-48] In the IR spectra from $WSCl_4$ and $AsEt_3$, there is no evidence of any W=S stretch and there is a stretch at 422 cm^{-1} which can be tentatively assigned to coordinated As=S.[49,50] Since arsine ligands are soft and poor σ-donors failure is not unexpected, especially considering [$WECl_4$(*o*-$C_6H_4(AsMe_2)_2$)] are not that stable. Although it should be noted that $AsEt_3$ formed complexes with WF_6 although it is much harder to reduce and a better Lewis acceptor.[8]

3.4 Conclusions

The main aim of the chapter was to continue the chemistry of tungsten(VI) oxo- and thio-tetrachlorides and develop a short series of neutral phosphine and arsine complexes under mild and ambient conditions. All compounds isolated were extremely hydrolytically unstable and were handled and stored under anhydrous conditions at all stages. Four examples of rare seven-coordinate complexes have been isolated and all fully characterised; two have been structurally characterised revealing pentagonal bipyramidal geometries. A number of W(V) reduction products have also been structurally characterised, including cationic salts and compared to the products of the failed attempt to isolate $[WOCl_4(o\text{-}C_6H_4(PPh_2)_2)]$ and known $[WF_4(o\text{-}C_6H_4(EMe_2)_2)_2]^{n+}$ species.

A small number of other complexes with the ligands PMe_3, dmpe and $AsEt_3$ were also attempted, but proved unsuccessful, with some side products shown to be chlorinated ligand and potentially some tungsten(V) reduction species. Spectroscopic data also showed chalcogen abstraction by the ligands to form possible reduced species. The reaction with $WOCl_4$ and PMe_3 showed that the complex $[WOCl_4(PMe_3)_2]$ could potentially be formed under the right conditions but is likely to be extremely sensitive to trace moisture.

3.5 Experimental

Syntheses were performed by using standard Schlenk and glove-box techniques under a dry N_2 atmosphere. Solvents were dried by distillation from CaH_2 (CH_2Cl_2) or Na/benzophenone ketyl (toluene, n-hexane). $AsEt_3$, 1,2-bis(dimethylphosphine)ethane and PMe_3 obtained from Strem and used as received. *o*-phenylenebis(diphenylphosphine) from Sigma-Aldrich and dried by heating *in vacuo* before use. *o*-phenylenebis(dimethylarsine) and *o*-phenylenebis(dimethylphosphine) were prepared *via* the literature methods,[51,52] and $WSCl_4$ and $WOCl_4$ were prepared *via* literature methods.[53,54] For further details regarding the instrumentation see Appendix A.

[$WOCl_4$(o-C_6H_4($AsMe_2$)$_2$)]

o-phenylenebis(dimethylarsine) (0.083 g, 0.29 mmol) in dichloromethane (2 mL) was added slowly to a solution of $WOCl_4$ (0.100 g, 0.29 mmol) in dichloromethane (4 mL). The solution was allowed to stir for 1 h., concentrated *in vacuo* to 2 mL, the green precipitate was filtered and dried *in vacuo.* Yield: 0.90 g, 49 %. Required for $C_{10}H_{16}As_2Cl_4OW$ (627.73): C: 19.13, H: 2.57 %. Found: C: 19.02, H: 2.46 %. IR spectrum (Nujol, ν / cm^{-1}): 955s W=O, 332s W-Cl. ^{1}H NMR (CD_2Cl_2): δ = 7.86 (m, [H], aromatic CH), 7.74 (m, [H], aromatic CH), 2.51 (s, [3H], CH_3), 2.42 (s, [3H], CH_3).

[$WSCl_4$(o-C_6H_4($AsMe_2$)$_2$)]

o-phenylenebis(dimethylarsine) (0.080 g, 0.28 mmol) in dichloromethane (2 mL) was added slowly to a solution of $WSCl_4$ (0.100 g, 0.28 mmol) in dichloromethane (4 mL). The solution was allowed to stir for 1 h., concentrated *in vacuo* to 2 mL, the red/brown precipitate was filtered and dried *in vacuo.* Yield: 0.230 g, 81 %. Required for $C_{10}H_{16}Cl_4As_2SW$ (643.79): C: 18.66, H: 2.50 %. Found: C: 18.52, H: 2.47 %. IR spectrum (Nujol, ν / cm^{-1}): 548s W=S, 330s W-Cl. ^{1}H NMR (CD_2Cl_2): δ = 7.71 (m, [2H], aromatic CH), 2.73 (s, [3H], CH_3), 2.39 (s, [3H], CH_3).

[$WOCl_4$(o-C_6H_4(PMe_2)$_2$)]

o-phenylenebis(dimethylphosphine) (0.087 g, 0.44 mmol) in dichloromethane (2 mL) added slowly to a solution of $WOCl_4$ (0.150 g, 0.42 mmol) in dichloromethane (4 mL). The solution was allowed to stir for 1 h., concentrated *in vacuo* to 2 mL, the green precipitate was filtered and dried *in vacuo* Yield: 0.170 g, 71 %. Required for $C_{10}H_{16}Cl_4OP_2W$ (539.83): C: 22.25, H: 2.99 %. Found: C: 22.31, H: 3.16 %. IR spectrum (Nujol/ cm^{-1}): 954s W=O, 319s, 302s W-Cl.^{1}H NMR (CD_2Cl_2): δ = 7.95 – 7.51 (m, [2H], aromatic CH), 2.61 (t, [3H], $^2J+^5J_{HH}$ = 8 Hz, CH_3), 2.53 (m, [3H] $^2J+^5J_{HH}$ = 8 Hz, CH_3). $^{31}P\{^1H\}$ NMR (CD_2Cl_2): +74.8 (s, $^1J_{WP}$ = 173 Hz).

[$WSCl_4$(o-C_6H_4(PMe_2)$_2$)]

o-phenylenebis(dimethylphosphine) (0.083 g, 0.42 mmol) in dichloromethane (2 mL) added slowly to a solution of $WSCl_4$ (0.150 g, 0.42 mmol) in dichloromethane (4 mL). The solution was allowed to stir for 1 h., concentrated *in vacuo* to 2 mL, the red/brown precipitate was filtered and dried *in*

vacuo. Yield: 0.172 g, 74 %. Required for $C_{10}H_{16}Cl_4P_2SW$ (555.90): C: 21.61, H: 2.90 %. Found: C: 21.72, H: 2.99 %. IR spectrum (Nujol, ν / cm^{-1}): 561s W=S, 313s, 297s W-Cl. ^1H NMR (CD_2Cl_2): δ = 8.92 (br, [H], aromatic CH), 8.72 (br [H], aromatic CH), 2.62 (m, [3H], CH_3), 2.54 (m, [3H], CH_3). $^{31}P\{^1H\}$ NMR (CD_2Cl_2): +74.8 (s, $^1J_{WP}$ = 168 Hz).

The products isolated from the following reactions were not satisfactorily characterised (see above) but are reported for completeness of work.

Reaction of $WOCl_4$ and PMe_3

A solution of trimethylphosphine (0.034 g, 0.44 mmol) in CH_2Cl_2 (5 mL) was added slowly to a suspension of $WSCl_4$ (0.150 g, 0.44 mmol) in CH_2Cl_2 (5 mL). The cherry red solution was then stirred for 1 h., concentrated to ~ 3 mL, filtered, and the red sticky solid dried *in vacuo.* IR spectrum (Nujol, ν / cm^{-1}): 954s, 898s br W=O, 351s W-Cl. ^1H NMR (CD_2Cl_2): δ = 2.54 (s, br), 1.94 (s, br). $^{31}P\{^1H\}$ NMR (CD_2Cl_2): +93.12 (s).

Reaction of $WSCl_4$ and PMe_3

A solution of trimethylphosphine (0.032 g, 0.42 mmol) in CH_2Cl_2 (5 mL) was added slowly to a suspension of $WOCl_4$ (0.150 g, 0.42 mmol) in CH_2Cl_2 (5 mL). The brown solution was then stirred for 1 h., concentrated to ~ 3 mL, filtered, and the brown solid dried *in vacuo.* IR spectrum (Nujol, ν / cm^{-1}): 528m, br W=S, 314s W-Cl. $^{31}P\{^1H\}$ NMR (CD_2Cl_2): +91.61 (s).

Reaction of $WOCl_4$ and dmpe

A solution of dmpe (0.033 g, 0.22 mmol) in CH_2Cl_2 (5 mL) was added slowly to a suspension of $WOCl_4$ (0.150 g, 0.44 mmol) in CH_2Cl_2 (5 mL). The orange solution was then stirred for 1 h., concentrated to ~ 3 mL, filtered, and the orange solid dried *in vacuo.* IR spectrum (Nujol, ν / cm^{-1}): 950s, 894s br W=O, 350s W-Cl. ^1H NMR (CD_2Cl_2): δ = 2.35 (s, br), 1.26 (s). $^{31}P\{^1H\}$ NMR (CD_2Cl_2): +74.4 (s).

Reaction of $WOCl_4$ and $AsEt_3$

A solution of triethylarsine (0.071 g, 0.44 mmol) in toluene (5 mL) was added slowly to a suspension of $WOCl_4$ (0.150 g, 0.44 mmol) in toluene (5 mL). The dark green solution was then stirred for 1 h., concentrated to ~ 3 mL, filtered, and the green solid dried *in vacuo.* IR spectrum (Nujol, ν / cm^{-1}): 956s W=O, 857s, br As=O, 349s, 334s W-Cl. ^1H NMR (CD_2Cl_2): δ = 3.03 (s, br), 1.63 (s).

Reaction of $WSCl_4$ and $AsEt_3$

A solution of triethylarsine (0.068 g, 0.42 mmol) in toluene (5 mL) was added slowly to a suspension of $WSCl_4$ (0.150 g, 0.42 mmol) in toluene (5 mL). The dark brown solution was then stirred for 1 h., concentrated to ~ 3 mL, filtered, and the dark brown solid dried *in vacuo*. IR spectrum (Nujol, ν / cm^{-1}): 422m, br As=S, 303s W-Cl. ^1H NMR (C_6D_6): δ = 2.68 (q, [2H], J_{HH} 7.7 Hz, CH_2), 1.2 (t, [3H], J_{HH} 7.6 Hz, CH_3).

3.5.1 Crystallographic Tables

Compound	[$WOCl_4$(o-$C_6H_4(AsMe_2)_2$)]	[$WSCl_4$(o-$C_6H_4(PMe_2)_2$)]	[$WOCl_3$(o-$C_6H_4(PMe_2)_2$)]
Formula	$C_{10}H_{16}As_2Cl_4OW$	$C_{10}H_{16}Cl_4P_2SW$	$C_{10}H_{16}Cl_3OP_2W$
M	627.72	555.88	504.37
Crystal system	Orthorhombic	Orthorhombic	Orthorhombic
Space group (no)	Pbca (61)	Pbca (61)	$P2_12_12_1$ (19)
a /Å	15.6918(3)	13.1473(4)	16.4487(3)
b /Å	13.7435(2)	15.8140(5)	13.9540(2)
c /Å	15.9443(3)	16.1052(6)	14.4660(2)
α /°	90	90	90
β /°	90	90	90
γ /°	90	90	90
U /$Å^3$	3438.55(10)	3348.48(19)	3320.31(9)
Z	8	8	8
μ(Mo-$K_α$) /mm^{-1}	1.114	7.834	7.617
F(000)	2336.0	2112.0	1912.0
Total number reflns	70940	27246	37813
R_{int}	0.0739	0.0562	0.0695
Unique reflns	5431	5218	9786
No. of params, restraints	194/132	165/18	325/20
GOF	1.275	1.091	1.050
R_1, wR_2 [$I > 2σ(I)$][b]	0.0510, 0.0794	0.0582, 0.1073	0.0657, 0.1512
R_1, wR_2 (all data)[b]	0.0596, 0.0814	0.0843, 0.1137	0.0812, 0.1613

Table 3.6: X-ray crystallography table. a: common data: wavelength (Mo-$K_α$) = 0.71073 Å; θ(max) = 27.5°; [b] $R_1 = Σ||Fo|-|Fc||/Σ|Fo|$; $wR_2=[Σw(Fo^2-Fc^2)^2/ΣwFo^4]^{1/2}$

Compound	$[WOCl_3(o\text{-}C_6H_4(PMe_2)(P(O)Me_2))]\cdot 0.5CH_2Cl_2$	$[WCl_4(o\text{-}C_6H_4(PPh_2)_2)_2][WCl_6]\cdot 2.5(C_7H_8)$	$[WCl_4(o\text{-}C_6H_4(PMe_2)_2)_2][WS_{0.5}O_{0.5}Cl_4]$
Formula	$C_{10.5}H_{17}Cl_4O_2P_2W$	$C_{77.5}H_{68}Cl_{10}P_4W_2$	$C_{20}H_{32}Cl_8O_{0.5}P_4S_{0.5}W_2$
M	562.83	1845.40	1071.66
Crystal system	Orthorhombic	Monoclinic	Triclinic
Space group (no)	Pbcn (60)	$P2_1/c$ (14)	$P\bar{1}$ (2)
a /Å	15.5425(2)	12.68450(10)	12.0846(4)
b /Å	17.6076(2)	22.62209(2)	12.4096(5)
c /Å	13.1080(2)	26.0710(2)	13.1385(4)
α /°	90	90	112.547(4)
β /°	90	100.0200(10)	107.746(3)
γ /°	90	90	99.743(3)
U /Å^3	3587.22(8)	7366.57(11)	1638.89(11)
Z	8	4	2
μ(Mo-K_α) /mm^{-1}	7.210	3.614	7.907
F(000)	2144.0	3644.0	1016.0
Total number reflns	38057	203082	35281
R_{int}	0.0567	0.0271	0.0631
Unique reflns	5453	23949	9848
No. of params, restraints	181/0	877/122	327/0
GOF	1.110	1.027	1.050
R_1, wR_2 [I > 2σ(I)][b]	0.0565, 0.1146	0.0196, 0.0370	0.0674, 0.1460
R_1, wR_2 (all data)[b]	0.0622, 0.1175	0.0250, 0.0381	0.0795, 0.1515

Table 3.6: Continued.

3.6 References

(1) Burt, J.; Levason, W.; Reid, G. *Coord. Chem. Rev.,* **2014,** *260*, 65-115
(2) Davis, M. F.; Levason, W.; Reid, G.; Webster, M. *Polyhedron,* **2006,** *25*, 930-36
(3) McAuliffe, C. A. *Comprehensive Coordination Chemistry I,* **1987,** *2*, 989-1066
(4) Kendall, A. J.; Tyler, D. R. *Dalton Trans.,* **2015,** *44*, 12473-83
(5) Arnaudet, L.; Bougon, R.; Ban, B.; Charpin, P.; Isabey, J.; Lance, M.; Nierlich, M.; Vigner, J. *Can. J. Chem.,* **1990,** *68*, 507-12
(6) Arnaudet, L.; Bougon, R.; Buu, B.; Lance, M.; Nierlich, M.; Thuéry, P.; Vigner, J. *J. Fluorine. Chem.,* **1995,** *71*, 123-29
(7) Greenacre, V. K.; Hector, A. L.; Levason, W.; Reid, G.; Smith, D. E.; Sutcliffe, L. *Polyhedron,* **2019,** *162*, 14-19
(8) Levason, W.; Monzittu, F. M.; Reid, G.; Zhang, W. *Chem. Commun.,* **2018,** *54*, 11681-84
(9) Crans, D. C.; Smee, J. J. *Comprehensive Coordination Chemistry II,* **2004,** *4*, 175-239
(10) Rice, D. A. *Coord. Chem. Rev.,* **1982,** *45*, 87-103
(11) Emsley, J. W.; Levason, W.; Reid, G.; Zhang, W.; De Luca, G. *J. Fluorine. Chem.,* **2017,** *197*, 74-79
(12) Young, C. G. *Comprehensive Coordination Chemistry II,* **2004,** *4*, 415-527
(13) Benjamin, S. L.; Levason, W.; Reid, G. *Chem. Soc. Rev.,* **2013,** *42*, 1460-99
(14) El-Kurdi, S.; Al-Terkawi, A.-A.; Schmidt, B. M.; Dimitrov, A.; Seppelt, K. *Chem. Eur. J.,* **2010,** *16*, 595-99
(15) Levason, W.; Monzittu, F. M.; Reid, G. *Coord. Chem. Rev.,* **2019,** *391*, 90-130
(16) Giese, S.; Seppelt, K. *Angew. Chem. Int. Ed.,* **1994,** *33*, 461-63
(17) Levason, W.; Monzittu, F. M.; Reid, G.; Zhang, W.; Hope, E. G. *J. Fluorine. Chem.,* **2017,** *200*, 190-97
(18) Butcher, R. J.; Penfold, B. R.; Sinn, E. *J. Chem. Soc., Dalton Trans.,* **1979**, 668-75
(19) Kergoat, R.; Calves, J. Y.; E, G. J.; Lenzi, M. *Compt. Rend., Ser. C* **1971,** *276*, 306-10
(20) Buslaey, Y. A.; Petrosyants, S. P. *Zh. Neorg. Khim.,* **1971,** *16*, 1330-34
(21) Wang, G.; Chen, G.; Luck, R. L.; Wang, Z.; Mu, Z.; Evans, D. G.; Duan, X. *Inorg. Chim. Acta,* **2004,** *357*, 3223-29
(22) Sens, I.; Stenger, H.; Mller, U.; Dehnicke, K. *Z. anorg. allg. Chem.,* **1992,** *610*, 117-20
(23) Arnaiz, F. J.; Aguado, R.; Martinez de Ilarduya, J. M. *Polyhedron,* **1994,** *13*, 3257-59
(24) Davis, M. F.; Levason, W.; Ratnani, R.; Reid, G.; Rose, T.; Webster, M. *Eur. J. Inorg. Chem.,* **2007**, 306-13
(25) Levason, W.; Reid, G.; Zhang, W. *J. Fluorine. Chem.,* **2016,** *184*, 50-57
(26) Davis, M. F.; Levason, W.; Light, M. E.; Ratnani, R.; Reid, G.; Saraswat, K.; Webster, M. *Eur. J. Inorg. Chem.,* **2007,** *13*, 1903-10
(27) Edwards, D. A. *J. Inorg. Nucl. Chem.,* **1965,** *27*, 303-07
(28) Saha, H. K.; Ray Chaudhuri, T. K. *J. Inorg. Nucl. Chem.,* **1977,** *39*, 698-700
(29) Butcher, A. V.; Chatt, J. *J. Chem. Soc. A,* **1971**, 2356-58
(30) Limberg, C.; Büchner, M.; Heinze, K.; Walter, O. *Inorg. Chem.,* **1997,** *36*, 872-79
(31) Blight, D. G.; Kepert, D. L.; Mandyczewsky, R.; Trigwell, K. R. *J. Chem. Soc., Dalton Trans.,* **1972**, 313-16
(32) Levason, W.; McAuliffe, C. A.; Sayle, B. J. *J. Chem. Soc., Dalton Trans.,* **1976**, 1177-81
(33) Levason, W.; McAuliffe, C. A.; McCullough, F. P. *Inorg. Chim. Acta,* **1977,** *24*, L13-L14
(34) Chow, K. K.; McAuliffe, C. A. *Inorg. Chim. Acta,* **1974,** *10*, 197-202
(35) Carmichael, W. M.; Edwards, D. A. *J. Inorg. Nucl. Chem.,* **1968,** *30*, 2641-46
(36) Lewis, J.; Whyman, R. *J. Chem. Soc.,* **1965**, 6027-31
(37) Levason, W.; McAuliffe, C. A.; McCullough, F. P. *Inorg. Chem.,* **1977,** *16*, 2911-16
(38) Agh-Atabay, N.; Ashmawy, F. M.; McAuliffe, C. A.; Hill, W. E. *Inorg. Chim. Acta,* **1985,** *104*, 73-76
(39) Fowles, G. W. A.; Frost, J. L. *J. Chem. Soc. A,* **1967**, 671-75
(40) Britnell, D.; Fowles, G. W. A.; Rice, D. A. *J. Chem. Soc., Dalton Trans.,* **1975**, 213-15
(41) Drew, M. G. B.; Mandyczewsky, R. *J. Chem. Soc. D,* **1970**, 292-93
(42) Gray, B. M.; Hector, A. L.; Levason, W.; Reid, G.; Webster, M.; Zhang, W.; Jura, M. *Polyhedron,* **2010,** *29*, 1630-38
(43) Garrou, P. E. *Chem. Rev.,* **1981,** *81*, 229-66
(44) Godfrey, S. M.; McAuliffe, C. A.; Pritchard, R. G.; Sheffield, J. M.; Thompson, G. M. *J. Chem. Soc., Dalton Trans.,* **1997**, 4823-28

(45) Verdonck, L.; Van Der Kelen, G. P. *Spectrochim. Acta A,* **1977,** *33*, 601-05
(46) Merijanian, A.; Zingaro, R. A. *Inorg. Chem.,* **1966,** *5*, 187-91
(47) Horner, S. M.; Tyree, S. Y. *Inorg. Chem.,* **1962,** *1*, 122-27
(48) Horner, S. M.; Tyree, S. Y. *Inorg. Chem.,* **1963,** *2*, 568-71
(49) Ablonin, B. E.; Lokhot-Skaya, L. A.; Shagidullin, R. R. *Zh. Obshch. Khim.,* **1991,** *61*, 1150 - 54
(50) Il'in, E. G.; Ignatov, M. E.; Buslaev, Y. A. *Dokl. Akad. Nauk SSSR,* **1979,** *247*, 113 - 15
(51) Feltham, R. D.; Kasenally, A.; Nyholm, R. S. *J. Organomet. Chem.,* **1967,** *7*, 285-88
(52) Kyba, E. P.; Liu, S. T.; Harris, R. L. *Organomet.,* **1983,** *2*, 1877-79
(53) Gibson, V. C.; Kee, T. P.; Shaw, A. *Polyhedron,* **1990,** *9*, 2293-98
(54) Dietz, S.; Allured, V.; DuBois, M. R. *Inorg. Chem.,* **1993,** *32*, 5418-20

Coordination Chemistry of $WOCl_4$, $WSCl_4$ and $WSCl_3$ with Neutral Sulfur and Selenium Donor Ligands

4.1 Introduction

In recent years there has been increasing interest in the development of early transition metal dichalcogenide semiconductor thin films, ME_2 (E = S, Se or Te) as discussed in Chapter 1; new methods to grow these films are becoming ever more important given their wide-ranging technological applications (Section 1.5). Chemical vapour deposition (CVD) is a versatile and cheap method for accessing a variety of these thin films. The primary focus of this chapter is to establish a systematic series of novel chalcogenoether complexes of tungsten(VI), to study the behaviour between the soft thio- and seleno-ether ligands and the hard tungsten(VI) centre. Complexes with suitable ligands will be identified as potential precursors for the production of WS_2 thin films *via* chemical vapour deposition. This chapter details the synthesis and characterisation of these complexes and the comparison between similar high oxidation state transition metal complexes.

4.2 Early Transition Metal Coordination Chemistry with Chalcogenoethers

Examples of soft donor coordination with high oxidation state early transition metals are less ubiquitous than their hard donor counterparts, as previously described (see Chapter 2). Properties of transition metal compounds that contain soft Group XVI donor ligands (thio-, seleno- or telluro-ethers) can differ quite drastically from hard donor and even phosphine donor complexes.[1] Due to the sporadic and limited reports of chalcogenoether complexes with high valent with Group VI metals, it is necessary to compare a range of early metals in a variety of oxidation states (including $W^{VI/\,V/\,IV}$, $Mo^{VI/\,V/\,IV}$, Ta^{V} and $Nb^{IV/V}$). All these high valent hard metal-soft donor systems are prone to both oxidation of the ligand and hydrolysis with adventitious water,[2-4] therefore the use of rigorously dried solvents and inert atmosphere is vital.

There is a large body of work on soft donor interactions with some high valent early transition metals, including TiX_4 (X = Cl, Br or I)[5,6] and MX_4 (M = Zr or Hf; X = Cl or Br)[7] and MX_5 (M = Nb or Ta; X = F, Cl or Br) discussed below. General trends show there are significant differences between the fluoride complexes and those of the other halides, with the fluoride analogues being difficult to isolate due to instability or strong fluoride bridges in the parent metal fluorides. The hard Lewis acidic nature of the metal fluorides means that efforts to make complexes with soft chalcogenoether donors is challenging, with many attempts leading to fluorination of the donor atom.[8,9] Some metal chloride complexes, $[MoCl_4(E^nBu_2)_2]$ or $[NbCl_5(E^nBu_2)]$, with terminal butyl substituents on the chalcogenoethers were identified as potential single-source precursors for the growth of metal dichalcogenide thin films, as the precursors had relatively high volatility and a low

energy decomposition pathway through potential β-hydride elimination and subsequent reduction.[4,6,10]

4.2.1 Coordination Complexes with Chalcogenoethers and Transition Metals in Their Highest Oxidation State

As stated in Chapter 3, there are no known neutral coordination complexes of MoF_6,[11] and early studies of WF_6 established the formation of $[WF_6(SMe_2)_n]$ (n = 1 or 2)[12,13] as white crystals and $[WF_6(SEt_2)_2]$, although characterisation is limited for $[WF_6(SEt_2)_2]$.[14] Subsequent studies with $RS(CH_2)_2SR$ (R = Me or ^{i}Pr) and WF_6 showed a colour change upon addition of the ligand to WF_6 in CH_2Cl_2 solution at 180 K, but the colour faded away when brought to room temperature.[11,15] It is unlikely that WF_6 chalcogenoether complexes will be stable in ambient conditions; those reported are isolated at low temperatures and are unstable at room temperature.[11-13,15] Attempts using $[M'OF_4(MeCN)]$ (M' = Mo or W) as the metal source and some chalcogenoethers (SMe_2, $SeMe_2$, $MeS(CH_2)_2SMe$ or $MeSe(CH_2)_2SeMe$) failed, as the ligands either could not displace the coordinated MeCN or brought about the reduction of the metal centre.[11,16] There are no reports of neutral $M'O_2F_2$ (M' = Mo or W) complexes with soft S- or Se- donor ligands, although accessing the parent compound is challenging. Thioether complexes of WCl_6 have been discussed previously in Chapter 2.

Corresponding metal pentafluorides, MF_5 (M = Nb or Ta), behave in a similar manner to $M'F_6$ (M' = Mo or W) analogues, with reactions between MF_5 and SR_2 (R = Me or Et) in the absence of solvent giving colourless $[MF_5(SR_2)]$ solids.[3,8,17] In contrast, MF_5 and excess SMe_2 in CH_2Cl_2 gave extremely moisture sensitive $[MF_4(SMe_2)_4][MF_6]$ crystals containing distorted dodecahedral cations (Figure 4.1).[8]

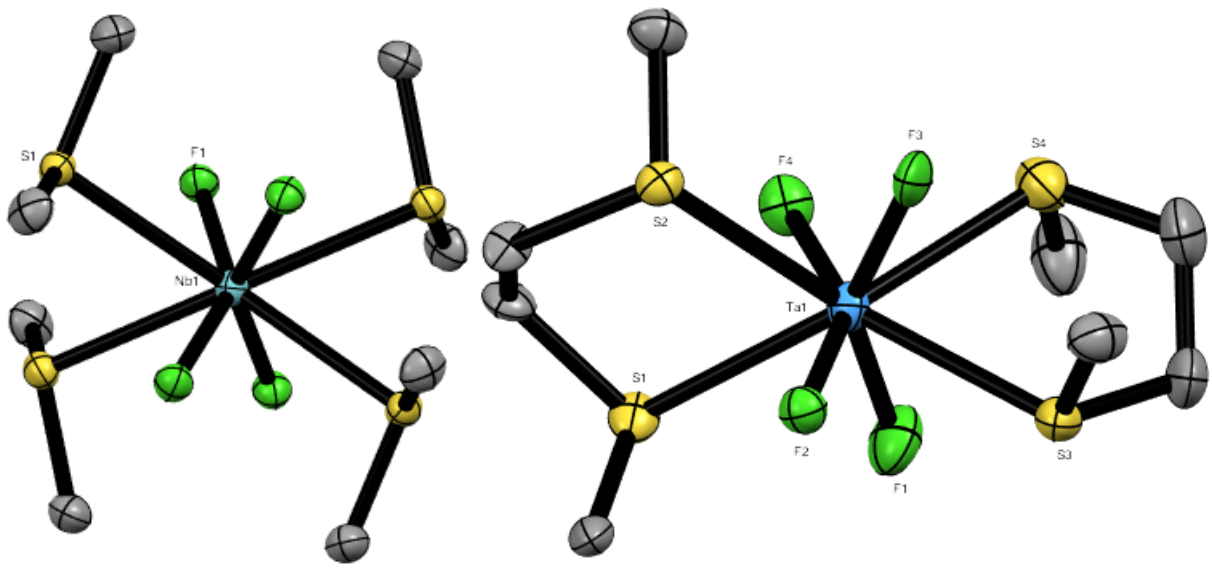

Figure 4.1: Crystal structures of the cations $[NbF_4(SMe_2)_4]^+$ (left) and $[TaF_4(MeS(CH_2)_2SMe)_2]^+$ (right). Hydrogen atoms and anions omitted for clarity.[3,8]

More stable complexes, $[MF_4(L\text{-}L)_2][MF_6]$ with dithioethers, L-L (L-L= $RS(CH_2)_2SR$; R = Me, Et or ^iPr) have also been formed as white powders from reaction with both NbF_5 and TaF_5 (see Figure 4.1). All of these compounds show rapid reversible dissociation or pyramidal inversion in solution even at low temperatures (190 K).[3,8] The xylyl ligand *o*-$C_6H_4(CH_2SMe)_2$ reacts with NbF_5 to form two structurally characterised products, an infinite chain cationic species in the complex, $[NbF_4(o\text{-}C_6H_4(CH_2SMe)_2)_2][Nb_2F_{11}]$, with two bridging thioether ligands between the Nb centres, and a very rare sulfonium salt $[(o\text{-}C_6H_4(CH_2SMe)_2)H][NbF_6]$, likely from trace moisture.[18] Highly sensitive $[MF_5(SeMe_2)]$[3,8] complexes have been isolated, but decompose rapidly within hours at ambient temperatures. Initial reactions with MF_5 and telluroethers gave insoluble black tarry materials,[3,8] but from TaF_5 and $TeMe_2$ at 0 ºC, $[TaF_5(TeMe_2)]$ was subsequently isolated, although this also decomposed rapidly.[4] Further examples of MF_5 complexes with neutral hard donors and phosphines are described in Chapter 6.

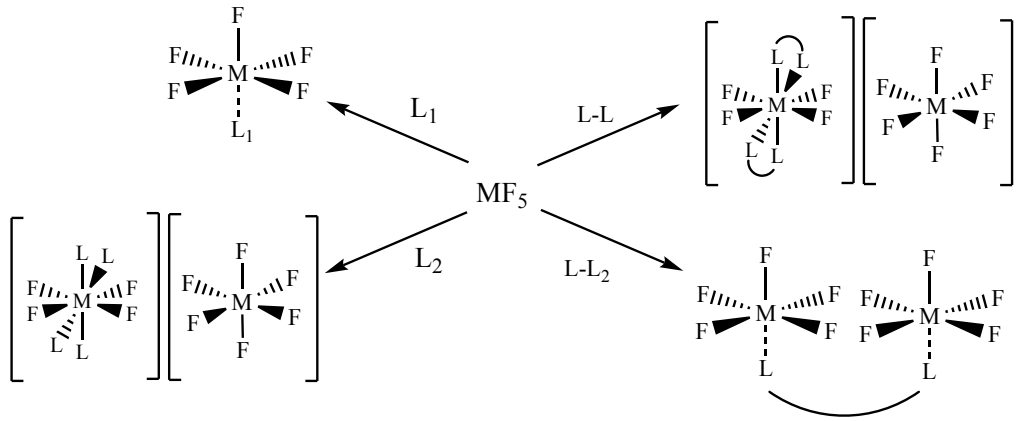

Figure 4.2: Reaction scheme showing complexes of MF_5 (M = Ta or Nb) with thio- and seleno-ethers.[3,8,18]

The majority of the complexes derived from MF_5 are extremely sensitive to trace moisture and decompose readily. Investigations into comparable complexes derived from MX_5 (X = Cl or Br) have shown complexes with heavier halides behave very differently to the fluoride analogues.[3,4,18] All the reactions between MF_5 and bidentate thioethers produced eight-coordinate salts (Figure 4.2). In contrast, only $MeS(CH_2)_2SMe$ produced this type of complex when reacted with MX_5 (X = Cl or Br), no matter the stoichiometry used.[3,8] Instead, MX_5 and bidentate chalcogenoether ligands formed bridged dimer complexes, $[(MX_5)_2(\mu\text{-}L\text{-}L)]$, where each donor heteroatom is coordinating with a different metal centre to give a distorted octahedral metal environment (Figure 4.3). The only examples of this occurring with the metal pentafluoride analogues are with the heavier chalcogen ligands $RSe(CH_2)_2SeR$ (R = Me or ^nBu), which form $[(MF_5)_2(\mu\text{-}L\text{-}L)]$.[3,8]

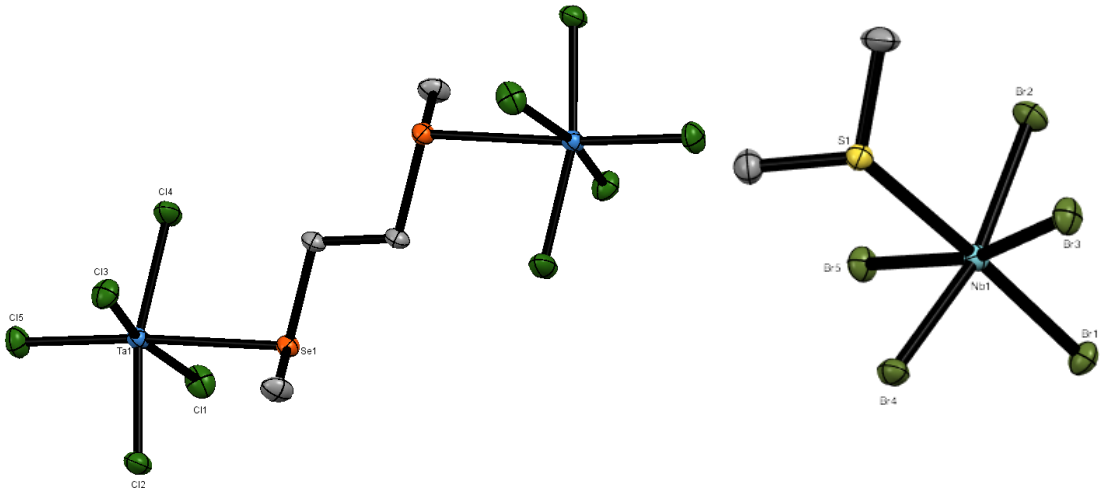

Figure 4.3: Crystal structures of [(TaCl$_5$)$_2$(MeSe(CH$_2$)$_2$SeMe)] (left) and [NbBr$_5$(SMe$_2$)] (right).. Hydrogen atoms omitted for clarity.[3,8]

The Group V pentahalides, MX_5 (X = Cl or Br), also form these bridged dimer complexes with *o*-xylyl backboned ligands containing either sulfur or selenium donor atoms (*o*-$C_6H_4(CH_2ER)_2$; E = S or Se; R = Me or Et), again showing the metal centre in a six-coordinate distorted octahedral environment. There are a very small number of examples of TaX_5 with telluroethers, [$TaX_5(TeR_2)$] (X = Cl or Br; R = Me or ^{n}Bu), being the first examples of the highest oxidation state transition metal complexes with telluroethers which are structurally characterised. High valent complexes with telluroethers are highly unusual as Te-C cleavage is common and the telluroether is also susceptible to oxidative halogenation.[19]

There is very little work on M'X_5 (M' = Mo or W) in the +V oxidation state and consequently few neutral complexes with chalcogenoethers. [WBr_5(MeS(CH$_2$)$_2$SMe)] has been reported, but there are no structurally characterised examples.[20]

4.2.2 Coordination Complexes of Metal(IV) Halides and Chalcogenoethers

There are a few early reports of $MoCl_4$ complexes with mono-, di-, poly-thioethers and thiamacrocycles.[1,21] Subsequent work has included structural characterisation of [$MoCl_4(SEt_2)_2$][22-24] and [$MoCl_4(tht)_2$].[25] A series of mildly moisture sensitive [$MoCl_4(L)_2$] and [$MoCl_4$(L-L)] complexes synthesised from $MoCl_5$ under ambient conditions have been described.[10] The easy reduction of the molybdenum centre by a variety of ligands under ambient conditions is likely to be the main reason why there is little or no $MoCl_5$ coordination chemistry that maintains the +V oxidation state.

Monodentate ligands (tht, SMe_2, S^nBu_2, $SeMe_2$ and Se^nBu_2) react in excess with $MoCl_5$ to produce the paramagnetic complexes *trans*-[$MoCl_4(ER_2)_2$]. These complexes can also be formed *via* a Mo(IV) precursor, [$MoCl_4(MeCN)_2$], where the chalcogenoether ligand displaces the MeCN ligand. Bidentate chalcogenoether ligands (MeE(CH$_2$)$_n$EMe; E = S or Se; n = 2 or 3) form *cis*-[$MoCl_4$(MeE(CH$_2$)$_n$EMe)] (Figure 4.5). All complexes are coordinatively saturated and are only

mildly hydrolytically sensitive. The crystal structures show the expected octahedral geometries with the chelating bidentate ligands causing a slight distortion from a perfect octahedron.[10]

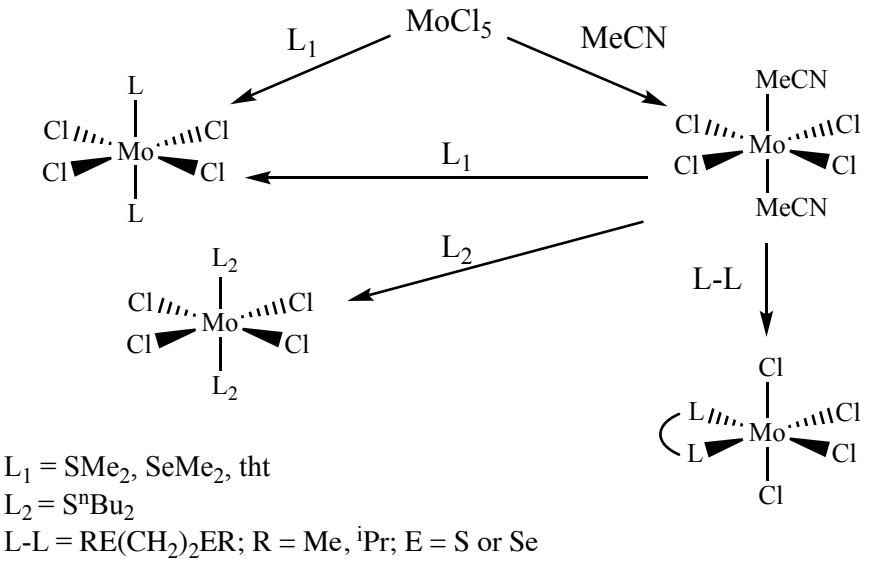

Figure 4.4: Reaction scheme for $[MoCl_4(L)_2]$ or $[MoCl_4(L\text{-}L)]$ complexes.[10]

The corresponding WCl_4 complexes are much rarer. But there are some examples of WCl_4 complexes with thioethers, $[WCl_4(SEt_2)_2]$[25] and $[WCl_4(MeS(CH_2)_2SMe)]$.[24] However these are early reports, so spectroscopic characterisation is limited, although $[WCl_4(SEt_2)_2]$ has been structurally characterised. These complexes are synthesised either by refluxing WCl_4 or $[WCl_4(MeCN)_2]$ in excess ligand, which also acts as a solvent. It is possible that because $[WCl_4(SEt_2)_2]$ has been isolated, other thioether complexes would be stable if they could be isolated, but since WCl_4 is strongly polymeric this could be challenging.

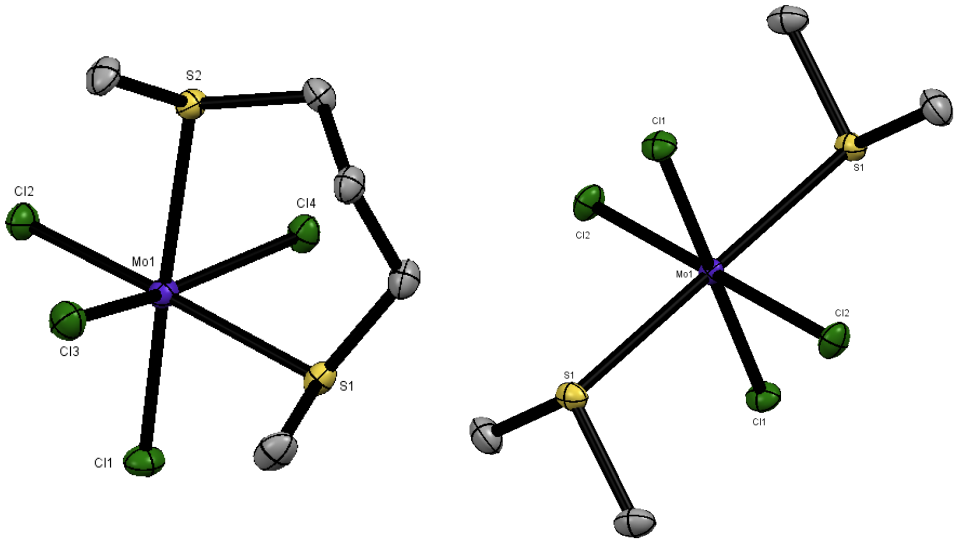

Figure 4.5: Crystal structures of $[MoCl_4(MeS(CH_2)_3SMe)]$ (left) and $[MoCl_4(SMe_2)_2]$ (right). Hydrogen atoms are omitted for clarity.[10]

Work on NbX_4 and TaX_4 is equally scarce, with only one tantalum(IV) literature report, where the complexes $[TaX_4(L)_2]$ (X = Cl or Br; R = tht or SMe_2) are described.[26] Work on niobium(IV)

complexes is more detailed; early reports show $[NbX_4(L)_2]$ (X = Cl, Br or I; R = tht or SMe_2), but $[NbCl_4(SMe_2)_2]$ rapidly loses an equivalent of SMe_2.[26,27] An example of eight-coordinate niobium(IV), $[NbCl_4(MeS(CH_2)_2SMe)_2]$,[28] was proposed, with the structure later confirmed as a distorted square antiprism (Figure 4.6).[19] The six-coordinate complex $[NbCl_4(MeS(CH_2)_2SMe)]$ was also isolated from $NbCl_4$ and a stoichiometric amount of ligand, but always had traces of the eight-coordinate species (shown by microanalysis and spectroscopic evidence). A series of six-coordinate $NbCl_4$ complexes with thioethers has been reported, $[NbCl_4(RS(CH_2)_nSR)]$ (R = Me or ^{i}Pr; n = 2 or 3) and $[NbCl_4(o\text{-}C_6H_4(CH_2SEt)_2)]$, isolated as moisture sensitive brown powders. Analogous selenoether complexes $[NbCl_4(L\text{-}L)]$ and $[NbCl_4(L)_2]$ have been isolated, there was no evidence of an eight-coordinate species when using $MeSe(CH_2)_2SeMe$, possibly due to steric effects around the metal centre or since selenoethers are weaker donor ligands.[19] Synthesis of telluroether complexes was attempted, but were unsuccessful due to Te-C cleavage, although it was speculated that $[NbCl_4(MeTe(CH_2)_3TeMe)_2]$ formed and rapidly decomposed, but with no crystallographic evidence. For examples of NbX_4 (X = Cl or Br) with phosphine ligands see Chapter 6.

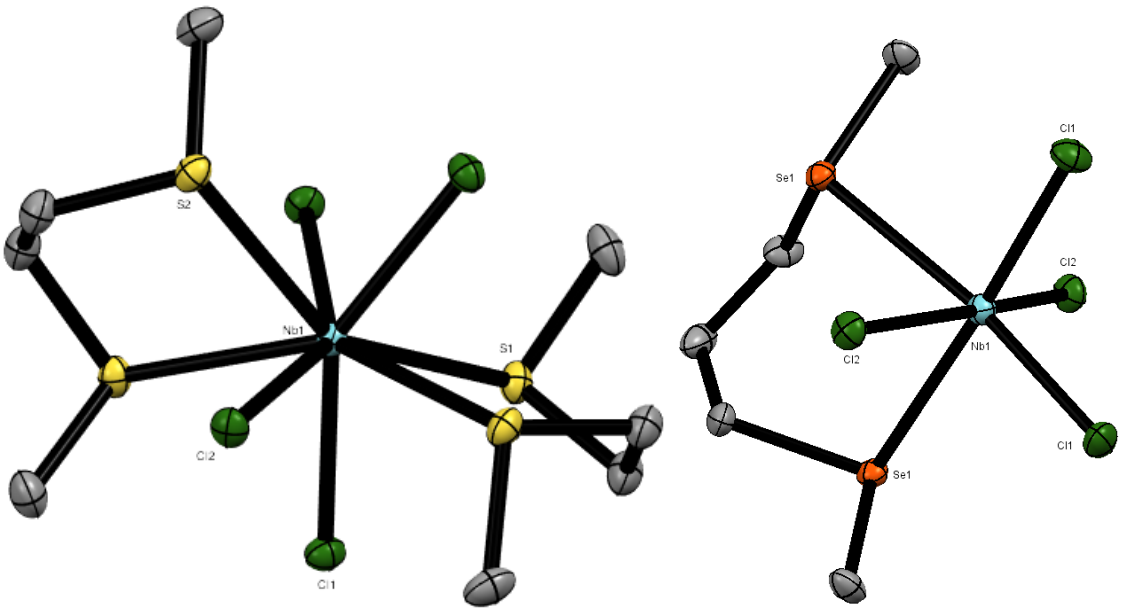

Figure 4.6: Crystal structures of $[NbCl_4(MeS(CH_2)_2SMe)_2]$ (left) and $[NbCl_4(MeSe(CH_2)_3SeMe)]$ (right). Hydrogen atoms omitted for clarity.[19]

4.2.3 Complexes of Metal Oxohalides with Chalcogenoethers

MOF_3 (M = Nb or Ta) do not react with thioethers, suggesting the ligands cannot bind strongly enough to prevent dissociation and polymerisation of the metal oxyfluoride.[29,30] An early example of $[NbOBr_3(tht)_2]$[31] was reported *via* direct reaction between $NbOBr_3$ and tht. Despite examples of $[NbOCl_3(L\text{-}L)]$ and $[NbOCl_3(L)_2]$ with hard donors and softer phosphine donor ligands (see Chapter 6), there are no complexes with thioethers from direct reactions between $NbOCl_3$ and thioether ligands.[30,32] The complexes $[NbOCl_3(MeS(CH_2)_2SMe)]$ and $[NbOCl_3(SMe_2)]$ were

identified as hydrolysis products and isolated as crystals; these are the only known thioether complexes, not surprising as $NbOCl_3$ is highly polymeric and needs a stable adduct to block the coordination sites.[19,33] In a similar vein, there are no known neutral complexes of $TaOX_3$ with thioethers, with only hard donor complexes known (see Chapter 6).[34]

As stated in Chapter 2, molybdenum in its highest oxidation state is highly reactive and often easily reduced; a detailed investigation of MoO_2X_2 (X = Cl or Br) and their reactions with thioethers has been reported.[35] Highly moisture sensitive complexes $[MoO_2X_2(RS(CH_2)_2SR)]$ (R = Me or Et) have been isolated and structurally characterised, but attempts with other ligands $(MeS(CH_2)_nSMe$, n = 1 or 3, SMe_2, $PhS(CH_2)_2SPh)$ proved unsuccessful, reducing the molybdenum centre. This indicates that only ligands where a five-membered chelate ring is formed and with terminal alkyl substituents (which increase σ-donor power) can form coordination complexes with MoO_2X_2. The thermally unstable complex $[MoO_2Cl_2(MeSe(CH_2)_2SeMe)]$ has also been isolated (decomposing at ambient temperatures), but the bromide analogue was not formed. Further studies expanded the thioether ligands used to include $^{i}PrS(CH_2)_2S^{i}Pr$, 1,4-dithiane and [14]aneS_4.[36] Interestingly, the ligand *o*-$C_6H_4(CH_2SMe)_2$ does not chelate, but forms a bridged dimer structure, $[(MoO_2Cl_2)_2(o\text{-}C_6H_4(CH_2SMe)_2)_2]$ (Figure 4.7).[36]

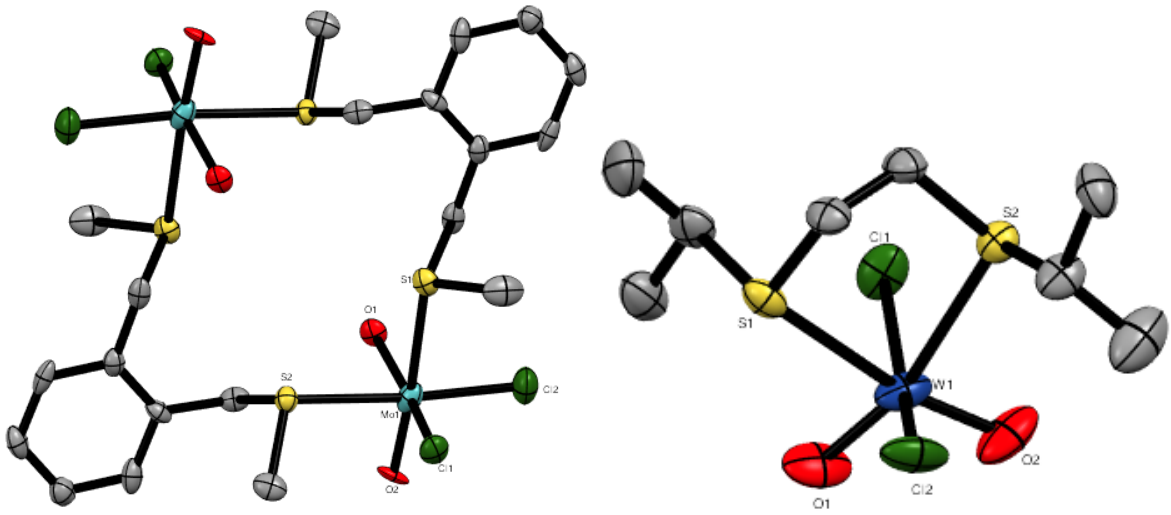

Figure 4.7: Crystal structures of $[(MoO_2Cl_2)_2(\mu\text{-}o\text{-}C_6H_4(CH_2SMe)_2)_2]$ (left) and $[MoO_2Cl_2(^{i}PrS(CH_2)_2S^{i}Pr)]$ (right). Hydrogen atoms omitted for clarity.[36]

Within the same study, WO_2X_2 complexes were also investigated and complexes in the form $[WO_2X_2(L\text{-}L)]$ (X = Cl or Br; L-L = $MeS(CH_2)_2SMe$, $^{i}PrS(CH_2)_2S^{i}Pr$ and dithiane) were isolated.[36] The tungsten(VI) complexes are more reactive than their molybdenum(VI) counterparts, consistent with WO_2X_2 being harder than MoO_2X_2. There is only one literature report that attempted to coordinate a thioether to $WOCl_4$, where SMe_2 is used in excess as the ligand, the report suggested SMe_2 reduced the tungsten centre.[37]

4.2.4 Complexes of Metal Thiohalides with Chalcogenoethers

Early work into $NbSCl_3$ complexes showed examples of $[NbSCl_3(SPPh_3)]$[38] and $[NbSCl_3(SEt_2)_2]$.[39] In other systems, rearrangements can occur to form compounds with dichalcogenide bridges including $[Nb_2Cl_4(\mu\text{-}Se_2)_2(L)_4]$ (L = SMe_2 or tht) and $[Nb_2Cl_4(\mu\text{-}S)(\mu\text{-}S_2)(tht)_4]$.[40-42] This work was followed by a series of complexes formed by reacting $NbCl_5$, $S(SiMe_3)_2$ and thioether, $[NbSCl_3(ER_2)]$ (E = S or Se; R = Me or ^{n}Bu) and $[NbSCl_3(L\text{-}L)]$ (L-L = $MeS(CH_2)_2SMe$, ^{i}PrS$(CH_2)_2$S^{i}Pr, $MeS(CH_2)_3SMe$, $MeSe(CH_2)_3SeMe$ and ^{n}BuS$(CH_2)_3$S^{n}Bu), which were isolated as green solids.[43] Crystals isolated from a solution of $[NbSCl_3(SMe_2)]$ were identified as $[(NbSCl_2)_2(\mu\text{-}Cl)_2(SMe_2)_2]$, showing highly asymmetric bridging chlorides (Figure 4.8). Unusually, the SMe_2 ligands lie *syn* rather than in the more common *anti* arrangement found in many *d* block dimers. Attempts to displace MeCN from $[NbSeCl_3(MeCN)_2]$ with thioether ligands were unsuccessful, while *in-situ* attempts from $NbCl_5$, $Se(SiMe_3)_2$ and Se^{n}Bu$_2$ produced a black solid tentatively assigned as $[NbSe_2Cl_3(Se^nBu_2)]$, which could contain Se_2^{2-} bridging groups.[43]

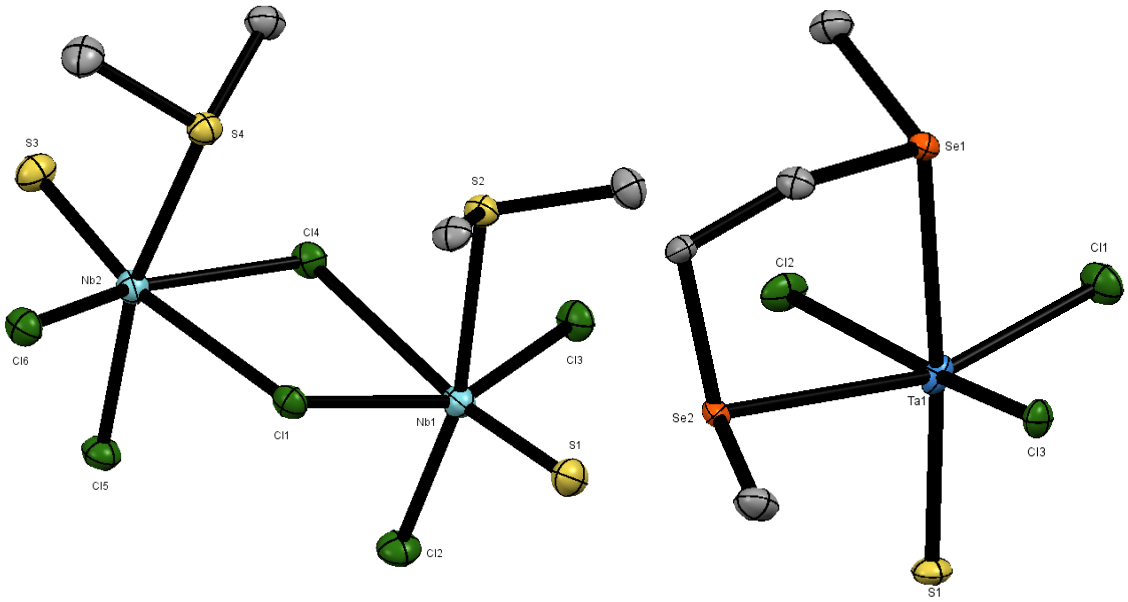

Figure 4.8: Crystal structures of $[(NbSCl_2)_2(\mu\text{-}Cl)_2(SMe_2)_2]$ (left) and $[TaSCl_3(MeSe(CH_2)_2SeMe)]$ (right). Hydrogen atoms omitted for clarity.[2,43]

Comparative work on $TaSCl_3$ complexes has also been undertaken, with complexes $[TaSCl_3(SMe_2)_2]$ and $[TaSCl_3(PhS(CH_2)_2SPh)]$ being described in the early 1980s.[44] Attempts to isolate $[TaSCl_3(E^nBu_2)_2]$ were unsuccessful, producing unidentifiable products.[2] A range of bidentate thioether complexes, $[TaSCl_3(RS(CH_2)_2SR)]$ (R = Me, ^{i}Pr or Ph) and $[TaSCl_3(RS(CH_2)_3SR)]$ (R = Me, ^{n}Bu) were shown to readily form and were isolated as dark coloured solids. Most of the bidentate thioether complexes have been structurally characterised, showing six-coordinate tantalum with *mer* chlorines and the thioether ligand lying *trans* to S/Cl, with some showing S/Cl disorder *trans* to ligand.[2] In addition, two selenoether complexes were also isolated, $[TaSCl_3(MeSe(CH_2)_2SeMe)]$ and $[TaSCl_3(^nBuSe(CH_2)_3Se\,^nBu)]$, where the ligands were shown to be relatively labile in solution.[2] Attempts to isolate $[TaSCl_3(MeSe(CH_2)_3SeMe)]$

were unsuccessful. All successful bidentate thioether complexes of the form $[MEX_3(L\text{-}L)]$ have been shown to have a six-coordinate distorted octahedral geometry where the neutral ligands lie *trans* to the M=E bond (see Figure 4.8 for example). A review of complexes of $MSCl_3$ (M = Nb, Ta or W) with hard donor ligands is presented in Chapter 6.

Complexes with $WSCl_4$ and thioethers are extremely rare; the bridged dimer $[(WSCl_4)_2(MeS(CH_2)_2SMe)]$, which was structurally characterised, being the first and only example to-date.[45,46] The ratio of the ligand to metal is shown to play a vital role in the complex that forms; if the ligand ratio is >1:1 then reduction to tungsten(V) occurs, resulting in isolation of the mononuclear compound, $[WSCl_3(MeS(CH_2)_2SMe)]$.[46,47] There is a similar report using the ether ligand $MeO(CH_2)_2OMe$ (dme) with $WSeCl_4$, which forms $[(WSeCl_4)_2(dme)]$. If it remains in solution for an extended time, isolated crystals show that $[WSeCl_3(OCH_2CH_2OMe)]$ forms, where cleavage of one of the ether linkages has occurred.[46,48]

High valent early transition metal halides and metal oxo- and thio-halides show a range of behaviours when reacting with chalcogenoethers. General trends seem to suggest that the complexes with monodentate ligands are less stable than their bidentate counterparts. Bidentate chalcogenoethers that have a C_2 backbone generally provide extra stability to complexes due to the formation of a five-membered chelate ring. Although, sometimes can make the ligand itself unstable and the C_2 linker can be eliminated and REER (E = S, Se or Te) is formed.[49] It is also clear the R substituents on the bidentate ligands play a role, not only sterically, but Me substituents seem to have a higher tendency to reduce metal centres.[47,48] These trends will be investigated when examining $WSCl_4$ complexes isolated in this work.

4.2.5 Aims

The aim of this chapter is to establish a systematic series of new $WSCl_4$ complexes with thioethers and compare these with the analogous $WOCl_4$ complexes. Softer selenium donor ligand complexes will also be investigated and their properties explored to allow comparisons with known literature. Complexes will be characterised by IR, ^1H NMR, $^{77}Se\{^1H\}$ NMR and UV-Vis spectroscopy, elemental analysis and single crystal X-ray diffraction. Potential precursors for chemical vapour deposition of WS_2 thin films will be identified based upon certain criteria i.e. neutral tungsten sulfide complexes containing thioether ligands bearing n-butyl substituents.

4.3 Results and Discussion

4.3.1 Bidentate Thioether Complexes of Tungsten(VI)

The six-coordinate bridged dimer complexes of tungsten(VI), $[(WSCl_4)_2(RS(CH_2)_2SR)]$ (R = Me, ^{i}Pr or Ph), $[(WSCl_4)_2(MeS(CH_2)_3SMe)]$ and $[(WOCl_4)_2(RS(CH_2)_2SR)]$ (R = ^{i}Pr or Ph) were obtained as dark coloured, highly moisture sensitive powders in moderate yields, ~45%, as shown

in Figure 4.9. All complexes were synthesised by direct reaction of pre-formed $WECl_4$ with stoichiometric amounts of ligands in an appropriate solvent (CH_2Cl_2 or toluene) in rigorously dry conditions.

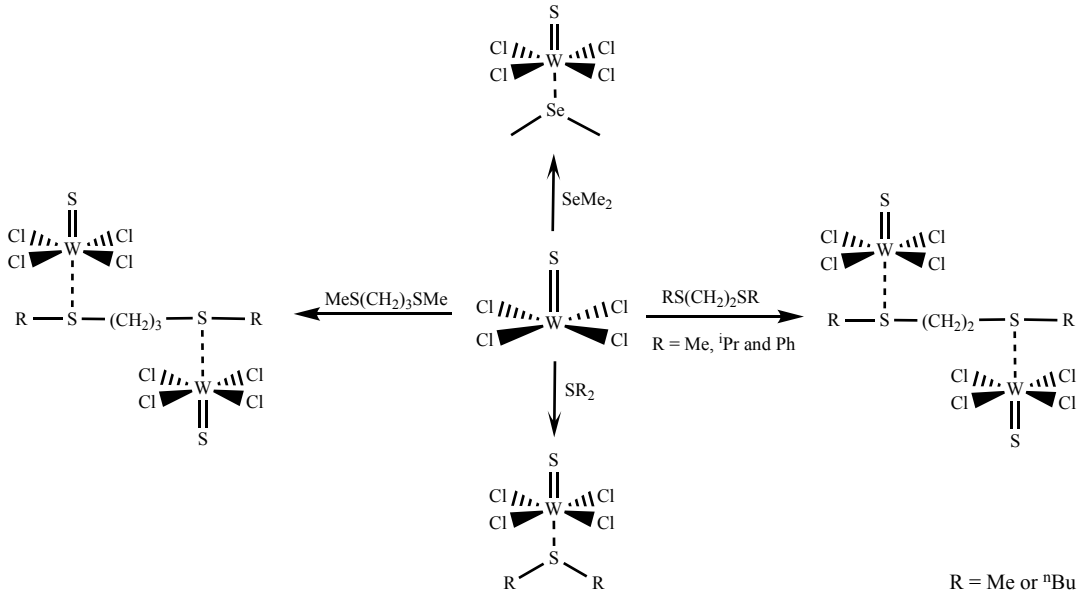

Figure 4.9: Reaction scheme for the synthesis of $[(WSCl_4)_2(L\text{-}L)]$ and $[WSCl_4(L)]$.

The complex, $[(WSCl_4)_2(MeS(CH_2)_2SMe)]$,[45,46] has been previously reported and was isolated from direct stoichiometric reaction of $WSCl_4$ with $MeS(CH_2)_2SMe$ in a 2:1 ratio in benzene; when a 1:1 ratio is used the W(V) complex, $[WSCl_3(MeS(CH_2)_2SMe)]$,[46,47] is isolated. The tungsten(V) complex was isolated after three weeks, whereas, in the present study it was isolated in a moderate yield after one hour (the yield could also be increased by using excess ligand as $MeS(CH_2)_2SMe$ would be lost as a ligand due to chlorination from the tungsten(VI) centre during reduction).

Complex	IR assignment		^{1}H NMR Data
	ν(W=S)	ν(W-Cl)	
$[(WSCl_4)_2(MeS(CH_2)_2SMe)]$	534 cm^{-1}	335 cm^{-1}	3.1(s), 2.4(s) ppm
$[WSCl_3(MeS(CH_2)_2SMe)]$	528 cm^{-1}	329 cm^{-1}	-
Literature data[46]			
$[(WSCl_4)_2(MeS(CH_2)_2SMe)]$	541 cm^{-1}	345 cm^{-1}	-
$[WSCl_3(MeS(CH_2)_2SMe)]$	535 cm^{-1}	315 cm^{-1}	-

Table 4.1: Comparison with the literature values for the complexes $[(WSCl_4)_2(MeS(CH_2)_2SMe)]$ and $[WSCl_3(MeS(CH_2)_2SMe)]$ with this work.

The complex $[WSCl_3(MeS(CH_2)_2SMe)]$ is a paramagnetic solid with a reported magnetic moment of 1.45 B.M., whereas $[(WSCl_4)_2(MeS(CH_2)_2SMe)]$ is a diamagnetic solid, like all tungsten(VI) complexes. The IR data shows a small shift to a lower wavenumber for the W=S stretch in the tungsten(V) complex (see Table 4.1) compared to the tungsten(VI) complex; this is expected when they have the same coordination number. The ^{1}H NMR data for $[(WSCl_4)_2(MeS(CH_2)_2SMe)]$ also

shows a small shift, +0.4 ppm, from uncoordinated ligand (2.67 and 2.09 ppm) due to deshielding of the protons upon coordination.

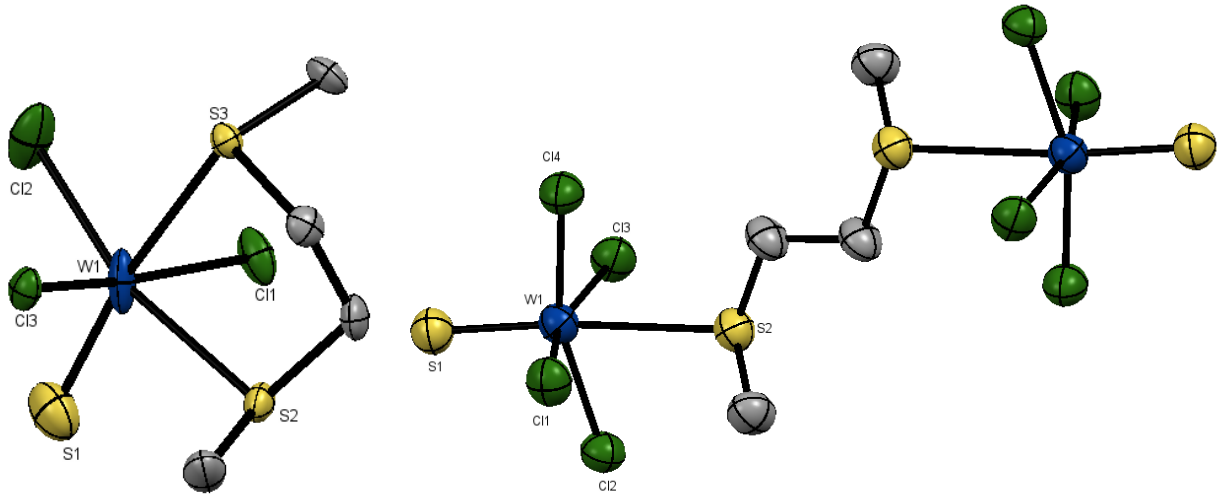

Figure 4.10: The structures of [$WSCl_3(MeS(CH_2)_2SMe)$] (left) and [$(WSCl_4)_2(MeS(CH_2)_2SMe)$] (right) showing the atom numbering scheme. Ellipsoids shown at 50% probability, hydrogen atoms are omitted for clarity. Note that the S/Cl were disordered in [$WSCl_3(MeS(CH_2)_2SMe)$], and were modelled using split atoms occupancies then refined to 0.25:0.75. Only the major form is shown.

[$WSCl_3(MeS(CH_2)_2SMe)$]			
Bond Lengths/ Å		**Bond Angles/ °**	
W1-Cl1	2.345(3)	Cl1-W1-Cl2	92.8(1)
W1-Cl2	2.279(3)	Cl1-W1-S1	96.4(1)
W1-Cl3	2.351(2)	Cl2-W1-Cl3	92.1(1)
W1-S1	2.075(4)	Cl2-W1-S3	86.34(8)
W1-S2	2.546(2)	S2-W1-S3	79.55(4)
W1-S3	2.704(2)		
**[$(WSCl_4)_2(MeS(CH_2)_2SMe$)] **			
Bond Lengths/ Å		**Bond Angles/ °**	
W1-Cl1	2.296(3)	S1-W1-Cl1	98.98(9)
W1-Cl2	2.310(2)	S1-W1-Cl2	101.0(1)
W1-Cl3	2.306(2)	S1-W1-Cl3	99.6(1)
W1-Cl4	2.299(2)	S1-W1-Cl4	97.8(1)
W1-S1	2.094(2)	Cl-W-Cl (*cis*)	88.74(9) - 90.24(9)
W1-S2	2.834(2)		

Table 4.2: Selected bond lengths and angles for [$WSCl_3(MeS(CH_2)_2SMe)$] and [$(WSCl_4)_2(MeS(CH_2)_2SMe)$].

Both structures above have been reported previously, but have been obtained with higher precision in this work (Figure 4.10). The complex [$WSCl_3(MeS(CH_2)_2SMe)$] was previously solved in the monoclinic space group $P2_1/c$, whereas the structure in this work was solved in the monoclinic

space group $P2_1/n$. The W=S bond is *trans* to the W-S bond from the thioether ligand, a similar arrangement to other structures of this nature. The structure of $[(WSCl_4)_2(MeS(CH_2)_2SMe)]$ crystallised in the monoclinic space group $P2_1/c$, compared to $P2_1/n$ in the reported structure, the chlorides sit slightly out of the equatorial plane, away from W=S bond, as is usual. Both complexes are in good agreement with the reported structures in terms of the W=S, W-Cl and W-S bond lengths. However, the W=S bond length in the previously reported structure of $[WSCl_3(MeS(CH_2)_2SMe)]$ has no mention of S/Cl disorder, a likely cause of the disparity between W=S bond distance in present structure (2.075(4) Å) and that reported (2.146 Å).[46]

The same reaction with $WOCl_4$ produced impure products from using both 1:1 and 2:1 M : ligand ratios. The major product is likely $[WOCl_3(MeS(CH_2)_2SMe)]$ and an unidentified minor species (potentially chlorinated ligand). A W=O stretch was observed in the IR spectrum, although at a lower frequency than observed for similar tungsten(VI) complexes, but there is no evidence of the bridged W(VI) dimer in the ^{1}H NMR spectrum.

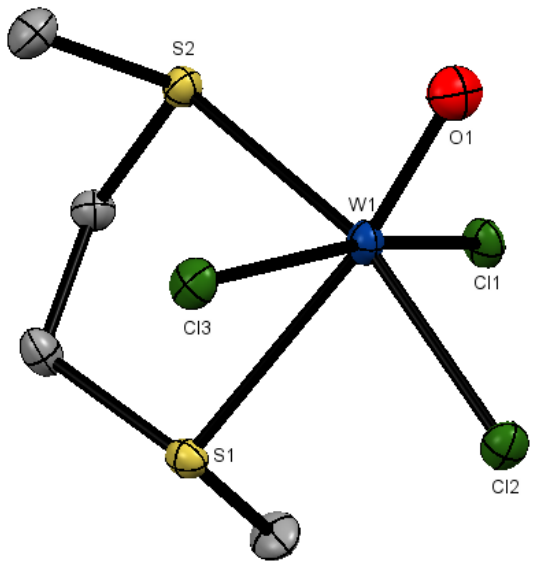

Figure 4.11: The structure of $[WOCl_3(MeS(CH_2)_2SMe)]$, showing the atom numbering scheme. Ellipsoids shown at 50% probability hydrogen atom are omitted for clarity.

$[WOCl_3(MeS(CH_2)_2SMe)]$			
Bond Lengths/ Å		**Bond Angles/ °**	
W1-Cl1	2.259(4)	Cl1-W1-Cl2	90.0(2)
W1-Cl2	2.338(7)	Cl1-W1-O1	90.0(2)
W1-Cl3	2.357(5)	Cl2-W1-Cl3	91.7(2)
W1-O1	1.72(2)	Cl2-W1-S2	82.1(2)
W1-S1	2.761(5)	Cl1–W1–S2	82.2(2)
W1-S2	2.520(6)	Cl3-W1–S1	77.1(2)

Table 4.3: Selected bond lengths and angles for $[WOCl_3(MeS(CH_2)_2SMe)]$.

Crystallisation attempts from a CH_2Cl_2 solution of the product isolated from this reaction yielded green crystals, which were identified as the previously unknown paramagnetic tungsten(V) complex, $[WOCl_3(MeS(CH_2)_2SMe)]$ (Figure 4.11). The thioether ligand lies *trans* to the W=O bond as is common and both the oxide and the analogous sulfide structures show slightly asymmetric W-S bonds with a difference of approximately ~0.2 Å, due to the *trans* influence. The W=O bond (1.72(2) Å) is slightly longer than the W=O bond in $[WOCl_3(dppmO_2)]$ (1.69(1) Å), but not significantly different.

The W(VI) complex, $[(WSCl_4)_2(MeS(CH_2)_3SMe)]$, has similar properties to $[(WSCl_4)_2(MeS(CH_2)_2SMe)]$, but has increased solubility in organic solvents, possibly caused by the C_3 backbone having more flexibility, which may influence the packing of the molecules in the solid state. The ^{1}H NMR spectrum shows three broad singlets, 2.72, 2.20 and 2.03 ppm, which indicates the compound may be dynamic in solution, whereas the resonances are sharp in the C_2 backboned complex.

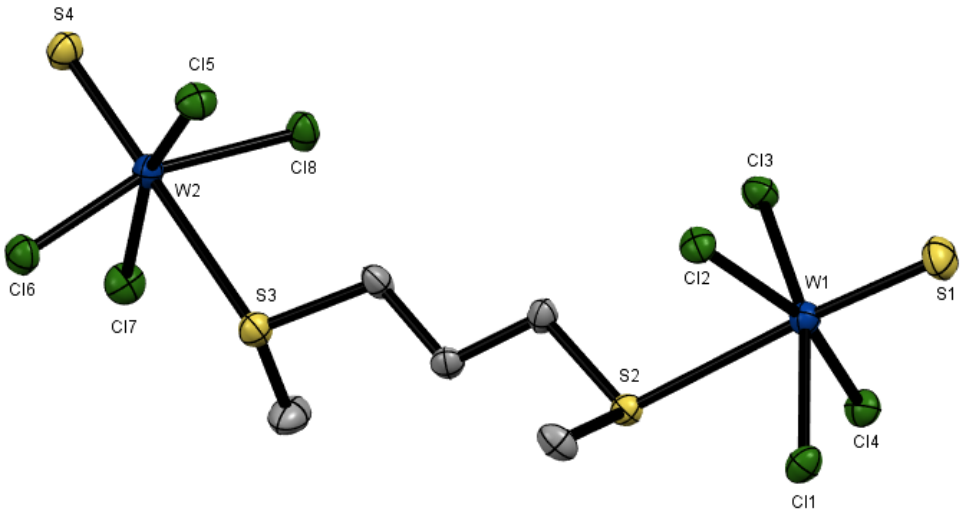

Figure 4.12: Crystal structure of $[(WSCl_4)_2(MeS(CH_2)_3SMe)]$, showing the atom numbering scheme. Ellipsoids shown at 50% probability, hydrogen atoms are omitted for clarity.

$[(WSCl_4)_2(MeS(CH_2)_3SMe)]$			
Bond Lengths/ Å		**Bond Angles/ °**	
W1-Cl1	2.295(2)	S1-W1-Cl1	98.84(9)
W1-Cl2	2.307(2)	S1-W1-Cl2	98.54(9)
W1-Cl3	2.329(2)	S1-W1-Cl3	99.51(9)
W1-Cl4	2.320(2)	S1-W1-Cl4	100.30(9)
W1-S1	2.102(3)	Cl-W-Cl (*cis*)	87.03(7) – 90.66(7)
W1-S2	2.816(2)		

Table 4.4: Selected bond lengths and angles for $[(WSCl_4)_2(MeS(CH_2)_3SMe)]$.

The structure of $[(WSCl_4)_2(MeS(CH_2)_3SMe)]$ also shows the tungsten(VI) in a distorted octahedral environment with the WCl_4 unit bent away from planarity (Figure 4.12). The W=S bond length in

$[(WSCl_4)_2(MeS(CH_2)_3SMe)]$, 2.102(3) Å, is not significantly different to that in $[(WSCl_4)_2(MeS(CH_2)_2SMe)]$, 2.094(2) Å.

Reaction between $WOCl_4$ and $MeS(CH_2)_3SMe$ behaved in the same way as with $MeS(CH_2)_2SMe$; it is reasonable to suggest that the ligand reduces the metal centre to tungsten(V) (with chlorination of the thioether), then the remaining thioether ligand chelates to form a six coordinate complex. Crystals of the tungsten(V) complex, $[WOCl_3(MeS(CH_2)_3SMe)]$ have been identified (Figure 4.13). The structure is similar to $[WOCl_3(MeS(CH_2)_2SMe)]$, showing six-coordinate tungsten(V) species where the dithioether is chelating. Interestingly, the two structures show different geometric isomers; $[WOCl_3(MeS(CH_2)_2SMe)]$ has the dithioether *trans* O/Cl, whilst $[WOCl_3(MeS(CH_2)_3SMe)]$ the dithioether is *trans* Cl/Cl. The isomers found in many $[MEX_3(L)_2]$ and $[MEX_3(L\text{-}L)]$ (E = O or S; X = halide) have the neutral ligand(s) *trans* E/X and frequently show disorder in this plane; unusually there is no evidence of disorder in either of the structures reported here.[2,43,50]

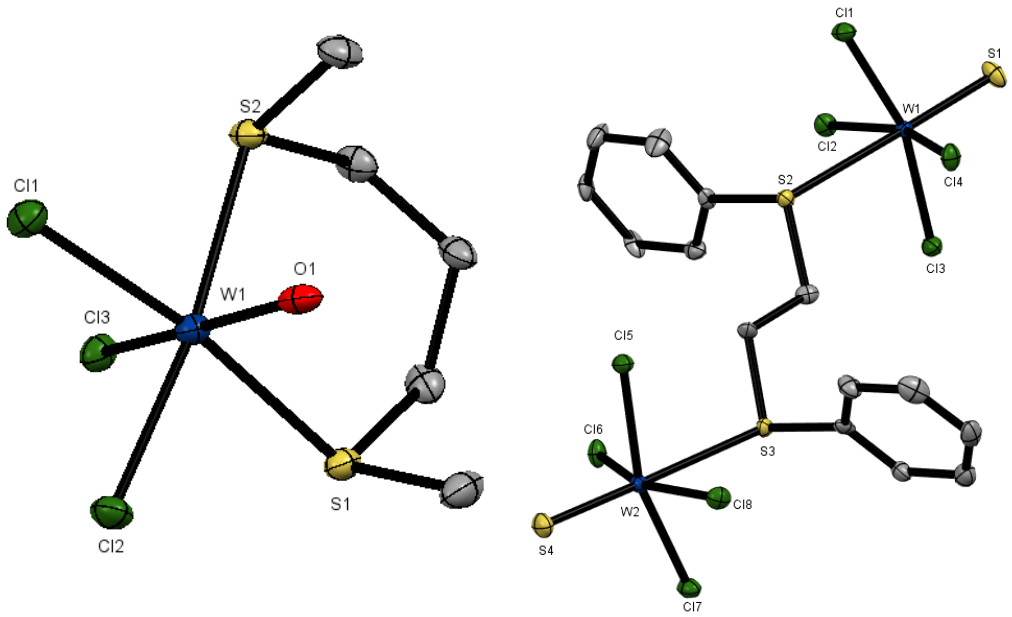

Figure 4.13: The structures of $[WOCl_3(MeS(CH_2)_3SMe)]$ (left) and $[(WSCl_4)_2(PhS(CH_2)_2SPh)]$ (right) showing the atom numbering scheme. Ellipsoids shown at 50% probability, hydrogen atoms are omitted for clarity.

$[WOCl_3(MeS(CH_2)_3SMe)]$			
Bond Lengths/ Å		**Bond Angles/ °**	
W1-Cl1	2.360(2)	Cl1-W1-Cl2	92.18(7)
W1-Cl2	2.331(2)	Cl1-W1-O1	91.61(6)
W1-Cl3	2.464(2)	Cl2-W1-Cl3	91.7(2)
W1-O1	1.721(6)	Cl2-W1-S2	82.1(2)
W1-S1	2.518(2)	Cl1–W1–S2	85.14(7)
W1-S2	2.521(2)	Cl3-W1–S1	77.20(6)
		S1-W1-S2	97.42(6)

[$(WSCl_4)_2(PhS(CH_2)_2SPh)$]			
Bond Lengths/ Å		**Bond Angles/ °**	
W1-Cl1	2.315(2)	S1-W1-Cl1	99.88(7)
W1-Cl2	2.285(2)	S1-W1-Cl2	100.37(7)
W1-Cl3	2.304(2)	S1-W1-Cl3	99.51(7)
W1-Cl4	2.321(2)	S1-W1-Cl4	99.80(7)
W1-S1	2.100(2)	Cl-W-Cl (*cis*)	87.39(6) – 89.55(6)
W1-S2	2.864(1)		

Table 4.5: Selected bond lengths and angles for [$WOCl_3(MeS(CH_2)_3SMe)$] and [$(WSCl_4)_2(PhS(CH_2)_2SPh)$].

The complexes, [$(WECl_4)_2(PhS(CH_2)_2SPh)$], have been prepared from direct reaction of $WECl_4$ and $PhS(CH_2)_2SPh$. Due to $PhS(CH_2)_2SPh$ being a poorer σ-donor compared to its methyl substituted analogue, the complexes have the potential to be more unstable compared to those described above. This was confirmed as [$(WOCl_4)_2(PhS(CH_2)_2SPh)$] decomposes within a few days to a black sticky solid, even under inert atmospheric conditions. There are some examples of ligand bridged complexes using $PhS(CH_2)_2SPh$ with niobium(V) and tantalum(V), [$(MCl_5)_2(PhS(CH_2)_2SPh)$], and the methyl complex, [$(MeMCl_4)_2(PhS(CH_2)_2SPh)$], where M = Nb or Ta.[51-53] In the ^1H NMR spectra of [$(WECl_4)_2(PhS(CH_2)_2SPh)$] two broad resonances are observed, indicating the complexes are dynamic in solution. For E=S, red crystals were isolated from a CH_2Cl_2 solution of the complex and were identified as [$(WSCl_4)_2(PhS(CH_2)_2SPh)$] (Figure 4.13); there are no significant differences in bond lengths between this structure and the other bridged thioether dimers described above.

The ligand $^iPrS(CH_2)_2S^iPr$ was used to identify the boundaries of dichalcogenoether ligands with $WOCl_4$, as the data suggested that $MeS(CH_2)_2SMe$ and $MeS(CH_2)_3SMe$ produced impure products that contained tungsten(V) species (shown by crystallographic studies), but $PhS(CH_2)_2SPh$ seemed to have coordinated, albeit forming a very unstable ligand-bridged complex of W(VI), [$(WOCl_4)_2(PhS(CH_2)_2SPh)$]. The ligand $^iPrS(CH_2)_2S^iPr$ is a stronger σ-donor than $PhS(CH_2)_2SPh$, but behaves subtly different from $MeS(CH_2)_2SMe$. In practice, the isolated complex, [$(WOCl_4)_2(^iPrS(CH_2)_2S^iPr)$], is extremely unstable, turning blue readily, and is more unstable than [$(WOCl_4)_2(PhS(CH_2)_2SPh)$], which is somewhat surprising, although $^iPrS(CH_2)_2S^iPr$ is more susceptible to oxidisation.

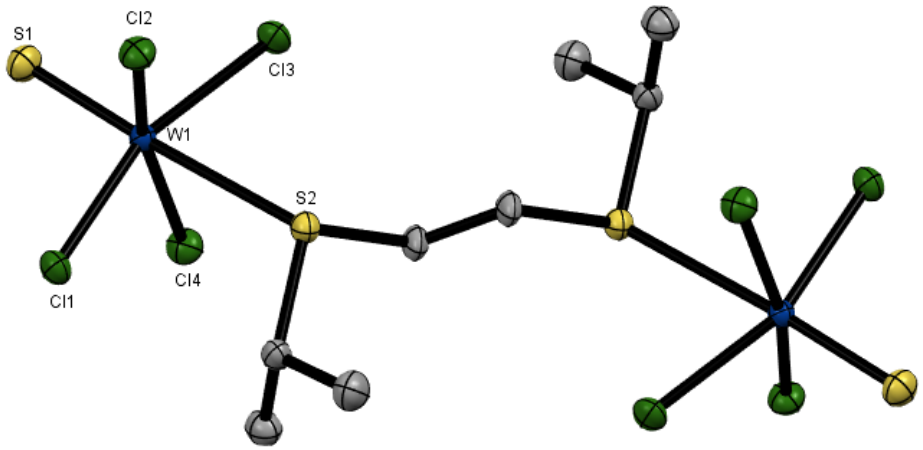

Figure 4.14: The structure of [(WSCl$_4$)$_2$(^{i}PrS(CH$_2$)$_2$S^{i}Pr)] showing the atom numbering scheme. Ellipsoids shown at 50% probability, hydrogen atoms are omitted for clarity.

[(WSCl$_4$)$_2$(^{i}PrS(CH$_2$)$_2$S^{i}Pr)]			
Bond Lengths/ Å		**Bond Angles/ °**	
W1-Cl1	2.210(2)	S1-W1-Cl1	99.27(7)
W1-Cl2	2.323(2)	S1-W1-Cl2	97.87(7)
W1-Cl3	2.310(2)	S1-W1-Cl3	100.12(7)
W1-Cl4	2.315(2)	S1-W1-Cl4	98.85(7)
W1-S1	2.097(2)	Cl-W-Cl (*cis*)	87.59(6) – 89.10(6)
W1-S2	2.864(2)		

Table 4.6: Selected bond lengths and angles for [(WSCl$_4$)$_2$(^{i}PrS(CH$_2$)$_2$S^{i}Pr)].

In contrast, the tungsten(VI) sulfide complex, [(WSCl$_4$)$_2$(^{i}PrS(CH$_2$)$_2$S^{i}Pr)], behaves like the other compounds in this series (data in Table 4.8) and is significantly more stable than the oxide analogue. The crystal structure is not significantly different to those described above (Figure 4.14).

The related tungsten(V) monomer, [WSCl$_3$(^{i}PrS(CH$_2$)$_2$S^{i}Pr)], was synthesised by using the 1:1 ratio of WSCl$_4$: dithioether and the spectroscopic data were shown to be consistent with those observed for [WSCl$_3$(MeS(CH$_2$)$_2$SMe)].

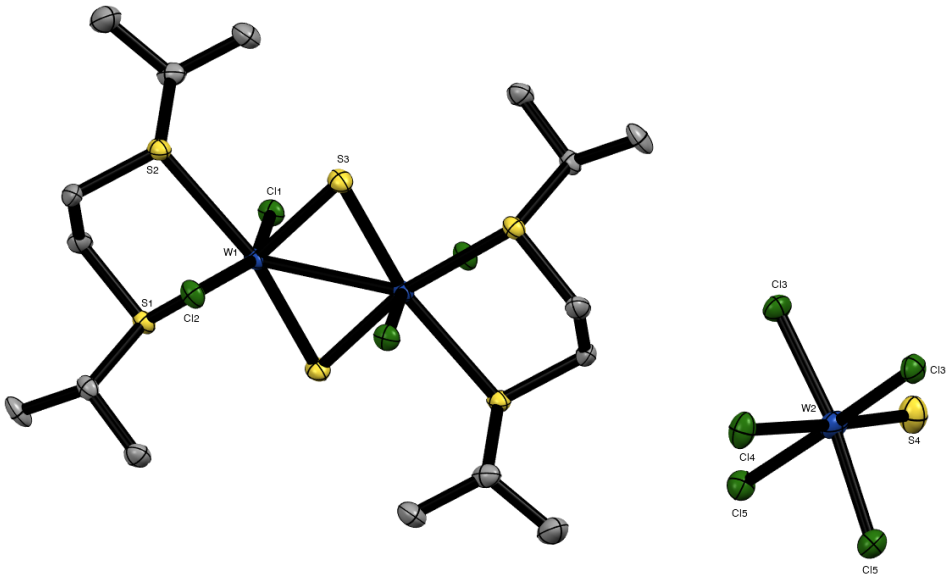

Figure 4.15: The structure of $[(WCl_2)_2(\mu\text{-}S)_2(^iPrS(CH_2)_2S^iPr)][WSCl_5]\bullet CH_2Cl_2$ showing the atom numbering scheme. Ellipsoids shown at 50% probability, hydrogen atoms and solvent are omitted for clarity.

$[(WCl_2)_2(\mu\text{-}S)_2(^iPrS(CH_2)_2S^iPr)][WSCl_5]\bullet CH_2Cl_2$			
Bond Lengths/ Å		**Bond Angles/ °**	
W1-Cl1	2.335(2)	Cl1-W1-Cl2	158.33(8)
W1-Cl2	2.326(2)	Cl1-W1-S3	96.89(8)
W1-S1	2.599(2)	W1-S3-W1	74.13(6)
W1-S2	2.601(2)	S4-W2-Cl_{cis}	93.9(2) – 96.1(3)
W1-S3	2.281(2)	Cl-W-Cl (*cis*)	90.29(3) – 90.73(4)
W2-S4	2.125(1)		
W2-Cl	2.329(3) – 2.486(4)		

Table 4.7: Selected bond lengths and angles for $[(WCl_2)_2(\mu\text{-}S)_2(^iPrS(CH_2)_2S^iPr)][WSCl_5]\bullet CH_2Cl_2$.

While attempting to isolate crystals of $[WSCl_3(^iPrS(CH_2)_2S^iPr)]$ from a solution of CH_2Cl_2, a few crystals formed that were shown to be an ionic salt (Figure 4.15). However, determining the specific nature of the bridging atoms has proved challenging. The bridging atoms are in doubt since Cl^- and S^{2-} are isoelectronic and therefore very difficult to distinguish by X-ray crystallography. The anion is $[WSCl_5]^{2-}$, therefore if the cation is sulfide bridged, then both the cation and anion would be tungsten(V), or alternatively, the dimer could be chloride bridged, making the cation tungsten(IV) and mixed valence – this seems less likely. Without further spectroscopic data it is not possible to confidently assign the structure. A similar structure was isolated with *o*-$C_6H_4(AsMe_2)_2$, which was equally ambiguous (Chapter 3).

Compound	IR Data		^{1}H NMR Data (δ / ppm)
	ν(W=E)	ν(W-Cl)	
$[WSCl_3(MeS(CH_2)_2SMe)]$	528 cm^{-1}	329 cm^{-1}	-
$[(WSCl_4)_2(MeS(CH_2)_2SMe)]$	534 cm^{-1}	335 cm^{-1}	3.07s, 2.40s
$[(WSCl_4)_2(PhS(CH_2)_2SPh)]$	539 cm^{-1}	336 cm^{-1}	7.33s br, 3.20s br
$[(WSCl_4)_2(MeS(CH_2)_3SMe)]$	529 cm^{-1}	332 cm^{-1}	2.72s br, 2.20s br, 2.03s br
$[(WSCl_4)_2(^iPrS(CH_2)_2S^iPr)]$	543 cm^{-1}	341 cm^{-1}	3.15dt, 2.86d, 1.32d
$[WSCl_3(^iPrS(CH_2)_2S^iPr)]$	527 cm^{-1}	323 cm^{-1}	-
$[WSCl_4(SMe_2)]$	537 cm^{-1}	327 cm^{-1}	2.32s br
$[WSCl_4(S^nBu_2)]$	537 cm^{-1}	348 cm^{-1}	2.74s br, 2.68s br, 1.52s, 0.96s
$[WSCl_4(SeMe_2)]$	525 cm^{-1}	331 cm^{-1}	2.23s br
$[WSCl_4(SPPh_3)]$	520 cm^{-1}	339 cm^{-1}	-
$[(WOCl_4)_2(PhS(CH_2)_2SPh)]$	982 cm^{-1}	356 cm^{-1}	7.39s br, 3.41s br
$[(WOCl_4)_2(^iPrS(CH_2)_2S^iPr)]$	998 cm^{-1}	332 cm^{-1}	3.20dt, 2.90d, 1.34d
$[WOCl_4(SMe_2)]$	993 cm^{-1}	345 cm^{-1}	2.54s br

Table 4.8: Selected IR and ^{1}H NMR data for complexes in this work.

4.3.2 Complexes with Monodentate Thioethers

Monodentate chalcogenoethers were reacted in a 1:1 ratio in a non-coordinating solvent (CH_2Cl_2 or toluene) in an attempt to form complexes of type $[WECl_4(L)]$ (L = SMe_2, S^nBu_2, SPh_2 or $SeMe_2$). The SMe_2 ligand is a moderately strong donor and coordinated with both $WOCl_4$ and $WSCl_4$, forming $[WECl_4(SMe_2)]$. The spectroscopic data for both compounds are comparable to that of the bidentate complexes (see Table 4.8) and bulk composition confirmed by elemental analysis. The ^{1}H NMR spectra for $[WECl_4(SMe_2)]$ shows a very broad singlet, which suggests the ligand is dynamic (reversibly dissociating) in solution. Attempts to isolate crystals of the W(VI) species were unsuccessful, however a few yellow crystals of a reduced tungsten dimer were isolated from the $[WSCl_4(SMe_2)]$ system (Figure 4.16).

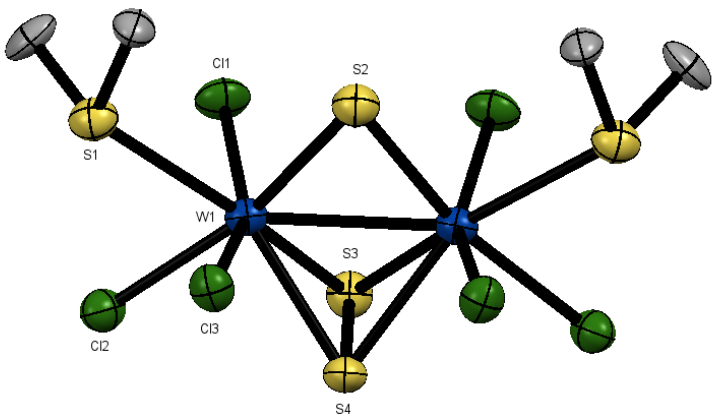

Figure 4.16: The structure of $[(WCl_3)_2(\mu\text{-}S_2)(\mu\text{-}S)(SMe_2)_2]$, showing the atom numbering scheme. Ellipsoids shown at 50% probability, hydrogen atoms are omitted for clarity.

There is some ambiguity for the determination of the bridging atoms as Cl^- and S^{2-} are isoelectronic, however, the most probable structure is shown in Figure 4.16. The structure is S_2^{2-} bridged, the S3-S4 bond length 2.00(3) Å is consistent with similar S_2^{2-} bridged coordination complexes. It is not uncommon for high valent metal thiohalides to rearrange to form S_2^{2-} bridges.[40-42] Therefore, it is likely the structure contains two tungsten(V) centres with a S_2^{2-}, a sulfide bridge and a single W-W bond.[54-57] This assignment is highly probable, but there are no other reported structures of this nature and single metal-metal bonds for high valent 5*d* metals are rare due to poor orbital overlap. Further spectroscopic investigation could categorically confirm the structure, but this is not currently possible in the absence of a bulk sample.

Since the binuclear compounds $[(WECl_4)_2(PhS(CH_2)_2SPh)]$ have been fully characterised, attempts to use the related ligand SPh_2 were investigated. The phenyl groups on the chalcogen were expected to help prevent reduction at the metal centre as the ligand is less basic and less susceptible to chlorination than alkyl ligands. However, it appears for both $WOCl_4$ and $WSCl_4$ that SPh_2 is not a strong enough donor and does not react with the $WECl_4$ in solution.

Following the successful isolation of the tungsten(VI) thioether bridged dimers, the ligand S^nBu_2 was used as it contains a low energy ß-hydride elimination pathway making complexes potential LPCVD precursors. If successful the precursor is likely to produce volatile by-products (butene and Cl_2) which would increase the chance of depositing clean film. An attempt to synthesise $[WOCl_4(S^nBu_2)]$ resulted in a deep green coloured oil, which is likely $[WOCl_4(S^nBu_2)]$, although very unstable. The compound decomposed within a few hours even under an inert atmosphere to leave yellow/brown oil. The extreme instability is probably due to the fact that the complex was an oil and therefore is intrinsically more susceptible to decomposition and hydrolysis than a solid. The reaction between $WSCl_4$ and S^nBu_2 produced $[WSCl_4(S^nBu_2)]$ as a deep red oil, which proved to be stable in an inert and rigorously dry atmosphere for ~2 weeks. Raman spectroscopy showed two strong peaks, a W=S peak at 538 cm^{-1}, which is coincident to the W=S peak in the IR spectrum at 535 cm^1. Group theory predicts two W-Cl bands, A_1 and E, with the A_1 band strong in the Raman spectrum and E strong in the IR spectrum. A band is observed at 379 cm^{-1} in the Raman spectrum (A_1) and 348 cm^{-1} in the IR spectrum (E). In some of the previous $WSCl_4$ complexes described above, the A_1 band is also observed in the IR spectrum, but is significantly weaker. Due to the oil's instability towards trace moisture, no elemental analysis could be obtained (as it is completed off-site), but all spectroscopic data are consistent with those of the other complexes in this work.

4.3.3 Complexes with Selenoethers

There are a few reported compounds of high valent early transition metal halides with dimethyl selenide including $[MCl_5(SeMe_2)]$ (M = Ta or Nb)[3,8] and the compound $[MoCl_4(SeMe_2)_2]$ but the molybdenum centre is in the +IV oxidation state.[10] However, there are no reports of dimethyl selenide coordinated to Group VI transition metals in the +VI oxidation state. There are some

bidentate selenoethers coordinated to MO_2X_2 (M = Mo or W; X = Cl or Br), but these are thermally unstable.[35,36] The compound [$WSCl_4(SeMe_2)$] has been successfully synthesised by reaction of $WSCl_4$ and $SeMe_2$ in toluene. A room temperature $^{77}Se\{^1H\}$ NMR experiment was attempted but showed no resonance. The sample was rerun at -90 ºC, which showed a strong resonance at +81.3 ppm, showing a clear and large coordination shift, (uncoordinated $SeMe_2$, 0 ppm). The broad peak clearly indicates the complex is dynamic in solution even at low temperature, within the appropriate NMR timescale. No ^{183}W satellites were observed, but the resonance was ~80 Hz wide so it is likely that the satellite coupling is masked by the peak width of the main resonance. ^1H NMR data showed a single resonance that was relatively broad and exhibited a coordination shift.

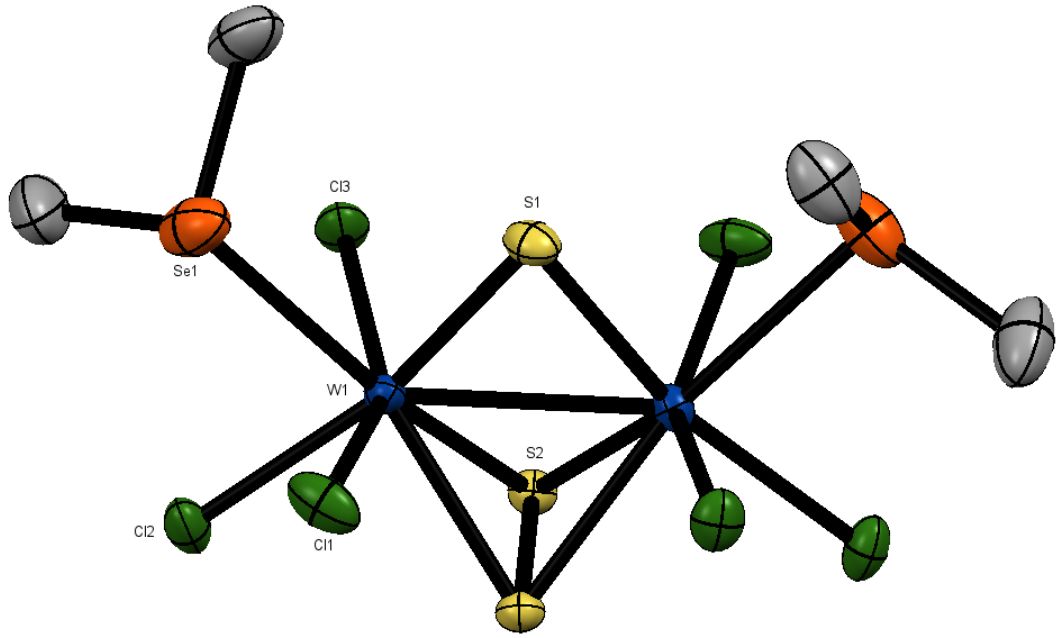

Figure 4.17: The structure of [$(WCl_3)_2$ (μ-S_2) (μ-S) $(SeMe_2)_2$], showing the atom numbering scheme. Ellipsoids shown at 50% probability, hydrogen atoms are omitted for clarity.

[$(WCl_3)_2(\mu\text{-}S_2)(\mu\text{-}S)(SeMe_2)_2$]			
Bond Lengths/ Å		**Bond Angles/ °**	
W1-Cl1	2.399(2)	S1-W1-S2	103.4(2)
W1-Cl2	2.424(4)	Cl1-W1-Cl2	85.2(1)
W1-Cl3	2.386(4)	Cl1-W1-Cl3	151.2(1)
W1-S1	2.280(2)	W1-S1-W1	74.0(2)
W1-S2	2.434(3)	W1-S2-W1	68.63(8)
S3-S3	2.012(4)		
W1-W1	2.7444(8)		

Table 4.9: Selected bond lengths and angles for [$(WCl_3)_2(\mu\text{-}S_2)(\mu\text{-}S)(SMe_2)_2$].

Attempts to isolate crystals also returned a structure which was identified as [$(WCl_3)_2(\mu\text{-}S_2)(\mu\text{-}S)(SeMe_2)_2$] (Figure 4.17). Although similar to [$(WCl_3)_2(\mu\text{-}S_2)(\mu\text{-}S)(SMe_2)_2$], they are not isomorphous. Interestingly, the complexes crystallise with different relative orientations of the

chalcogenoether ligands, resulting in different mirror planes. These dimer structures are clearly favourable decomposition products that occur across a variety of complexes with different ligands, with the S_2^{2-} most likely to be derived from $WSCl_4$ in this instance.

The synthesis of $[WOCl_4(SeMe_2)]$ was also investigated in a similar manner. The solution turned green immediately after addition of ligand, suggesting coordination. However, within ~30 minutes or when the reaction flask was placed under vacuum, the solution/solid turned purple and the isolated purple product was very stable but is unidentified. The IR data are not consistent with similar tungsten(VI) thioether compounds. There is a strong peak at 832 cm^{-1} likely to be W=O-W and due to the very poor solubility of the purple solid in organic solvents, NMR data could not be obtained. This insolubility may suggest that the product is dimeric or polymeric.

Investigation into the formation of bidentate selenoether complexes was also undertaken, but the reaction between $MeSe(CH_2)_2SeMe$ and $WOCl_4$ seemed to be unsuccessful, with the IR spectrum showing that the isolated product is impure with $WOCl_4$ still present. The same reaction with $WSCl_4$ was also intractable, a W=S stretch was observed in the IR spectrum at 528 cm^{-1} and a W-Cl stretch at 315 cm^{-1} (similar to stretch observed in $[WSCl_3(MeS(CH_2)_2SMe)]$) but no solution spectroscopy could be obtained due to very limited solubility and elemental analysis is inconclusive. Without a crystal structure it is impossible to confidently say whether the bridged dimer or a reduced species formed.

4.3.4 Complexes with Triphenylphosphine Sulfide

Attempts to synthesise $[WOCl_4(SPPh_3)]$ and $[WSCl_4(SPPh_3)]$ have been investigated to compare behaviour observed between phosphine oxide complexes, explored in Chapter 2, and thioether complexes and $SPPh_3$ provides a convenient $^{31}P\{^1H\}$ NMR handle, and the lone pairs on the sulfur behave very differently. Both compounds are unknown and there are few simple high oxidation state early transition metal complexes using $SPPh_3$ as a ligand, with the most similar being $[MoOCl_3(SPPh_3)]$ and $[WCl_5(SPPh_3)_2]$.[58-60] The complex $[WSCl_4(SPPh_3)]$ was obtained by reaction of $WSCl_4$ and $SPPh_3$ in CH_2Cl_2 and shows a P=S stretch in the IR spectrum at 598 cm^{-1}, shifted from 638 cm^{-1} in the uncoordinated ligand, consistent with the trends seen in the phosphine oxide complexes in Chapter 2. The IR spectra also shows a W=S stretch at 521 cm^{-1} and a W-Cl stretch at 339 cm^{-1}. However, the ^1H and $^{31}P\{^1H\}$ NMR data both show uncoordinated ligand only, even at -90 °C, suggesting either the compound is extremely labile in solution even at low temperatures or the complex is unstable in solution, as all the solid-state data (IR spectroscopy and elemental analysis) suggests the complex $[WSCl_4(SPPh_3)]$.

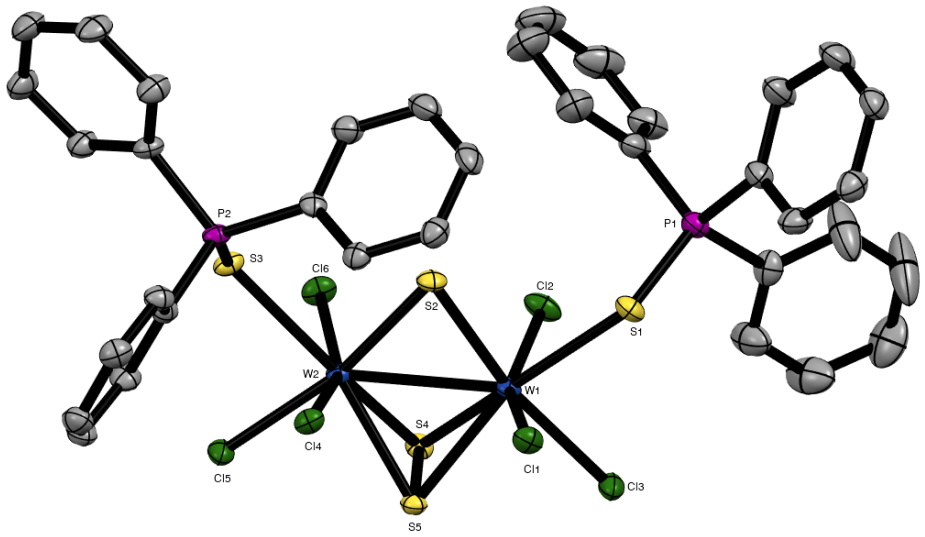

Figure 4.18: The structure of $[(WCl_3)_2(S_2)(\mu\text{-}S)(SPPh_3)_2]\bullet 2CH_2Cl_2$ showing the atom numbering scheme. Ellipsoids shown at 50% probability, hydrogen atoms and solvent are omitted for clarity.

$[(WCl_3)_2(\mu\text{-}S_2)(\mu\text{-}S)(SPPh_3)_2]\bullet 2CH_2Cl_2$			
Bond Lengths/ Å		**Bond Angles/ °**	
W1-Cl	2.368(1) – 2.421(1)	S2-W1-S4	102.53(4)
W1-S2	2.486(1)	S2-W1-S5	103.38(4)
W1-S4	2.419(1)	Cl1-W1-Cl2	152.82(4)
W1-S5	2.430(1)	Cl1-W1-Cl3	87.29(4)
S4-S5	1.997(2)	W1-S2-W2	74.21(3)
W1-W2	2.7582(7)	W1-S4-W2	69.50(3)

Table 4.10: Selected bond lengths and angles for $[(WCl_3)_2(\mu\text{-}S_2)(\mu\text{-}S)(SPPh_3)_2]\bullet 2CH_2Cl_2$.

The crystals of $[(WCl_3)_2(\mu\text{-}S_2)(\mu\text{-}S)(SPPh_3)_2]\bullet 2CH_2Cl_2$ were obtained from a saturated CH_2Cl_2 solution of $[WSCl_4(SPPh_3)]$, (Figure 4.18), the structural determination presented is the most probable. All three structures $[(WCl_3)_2(\mu\text{-}S_2)(\mu\text{-}S)(SPPh_3)_2]\bullet 2CH_2Cl_2$, $[(WCl_3)_2(\mu\text{-}S_2)(\mu\text{-}S)(EMe_2)_2]$ (E = S or Se) have similar W-S_{bridge} and W-S_2^{2-} bond lengths, suggesting that they all have the same bridging atoms and the metals are in the same oxidation state further indicating they are all sulfur bridged. Usually, $SPPh_3$ behaves very differently to the sulfur donor in thioethers so it is interesting they form the same decomposition systems.

In contrast, the product isolated from an attempt to prepare $[WOCl_4(SPPh_3)]$ shows a resonance in the $^{31}P\{^1H\}$ NMR spectrum at +66.4 ppm, which can be assigned as PPh_3Cl_2.[61] Therefore, it can be concluded that the product has reduced and chlorinated $SPPh_3$, which was also seen in WCl_6 chemistry in Chapter 2.

4.4 Conclusions

The aim of this work was to probe the boundaries of tungsten(VI) coordination chemistry by building on the hard N- and O-donor ligand complexes (Chapter 2), and the soft phosphine and arsine work described in Chapter 3. A systematic series of $WSCl_4$ complexes with monodentate and bidentate thioethers has been established and comparative analogues of $WOCl_4$ have also been isolated. Complexes with softer selenoether donor ligands were attempted, but $[WSCl_4(SeMe_2)]$ was the only stable complex that could be isolated.

Complexes were characterised by IR, ^{1}H NMR, ^{77}Se{^{1}H} NMR spectroscopy and solid-state UV-Vis spectroscopy, elemental analysis, single crystal X-ray diffraction and $[WSCl_4(S^nBu_2)]$ characterised by Raman spectroscopy. All the complexes isolated were six-coordinate and controlling the W : ligand stoichiometry is paramount for the isolation of tungsten(VI) species, as excess ligand reduces the metal centre. A number of reduced tungsten (V) decomposition products have also been identified by X-ray crystallography.

Thioether complexes with terminal substituents bearing β-hydrogens have the possibility to be single-source precursors for the production of WS_2 thin films *via* LPCVD providing the potential of a low energy decomposition pathway. The complexes $[(WSCl_4)_2(^iPrS(CH_2)_2S^iPr)]$, $[WSCl_3(^iPrS(CH_2)_2S^iPr)]$ and $[WSCl_4(S^nBu_2)]$ all meet this criterion, while also containing the 1:2 W:S ratio required for WS_2 formation. The suitability of these compounds as CVD precursors will be investigated in the following chapter.

4.5 Experimental

Syntheses were performed by using standard Schlenk and glove-box techniques under a dry N_2 atmosphere. Solvents were dried by distillation from CaH_2 (CH_2Cl_2) or Na/benzophenone ketyl (toluene, n-hexane). $SPPh_3$ was obtained from Sigma-Aldrich and dried by heating *in vacuo.* Dichalcogenoethers, $RE(CH_2)_nER$ (*n* = 2 or 3; E = S or Se; R = Me, Ph, ^iPr) were prepared *via* literature methods.[62,63] Me_2S, Ph_2S and $^nBu_2S$ were purchased from Sigma-Aldrich and Me_2Se from Strem and used as received. $WSCl_4$ and $WOCl_4$ were prepared *via* literature methods.[64,65] For further details regarding the instrumentation see Appendix A.

[(WSCl$_4$)$_2$(MeS(CH$_2$)$_2$SMe)]

A solution of $MeS(CH_2)_2SMe$ (0.030 g, 0.21 mmol) in dichloromethane (5 mL) was slowly added to a suspension of $WSCl_4$ (0.150 g, 0.42 mmol) in dichloromethane (5 mL). The dark red solution was then stirred for 1 h., concentrated to ~ 3 mL, filtered, and the red/brown solid dried *in vacuo*. Yield: 0.050 g, 28 %. Required for $C_4H_{10}Cl_8S_4W_2$ (837.7): C: 5.96, H: 1.25 %. Found: C: 5.85, H: 1.19 %. IR spectrum (Nujol, ν / cm^{-1}): 534s W=S, 376m, 335s W-Cl. ^1H NMR (CD_2Cl_2): δ = 3.07 (s, [2H], CH_2), 2.40 (s, [3H], CH_3). UV/Vis spectrum (diffuse reflectance) ν / cm^{-1}: 35,500, 32,250 sh, 20,200.

[(WSCl$_4$)$_2$(MeS(CH$_2$)$_3$SMe)]

A solution of $MeS(CH_2)_3SMe$ (0.029 g, 0.21 mmol) in dichloromethane (2 mL) was slowly added to a suspension of $WSCl_4$ (0.150 g, 0.42 mmol) in dichloromethane (5 mL). The dark red solution was then stirred for 1 h., concentrated to ~ 3 mL, filtered, and the red/brown solid dried *in vacuo*. Yield: 0.096 g, 54 %. Required for $C_5H_{12}Cl_8S_4W_2$ (851.7): C: 7.05, H: 1.42 %. Found: C: 7.24, H: 1.53 %. IR spectrum (Nujol, ν / cm^{-1}): 529s W=S, 360m, 332s W-Cl. ^1H NMR (CD_2Cl_2): δ = 2.72 (s br, [2H], CH_2), 2.20 (s br, [H], CH_2), 2.03 (s br, [3H], CH_3). UV/Vis spectrum (diffuse reflectance) ν / cm^{-1}: 34,750, 32,200sh, 20,000.

[(WSCl$_4$)$_2$(^{i}PrS(CH$_2$)$_2$S^{i}Pr)]

Was prepared similarly to $[(WSCl_4)_2(MeS(CH_2)_2SMe)]$ and isolated as a red/brown solid. Yield: 0.101 g, 54 %. Required for $C_8H_{18}Cl_8S_4W_2$ (893.8): C: 10.75, H: 2.03 %. Found: C: 10.90, H: 1.95 %. IR spectrum (Nujol, ν / cm^{-1}): 543s W=S, 370m, 341s W-Cl. ^1H NMR (CD_2Cl_2): δ = 3.15 (sep, [H], CH, $^3J_{HH}$, 8 Hz), 2.86 (s, [2H], CH_2), 1.32 (d, [6H], $^3J_{HH}$ 6.6 Hz, CH_3). UV/Vis spectrum (diffuse reflectance) ν / cm^{-1}: 36,500, 32,250 sh, 20,800.

[(WSCl$_4$)$_2$(PhS(CH$_2$)$_2$SPh)]

Was prepared similarly to $[(WSCl_4)_2(MeS(CH_2)_2SMe)]$ and isolated as a dark red solid. Yield: 0.090 g, 45 %. Required for $C_{14}H_{14}Cl_8S_4W_2$ (961.82): C: 17.48, H: 1.47 %. Found: C: 17.52, H:

1.60 %. IR spectrum (Nujol, ν / cm^{-1}): 539s W=S, 355m, 337s W-Cl. ^1H NMR (CD_2Cl_2): δ = 7.33 (s br, [5H], aromatic CH), 3.20 (s br, [2H], CH_2).

[$WSCl_3(MeS(CH_2)_2SMe)$]

A solution of $MeS(CH_2)_2SMe$ (0.051 g, 0.42 mmol) in dichloromethane (5 mL) was slowly added to a suspension of $WSCl_4$ (0.150 g, 0.42 mmol) in dichloromethane (5 mL). The dark red solution was then stirred for 1 h., concentrated to ~ 3 mL, layered with hexane, filtered, and the red/brown solid dried *in vacuo*. Yield: 0.070 g, 37 %. Required for $C_4H_{10}Cl_3S_3W$ (444.5): C: 10.81, H: 2.27 %. Found: C: 11.07, H: 2.26 %. IR spectrum (Nujol, ν / cm^{-1}): 528m W=S, 329s, br W-Cl.

[$WSCl_3(^iPrS(CH_2)_2S^iPr)$]

A solution of $^iPrS(CH_2)_2S^iPr$ (0.112 g, 0.42 mmol) in dichloromethane (2 mL) was slowly added to a suspension of $WSCl_4$ (0.150 g, 0.42 mmol) in dichloromethane (5 mL). The dark red/brown solution was then stirred for 1 h., concentrated to ~ 3 mL, filtered, and the red/brown solid dried *in vacuo*. Yield: 0.101 g, 54 %. Required for $C_8H_{18}Cl_3S_3W$ (500.62): C: 19.19, H: 23.62 %. Found: C: 19.50, H: 3.77 %. IR spectrum (Nujol, ν / cm^{-1}): 527s W=S, 340m, 323s W-Cl. UV/Vis spectrum (diffuse reflectance) ν / cm^{-1}: 34,000, 27,200, 20,400

[$WSCl_4(SMe_2)$]•CH_2Cl_2

A solution of dimethyl sulfide (0.026 g, 0.42 mmol) in dichloromethane (5 mL) was slowly added to a suspension of $WSCl_4$ (0.150 g, 0.42 mmol) in dichloromethane (5 mL). The dark red solution was then stirred for 1 h., concentrated to ~ 3 mL, filtered, and the brown/red solid dried *in vacuo*. Yield: 0.101 g, 57%. Required for $C_2H_6Cl_4S_2W$•CH_2Cl_2 (504.78): C: 7.14, H: 1.60 %. Found: C: 7.26, H: 1.73 %. IR spectrum (Nujol, ν / cm^{-1}): 538s W=S, 347s W-Cl. ^1H NMR (CD_2Cl_2): δ = 5.32 (s, CH_2Cl_2), 2.32 (s, br, SMe_2).

[$WSCl_4(S^nBu_2)$]

A solution of dibutyl sulfide (0.041 g, 0.28 mmol) in dichloromethane (5 mL) was slowly added to a suspension of $WSCl_4$ (0.100 g, 0.28 mmol) in dichloromethane (5 mL). The dark red solution was then stirred for 1 h., reduced to dryness, collecting a dark red oil. IR spectrum (Nujol, ν / cm^{-1}): 538 W=S, 348s W-Cl. Raman spectrum (ν / cm^{-1}): 535s W=S, 379s W-Cl. ^1H NMR (CD_2Cl_2): 2.74 (s br, [2H], CH_2), 2.68 (s br, [2H], CH_2), 1.52 (s, [2H], CH_2), 0.96 (s, [3H], CH_3). UV/Vis spectrum (diffuse reflectance) ν /cm^{-1}: 32000, 26900, 22700.

[$(WOCl_4)_2(^iPrS(CH_2)_2S^iPr)$]

A solution of $^iPrS(CH_2)_2S^iPr$ (0.039 g, 0.22 mmol) in dichloromethane (2 mL) was slowly added to a suspension of $WOCl_4$ (0.150 g, 0.44 mmol) in dichloromethane (5 mL). The dark green solution was then stirred for 1 h., concentrated to ~ 3 mL, filtered, and the green solid dried *in vacuo*. Yield:

0.089 g, 47 %. Required for $C_8H_{18}Cl_8O_2S_2W_2$ (861.6): C: 11.15, H: 2.11 %. Found: C: 11.24, H: 2.14 %. IR spectrum (Nujol, ν / cm^{-1}): 998s W=O, 325s W-Cl. ^1H NMR (CD_2Cl_2): δ = 3.20 (sep, [H], $^3J_{HH}$ 13.5, 6.8, CH), 2.90 (s, [2H], CH_2), 1.34 (d, [6H], $^3J_{HH}$ 6.9, CH_3)

[$(WOCl_4)_2(PhS(CH_2)_2SPh)$]

A solution of $PhS(CH_2)_2SPh$ (0.054 g, 0.22 mmol) in dichloromethane (5 mL) was slowly added to a suspension of $WOCl_4$ (0.150 g, 0.44 mmol) in dichloromethane (5 mL). The dark brown solution was then stirred for 1 h., concentrated to ~ 3 mL, filtered, and the dark pink solid dried *in vacuo*. Yield: 0.070 g, 34 %. Required for $C_{14}H_{14}Cl_8O_2S_2W_2$ (929.69): C: 18.09, H: 1.52 %. Found: C: 18.18, H: 1.60 %. IR spectrum (Nujol, ν / cm^{-1}): 982s W=O, 356s W-Cl. ^1H NMR (CD_2Cl_2): δ = 7.39 (s br, [5H], aromatic CH), 3.43 (s br, [2H], CH_2).

[$WOCl_4(SMe_2)$]

A solution of dimethyl sulfide (0.027 g, 0.44 mmol) in dichloromethane (5 mL) was slowly added to a suspension of $WOCl_4$ (0.150 g, 0.44 mmol) in dichloromethane (5 mL). The dark orange solution was then stirred for 1 h., concentrated to ~ 3 mL, filtered, and the brown/yellow solid dried *in vacuo*. Yield: 0.096 g, 54 %. Required for $C_2H_6Cl_4OSW$ (419.85): C: 5.95, H: 1.50 %. Found: C: 5.86, H: 1.39 %. IR spectrum (Nujol, ν / cm^{-1}): 979s W=O, 352s W-Cl. ^1H NMR (CD_2Cl_2): δ = 2.54 (s, br, SMe_2).

[$WSCl_4(SeMe_2)$]

A solution of dimethyl selenide (0.046 g, 0.42 mmol) in dichloromethane (5 mL) was slowly added to a suspension of $WSCl_4$ (0.150 g, 0.42 mmol) in dichloromethane (5 mL). The dark red solution was then stirred for 1 h., and brought to dryness *in vacuo* collecting a brown solid. Yield: 0.134 g, 68 %. Required for $C_2H_6Cl_4SSeW$ (466.75): C: 5.15, H: 1.30 %. Found: C: 5.22, H: 1.36 %. IR spectrum (Nujol, ν / cm^{-1}): 525s W=S, 331m W-Cl. ^1H NMR (CD_2Cl_2): δ = 2.23 (s, br, $SeMe_2$). $^{77}Se\{^1H\}$ NMR (CD_2Cl_2, 295 K) : no resonance; (183 K): δ = +81.3.

[$WSCl_4(SPPh_3)$]

$SPPh_3$ (0.082 g, 0.28 mmol) in dichloromethane (2 mL) was slowly added to a red solution of $WSCl_4$ (0.100 g, 0.28 mmol) in dichloromethane (5 mL). The solution was then stirred for 1 h., concentrated in *vacuo* to ~ 3 mL. The brown precipitate was filtered, washed with hexane (2 x 1 mL) and dried *in vacuo*. Yield: 0.120 g, 65 %. Required for $C_{18}H_{15}Cl_4PS_2W$ (652.1): C: 33.15, H: 2.32 %. Found: C: 32.98, H: 2.39 %. IR spectrum (Nujol, ν / cm^{-1}): 598s P=S, 337s W-Cl.

The products isolated from the following reactions were not satisfactorily characterised (see above) but are reported for completeness of work.

Reaction of $WOCl_4$ and $MeS(CH_2)_2SMe$

A solution of $MeS(CH_2)_2SMe$ (0.026 g, 0.22 mmol) in dichloromethane (5 mL) was slowly added to a suspension of $WOCl_4$ (0.150 g, 0.44 mmol) in dichloromethane (5 mL). The dark solution was then stirred for 1 h., concentrated to ~ 3 mL, filtered, and the green solid dried *in vacuo*. IR spectrum (Nujol, ν / cm^{-1}): 956m W=O, 325s W-Cl.

Reaction of $WOCl_4$ and $SeMe_2$

A solution of dimethyl selenide (0.048 g, 0.44 mmol) in dichloromethane (5 mL) was slowly added to a suspension of $WOCl_4$ (0.150 g, 0.44 mmol) in dichloromethane (5 mL). The dark green solution was then stirred for 1 h, which had turned purple, and brought to dryness *in vacuo* collecting a purple solid. IR spectrum (Nujol, ν / cm^{-1}): 976m, 832s W=O, 329s, 306s W-Cl. ^1H NMR (CD_2Cl_2): δ = 2.54 (s, br).

Reaction of $WSCl_4$ and $MeSe(CH_2)_2SeMe$

A solution of $MeSe(CH_2)_2SeMe$ (0.023 g, 0.21 mmol) in dichloromethane (5 mL) was slowly added to a suspension of $WSCl_4$ (0.150 g, 0.42 mmol) in dichloromethane (5 mL). The dark brown solution was then stirred for 1 h., concentrated to ~ 3 mL, filtered, and the beige solid dried *in vacuo*. IR spectrum (Nujol, ν / cm^{-1}): 528s W=S, 315s W-Cl.

Reaction of $WOCl_4$ and $SPPh_3$

$SPPh_3$ (0.082 g, 0.28 mmol) in toluene (2 mL) was slowly added to a red solution of $WOCl_4$ (0.100 g, 0.28 mmol) in toluene (5 mL). The solution was then stirred for 1 h., concentrated *in vacuo* to ~ 3 mL. The brown precipitate was filtered off, washed with hexane (2 x 1 mL) and dried *in vacuo*. $^{31}P\{^1H\}$ NMR (CD_2Cl_2): δ = +66.4 (PPh_3Cl_2).

4.5.1 Crystallographic Tables

Compound	$[WSCl_3(MeS(CH_2)_2SMe)]$	$[(WSCl_4)_2(MeS(CH_2)_2SMe)]$	$[WOCl_3(MeS(CH_2)_2SMe)]$	$[WOCl_3(MeS(CH_2)_3SMe)]$
Formula	$C_4H_{10}Cl_3S_3W$	$C_4H_{10}Cl_8S_4W_2$	$C_4H_{10}Cl_3OS_2W$	$C_5H_{12}Cl_3OS_2W$
M	444.50	837.66	428.44	442.47
Crystal system	Monoclinic	Monoclinic	Triclinic	Triclinic
Space group (no)	$P2_1/n$ (14)	$P2_1/c$ (14)	P1 (1)	$P\bar{1}$ (2)
a /Å	6.87590(10)	7.6847(2)	6.7344(3)	6.7576(4)
b /Å	13.2594(2)	10.5083(3)	6.9606(3)	7.3941(4)
c /Å	12.5785(2)	11.8250(4)	7.1931(4)	12.4200(5)
α /°	90	90	108.979(4)	78.514(4)
β /°	94.540(2)	91.882(3)	98.852(4)	81.724(4)
γ /°	90	90	114.329(4)	72.508(5)
U /Å^3	1143.19(3)	954.39(5)	273.84(3)	577.68(5)
Z	4	2	1	2
μ(Mo-K_α) /mm^{-1}	11.296	13.580	11.606	11.008
F(000)	828.0	764.0	199.0	414.0
Total number reflns	30789	13759	5307	15490
R_{int}	0.0259	0.1334	0.0731	0.0692
Unique reflns	3660	1870	2895	3458
No. of params, restraints	102/0	83/0	102/3	111/0
GOF	1.204	1.116	1.042	1.097
R_1, wR_2 $[I > 2\sigma(I)]^b$	0.0648, 0.1340	0.0615, 0.1582	0.0546, 0.1272	0.0501, 0.1169
R_1, wR_2 (all data)^b	0.0699, 0.1366	0.0639, 0.1622	0.0555, 0.1281	0.0558, 0.1207

Table 4.11: X-ray crystallography table. a: common data: wavelength (Mo-K_α) = 0.71073 Å; θ(max) = 27.5°; ^{b} $R_1 = \Sigma||Fo|-|Fc||/\Sigma|Fo|$; $wR_2=[\Sigma w(Fo^2-Fc^2)^2/\Sigma wFo^4]^{1/2}$

Compound	$[(WSCl_4)_2(MeS(CH_2)_3SMe)]$	$[(WSCl_4)_2(PhS(CH_2)_2SPh)]$	$[(WSCl_4)_2(^iPrS(CH_2)_2S^iPr)]$
Formula	$C_5H_{12}Cl_8S_4W_2$	$C_{14}H_{14}Cl_8S_4W_2$	$C_8H_{18}Cl_8S_4W_2$
M	851.69	961.79	893.76
Crystal system	Triclinic	Monoclinic	Monoclinic
Space group (no)	$P\bar{1}$ (2)	$P2_1/n$ (14)	$P2_1/c$ (14)
a /Å	6.6665(2)	10.5790(2)	10.7903(2)
b /Å	11.1479(2)	13.9272(3)	8.89710(10)
c /Å	13.8916(3)	17.2182(4)	12.1898(2)
α /°	101.979(2)	90	90
β /°	100.011(2)	96.368(2)	106.732(2)
γ /°	95.717(2)	90	90
U /Å^3	984.61(4)	2521.21(9)	1120.70(3)
Z	2	4	2
μ(Mo-K_α) /mm^{-1}	2.873	10.300	2.649
F(000)	780.0	1784.0	828.0
Total number reflns	15275	17788	18750
R_{int}	0.0394	0.0698	0.0613
Unique reflns	5051	6811	2199
No. of params, restraints	174/0	253/0	102/0
GOF	1.177	0.968	1.180
R_1, wR_2 $[I > 2\sigma(I)]^b$	0.0495, 0.1182	0.0420, 0.0711	0.0391, 0.0869
R_1, wR_2 (all data)^b	0.0580, 0.1279	0.0625, 0.0816	0.0413, 0.0884

Figure 4.11: X-ray crystallography table continued.

Compound	$[(WCl_3)_2(\mu\text{-}S_2)(\mu\text{-}S)(SPPh_3)_2]\bullet 2CH_2Cl_2$	$[(WCl_3)_2(\mu\text{-}S_2)(\mu\text{-}S)(SeMe_2)_2]$	$[(WCl_2)_2(\mu\text{-}S)_2(^iPrS(CH_2)_2S^iPr)][WSCl_5]\bullet CH_2Cl_2$
Formula	$C_{38}H_{34}Cl_{10}P_2S_5W_2$	$C_4H_{12}Cl_6S_3Se_2W_2$	$C_{17}H_{38}Cl_{13}S_5W_3$
M	1435.09	894.64	1415.17
Crystal system	Monoclinic	Monoclinic	Orthorhombic
Space group (no)	$P2_1/n$ (14)	C2/c (15)	Pnma (62)
a /Å	10.03090(10)	18.3641(5)	10.8463(2)
b /Å	26.3151(3)	9.1641(5)	31.8463(7)
c /Å	18.2867(2)	10.5536(3)	11.5026(2)
α /°	90	90	90
β /°	97.7900(1)	101.238(3)	90
γ /°	90	90	90
U /Å^3	4782.43(9)	1742.13(8)	3973.31(13)
Z	4	4	4
μ(Mo-K$_\alpha$) /mm^{-1}	5.681	18.629	9.815
F(000)	2760.0	1608.0	2652.0
Total number reflns	75427	22340	75427
R_{int}	0.0450	0.0775	0.0879
Unique reflns	15411	2696	6254
No. of params, restraints	514/0	80/0	188/22
GOF	1.113	1.058	1.295
R_1, wR_2 $[I > 2\sigma(I)]^b$	0.0410, 0.0782	0.0726, 0.1937	0.0682, 0.1242
R_1, wR_2 (all data)^b	0.0528, 0.0811	0.0815, 0.1983	0.0761, 0.1267

Figure 4.11: X-ray crystallography table continued.

4.6 References

(1) Young, C. G. *Comprehensive Coordination Chemistry II,* **2004,** *4*, 415-527
(2) Bannister, R. D.; Levason, W.; Reid, G.; Robinson, F. *Polyhedron,* **2019,** *169*, 129-34
(3) Benjamin, S. L.; Hyslop, A.; Levason, W.; Reid, G. *J. Fluorine. Chem.,* **2012,** *137*, 77-84
(4) Benjamin, S. L.; Chang, Y. P.; Gurnani, C.; Hector, A. L.; Huggon, M.; Levason, W.; Reid, G. *Dalton Trans.,* **2014,** *43*, 16640-48
(5) Levason, W.; Patel, B.; Reid, G.; Tolhurst, V.-A.; Webster, M. *J. Chem. Soc., Dalton Trans.,* **2000**, 3001-06
(6) Reid, S. D.; Hector, A. L.; Levason, W.; Reid, G.; Waller, B. J.; Webster, M. *Dalton Trans.,* **2007**, 4769-77
(7) Hart, R.; Levason, W.; Patel, B.; Reid, G. *J. Chem. Soc., Dalton Trans.,* **2002**, 3153-59
(8) Jura, M.; Levason, W.; Ratnani, R.; Reid, G.; Webster, M. *Dalton Trans.,* **2010,** *39*, 883-91
(9) Davis, M. F.; Levason, W.; Paterson, J.; Reid, G.; Webster, M. *Eur. J. Inorg. Chem.,* **2008**, 802-11
(10) Chang, Y. P.; Hector, A. L.; Levason, W.; Reid, G.; Whittam, J. *Dalton Trans.,* **2018,** *47*, 2406-14
(11) Levason, W.; Monzittu, F. M.; Reid, G. *Coord. Chem. Rev.,* **2019,** *391*, 90-130
(12) Tebbe, F. N.; Muetterties, E. L. *Inorg. Chem.,* **1968,** *7*, 172-74
(13) Brownstein, S.; Christian, B. H.; Latremouille, G.; Steigel, A. *Can. J. Chem.,* **1976,** *54*, 2343-48
(14) Noble, A. M.; Winfield, J. M. *Inorg. Nucl. Chem. Lett.,* **1968,** *4*, 339-42
(15) Levason, W.; Monzittu, F. M.; Reid, G.; Zhang, W. *Chem. Commun.,* **2018,** *54*, 11681-84
(16) Benjamin, S. L.; Levason, W.; Reid, G. *Chem. Soc. Rev.,* **2013,** *42*, 1460-99
(17) Fairbrother, F.; Grundy, K. H.; Thompson, A. *J. Chem. Soc.,* **1965**, 765-70
(18) Jura, M.; Levason, W.; Reid, G.; Webster, M. *Dalton Trans.,* **2009**, 7610-12
(19) Chang, Y. P.; Levason, W.; Light, M. E.; Reid, G. *Dalton Trans.,* **2016,** *45*, 16262-74
(20) Boorman, P. M.; Islip, M.; Reimer, M. M.; Reimer, K. J. *J. Chem. Soc., Dalton Trans.,* **1972**, 890-93
(21) Dori, Z. *Comprehensive Coordination Chemistry I,* **1987,** *3*, 973-1022
(22) Westland, A. D.; Uzelac, V. *Can. J. Chem.,* **1970,** *48*, 2871-76
(23) Sevdić, D.; Fekete, L. *Inorg. Chim. Acta,* **1982,** *57*, 111-17
(24) Levason, W.; McAuliffe, C. A.; McCullough, F. P.; Murray, S. G.; Rice, C. A. *Inorg. Chim. Acta,* **1977,** *22*, 227-31
(25) Dierkes, P.; Frenzen, G.; Wocadlo, S.; Massa, W.; Berger, S.; Pebler, J.; Dehnicke, K. *Z. Naturforsch. B,* **1995,** *50*, 159-67
(26) Fowles, G. W. A.; Tidmarsh, D. J.; Walton, R. A. *J. Inorg. Nucl. Chem.,* **1969,** *31*, 2373-79
(27) Hamilton, J. B.; McCarley, R. E. *Inorg. Chem.,* **1970,** *9*, 1333-39
(28) Hamilton, J. B.; McCarley, R. E. *Inorg. Chem.,* **1970,** *9*, 1339-43
(29) Levason, W.; Reid, G.; Zhang, W. *J. Fluorine. Chem.,* **2015,** *172*, 62-67
(30) Levason, W.; Reid, G.; Trayer, J.; Zhang, W. *Dalton Trans.,* **2014,** *43*, 3649-59
(31) Behzadi, K.; Iran, A. I. T. A.; Thompson, A. *J. Less Common Met.,* **1986,** *124*, 135-39
(32) Levason, W.; Light, M. E.; Reid, G.; Zhang, W. *Dalton Trans.,* **2014,** *43*, 9557-66
(33) Hubert-Pfalzgraf, L. G.; Postel, M.; Reiss, J. G. *Comprehensive Coordination Chemistry I,* **1987,** *3*, 585-698
(34) Bannister, R. D.; Levason, W.; Light, M. E.; Reid, G.; Zhang, W. *Polyhedron,* **2019,** *167*, 1-10
(35) Brown, M. D.; Hursthouse, M. B.; Levason, W.; Ratnani, R.; Reid, G. *Dalton Trans.,* **2004**, 2487-91
(36) Davis, M. F.; Levason, W.; Light, M. E.; Ratnani, R.; Reid, G.; Saraswat, K.; Webster, M. *Eur. J. Inorg. Chem.,* **2007,** *13*, 1903-10
(37) Fowles, G. W. A.; Frost, J. L. *J. Chem. Soc. A,* **1967**, 671-75
(38) Drew, M. G. B.; Hobson, R. J. *Inorg. Chim. Acta,* **1983,** *72*, 233-37
(39) Behzadi, K.; Baghlaf, A. O.; Thompson, A. *J. Less Common Met.,* **1987,** *128*, 195-206
(40) Drew, M. G. B.; Rice, D. A.; Williams, D. M. *J. Chem. Soc., Dalton Trans.,* **1984**, 1087-90
(41) Drew, M. G. B.; Rice, D. A.; Williams, D. M. *J. Chem. Soc., Dalton Trans.,* **1983**, 2251-56
(42) Drew, M. G. B.; Rice, D. A.; Williams, D. M. *Acta Cryst. C,* **1984,** *40*, 1547-49
(43) Chang, Y. P.; Hector, A. L.; Levason, W.; Reid, G. *Dalton Trans.,* **2017,** *46*, 9824-32
(44) Drew, M. G. B.; Rice, D. A.; Williams, D. M. *J. Chem. Soc., Dalton Trans.,* **1984**, 845-48

(45) Britnell, D.; Drew, M. G. B.; Fowles, G. W. A.; Rice, D. A. *Inorg. Nucl. Chem. Lett.,* **1973,** *9*, 501-04
(46) Britnell, D.; Fowles, G. W. A.; Rice, D. A. *J. Chem. Soc., Dalton Trans.,* **1975**, 213-15
(47) Drew, M. G. B.; Griffin, G. F.; Rice, D. A. *Inorg. Chim. Acta,* **1979,** *34*, L192
(48) Britnell, D.; Drew, M. G. B.; Fowles, G. W. A.; Rice, D. A. *Inorg. Nucl. Chem. Lett.,* **1973,** *9*, 415-17
(49) Hope, E. G.; Kemmitt, T.; Levason, W. *Organomet.,* **1988,** *7*, 78-83
(50) Walton, R. A. *Prog. Inorg. Chem.,* **1972,** *16*, 1 -194
(51) Fowles, G. W. A.; Rice, D. A.; Wilkins, J. D. *J. Chem. Soc., Dalton Trans.,* **1972**, 2313-18
(52) Fowles, G. W. A.; Rice, D. A.; Wilkins, J. D. *J. Chem. Soc., Dalton Trans.,* **1973**, 961-65
(53) Wilkins, J. D. *J. Inorg. Nucl. Chem.,* **1975,** *37*, 2095-97
(54) Müller, U.; Klingelhöfer, P.; Friebel, C.; Pebler, J. *Angew. Chem. Int. Ed.,* **1985,** *24*, 689-90
(55) Fedin, V. P.; Sokolov, M. N.; Myakishev, K. G.; Geras'ko, O. A.; Fedorov, V. Y.; Maciček, J. *Polyhedron,* **1991,** *10*, 1311-17
(56) Rabe, S.; Müller, U. *Z. anorg. allg. Chem.,* **1999,** *625*, 1367-70
(57) Fenske, D.; Czeska, B.; Schumacher, C.; Schmidt, R. E.; Dehnicke, K. *Z. anorg. allg. Chem.,* **1985,** *520*, 7-17
(58) Boorman, P. M.; Garner, C. D.; Mabbs, F. E.; King, T. J. *J. Chem. Soc., Chem. Commun.,* **1974**, 663-64
(59) Boorman, P. M.; Reimer, K. J. *Can. J. Chem.,* **1971,** *49*, 2926-30
(60) Garner, C. D.; Howlader, N. C.; Mabbs, F. E.; McPhail, A. T.; Onan, K. D. *J. Chem. Soc., Dalton Trans.,* **1978**, 1848
(61) Godfrey, S. M.; McAuliffe, C. A.; Pritchard, R. G.; Sheffield, J. M.; Thompson, G. M. *J. Chem. Soc., Dalton Trans.,* **1997**, 4823-28
(62) Hartley, F. R.; Murray, S. G.; Levason, W.; Soutter, H. E.; McAuliffe, C. A. *Inorg. Chim. Acta,* **1979,** *35*, 265-77
(63) Gulliver, D. J.; Hope, E. G.; Levason, W.; Murray, S. G.; Potter, D. M.; Marshall, G. L. *J. Chem. Soc., Perkin Trans. II,* **1984,** *2*, 429-34
(64) Gibson, V. C.; Kee, T. P.; Shaw, A. *Polyhedron,* **1990,** *9*, 2293-98
(65) Dietz, S.; Allured, V.; DuBois, M. R. *Inorg. Chem.,* **1993,** *32*, 5418-20

Single Source Precursors for the Low-Pressure Chemical Vapour Deposition of WS_2 Films

5.1 Introduction

Layered transition metal dichalcogenides have been the focus of much interest in recent years, due to their desirable properties and structural relationship as inorganic analogues of graphene. Common methods of forming ME_2 (E = S, Se or Te) 2D films are mechanical and liquid exfoliation[1] from bulk crystalline samples or heating metal oxides with elemental chalcogens for the vapour to deposit onto substrates.[2-10] Chemical vapour deposition (CVD) is a versatile and a cheap method for accessing a variety of these thin films. Complexes with suitable ligands have been identified as potential precursors for the production of WS_2 thin films *via* low-pressure chemical vapour deposition (LPCVD). This chapter details the low-pressure chemical vapour deposition of WS_2 from a selection of complexes (synthesised in Chapter 4) and subsequent materials characterisation.

5.2 Transition Metal Dichalcogenides *via* Chemical Vapour Deposition

The use of CVD for the production of transition metal dichalcogenide thin films has advanced significantly in recent years.[11,12] Traditionally, CVD uses two chemicals, each containing one of the elements, and passing them over heated substrates, where the vapour decomposes depositing ME_2 films onto the substrate.[13] Typically, chemicals with low molecular weights and high volatility are used; such as $NbCl_5$ and Se^nBu_2 to produce $NbSe_2$ thin films or $WOCl_4$ and $HS(CH_2)_2SH$ for WS_2 films.[14,15] Single source low-pressure CVD uses a single reagent that contains all the elements required to deposit ME_2 films (experiments need to be carried out at low pressure to increase vaporisation of the less volatile precursor). Single source precursors provide the ability to control more variables and therefore have more influence over the films produced. In some cases, predetermining the stoichiometry of the metal, the chalcogen and the molecular weight allows greater control over the deposition conditions and subsequent film characteristics, including film phase, dopant concentration and orientation of crystals within the film. In addition there are examples of LPCVD enabling highly substrate-selective deposition onto micro- or nano-patterned substrates.[16,17] Metal halide complexes with chalcogenoether ligands and metal chalcogenide halides possess many properties that are desirable to make suitable CVD precursors, including having suitable volatility and removal of Cl_2 *in-vacuo* as a by-product. Coordination of chalcogenoethers ligands with alkyl substituents provides a low energy decomposition pathway *via* ß-hydride elimination and subsequent release of alkenes.[18,19]

5.2.1 Group IV Transition Metal Dichalcogenides

Titanium dichalcogenides are reported as semiconducting diamagnetic materials,[20,21] their layered structure also makes them suitable for a range of applications, including but not limited to cathode materials for Li ion batteries,[11,22-24] as well as for the removal of impurities from crude oil as some examples.[25] Reaction of elemental titanium with elemental sulfur or hydrogen sulfide under vacuum in sealed ampoules (625 or 800 ºC) has been shown to deposit TiS_2 films of varying thickness.[26,27] Dual source CVD has been used for the successful preparation of TiS_2 using $TiCl_4$ and $S_2{}^tBu_2$ at 300 ºC for 2 hours in ultra-high vacuum.[28] $TiCl_4$ has also been used with hydrogen sulfide at 350 ºC *via* plasma enhanced CVD, however, this produced a non-continuous film.[29,30] Further examples from Parkin and co-workers demonstrated the use of ambient pressure CVD with $[Ti(NMe_2)_4]$ and ^{t}BuSH or $^tBu_2S_2$, using ^{t}BuSH as the sulfur source allowed deposition of TiS_2 films at lower temperatures (200 ºC).[25] Following this, the compounds $[Ti(NMe_2)_4]$ and ^{t}BuSH were mixed in solvent and it is suggested the complex $[Ti(S^tBu_2)_4]$ forms *in-situ* and is subsequently used in aerosol assisted CVD (AACVD) between 150-300 ºC.[31] Initial work into single source precursors for the deposition of TiS_2 using $[TiCl_4(L)_2]$ (L = thiane or tht) concluded that the precursors were not suitable as the cyclic group slows down the rate of C-S cleavage.[32] Following the *in-situ* work using $[Ti(NMe_2)_4]$ and ^{t}BuSH, complexes of $[Ti(S^tBu_2)_4]$ and $[Ti(S^tBu_2)_3(NEt_2)]$ were isolated and then used as precursors to deposit gold coloured TiS_2 thin films.[33]

Titanium diselenide and ditelluride are both studied for their superconductive properties either at low temperature with Cu intercalation[34] or high pressure,[35] with $TiTe_2$ also a candidate for field-effect transistors.[36] Preparations of $TiSe_2$ are much less numerous than TiS_2, elemental titanium and selenium have been shown to react and deposit 1T-$TiSe_2$ thin films onto graphene/SiC substrates.[37] Thin film studies have been carried out, exfoliation from bulk 1T-$TiSe_2$ crystals and the films' properties investigated as the films move from tri- to bi- to mono-layer.[38] Examples of dual source CVD include using $TiCl_4$ and $SeEt_2$ or $Se_2{}^tBu_2$, at ambient pressure, to deposit blue $TiSe_2$ onto glass substrates with plate-like crystallites orientated parallel to the substrate.[39] Single source precursors $[TiCl_4(SeR_2)_2]$ (R = Et or ^{n}Bu),[40] $[(Cp)_2Ti(Se^tBu_2)_2]$[41] or $[TiCl_4(o\text{-}C_6H_4(CH_2SeMe)_2)]$[18] have been used in LPCVD and shown to deposit 1T-$TiSe_2$ thin films at 500-600 ºC onto SiO_2 substrates. The complex $[TiCl_4(Se^nBu_2)_2]$ is shown to deposit 1T-$TiSe_2$ selectively onto the TiN regions of photolithographically micropatterned TiN/SiO_2 substrates with recesses of 2 µm. Attempts to isolate $[(Cp)_2Ti(Te^tBu_2)_2]$ for a potential $TiTe_2$ precursor were unsuccessful[41] and currently $TiTe_2$ thin films are only reported *via* exfoliation from bulk $TiTe_2$ crystals.[36]

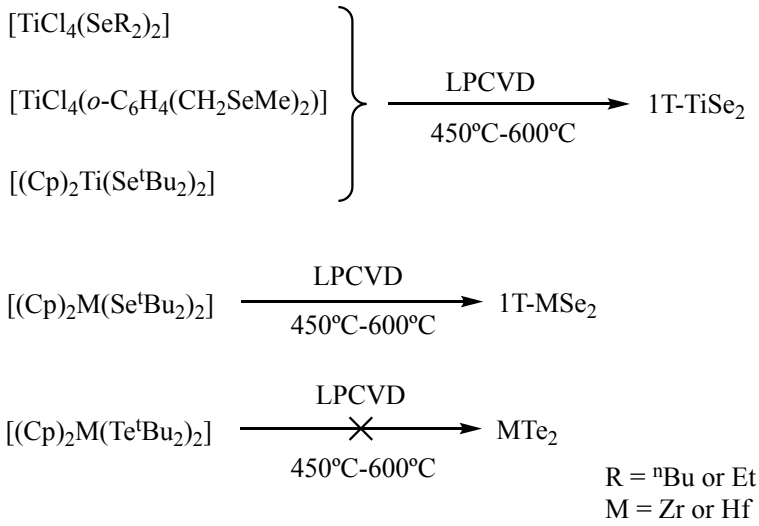

Figure 5.1: Scheme showing single source precursors for the LPCVD of MSe_2 and MTe_2 (M = Ti, Zr or Hf) attempts.[19,41-43]

Other Group IV transition metal dichalcogenides ME_2 (M = Zr or Hf) are studied for electrical transport properties[44-46] and are potential materials for large scale solar cells with high short circuit currents.[47] Synthesis of ZrS_2 and HfS_2 has been shown from the elemental metal or the metal iodide (MI_4) and elemental sulfur under vacuum[27] or using MCl_4 and sulfur *via* CVD depositing onto *h*-BN or Si/SiO_2 substrates.[48-53] Under similar conditions, MSe_2 films can be produced with metal powder and elemental selenium with iodine as a transporting agent when heated to high temperatures (700-900ºC).[54-56] Analogous to $[(Cp)_2Ti(Se^tBu_2)_2]$, the single source precursors $[(Cp)_2M(Se^tBu_2)_2]$ (M = Zr or Hf) can produce thin 1T films *via* LPCVD.[41] The complexes $[(Cp)_2M(Te^tBu_2)_2]$ (M = Zr or Hf) were the first tellurolate complexes of their type, however were unsuccessful as LPCVD precursors as the weak Te-alkyl bonds led to facile Te elimination and deposited only elemental Te.[41] The only reports of MTe_2 films are from heating metal powders, tellurium and iodine, and using CBr_4 as a transporting agent.[57-59]

5.2.2 Group V Transition Metal Dichalcogenides

Thin films of ME_2 (M = V, Nb or Ta; E = S, Se or Te) are of interest due to their superconducting properties[60] which makes them potential materials for charge density wave transitors[61-63] and their intercalation properties.[64] VS_2 was first reported using $LiCO_3$, V_2O_5 and H_2S using CVD[65-68] following this, washing $LiVS_2$ with deionised water and ethanol results in the formation of VS_2.[69] There are currently no reported single source precursors for the CVD of 1T-VS_2 although there is an example of dual source ambient pressure CVD using VCl_3 and elemental sulfur at 500ºC.[63]

Vanadium diselenide thin films can be produced with elemental vanadium and selenium at 700-800ºC and crystals have been grown with iodine as a transporting agent.[62,63,65] Dual source precursors ($VOCl_3$ or $[V(NMe_2)_4]$ and Se^tBu_2) for APCVD at 250-600 ºC were shown to produce films 1T-VSe_2 with a range of stoichiometric ratio (0.7 – 2.1) however using $VOCl_3$ as the vanadium source caused impurities of VO_x in the films and low Se content.[14] Using $[V(NMe_2)_4]$ as

the vanadium source produced films much closer to VSe_2 shown by EDX (1:2.1). A recent report demonstrates heating VCl_3 and Se together using 10% H_2/Ar as a carrier gas deposits 1T-VSe_2 thin films onto sapphire substrates.[70]

A series of VCl_4 and VCl_3 diselenoether complexes [VCl_x(L-L)] have been prepared, but they were not sufficiently volatile to produce VSe_2 thin films.[19] Within the same study, the complexes [$VCl_3(SeMe_2)_2$] and [$(Cp)_2V(Se^tBu_2)_2$] were isolated and shown to be suitable as single source precursors to deposit 1T-VSe_2 thin films at 500-600 ºC.[19] Recently, nanoplates of 1T-VTe_2 have been deposited from sublimed salt-assisted atmospheric pressure CVD using V_2O_5, NH_4Cl and Te at 750 ºC, however, there are no single source precursors for the deposition of VTe_2.[71]

The production of NbE_2 thin films *via* CVD has been studied more extensively than other transition metal dichalcogenides. Crystals of NbS_2 suitable for X-ray diffraction have been grown by vapour transport methods.[72,73] 2H-NbS_2 thin films have only been reported when using dual source precursors [$Nb(NMe_2)_5$] and ^{t}BuSH using AACVD from CH_2Cl_2 or *n*-hexane solution.[74] Whereas, 1T-NbS_2 thin films have been prepared from $NbCl_5$ and $S(SiMe_3)_2$ or $^tBu_2S_2$ at 500ºC onto float glass.[75,76] The more common 3R-polymorph has been shown *via* the reaction of elemental niobium and sulfur and using dual source APCVD with $NbCl_5$ and $HS(CH_2)_2SH$ or ^{t}BuSH.[77-80]

3R-NbS_2 thin films have also been deposited from a variety of single source precursors, the first report was using [$NbCl_4(S_2R_2)_2$][$NbCl_6$] in LPCVD at 500 ºC as confirmed by XRD and XPS.[81] Following this, reflective brown 3R-NbS_2 thin films were deposited *via* LPCVD from [$NbCl_5(S^nBu_2)$] onto silica.[82] Subsequently a series of coordination complexes with $NbCl_4$ and thioethers with the desired 1:2 ratio were isolated, however attempts to use them for LPCVD failed, with failure attributed to insufficient volatility and loss of thioether at elevated temperatures, leaving $NbCl_4$ residue.[83] The metal chalcogenide halide, $NbSCl_3$, is shown to vaporise upon heating[84] but CVD attempts using this directly failed to produce any deposit.[85] A series of niobium sulfide halides with thioethers was therefore established and precursors with ß-hydrogens, [$NbSCl_3(S^nBu_2)_2$] and [$NbSCl_3(^nBuS(CH_2)_3S^nBu)$], were shown to deposit 3R-NbS_2 thin films with <00*l*> preferred orientation.[85]

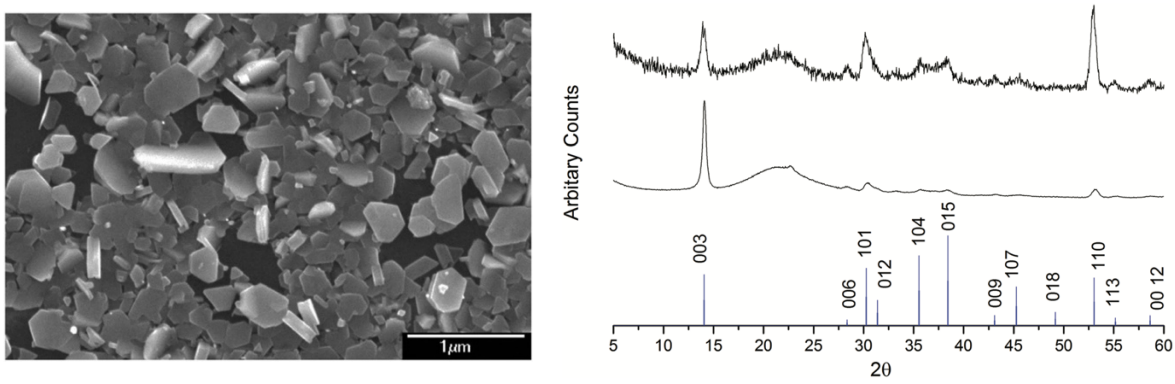

Figure 5.2: Scanning electron microscope image of polycrystalline NbS_2 films. Deposited by low pressure CVD from [$NbSCl_3(S^nBu_2)$] at 700 ºC (left).[85] Right: IPXRD (top), GIXRD (middle) from $NbSe_2$ deposited by LPCVD of [$NbCl_5(Se^nBu_2)$] at 650 ºC and literature pattern for $NbSe_2$ bulk (bottom).[82]

In contrast, $NbSe_2$ thin films favour the polymorph 2H over 3R, there is only one report of 3R-$NbSe_2$ deposition, which used the single source precursor $[NbCl_5(Se^nBu_2)]$ in LPCVD at 650 ºC to produce dark brown 3R-$NbSe_2$ thin films.[82] 2H-$NbSe_2$ thin films have been deposited *via* chemical vapour transport and dual source APCVD using $NbCl_5$ and Se^tBu_2.[74,86-89] As with the attempts to produce NbS_2 films from $NbCl_4$ complexes with thioether complexes, the corresponding Nb(IV) selenoether complexes also did not produce thin films.[83] However 2H-$NbSe_2$ thin films were deposited *via* LPCVD at 650 ºC using $[NbSe_2Cl_3(Se^nBu_2)]$ onto silica, but show significantly less preferred orientation compared to the 3R-NbS_2 thin films.[85] The complex $[NbCl_5(Te^nBu_2)]$ was prepared but decomposed within a few hours therefore was not tested for LPCVD for the production of $NbTe_2$.

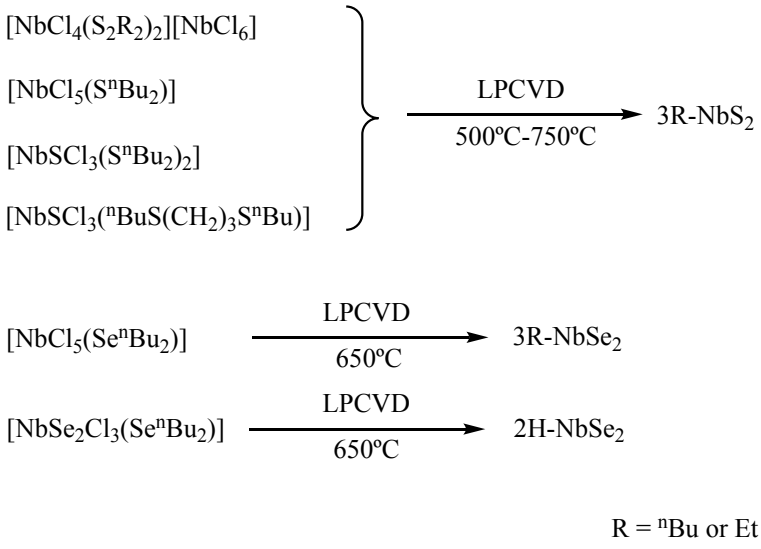

Figure 5.3: Scheme showing single source precursors for the LPCVD of NbE_2 (E = S or Se). [82,85]

Films of tantalum dichalcogenides are considerably rarer compared to their 4*d* counterparts, NbE_2 films. The crystal structures of TaS_2 and $TaSe_2$ have been obtained using a temperature gradient and sintered powder at 900 ºC under vacuum. Complexes analogous to the niobium counterparts $[TaCl_5(E'^nBu_2)]$ (E' = S, Se or Te) all failed to produce any deposit by CVD.[82] This is also the case with $[TaSCl_3(^nBuE'(CH_2)_3E'^nBu)]$ (E' = S or Se) complexes, the relatively high molecular weights may be a factor, although the lower stability of the tantalum complexes is also likely to hinder film growth by CVD.[90] The only successful deposition of TaS_2 reported used $[Ta(NMe_2)_5]$ and ^{t}BuSH in AACVD with CH_2Cl_2 or *n*-hexane[74] and the only 2H-$TaSe_2$ thin film is from the chemical vapour transport method.[91,92] A recent report has shown 3R-$TaSe_2$ thin films deposited from APCVD using $TaCl_5$, Ta and Se in a 10:1 ratio of halide to metal under H_2/Ar flow.[93] Currently there are no reports of MTe_2 (M = Nb or Ta) deposited thin films and LPCVD attempts using $[TaCl_5(Te^nBu_2)]$ deposited a small amount of crystallised tellurium.[82]

5.2.3 Group VI Transition Metal Dichalcogenides

MoE_2 (E = S or Se) thin films are probably some of the most explored and most interesting 2D transition metal dichalcogenides, they are promising materials for a variety of applications including spintronics,[94] electrocatalysts for hydrogen evolution,[95,96] optoelectronics[9] and environmental sensors.[97] Increasingly, MoS_2 is also being investigated for its thermoelectric properties,[98] traditionally MoE_2 films or powders were prepared by heating MoO_3 with elemental sulfur or selenium at 800 ºC under vacuum.[3-8,99-115] Some of these reports have claimed to have deposited films <1 nm thick[3,5] or monolayer MoE_2; these ultra-thin 2D films are extremely desirable due to the transition from indirect to direct bandgap material.[4,102] There are reports of using $[NH_4]_2[MoS_4]$ with H_2 gas in the gas phase to deposit MoS_2 films, as well as using $[NH_4]_2[MoS_4]$ in DMF *via* AACVD at 400 ºC.[10,110] Reports of using molybdenum halides for CVD are rare; an initial example of using $[Mo(S^tBu)_4]$ has been shown to deposit MoS_2 at moderate temperatures (110-350 ºC).[116] Following this early report, a series of $MoCl_4$ complexes with thioethers of the form $[MoCl_4(L)_2]$ and $[MoCl_4(L\text{-}L)]$ were synthesised. Using the terminal butyl complex $[MoCl_4(S^nBu_2)_2]$ in LPCVD at 750 ºC thin films of 2H-MoS_2 were deposited. These were too thin to generate an XRD pattern, but were identified as 2H-MoS_2 by Raman spectroscopy.[117]

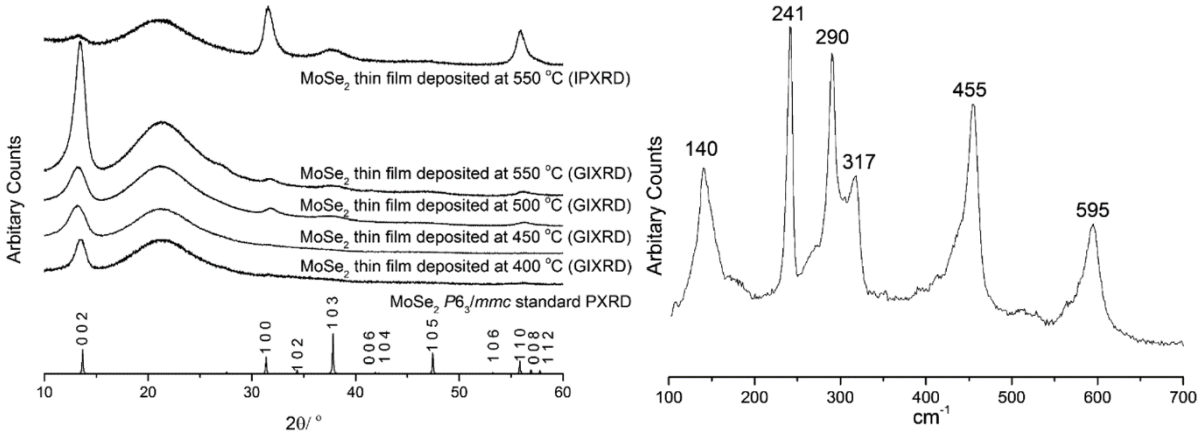

Figure 5.4: GIXRD and IPXRD (top) of 2H-$MoSe_2$. Deposited by LPCVD at 400 ºC–550 ºC from $[MoCl_4(Se^nBu_2)_2]$ (left) and Raman spectrum of $MoSe_2$ deposited by LPCVD at 550 ºC from $[MoCl_4(Se^nBu_2)_2]$ (right).[117]

Within the same report, using the analogous complex $[MoCl_4(Se^nBu_2)_2]$ at 550 ºC produced 2H-$MoSe_2$ thin films, which showed strong preferred orientation for the <00*l*> plane with platelets growing parallel to the substrate and with a film thickness of 130 nm.[117] The only other report of using CVD to deposit $MoSe_2$ is using $MoCl_5$ and either $SeEt_2$ or $^nBu_2Se$ at 200 ºC *via* APCVD, with XRD data suggesting mixed polymorphs of 3R and 2H.[118]

Similarly to MoE_2 thin films, WE_2 (E = S or Se) thin films have commonly been made by heating WO_3 and elemental chalcogen at 925 ºC under vacuum.[6,114,115,119,120] Compared to MoE_2 films, the WE_2 films are underdeveloped; there is only a single report of using AACVD for the deposition of 2H-WS_2 from the dithiocarbamate complex $[WS(S_2)(S_2CNEt_2)_2]$ at 350 ºC.[121]

The deposition of MTe_2 (M = Mo or W) thin films has received little attention, probably as the precursors are less stable and the materials decompose rapidly to release tellurium vapour.[122] A few examples of heating the metal with tellurium using CVD at 650-700 ºC ($MoTe_2$)[123,124] and 1000 ºC (WTe_2) are known.[125] Recently a dual source precursor using metal oxides (MoO_3 or WO_3), metal halides ($MoCl_5$ or WCl_6) and tellurium powder in a 1:1:1 ratio deposited MTe_2 thin films at 700-800 ºC, confirmed by Raman spectroscopy.[122] An example of 1T'-WTe_2 thin films has been demonstrated by using WCl_6 and Te in a three zone furnace depositing onto SiO_2/Si substrates under N_2/H_2.[126]

The application of various CVD methods has been of particular interest in the last 20 years, with significant advances in the variety of materials deposited and complexes used as precursors. It is not yet entirely clear what makes a 'good' single source LPCVD precursor, but complexes with a low energy decomposition pathway (ß-hydride elimination) seem to play a vital role. However, other factors, including the molecular weight of precursors and the stability of the molecules is particularly problematic for deposition of heavier transition metals, as the metal generally becomes harder going down the group, meaning M-E bonds become weaker. Also, some precursors allow the incorporation of impurities into the deposited films, common impurities are Cl, O and C but a 'good' precursor facilitates the removal of these impurities *in vacuo.*

5.2.4 Aims

This chapter investigates and details the potential of single source LPCVD precursors identified and synthesised in Chapter 4 for the deposition of WS_2 thin films. The precursors have been fully characterised in the previous chapter and the deposited WS_2 thin films will be characterised by Raman spectroscopy, X-ray diffraction, X-ray photoelectron spectroscopy, SEM and their electrical properties investigated.

5.3 Results and Discussion

The complexes $[(WSCl_4)_2(^iPrS(CH_2)_2S^iPr)]$, $[WSCl_3(^iPrS(CH_2)_2S^iPr)]$ and $[WSCl_4(S^nBu_2)]$ were tested as single source low pressure chemical vapour deposition precursors at 550-700 ºC, *ca.* 0.1 mmHg. No significant deposits were obtained at lower temperatures and the complex $[WSCl_3(^iPrS(CH_2)_2S^iPr)]$ did not produce any deposits across the range 600-700 ºC. Material analyses were performed by Dr Roumeng Huang (XPS, SEM and Raman spectroscopy) and Dr Shibin Thomas (EDX and WDX) from ECS and the School of Chemistry at the University at Southampton, respectively.

5.3.1 Low Pressure CVD using $[(WSCl_4)_2(^iPrS(CH_2)_2S^iPr)]$

The complex $[(WSCl_4)_2(^iPrS(CH_2)_2S^iPr)]$ would not be considered to be a 'traditional' single source LPCVD precursor due to its high molecular weight. However, the terminal isopropyl groups may still provide a suitable ß-hydride elimination pathway. Despite the high molecular weight, the precursor produces bronze films with uniform coverage across a number of SiO_2 tiles. The films were identified as 4H-WS_2 and were deposited at 590-620 ºC/0.1 mmHg , although the precursor does leave a large amount of (unidentified) amorphous black residue in the precursor bulb.

Surprisingly, the W(V) complex, $[WSCl_3(^iPrS(CH_2)_2S^iPr)]$, did not produce any deposit despite its molecular weight being almost half that of $[(WSCl_4)_2(^iPrS(CH_2)_2S^iPr)]$. It also seemed to decompose into an amorphous black powder in the precursor bulb upon heating. The very different behaviour of these two very similar complexes highlights that the factors that make an effective precursor are not yet well understood.

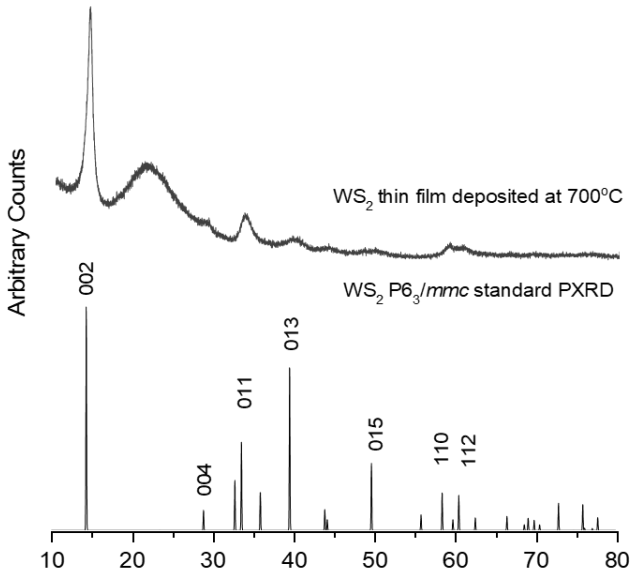

Figure 5.5: Grazing incidence XRD pattern (top) from a WS_2 thin film deposited by low pressure CVD using $[(WSCl_4)_2(^iPrS(CH_2)_2S^iPr)]$ at 700 ºC. The broad feature at $2\theta = 20$ -25° is from the SiO_2 substrate, XRD pattern for bulk WS_2 (bottom).[127]

Analysis of the films deposited from $[(WSCl_4)_2(^iPrS(CH_2)_2S^iPr)]$ are consistent with polycrystalline 4H-WS_2 in the space group $P6_3/mmc$ and the lattice parameters were refined as a = 3.1523(11), c = 12.381(4) Å (R_{wp} = 7.67%, literature: a = 3.1532(4), c = 12.323(5) Å).[127] The grazing incidence XRD pattern is dominated by the 002 reflection, suggesting preferred orientation in the <00*l*> direction. This is not unusual in 2D layered materials as they typically grow initially along the c axis parallel to the substrate, resulting in flat platelets,[85,117] although this preferred orientation is commonly suppressed as the films get thicker. Attempts to obtain an in-plane XRD pattern, even over an extended period, were unsuccessful as the films were unfortunately too thin. The average crystallite size was calculated from the grazing incidence XRD data (Figure 5.5) using the Williamson-Hall method (see Section 1.10.1), giving an estimated size of 9.1(3) nm.

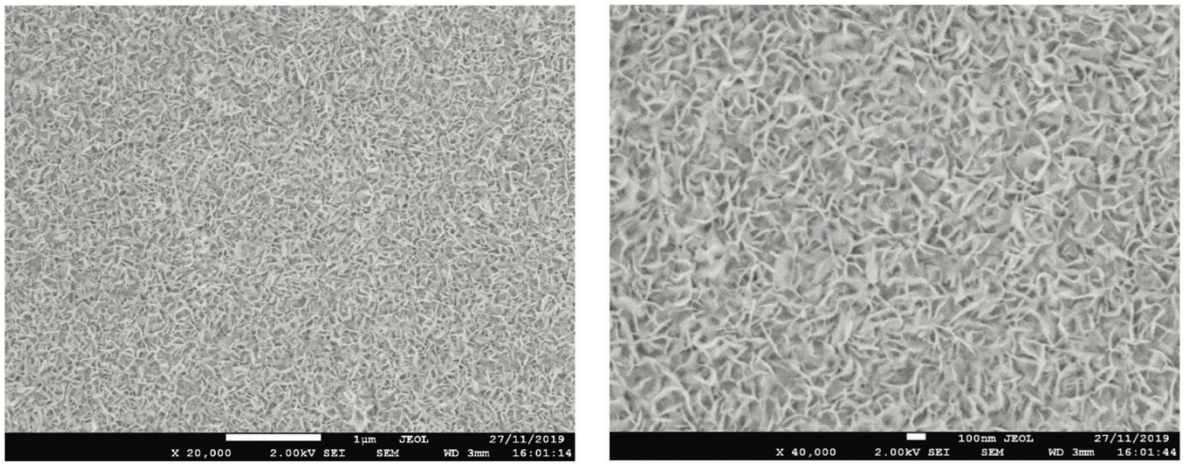

Figure 5.6: SEM image showing a continuous WS_2 thin film produced via low pressure CVD using $[(WSCl_4)_2(^tPrS(CH_2)_2S^iPr)]$ at 700 ºC.

Scanning electron microscopy (SEM) showed uniform and continuous coverage of the substrate by small hexagonal platelet crystallites (Figure 5.6). Accurate determination of composition was attempted using EDX analysis, however, due to overlap of the emission peaks from tungsten and silicon within the substrate (W $M\alpha_1$: 1.775 keV and Si $K\alpha_1$: 1.740 keV),[128] this was not possible. However, the EDX spectrum has no C or Cl impurity peaks indicating a clean deposition. A subsequent attempt using WDX (which has higher resolution) confirmed the presence of both tungsten and sulfur, but a reliable ratio could not be obtained as films were too thin.

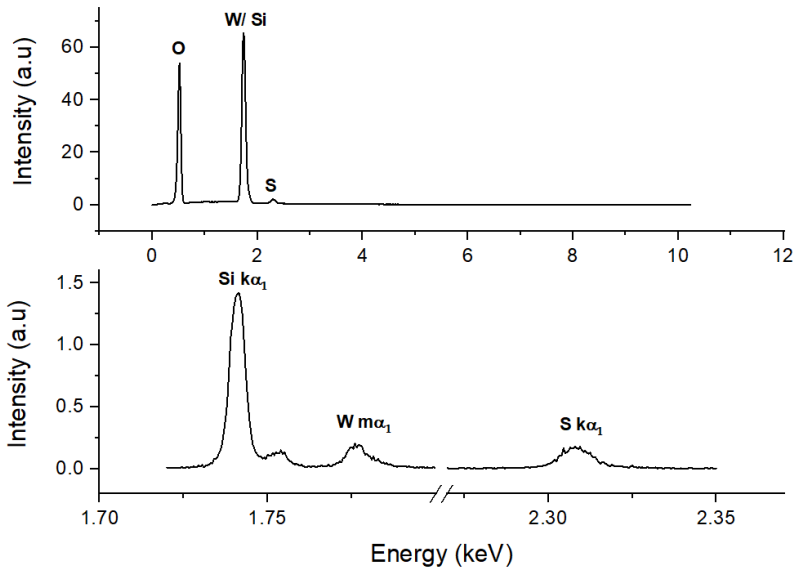

Figure 5.7: EDX spectrum (top) and WDX spectrum (bottom) from WS_2 thin film via low pressure CVD using $[(WSCl_4)_2(^tPrS(CH_2)_2S^iPr)]$ at 700 ºC.

To obtain accurate determination of composition X-ray photoelectron spectroscopy (XPS) was carried out on the as-deposited films (Figure 5.8). The W peaks at 32.6, 34.7, 28.2 eV can be assigned to W $4f_{7/2}$, W $4f_{5/2}$, W $5p_{3/2}$ from which it can be concluded that the films are not oxidised. The S peaks at 162.2 and 163.4 eV are attributed to S $p_{1/2}$ and $Sp_{3/2}$ and are characteristic of S^{2-} in WS_2.[129] The W : S ratio (1 : 2.2) was estimated by integrating the W 4f and the S 2p peaks.

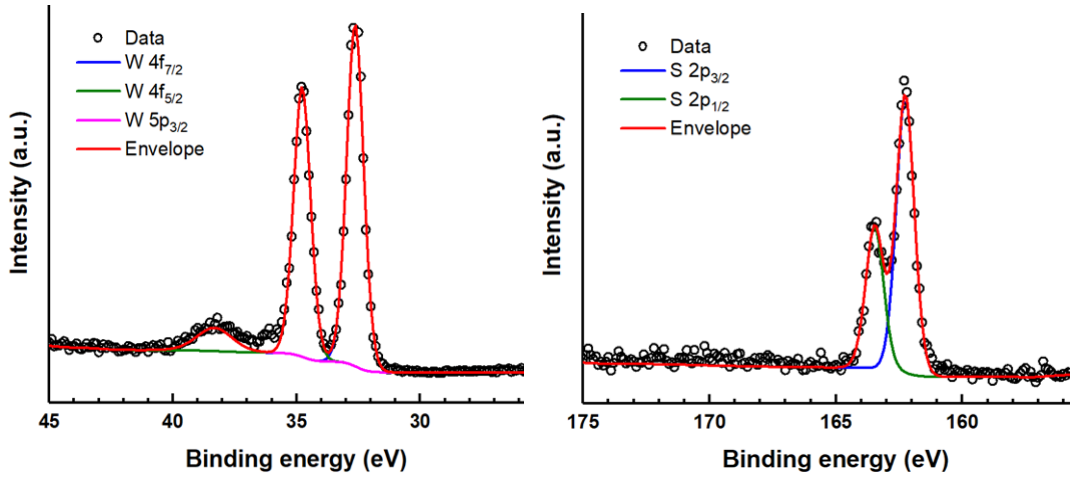

Figure 5.8: Representative XPS data for an as-deposited WS_2 film thin film via low pressure CVD using $[(WSCl_4)_2(^iPrS(CH_2)_2S^iPr)]$. Showing the peaks associated with tungsten (left) and sulfur (right).

Raman spectra were collected using a 532 nm excitation laser and the spectra show the two main peaks at 352 and 419 cm^{-1}, which are assigned to the E_{2g} and A_{1g} vibrational modes of WS_2, respectively; the weaker features present in the spectra are also consistent with WS_2 peaks.[130]

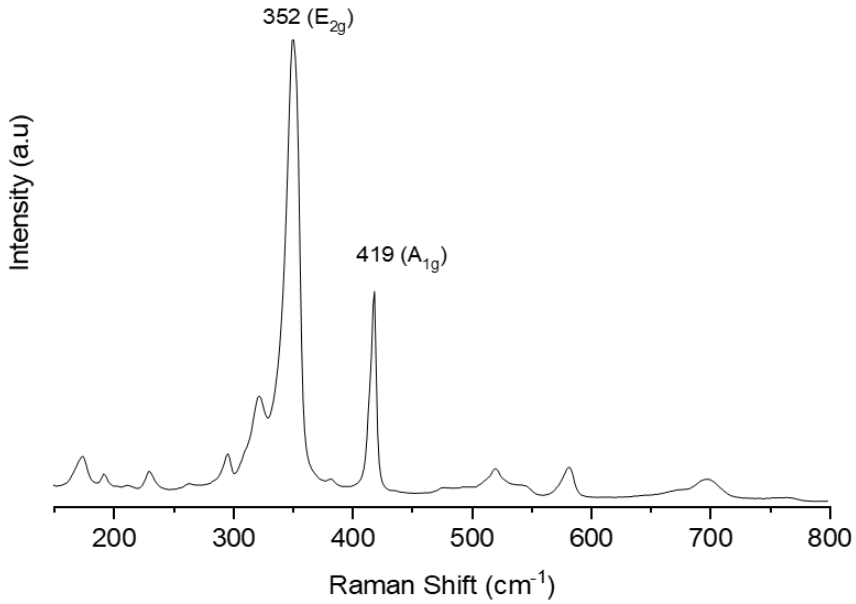

Figure 5.9: Raman spectra for as-deposited WS_2 thin films via low pressure CVD using $[(WSCl_4)_2(^iPrS(CH_2)_2S^iPr)]$ at 700 °C.

5.3.2 Low Pressure CVD using $[WSCl_4(S^nBu_2)]$

Following the success of the precursor, $[(WSCl_4)_2(^iPrS(CH_2)_2S^iPr)]$, for WS_2 film growth, it was decided to investigate the simpler mononuclear W(VI) complex, $[WSCl_4(S^nBu_2)]$, for LPCVD. Initially this precursor was overlooked due to its extreme sensitivity to moisture, but if the complex was isolated and used immediately it was possible to perform a series of LPCVD experiments.

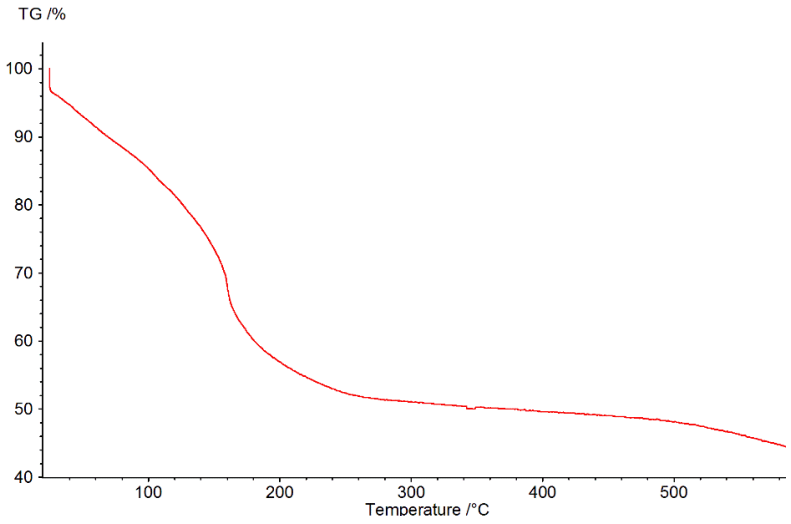

Figure 5.10: TGA profile for [$WSCl_4(S^nBu_2)$] 0 – 600ºC.

Thermogravimetric analysis (TGA) was undertaken in order to gain an insight into the decomposition pathway of the precursor. The TGA profile shows an initial weight loss step (25 to 125 ºC) then a significant loss (130 to180 ºC). Followed by a plateau between 350 to 425 ºC at ~50 % weight loss, WS_2 would be expected to correspond to 49.2 % of the original mass. A further gradual weight loss from 450 ºC to 600 ºC is observed which could be further loss of sulfur. This precursor was therefore considered to merit testing *via* LPCVD. Although deposition temperatures would not be comparable as TGA is undertaken at ambient pressure. The precursor [$WSCl_4(S^nBu_2)$] successfully deposited WS_2 thin films as described below.

When using small amounts of [$WSCl_4(S^nBu_2)$] (*ca*. 30-80 mg), low pressure CVD onto SiO_2 substrates at 700 ºC (0.1 mmHg) resulted in dark almost black thin films across a number of tiles (624 to 652 ºC). Coverage of tiles was uniform and with increased amounts of precursor thicker matte films were produced. Unlike [$(WSCl_4)_2(^iPrS(CH_2)_2S^iPr)$], [$WSCl_4(S^nBu_2)$] does not leave any significant residue in the precursor bulb, suggesting a better LPCVD precursor. Grazing incidence X-ray analysis of these films (Figure 5.11) is consistent with 4H-WS_2 in space group $P6_3/mmc$ (lattice parameters were refined as: a = 3.1185(16), c = 12.771(8) Å R_{wp} = 8.10%, literature: a = 3.1532(4), c = 12.323(5) Å).[127] The grazing incidence pattern is dominated by the 002 reflection, suggesting platelets lying flat and parallel to the substrate (with the c-axis normal to the substrate). An in-plane XRD measurement shows the suppression of the 002 reflection and has enhanced the 011, 110 and 112 reflections, supporting this conclusion. The crystallite size in the WS_2 film produced at 650 ºC was calculated from the grazing incidence XRD data using the Williamson-Hall method, which resulted in crystals of 3.8(2) nm. These crystallites are significantly smaller than for the WS_2 deposits from [$(WSCl_4)_2(^iPrS(CH_2)_2S^iPr)$], possibly due to increased volatility of [$WSCl_4(S^nBu_2)$]. Increased volatility results in higher vapour concentration, meaning there is an increased number of nucleation sites above the substrate and therefore faster deposition resulting in smaller crystals.

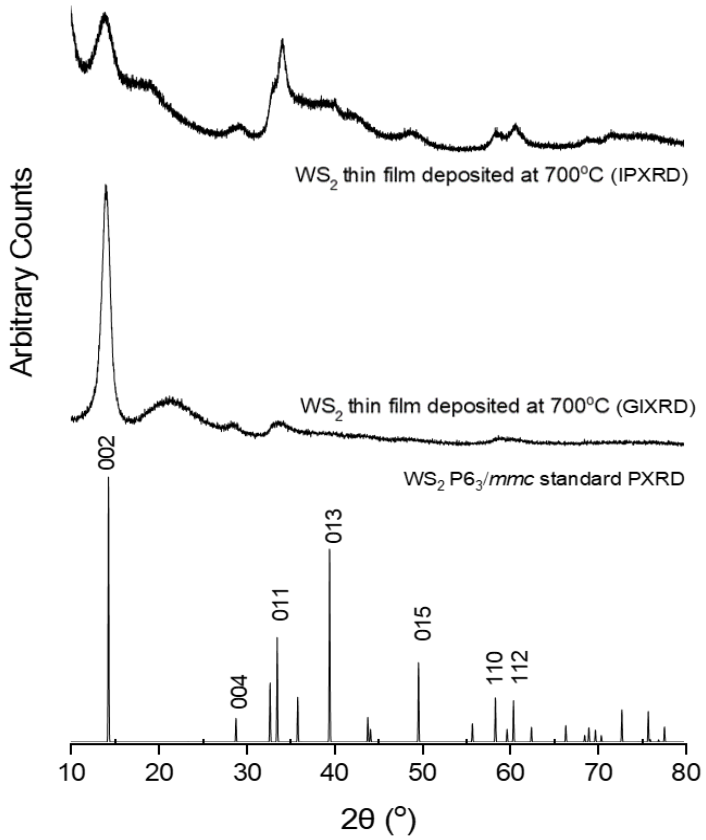

Figure 5.11: In-plane XRD pattern (top), grazing incidence XRD pattern (middle) from a WS_2 thin film deposited by low pressure CVD using [$WSCl_4(S^nBu_2)$] at 700 ºC. The broad feature at 2θ = 20 -25° is from the SiO_2 substrate, XRD pattern for bulk WS_2 (bottom).[127]

Scanning electron microscopy (SEM) showed uniform and continuous coverage over the entire substrate (2 cm x 0.8 cm, deposited at 639 ºC) by small hexagonal crystallites (Figure 5.12). The calculated crystallite size from the GIXRD pattern is significantly smaller than the largest dimensions of the platelets observed in Figure 5.12 (*ca.* 100 nm) suggesting a dense underlying material. The GIXRD pattern suggests the platelets are parallel to the substrate, with a small crystallite size. The SEM images show the top layer has different directional growth to the underlying film, this is quite a common observation for TMDC materials.[117]

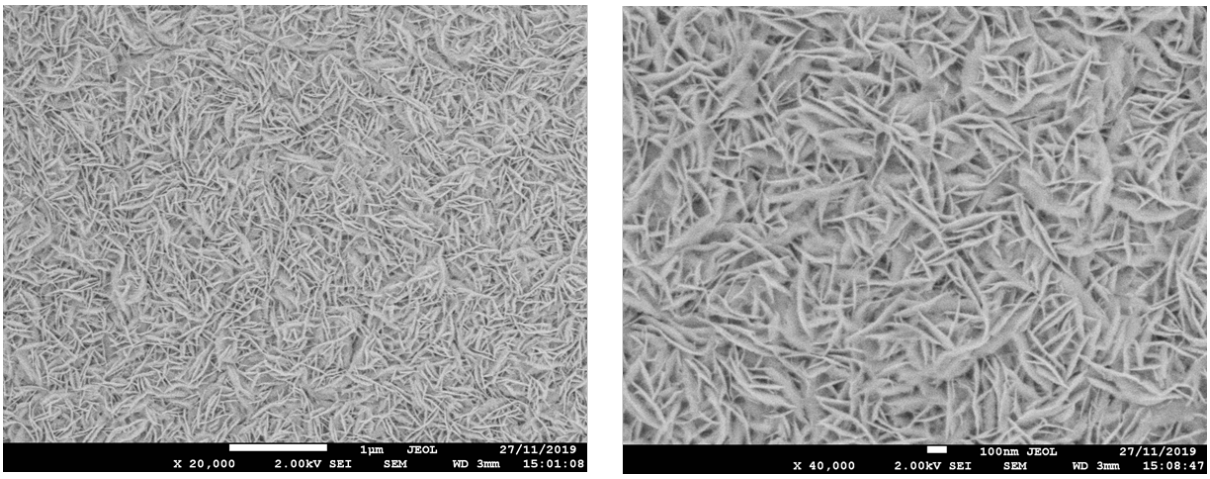

Figure 5.12: SEM image of continuous WS_2 thin film produced via low pressure CVD using [$WSCl_4(S^nBu_2)$] at 700 ºC.

Attempts to quantify the W:S ratio by EDX or WDX analysis were unsuccessful, due to the overlap of emission peaks (W $M\alpha_1$: 1.775 keV and Si $K\alpha_1$: 1.740 keV) in EDX.[128] WDX confirmed the presence of W and S but the ratio was estimated W:S (1.2:1) which is contradictory to all other collected data. The high errors of WDX is likely from the films being too thin (estimated to be <1 μm) to obtain an accurate W : S ratio.

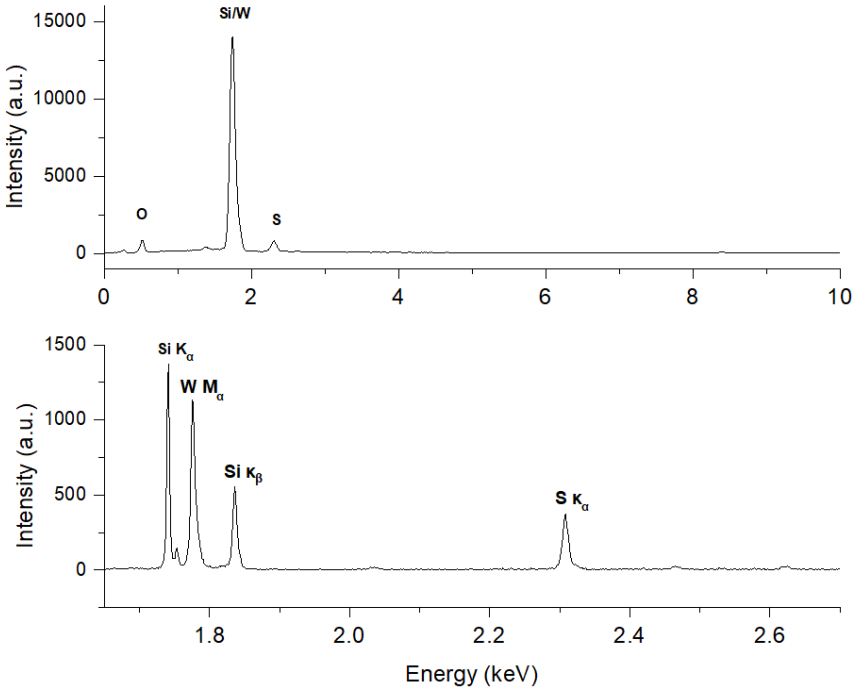

Figure 5.13: EDX spectrum (top) showing overlap of the W and Si peaks and WDX spectrum (bottom) from WS_2 thin film via low pressure CVD using [$WSCl_4(S^nBu_2)$] at 700 °C.

To obtain accurate determination of composition X-ray photoelectron spectroscopy (XPS) was carried out on the as-deposited films (Figure 5.8). XPS is a surface technique and only samples 5-10 nm of the sample. The W peaks at 32.5, 35.0, 28.1 eV can be assigned to W $4f_{7/2}$, W $4f_{5/2}$, W $5p_{3/2}$ from which it can be concluded that the films were not oxidised. The S peaks at 162.5 and 163.8 eV are attributed to S $p_{1/2}$ and $Sp_{3/2}$ and are characteristic of S^{2-} in WS_2.[129] The W : S ratio (1 : 2.2) was estimated by integrating the W 4f and the S 2p peaks.

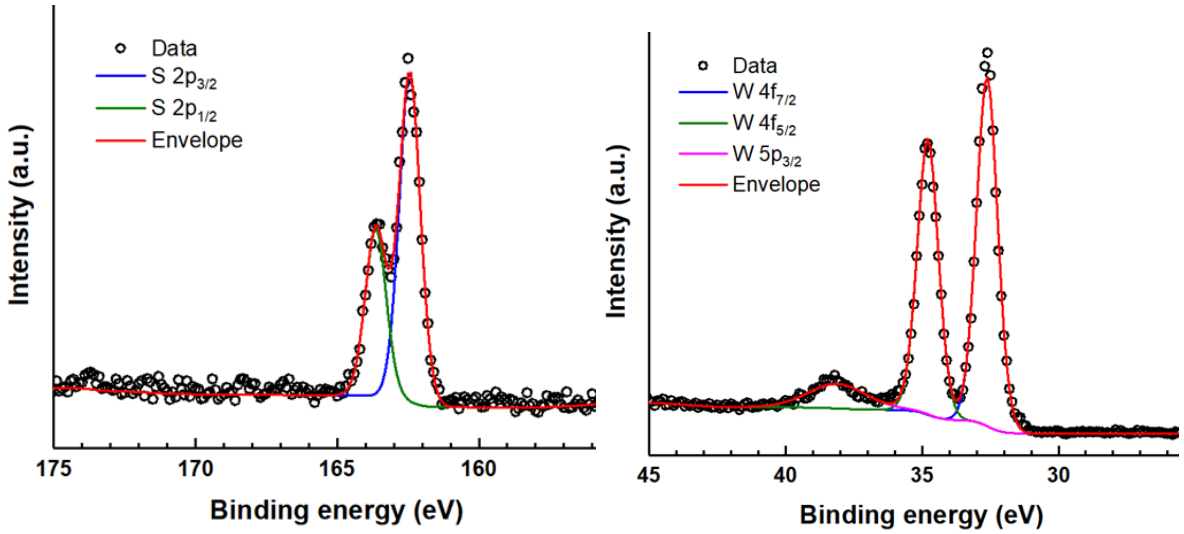

Figure 5.14: Representative XPS data for an as-deposited WS_2 thin film via low pressure CVD using [$WSCl_4(S^nBu_2)$]. Showing the peaks associated with tungsten (right) and sulfur (left).

Raman spectra were collected using a 532 nm excitation laser and the spectra show the two main peaks at 351 and 418 cm^{-1}, which are assigned to the E_{2g} and A_{1g} vibrational modes of WS_2, respectively; the weaker features present in the spectra are also consistent with WS_2 peaks.[130] This spectrum is practically identical to the spectra obtained for WS_2 deposited from [$(WSCl_4)_2(^iPrS(CH_2)_2S^iPr)$], as are the other data, suggesting the films deposited from the two precursors are very similar.

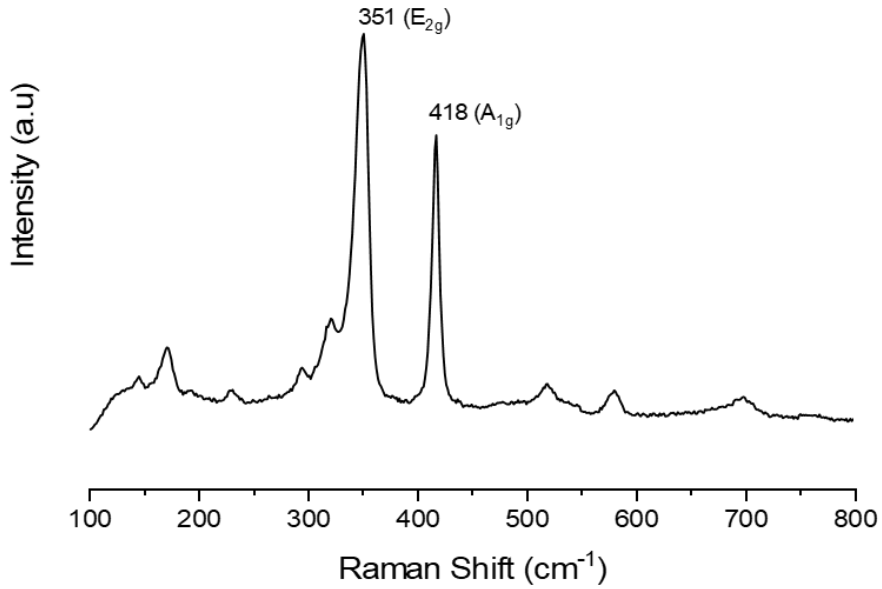

Figure 5.15: Raman spectra for as-deposited WS_2 film thin film via low pressure CVD using [$WSCl_4(S^nBu_2)$] at 700 ºC.

5.3.3 Electrical Measurements

Structural and compositional analysis on the films produced from both [$(WSCl_4)_2(^iPrS(CH_2)_2S^iPr)$] and [$WSCl_4(S^nBu_2)$] showed the WS_2 thin films produced *via* LPCVD were very similar. However,

electrical measurements, carried out by Dr Roumeng Huang, showed the films from the different precursors behaved differently.

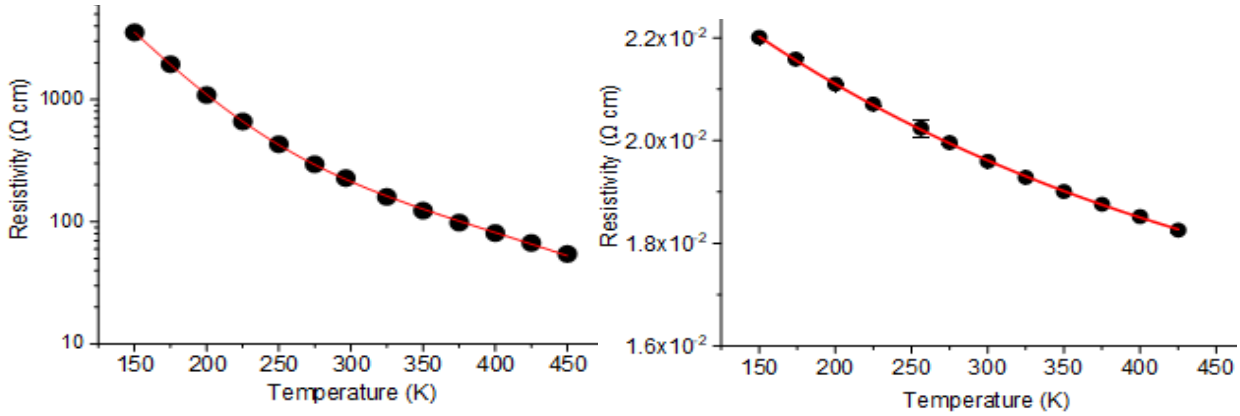

Figure 5.16: Resistivity measurements from WS_2 thin films produced from [$(WSCl_4)_2(^iPrS(CH_2)_2S^iPr)$] (left) and [$WSCl_4(S^nBu_2)$] (right).

Films from [$(WSCl_4)_2(^iPrS(CH_2)_2S^iPr)$] exhibited typical semiconducting behaviour, showing that the resistivity decreases significantly with increasing temperature. In contrast, the WS_2 films produced from the [$WSCl_4(S^nBu_2)$] precursor showed significantly lower resistivity (much higher conductivity), more consistent with a conductor or semi-metal.[131] Figure 5.16 shows both films have increasing charge carriers as the temperature increases, however films from [$WSCl_4(S^nBu_2)$] show increased electron scattering effects (Figure 5.17) compared to WS_2 films from [$(WSCl_4)_2(^iPrS(CH_2)_2S^iPr)$], which is typical for a semi-metal/conductor..

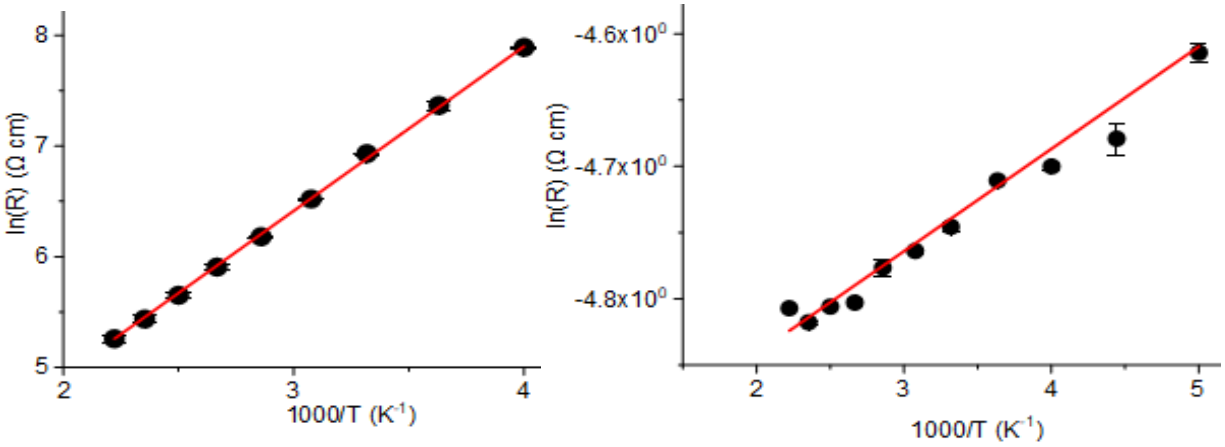

Figure 5.17: Graph showing activation energy from WS_2 thin films produced from [$(WSCl_4)_2(^iPrS(CH_2)_2S^iPr)$] (left) and [$WSCl_4(S^nBu_2)$] (right).

This behaviour is also confirmed with the calculated activation energy values with films from [$(WSCl_4)_2(^iPrS(CH_2)_2S^iPr)$] having an activation value of ~100 meV and those from [$WSCl_4(S^nBu_2)$] having an activation energy ~6 meV. Again, this is consistent with semiconductor and semi-metal WS_2 films, respectively.[131]

The differences in behaviour from the films from different precursors is unusual given the similarity between precursors and experimental conditions employed. The deposition temperature

does not seem to influence the electrical properties of the films, as the temperature range used was consistent for both precursors. It is likely that the differences in electrical properties stem from different defects within the films, most probably sulfur deficiencies. Thus, films with higher S deficiency would be expected to exhibit increased conductivity due to the increased number of holes in the film. The potential cause of this sulfur deficiency could be the time required for the deposition as [$WSCl_4(S^nBu_2)$] is much more volatile and may therefore need a shorter deposition time. The increased deposition times could cause small amounts of volatile sulfur to be lost during the deposition experiment.

5.4 Conclusions

Complexes of [$(WSCl_4)_2(^iPrS(CH_2)_2S^iPr)$], [$WSCl_3(^iPrS(CH_2)_2S^iPr)$] and [$WSCl_4(S^nBu_2)$] were tested as single source low pressure chemical vapour deposition precursors at 550-700 ºC. The complex [$WSCl_3(^iPrS(CH_2)_2S^iPr)$] was found to be unsuitable for LPCVD and did not deposit any material onto the substrates. [$(WSCl_4)_2(^iPrS(CH_2)_2S^iPr)$] and [$WSCl_4(S^nBu_2)$] were found to deposit 4H-WS_2 thin films successfully between 650 ºC and 700 ºC. The two novel single source precursors deposited continuous uniform coverage of the substrate and the films have been shown to have a W:S ratio of 1:2.2 consistent with WS_2.

These are the first examples of single source LPCVD precursors to deposit WS_2 thin films and the films have been characterised by Raman spectroscopy, grazing incidence XRD and in-plane XRD, EDX, WDX, XPS and SEM. The films have preferred orientation in <00*l*> direction with SEM confirming the crystallites parallel to the substrate surface. These precursors potentially provide a viable route for the growth of thin films of this important semiconducting material if conditions and optimisation of reagent can be achieved.

Surprisingly, the two precursors produce films with different electrical behaviour with [$(WSCl_4)_2(^iPrS(CH_2)_2S^iPr)$] behaving as a typical semiconductor and [$WSCl_4(S^nBu_2)$] behaving as a semi-metal/conductor. The difference probably stems from defects, likely sulfur deficiency which is not due to the deposition temperature, but may be caused by evaporation of some sulfur during the deposition experiment. This can be investigated by running a series of CVD experiments with the same conditions but varying the deposition time.

5.5 Experimental

In an N_2 purged glove box the precursor (20-30 mg) was loaded into the precursor bulb at the closed end of a silica tube, silica substrates (*ca.* 1 x 8 x 20 mm^3) were then positioned end-to-end lengthways along the tube outwards from the precursor. The tube was then set in a furnace so that the substrates were in the heated zone and the precursor protruded *ca.* 1 cm out of the furnace. The tube was evacuated to 0.1 mmHg and the furnace heated to 700 ºC and left for 10 minutes to allow for the temperature to stabilise. The tube was gradually moved towards the hot zone until evaporation of the precursor was observed. The position was maintained until no further evaporation occurred, leaving a black solid in the precursor bulb for $[(WSCl_4)_2(^iPrS(CH_2)_2S^iPr)]$; no residue remained from the $[WSCl_4(S^nBu_2)]$. A brown/bronze film was observed at the opposite end of the tube. After *ca.* 20 min. the tube was cooled to room temperature and the tiles were unloaded in the glove box where they were stored for characterisation. Brown/bronze films were observed on the second and third substrates (actual T range = 590-625 ºC, determined by temperature profiling) using $[(WSCl_4)_2(^iPrS(CH_2)_2S^iPr)]$, and brown films were obtained across all of the substrates using $[WSCl_4(S^nBu_2)]$ (actual T range = 624-650 °C).

5.6 References

(1) Coleman, J. N.; Lotya, M.; O'Neill, A.; Bergin, S. D.; King, P. J.; Khan, U.; Young, K.; Gaucher, A.; De, S.; Smith, R. J.; Shvets, I. V.; Arora, S. K.; Stanton, G.; Kim, H. Y.; Lee, K.; Kim, G. T.; Duesberg, G. S.; Hallam, T.; Boland, J. J.; Wang, J. J.; Donegan, J. F.; Grunlan, J. C.; Moriarty, G.; Shmeliov, A.; Nicholls, R. J.; Perkins, J. M.; Grieveson, E. M.; Theuwissen, K.; McComb, D. W.; Nellist, P. D.; Nicolosi, V. *Science,* **2011,** *331*, 568-71

(2) Rhyee, J. S.; Kwon, J.; Dak, P.; Kim, J. H.; Kim, S. M.; Park, J.; Hong, Y. K.; Song, W. G.; Omkaram, I.; Alam, M. A.; Kim, S. *Adv. Mater.,* **2016,** *28*, 2316-21

(3) Chang, Y. H.; Zhang, W.; Zhu, Y.; Han, Y.; Pu, J.; Chang, J. K.; Hsu, W. T.; Huang, J. K.; Hsu, C. L.; Chiu, M. H.; Takenobu, T.; Li, H.; Wu, C. I.; Chang, W. H.; Wee, A. T.; Li, L. J. *ACS Nano,* **2014,** *8*, 8582-90

(4) Wang, X.; Gong, Y.; Shi, G.; Chow, W. L.; Keyshar, K.; Ye, G.; Vajtai, R.; Lou, J.; Liu, Z.; Ringe, E.; Tay, B. K.; Ajayan, P. M. *ACS Nano,* **2014,** *8*, 5125-31

(5) Lu, X.; Utama, M. I.; Lin, J.; Gong, X.; Zhang, J.; Zhao, Y.; Pantelides, S. T.; Wang, J.; Dong, Z.; Liu, Z.; Zhou, W.; Xiong, Q. *Nano Lett.,* **2014,** *14*, 2419-25

(6) Pawbake, A. S.; Pawar, M. S.; Jadkar, S. R.; Late, D. J. *Nanoscale,* **2016,** *8*, 3008-18

(7) Chen, J.; Zhao, X.; Tan, S. J.; Xu, H.; Wu, B.; Liu, B.; Fu, D.; Fu, W.; Geng, D.; Liu, Y.; Liu, W.; Tang, W.; Li, L.; Zhou, W.; Sum, T. C.; Loh, K. P. *J. Am. Chem. Soc.,* **2017,** *139*, 1073-76

(8) Lee, Y. H.; Zhang, X. Q.; Zhang, W.; Chang, M. T.; Lin, C. T.; Chang, K. D.; Yu, Y. C.; Wang, J. T.; Chang, C. S.; Li, L. J.; Lin, T. W. *Adv. Mater.,* **2012,** *24*, 2320-25

(9) Pu, J.; Yomogida, Y.; Liu, K. K.; Li, L. J.; Iwasa, Y.; Takenobu, T. *Nano Lett.,* **2012,** *12*, 4013-17

(10) Liu, K. K.; Zhang, W.; Lee, Y. H.; Lin, Y. C.; Chang, M. T.; Su, C. Y.; Chang, C. S.; Li, H.; Shi, Y.; Zhang, H.; Lai, C. S.; Li, L. J. *Nano Lett.,* **2012,** *12*, 1538-44

(11) Chhowalla, M.; Shin, H. S.; Eda, G.; Li, L. J.; Loh, K. P.; Zhang, H. *Nat. Chem.,* **2013,** *5*, 263-75

(12) Chhowalla, M.; Liu, Z.; Zhang, H. *Chem. Soc. Rev.,* **2015,** *44*, 2584-86

(13) Ji, Q.; Zhang, Y.; Zhang, Y.; Liu, Z. *Chem. Soc. Rev.,* **2015,** *44*, 2587-602

(14) Boscher, N. D.; Blackman, C. S.; Carmalt, C. J.; Parkin, I. P.; Prieto, A. G. *Appl. Surf. Sci.,* **2007,** *253*, 6041-46

(15) Carmalt, C. J.; Parkin, I. P.; Peters, E. S. *Polyhedron,* **2003,** *22*, 1499-505

(16) Benjamin, S. L.; de Groot, C. H.; Gurnani, C.; Hawken, S. L.; Hector, A. L.; Huang, R.; Jura, M.; Levason, W.; Reid, E.; Reid, G.; Richards, S. P.; Stenning, G. B. G. *J. Mater. Chem. C,* **2018,** *6*, 7734-39

(17) de Groot, C. H.; Gurnani, C.; Hector, A. L.; Huang, R.; Jura, M.; Levason, W.; Reid, G. *Chem. Mater.,* **2012,** *24*, 4442-49

(18) Reid, S. D.; Hector, A. L.; Levason, W.; Reid, G.; Waller, B. J.; Webster, M. *Dalton Trans.,* **2007**, 4769-77

(19) Hector, A. L.; Jura, M.; Levason, W.; Reid, S. D.; Reid, G. *New J. Chem.,* **2009,** *33*, 641-45

(20) Xu, M.; Liang, T.; Shi, M.; Chen, H. *Chem. Rev.,* **2013,** *113*, 3766-98

(21) Mas-Balleste, R.; Gomez-Navarro, C.; Gomez-Herrero, J.; Zamora, F. *Nanoscale,* **2011,** *3*, 20-30

(22) Kanehori, K. *J. Electrochem. Soc.,* **1989,** *136*, 1265-70

(23) Whittingham, M. S. *Chem. Rev.,* **2004,** *104*, 4271-301

(24) Trevey, J. E.; Stoldt, C. R.; Lee, S.-H. *J. Electrochem. Soc.,* **2011,** *158*, A1282-A89

(25) Peters, E. S.; Carmalt, C. J.; Parkin, I. P. *J. Mater. Chem.,* **2004,** *14*, 3474-77

(26) Perry, P. B. *Phys. Rev. B,* **1976,** *13*, 5211-13

(27) Conroy, L. E.; Bouchard, R. J. *Inorg. Synth.,* **1970,** *12*, 158 - 65

(28) Tonti, D.; Pettenkofer, C.; Jaegermann, W. *Ionics,* **2000,** *6*, 196-202

(29) Kikkawa, S.; Miyazaki, M.; Liu, Y.; Kanamaru, F. *Solid State Ionics,* **1990,** *40-41*, 553-56

(30) Shimanouchi, R.; Yamamoto, T.; Kikkawa, S.; Koizumi, M. *Chem. Lett.,* **1985,** *14*, 1323-26

(31) Carmalt, C. J.; O'Neill, S. A.; Parkin, I. P.; Peters, E. S. *J. Mater. Chem.,* **2004,** *14*, 830-34

(32) Suren Lewkebandara, T.; McKarns, P. J.; Haggerty, B. S.; Yap, G. P. A.; Rheingold, A. L.; Winter, C. H. *Polyhedron,* **1998,** *17*, 1-9

(33) Carmalt, C. J.; Dinnage, C. W.; Parkin, I. P.; White, A. J. P.; Williams, D. J. *J. Chem. Soc., Dalton Trans.,* **2001**, 2554-58
(34) Morosan, E.; Zandbergen, H. W.; Dennis, B. S.; Bos, J. W. G.; Onose, Y.; Klimczuk, T.; Ramirez, A. P.; Ong, N. P.; Cava, R. J. *Nat. Phys.,* **2006,** *2*, 544-50
(35) Xiao, R. C.; Lu, W. J.; Shao, D. F.; Li, J. Y.; Wei, M. J.; Lv, H. Y.; Tong, P.; Zhu, X. B.; Sun, Y. P. *J. Mater. Chem. C,* **2017,** *5*, 4167-73
(36) Khan, J.; Nolen, C. M.; Teweldebrhan, D.; Wickramaratne, D.; Lake, R. K.; Balandin, A. A. *Appl. Phys. Lett.,* **2012,** *100*, 043109
(37) Sugawara, K.; Nakata, Y.; Shimizu, R.; Han, P.; Hitosugi, T.; Sato, T.; Takahashi, T. *ACS Nano,* **2016,** *10*, 1341-45
(38) Duong, D. L.; Ryu, G.; Hoyer, A.; Lin, C.; Burghard, M.; Kern, K. *ACS Nano,* **2017,** *11*, 1034-40
(39) Boscher, N. D.; Carmalt, C. J.; Parkin, I. P. *Chem. Vap. Deposition,* **2006,** *12*, 54-58
(40) Benjamin, S. L.; de Groot, C. H.; Gurnani, C.; Hector, A. L.; Huang, R.; Ignatyev, K.; Levason, W.; Pearce, S. J.; Thomas, F.; Reid, G. *Chem. Mater.,* **2013,** *25*, 4719-24
(41) Hector, A. L.; Levason, W.; Reid, G.; Reid, S. D.; Webster, M. *Chem. Mater.,* **2008,** *20*, 5100-06
(42) Levason, W.; Patel, B.; Reid, G.; Tolhurst, V.-A.; Webster, M. *J. Chem. Soc., Dalton Trans.,* **2000**, 3001-06
(43) Hart, R.; Levason, W.; Patel, B.; Reid, G. *J. Chem. Soc., Dalton Trans.,* **2002**, 3153-59
(44) Fiori, G.; Bonaccorso, F.; Iannaccone, G.; Palacios, T.; Neumaier, D.; Seabaugh, A.; Banerjee, S. K.; Colombo, L. *Nat. Nanotechnol.,* **2014,** *9*, 768-79
(45) Li, L.; Fang, X.; Zhai, T.; Liao, M.; Gautam, U. K.; Wu, X.; Koide, Y.; Bando, Y.; Golberg, D. *Adv. Mater.,* **2010,** *22*, 4151-56
(46) Li, Y.; Kang, J.; Li, J. *RSC Adv.,* **2014,** *4*, 7396-401
(47) Blochl, P. E. *Phys. Rev. B* **1994,** *50*, 17953-79
(48) Zhu, Y.; Wang, X.; Zhang, M.; Cai, C.; Xie, L. *Nano Res.,* **2016,** *9*, 2931-37
(49) Zhang, M.; Zhu, Y.; Wang, X.; Feng, Q.; Qiao, S.; Wen, W.; Chen, Y.; Cui, M.; Zhang, J.; Cai, C.; Xie, L. *J. Am. Chem. Soc.,* **2015,** *137*, 7051-54
(50) Zhang, W.; Huang, Z.; Zhang, W.; Li, Y. *Nano Res.,* **2014,** *7*, 1731-37
(51) Wang, X.; Huang, L.; Jiang, X.-W.; Li, Y.; Wei, Z.; Li, J. *J. Mater. Chem. C,* **2016,** *4*, 3143-48
(52) Leem, M.; Lee, H.; Park, T.; Ahn, W.; Kim, H.; Lee, E.; Kim, H. *Appl. Surf. Sci.,* **2020,** *509*, 144701
(53) Zheng, B.; Wang, Z.; Qi, F.; Wang, X.; Yu, B.; Zhang, W.; Chen, Y. *Appl. Surf. Sci.,* **2018,** *435*, 563-67
(54) Zheng, X.-g.; Kuriyaki, H.; Hirakawa, K. *J. Phys. Soc. Jpn.,* **1989,** *58*, 622-26
(55) Amberg, M. *Solid State Ionics,* **1996,** *84*, 313-21
(56) Mleczko, M. J.; Zhang, C.; Lee, H. R.; Kuo, H. H.; Magyari-Kope, B.; Moore, R. G.; Shen, Z. X.; Fisher, I. R.; Nishi, Y.; Pop, E. *Sci. Adv.,* **2017,** *3*, e1700481
(57) Aoki, Y.; Sambongi, T.; Levy, F.; Berger, H. *J. Phys. Soc. Jpn.,* **1996,** *65*, 2590-93
(58) Harbrecht, B.; Conrad, M.; Degen, T.; Herbertz, R. *J. Alloys Compd.,* **1997,** *255*, 178-82
(59) Bhavsar, D. N.; Jani, A. R. *Optoelectronics Adv. Mater.,* **2014,** *16*, 215-20
(60) Feng, J.; Sun, X.; Wu, C.; Peng, L.; Lin, C.; Hu, S.; Yang, J.; Xie, Y. *J. Am. Chem. Soc.,* **2011,** *133*, 17832-38
(61) Terashima, K.; Sato, T.; Komatsu, H.; Takahashi, T.; Maeda, N.; Hayashi, K. *Phys. Rev. B,* **2003,** *68*, 155108
(62) Eaglesham, D. J.; Withers, R. L.; Bird, D. M. *J. Phys. C: Solid State Phys.,* **1986,** *19*, 359-67
(63) Giambattista, B.; Slough, C. G.; McNairy, W. W.; Coleman, R. V. *Phys. Rev. B* **1990,** *41*, 10082-103
(64) Brauer, H. E.; Ekvall, I.; Olin, H.; Starnberg, H. I.; Wahlström, E.; Hughes, H. P.; Strocov, V. N. *Phys. Rev. B,* **1997,** *55*, 10022-26
(65) DiSalvo, F. J.; Waszczak, J. V. *Phys. Rev. B,* **1981,** *23*, 457-61
(66) Therese, H. A.; Rocker, F.; Reiber, A.; Li, J.; Stepputat, M.; Glasser, G.; Kolb, U.; Tremel, W. *Angew. Chem. Int. Ed.,* **2004,** *44*, 262-65
(67) Homyonfer, M.; Alperson, B.; Rosenberg, Y.; Sapir, L.; Cohen, S. R.; Hodes, G.; Tenne, R. *J. Am. Chem. Soc.,* **1997,** *119*, 2693-98

(68) Murphy, D. W.; Cros, C.; Di Salvo, F. J.; Waszczak, J. V. *Inorg. Chem.,* **2002,** *16*, 3027-31
(69) Feng, J.; Peng, L.; Wu, C.; Sun, X.; Hu, S.; Lin, C.; Dai, J.; Yang, J.; Xie, Y. *Adv. Mater.,* **2012,** *24*, 1969-74
(70) Xue, Y.; Zhang, Y.; Wang, H.; Lin, S.; Li, Y.; Dai, J. Y.; Lau, S. P. *Nanotechnology,* **2020,** *31*, 145712
(71) Liu, H.; Xue, Y.; Shi, J. A.; Guzman, R. A.; Zhang, P.; Zhou, Z.; He, Y.; Bian, C.; Wu, L.; Ma, R.; Chen, J.; Yan, J.; Yang, H.; Shen, C. M.; Zhou, W.; Bao, L.; Gao, H. J. *Nano Lett.,* **2019,** *19*, 8572-80
(72) Dash, J. K.; Chen, L.; Dinolfo, P. H.; Lu, T.-M.; Wang, G.-C. *J. Phys. Chem. C,* **2015,** *119*, 19763-71
(73) Morosin, B. *Acta Cryst. B,* **1974,** *30*, 551-52
(74) Peters, E. S.; Carmalt, C. J.; Parkin, I. P.; Tocher, D. A. *Eur. J. Inorg. Chem.,* **2005**, 4179-85
(75) Carmalt, C. J.; Manning, T. D.; Parkin, I. P.; Peters, E. S.; Hector, A. L. *J. Mater. Chem.,* **2004,** *14*, 290-91
(76) Carmalt, C. J.; Manning, T. D.; Parkin, I. P.; Peters, E. S.; Hector, A. L. *Thin Solid Films,* **2004,** *469*, 495-99
(77) Zhao, S.; Hotta, T.; Koretsune, T.; Watanabe, K.; Taniguchi, T.; Sugawara, K.; Takahashi, T.; Shinohara, H.; Kitaura, R. *2D Mater.,* **2016,** *3*, 025027
(78) Yanase, T.; Watanabe, S.; Weng, M.; Wakeshima, M.; Hinatsu, Y.; Nagahama, T.; Shimada, T. *Cryst. Growth Des.,* **2016,** *16*, 4467-72
(79) Ge, W.; Kawahara, K.; Tsuji, M.; Ago, H. *Nanoscale,* **2013,** *5*, 5773-78
(80) Carmalt, C. J.; Peters, E. S.; Parkin, I. P.; Manning, T. D.; Hector, A. L. *Eur. J. Inorg. Chem.,* **2004**, 4470-76
(81) McKarns, P. J.; Heeg, M. J.; Winter, C. H. *Inorg. Chem.,* **1998,** *37*, 4743-47
(82) Benjamin, S. L.; Chang, Y. P.; Gurnani, C.; Hector, A. L.; Huggon, M.; Levason, W.; Reid, G. *Dalton Trans.,* **2014,** *43*, 16640-48
(83) Chang, Y. P.; Levason, W.; Light, M. E.; Reid, G. *Dalton Trans.,* **2016,** *45*, 16262-74
(84) Nowak, I.; Page, E. M.; Rice, D. A.; Richardson, A. D.; French, R. J.; Hedberg, K.; Ogden, J. S. *Inorg. Chem.,* **2003,** *42*, 1296-305
(85) Chang, Y. P.; Hector, A. L.; Levason, W.; Reid, G. *Dalton Trans.,* **2017,** *46*, 9824-32
(86) Boscher, N. D.; Carmalt, C. J.; Parkin, I. P. *Eur. J. Inorg. Chem.,* **2006,** *6*, 1255-59
(87) Huang, Y. H.; Chen, R. S.; Zhang, J. R.; Huang, Y. S. *Nanoscale,* **2015,** *7*, 18964-70
(88) Hitz, E.; Wan, J.; Patel, A.; Xu, Y.; Meshi, L.; Dai, J.; Chen, Y.; Lu, A.; Davydov, A. V.; Hu, L. *ACS Appl. Mater. Interfaces,* **2016,** *8*, 11390-95
(89) Boscher, N. D.; Carmalt, C. J.; Parkin, I. P. *Appl. Surf. Sci.,* **2010,** *256*, 3178-82
(90) Bannister, R. D.; Levason, W.; Reid, G.; Robinson, F. *Polyhedron,* **2019,** *169*, 129-34
(91) Renteria, J.; Samnakay, R.; Jiang, C.; Pope, T. R.; Goli, P.; Yan, Z.; Wickramaratne, D.; Salguero, T. T.; Khitun, A. G.; Lake, R. K.; Balandin, A. A. *J. Appl. Phys.,* **2014,** *115*, 034305
(92) Papageorgopoulos, D. C.; Saltas, V.; Papageorgopoulos, C. A.; Tonti, D.; Pettenkofer, C.; Jaegermann, W. *Appl. Surf. Sci.,* **2000,** *161*, 347-54
(93) Deng, Y.; Lai, Y.; Zhao, X.; Wang, X.; Zhu, C.; Huang, K.; Zhu, C.; Zhou, J.; Zeng, Q.; Duan, R.; Fu, Q.; Kang, L.; Liu, Y.; Pennycook, S. J.; Wang, X. R.; Liu, Z. *J. Am. Chem. Soc.,* **2020,** *142*, 2948-55
(94) Zeng, H.; Dai, J.; Yao, W.; Xiao, D.; Cui, X. *Nat. Nanotechnol.,* **2012,** *7*, 490-93
(95) Xiang, Q.; Yu, J.; Jaroniec, M. *J. Am. Chem. Soc.,* **2012,** *134*, 6575-78
(96) Wang, J.; Liu, J.; Zhang, B.; Ji, X.; Xu, K.; Chen, C.; Miao, L.; Jiang, J. *Phys. Chem. Chem. Phys.,* **2017,** *19*, 10125-32
(97) Lee, K.; Gatensby, R.; McEvoy, N.; Hallam, T.; Duesberg, G. S. *Adv. Mater.,* **2013,** *25*, 6699-702
(98) Zhang, G.; Zhang, Y.-W. *J. Mater. Chem. C,* **2017,** *5*, 7684-98
(99) Bachmatiuk, A.; Abelin, R. F.; Quang, H. T.; Trzebicka, B.; Eckert, J.; Rummeli, M. H. *Nanotechnology,* **2014,** *25*, 365603
(100) Jung, C.; Kim, S. M.; Moon, H.; Han, G.; Kwon, J.; Hong, Y. K.; Omkaram, I.; Yoon, Y.; Kim, S.; Park, J. *Sci. Rep.,* **2015,** *5*, 15313
(101) Shaw, J. C.; Zhou, H.; Chen, Y.; Weiss, N. O.; Liu, Y.; Huang, Y.; Duan, X. *Nano Res.,* **2015,** *7*, 511-17

(102) Krustok, J.; Raadik, T.; Jaaniso, R.; Kiisk, V.; Sildos, I.; Marandi, M.; Komsa, H. P.; Li, B.; Zhang, X.; Gong, Y.; Ajayan, P. M. *Appl. Phys. Lett.,* **2016,** *109*, 253106
(103) Mitioglu, A. A.; Galkowski, K.; Surrente, A.; Klopotowski, L.; Dumcenco, D.; Kis, A.; Maude, D. K.; Plochocka, P. *Phys. Rev. B,* **2016,** *93*, 165412
(104) Wang, B. B.; Ostrikov, K.; van der Laan, T.; Zheng, K.; Shao, R.; Zhu, M. K.; Zou, S. S. *RSC Adv.,* **2016,** *6*, 37236-45
(105) Umrao, S.; Jeon, J.; Jeon, S. M.; Choi, Y. J.; Lee, S. *Nanoscale,* **2017,** *9*, 594-603
(106) Wang, B. B.; Zheng, K.; Zhong, X. X.; Gao, D.; Gao, B. *J. Alloys Compd.,* **2017,** *695*, 27-34
(107) Park, W.; Baik, J.; Kim, T. Y.; Cho, K.; Hong, W. K.; Shin, H. J.; Lee, T. *ACS Nano,* **2014,** *8*, 4961-68
(108) van der Zande, A. M.; Huang, P. Y.; Chenet, D. A.; Berkelbach, T. C.; You, Y.; Lee, G. H.; Heinz, T. F.; Reichman, D. R.; Muller, D. A.; Hone, J. C. *Nat. Mater.,* **2013,** *12*, 554-61
(109) Schmidt, H.; Wang, S.; Chu, L.; Toh, M.; Kumar, R.; Zhao, W.; Neto, A. H.; Martin, J.; Adam, S.; Ozyilmaz, B.; Eda, G. *Nano Lett.,* **2014,** *14*, 1909-13
(110) Shi, Y.; Zhou, W.; Lu, A. Y.; Fang, W.; Lee, Y. H.; Hsu, A. L.; Kim, S. M.; Kim, K. K.; Yang, H. Y.; Li, L. J.; Idrobo, J. C.; Kong, J. *Nano Lett.,* **2012,** *12*, 2784-91
(111) Wu, J.; Schmidt, H.; Amara, K. K.; Xu, X.; Eda, G.; Ozyilmaz, B. *Nano Lett.,* **2014,** *14*, 2730-34
(112) Zafar, A.; Nan, H.; Zafar, Z.; Wu, Z.; Jiang, J.; You, Y.; Ni, Z. *Nano Res.,* **2016,** *10*, 1608-17
(113) Najmaei, S.; Liu, Z.; Zhou, W.; Zou, X.; Shi, G.; Lei, S.; Yakobson, B. I.; Idrobo, J. C.; Ajayan, P. M.; Lou, J. *Nat. Mater.,* **2013,** *12*, 754-59
(114) Zhang, W.; Li, X.; Jiang, T.; Song, J.; Lin, Y.; Zhu, L.; Xu, X. *Nanoscale,* **2015,** *7*, 13554-60
(115) O'Brien, M.; McEvoy, N.; Hanlon, D.; Hallam, T.; Coleman, J. N.; Duesberg, G. S. *Sci. Rep.,* **2016,** *6*, 19476
(116) Cheon, J.; Gozum, J. E.; Girolami, G. S. *Chem. Mater.,* **1997,** *9*, 1847-53
(117) Chang, Y. P.; Hector, A. L.; Levason, W.; Reid, G.; Whittam, J. *Dalton Trans.,* **2018,** *47*, 2406-14
(118) Boscher, N. D.; Carmalt, C. J.; Palgrave, R. G.; Gil-Tomas, J. J.; Parkin, I. P. *Chem. Vap. Deposition,* **2006,** *12*, 692-98
(119) Gao, Y.; Liu, Z.; Sun, D. M.; Huang, L.; Ma, L. P.; Yin, L. C.; Ma, T.; Zhang, Z.; Ma, X. L.; Peng, L. M.; Cheng, H. M.; Ren, W. *Nat. Commun.,* **2015,** *6*, 8569
(120) Huang, J. K.; Pu, J.; Hsu, C. L.; Chiu, M. H.; Juang, Z. Y.; Chang, Y. H.; Chang, W. H.; Iwasa, Y.; Takenobu, T.; Li, L. J. *ACS Nano,* **2014,** *8*, 923-30
(121) Richey, N. E.; Haines, C.; Tami, J. L.; McElwee-White, L. *Chem. Commun.,* **2017,** *53*, 7728-31
(122) Zhou, J.; Liu, F.; Lin, J.; Huang, X.; Xia, J.; Zhang, B.; Zeng, Q.; Wang, H.; Zhu, C.; Niu, L.; Wang, X.; Fu, W.; Yu, P.; Chang, T. R.; Hsu, C. H.; Wu, D.; Jeng, H. T.; Huang, Y.; Lin, H.; Shen, Z.; Yang, C.; Lu, L.; Suenaga, K.; Zhou, W.; Pantelides, S. T.; Liu, G.; Liu, Z. *Adv. Mater.,* **2017,** *29*, 1603471
(123) Keum, D. H.; Cho, S.; Kim, J. H.; Choe, D.-H.; Sung, H.-J.; Kan, M.; Kang, H.; Hwang, J.-Y.; Kim, S. W.; Yang, H.; Chang, K. J.; Lee, Y. H. *Nat. Phys.,* **2015,** *11*, 482-86
(124) Park, J. C.; Yun, S. J.; Kim, H.; Park, J. H.; Chae, S. H.; An, S. J.; Kim, J. G.; Kim, S. M.; Kim, K. K.; Lee, Y. H. *ACS Nano,* **2015,** *9*, 6548-54
(125) Naylor, C. H.; Parkin, W. M.; Ping, J.; Gao, Z.; Zhou, Y. R.; Kim, Y.; Streller, F.; Carpick, R. W.; Rappe, A. M.; Drndic, M.; Kikkawa, J. M.; Johnson, A. T. *Nano Lett.,* **2016,** *16*, 4297-304
(126) Li, J.; Cheng, S.; Liu, Z.; Zhang, W.; Chang, H. *J. Phys. Chem. C,* **2018,** *122*, 7005-12
(127) Schutte, W. J.; De Boer, J. L.; Jellinek, F. *J. Solid State Chem.,* **1987,** *70*, 207-09
(128) Thompson, A. C.; Vaughan, D. *X-ray data booklet*; Lawrence Berkeley National Laboratory, University of California: Berkely, CA, 2001.
(129) Huang, J.; Wang, X.; Li, J.; Cao, L.; Xu, Z.; Wei, H. *J. Alloys Compd.,* **2016,** *673*, 60-66
(130) Berkdemir, A.; Gutiérrez, H. R.; Botello-Méndez, A. R.; Perea-López, N.; Elías, A. L.; Chia, C.-I.; Wang, B.; Crespi, V. H.; López-Urías, F.; Charlier, J.-C.; Terrones, H.; Terrones, M. *Sci. Rep.,* **2013,** *3*, 1755

(131) Nayak, A. P.; Yuan, Z.; Cao, B.; Liu, J.; Wu, J.; Moran, S. T.; Li, T.; Akinwande, D.; Jin, C.; Lin, J. F. *ACS Nano,* **2015,** *9*, 9117-23

Coordination Chemistry of $MoOCl_3$ and $MoOCl_4$ with Neutral Donor Ligands

6.1 Introduction

Following the investigation into the coordination complexes of $WECl_4$ (E = O or S) with a range of neutral ligands (see Chapters 2 to 4), the chemistry of the molybdenum(VI) analogue, $MoOCl_4$, with a range of comparative neutral donor ligands is described in this Chapter. A series of analogous molybdenum(V) complexes, $MoOCl_3$, with hard donors will be isolated and compared to products from reactions of $MoOCl_4$. Coordination complexes of $MoOCl_4$ have not been reported in the literature, as the metal centre is less stable than the tungsten(VI) analogue and is very susceptible to reduction upon addition of ligands.

A subsequent series of $MoOCl_3$ complexes with bi- and mono-dentate chalcogenoether ligands will also be explored, including the aim to isolate the first molybdenum(V) telluroether complexes. This chapter details the attempted synthesis of the first examples of coordination complexes of $MoOCl_4$, along with characterisation of a systematic series of $MoOCl_3$ coordination complexes with a range of neutral hard and soft donor ligands and comparisons with their tungsten analogues.

6.2 High Valent Early Transition Metal Coordination Complexes

Much of the coordination chemistry of early transition high valent coordination complexes originates pre-1980, meaning there are few systematic studies that investigate the behaviour of these metal species towards particular ligand classes. Coordination complexes of WX_6 (X = F, Cl or Br) with chalcogenoethers, phosphine and arsine donors have been discussed in Chapters 2, 3 and 4, some further examples are included here.

The pentafluorides, MF_5 (M = Nb or Ta), are very hydroscopic powders and their respective coordination chemistry has been quite extensively investigated and summarised in a recent review.[1] MF_5 reactions with chalcogenoethers has been reviewed in Chapter 4.

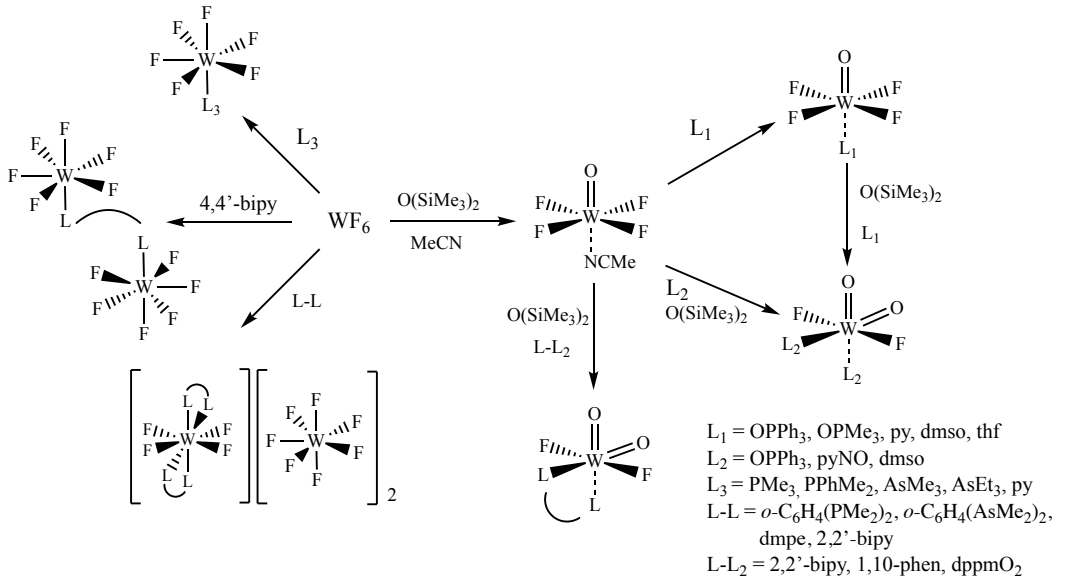

Figure 6.1: Scheme showing coordination complexes of tungsten fluoride complexes. WF_6,[2-6] WOF_4[7,8] and WO_2F_2.[7,9,10]

Reactions of MF_5 and neutral donor ligands typically form complexes of either six-coordinate $[MF_5(L)]$, seven-coordinate $[MF_5(L\text{-}L)]$ or eight-coordinate $[MF_4(L_4)][MF_6]$.[11-13] Neutral complexes, $[MF_5(L)]$ and $[MF_5(L\text{-}L)]$ (L = dmf, dmso, OPR_3; L-L = 2,2'-bipy, 1,10-phen and 4,4'-bipy), have all been reported, although much of the literature is early and spectroscopic characterisation is limited.[14-17] More recently, $[MF_4(py)_4][MF_6]$ have been isolated and structurally characterised, with structures revealing a distorted square antiprismatic geometry; also reported is $[MF_4(2,2'\text{-bipy})_2][MF_6]$.[18] The same study described complexes with the softer phosphine ligand, dppe, which forms $[MF_4(dppe)_2][MF_6]$, also showing an eight-coordinate cation with a octahedral anion.[18]

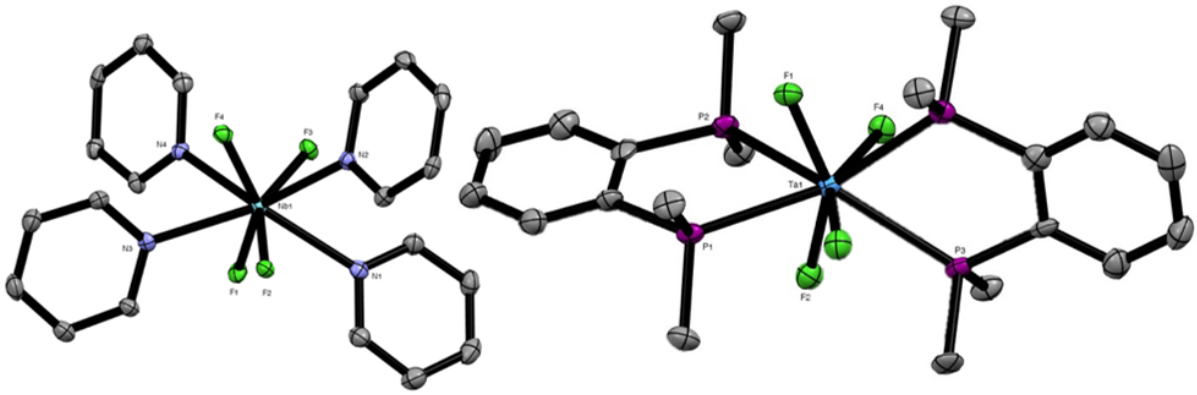

Figure 6.2: Crystal structures of $[NbF_4(py)_4]^+$ (left) and $[TaF_4(o\text{-}C_6H_4(PMe_2)_2)_2]^+$ (right). Anions and hydrogen atoms omitted for clarity.[18,19]

Further reports in the literature include the complexes $[MF_4(R_2P(CH_2)_2PR_2)_2][MF_6]$ and $[MF_4(o\text{-}C_6H_4(EMe_2)_2)_2][MF_6]$ (M = Nb or Ta; R = Me or Et; E = P or As), which were isolated as orange or white solids and crystal structures revealed the cation in a dodecahedral geometry.[19] As discussed in Chapter 3, the reaction of WF_6 and $o\text{-}C_6H_4(EMe_2)_2$ forms $[WF_4(o\text{-}C_6H_4(EMe_2)_2)_2]^{2+}$ cations[2] and

similar cations, $[WCl_4(o\text{-}C_6H_4(EMe_2)_2)_2]^+$, have been crystallographically characterised, formed from reaction of $WECl_4$ and $o\text{-}C_6H_4(EMe_2)_2$ in this work (Chapter 3). A subsequent study showed examples of MF_5 with monodentate phosphine and arsine donor ligands in the form of $[MF_5(L)]$ (L = AsR_3, PPh_3 and PMe_3), all of which were extremely moisture sensitive; attempts using the pnictogen ligand $SbMe_3$ with a heavier donor atom were unsuccessful.[20] The complexes were shown to only form under specific reaction conditions and were very solvent dependent (only diethyl ether being successful). Reactions in MeCN found the ligands were not competitive enough to displace the MeCN and in CH_2Cl_2 the major products were $[PR_3H][MF_6]$. Chloride analogues, $[MCl_4(R_2P(CH_2)_2PR_2)_2][MCl_6]$ and $[MCl_4(o\text{-}C_6H_4(EMe_2)_2)_2][MCl_6]$ (R = Me or Et; E = P or As), have been isolated and showed little difference in behaviour compared to the fluorides.[20] The complex $[TaCl_5(PPh_3)]$[21] has been reported to form under mild conditions and has recently been structurally characterised, while harder ligand complexes $[MCl_5(E'PPh_3)]$ (E' = O, S or Se) are known and some structurally characterised.[22-24]

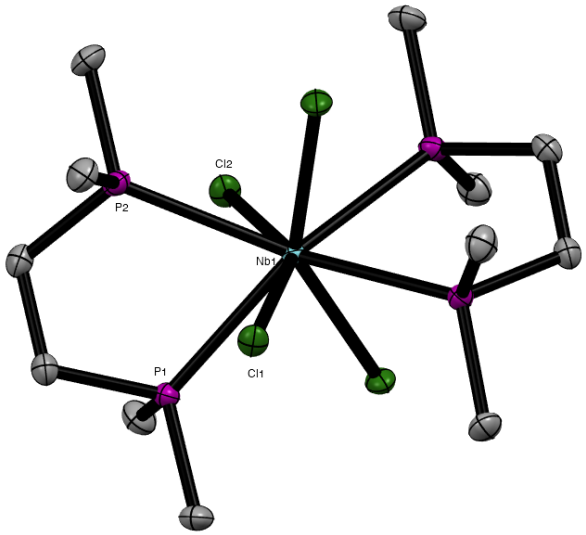

Figure 6.3: Crystal structure of [$NbCl_4$($Me_2P(CH_2)_2PMe_2$)$_2$]. Hydrogen atoms omitted for clarity.[25]

A series of $NbCl_4$ and $NbBr_4$ complexes with bidentate phosphines and thioethers (Chapter 4) have been isolated and the eight-coordinate complexes $[NbCl_4(L\text{-}L)_2]$ (L-L = $o\text{-}C_6H_4(PMe_2)_2$, $R_2P(CH_2)_2PR_2$; R = Me or Et) were isolated as green powders.[25] The compounds with ethylene backbone ligands were shown as having a distorted square antiprism geometry, whereas $[NbCl_4(o\text{-}C_6H_4(PMe_2)_2)_2]$ is distorted dodecahedral. Within the same study unstable 1:1 metal to ligand complexes were isolated, but could not be structurally characterised. It is tentatively suggested that the complexes are the chloride bridged dimers, $[(NbCl_2)_2(\mu\text{-}Cl)_4(L\text{-}L)_2]$ based on elemental composition, magnetic behaviour and structural analgoues.[25-28] There are a small number of $NbCl_4$ complexes with monodentate phosphines, six-coordinate $[NbCl_4(PEtPh_2)_2]$[26] and seven-coordinate $[NbCl_4(PMe_3)_3]$[29] and $[NbBr_4(PMe_2Ph)_3]$[30] have been isolated. The dinuclear complex $[(NbCl_2)_2(\mu\text{-}$

$Cl)_4(PMe_3)_4]$ has a crystalographically confirmed Nb-Nb bond and dissociates into a six-coordinate monomer in solution.[27,28] Reported literature of MX_5 and MX_4 (M = Nb or Ta) complexes with chalcogenoethers were reviewed in Chapter 4.

6.2.1 Coordination Complexes of Transition metal(V) Oxohalides

There are no known neutral coordination complexes of $TaOF_3$, $MoOF_3$ or WOF_3,[1] however, $NbOF_3$ has been shown to form neutral complexes with a selection of hard donor ligands.[31] The complex $[NbOF_3(OPPh_3)_2]$ was shown to form *via* reaction of $[NbF_5(OPPh_3)]$ and $O(SiMe_3)_2$ in CH_2Cl_2, resulting in a white precipitate. Subsequent reactions with NbF_5, $O(SiMe_3)_2$ and ligands produced a more extended series, including $[NbOF_3(L)_2]$ or $[NbOF_3(L\text{-}L)]$ (L = $OPMe_3$, dmso; L-L = $dppmO_2$, 2,2'-bipy, 1,10-phen and tmeda), which were isolated as white, mildly hydrolytically sensitive powders.[31] A full range of chloride analogues, $[NbOCl_3(L)_2]$ or $[NbOCl_3(L\text{-}L)]$, were also isolated under similar conditions and structural investigations showed little difference in the Nb=O bond lengths between different halides. All structures show six-coordinate niobium in distorted octahedral geometry with the ligand *trans* to the Nb=O bond. The main difference between the halides is how $NbOF_3$ and $NbOCl_3$ behave as acceptors towards weaker donor ligands, with complexes of $NbOCl_3$ and ethers or nitriles (THF, MeCN and $MeO(CH_2)_2OMe$) forming stable complexes, while $NbOF_3$ analogues producing intractable ligand-free products, assumed to be mainly polymeric $NbOF_3$.[32-34]

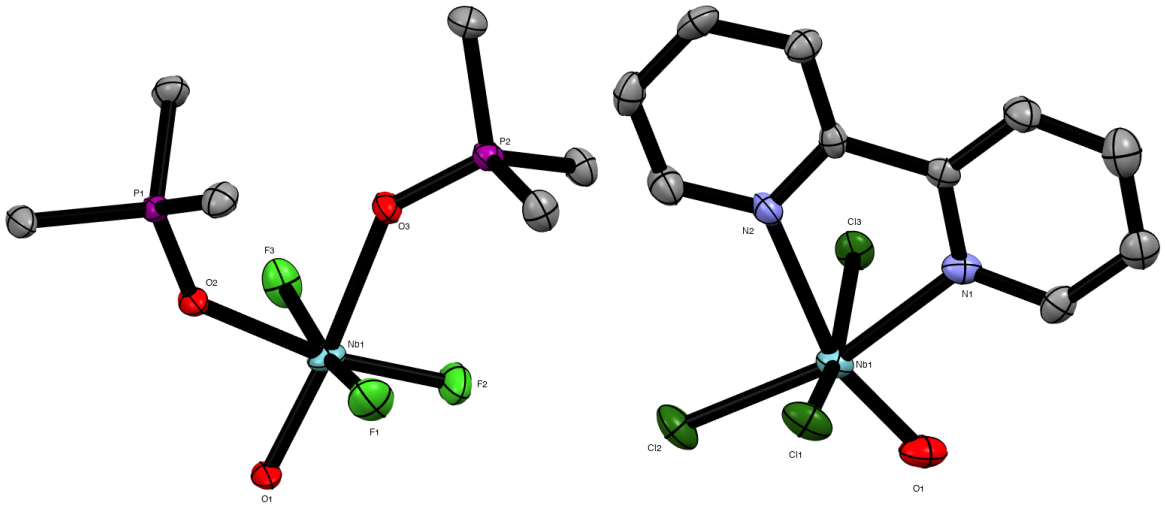

Figure 6.4: Crystal structures of $[NbOF_3(OPMe_3)_2]$ (left) and $[NbOCl_3(2,2'\text{-bipy})]$ (right). Hydrogen atoms and solvent omitted for clarity.[31]

$NbOCl_3$ has been reported to form complexes with tertiary mono- and bi-dentate phosphines; a series of six-coordinate complexes $[NbOCl_3(L)_2]$ (L = PPh_3, $PMePh_2$, PMe_3 or PEt_3) have been isolated using stoichiometric amounts of ligand.[35] Interestingly, when using less sterically demanding and strong σ-donors (PMe_3 and PMe_2Ph), seven-coordinate complexes $[NbOCl_3(L)_3]$ form,[35,36] with the

crystal structures revealing a distorted capped octahedral with a *fac* arrangement of chlorides; this is a similar coordination environment to that seen in $[NbCl_4(PMe_3)_3]$.[29] Two pairs of apparently isomorphous/isostructural crystals of $[NbECl_3(PMe_3)_3]$ (E = O or S) have been reported (green and yellow; orange and green) as examples of "bond-length isomerism", but subsequently it was suggested to result from co-crystallised $[NbCl_4(PMe_3)_3]$, which could explain the different colours and the differences in reported bond lengths.[37,38] Many examples of "bond-length isomerism" have now been disproved and the concept is now disregarded by most.[37]

In contrast to $NbOCl_3$, $TaOCl_3$ has been shown to be considerably less stable[39] and forms readily from trace hydrolysis of $TaCl_5$ or by oxygen abstraction from oxo-ligands.[16,40,41] Crystallographic examples of mononuclear $TaOCl_3$ complexes are limited, with considerably more examples of dinuclear oxide bridged structures, $[LCl_4Ta(\mu\text{-}O)TaCl_4L]$[22] or $[(L\text{-}L)Cl_3Ta(\mu\text{-}O)TaCl_5]$.[42] A systematic series of $[TaOCl_3(L)_2]$ and $[TaOCl_3(L\text{-}L)]$ complexes with a range of hard donor ligands (1,10-phen, 2,2'-bipy, $OPPh_3$, $dppmO_2$, $dppeO_2$ and PPO_2) has been reported, all of which were shown to be six-coordinate, crystallographic studies showed the hard donor ligands positioned *trans* to the Ta=O bond and with most structures exhibiting O/Cl disorder.[43]

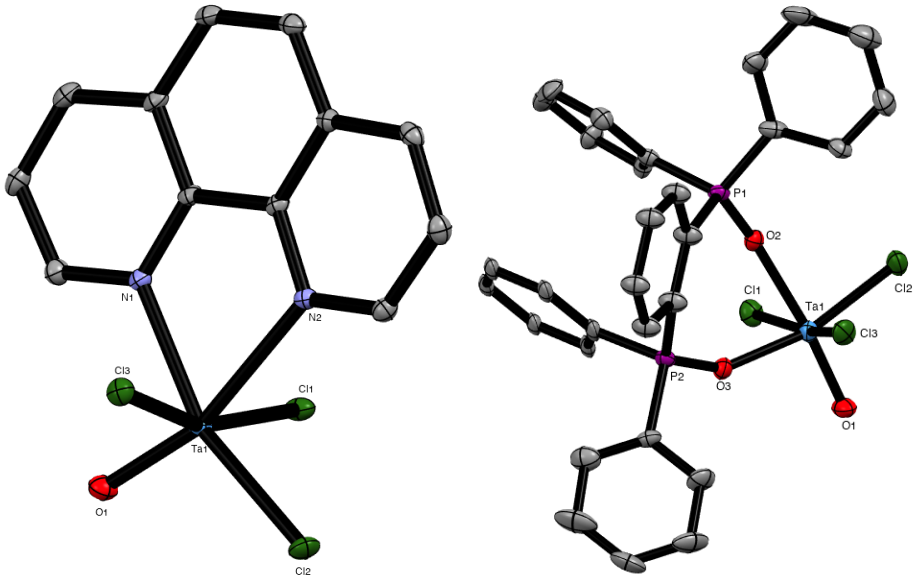

Figure 6.5: Crystal structures of $[TaOCl_3(2,2'\text{-bipy})]$ (left) and $[TaOCl_3(PPO_2)]$ (right) Hydrogen atoms omitted for clarity.[43]

The compound $MoOCl_3$ has been investigated quite extensively in the early literature.[44] Initial reports of simple complexes of $MoOCl_3$ with ethers showed the formation of $[MoOCl_3(L)]$ and $[MoOCl_3(L')_2]$ (L = 1,4-diox, 1,4-thiox, OR_2; L' = THF, tht, THP and thiane), all isolated from the reaction of $MoCl_5$ and excess ligand.[45] It is likely the 1:1 adducts are chloride bridged dimers, $[(LMoOCl_2)_2(\mu\text{-}Cl)_2]$, and the 2:1 adducts are six-coordinate monomers. Following this, $MoOCl_3$ was reacted with aliphatic nitriles, and subsequently $[MoOCl_3(MeCN)_2]$ was reacted with 2,2'-bipy or

1,10-phen, which displaced the MeCN, forming the six-coordinate $[MoOCl_3(L\text{-}L)]$.[46] $[MoOCl_3(OPPh_3)_2]$ has been isolated, as well as a range of $[MoOBr_3(L)_2]$ (L = $OPPh_3$, $OAsPh_3$, MeCN) analogues.[47,48] A short investigation into the reaction of $[MoOCl_3(THF)_2]$ and $R_2P(S)(CH_2)_2P(S)R_2$ (R = Me or Et) showed the formation of two different types of complex; the first, $[MoOCl_3(Et_2P(S)(CH_2)_2P(S)Et_2)]$, forming a six-coordinate chelated species,[49] the second, a seven-coordinate bridged species, $[(MoOCl_3(dmpeS_2))_2(\mu\text{-}dmpeS_2)]$. The difference in behaviour can be attributed to the steric requirements of the ligand.[49] An investigation into the use of open-chain tetrathioether ligands with $MoOCl_3$ showed the formation of a six-coordinate species similar to the isolated structure of $[MoOCl_3(MeS(CH_2)_2SMe)]$ (Figure 6.6).[50]

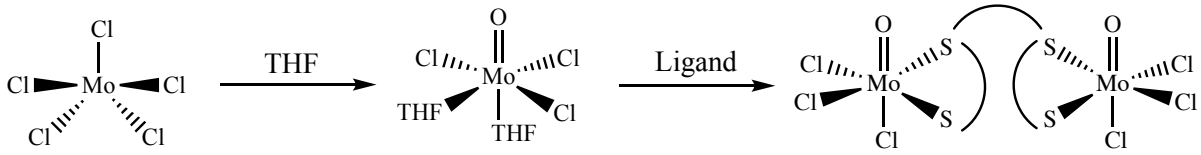

Figure 6.6: Scheme showing the synthesis of six-coordinate $MoOCl_3$ species with open chain thioethers.[50]

Two of the sulfur donors have coordinated to one $MoOCl_3$, forming the six-coordinate species. The alkyl backbone forms a bridge, whereas the other two donor atoms coordinate to a different molybdenum(V) centre.[50] A small number of bidentate thioether complexes with $MoOCl_3$ have been reported, $[MoOCl_3(RS(CH_2)_2SR)]$ (R = Me or Et), isolated from reaction of $[MoOCl_3(THF)_2]$ and ligand.[51] Prior to this work, there was a single report of a selenoether complex, $[MoOCl_3(MeSe(CH_2)_3SeMe)]$ although characterisation is limited.[52] Complexes of $MoOCl_3$ with mono- and bi-dentate phosphine and arsine ligands has been reviewed in Chapter 3.[53]

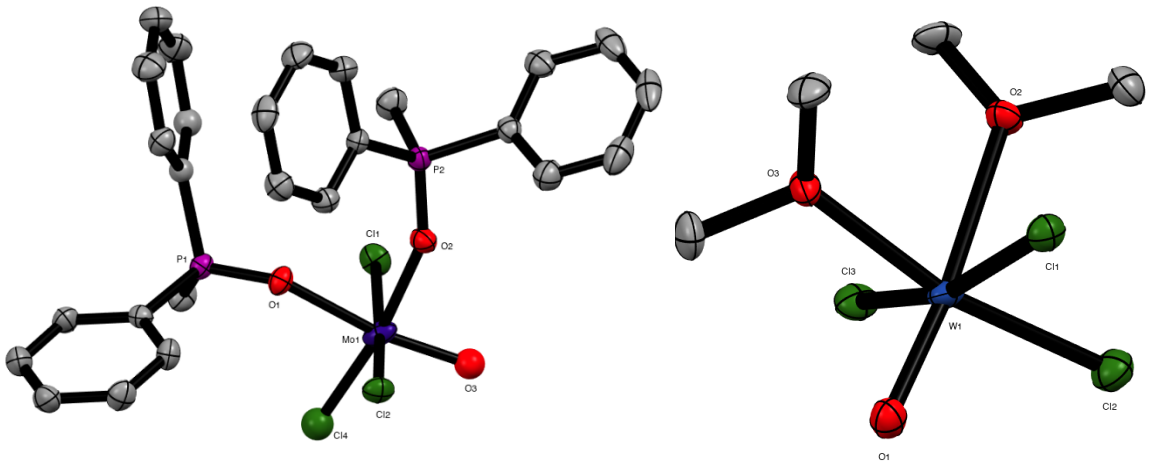

Figure 6.7: Crystals structures of $[MoOCl_3(OPPh_2Me)_2]$ (left) and $[WOCl_3(OMe_2)_2]$ (right). Hydrogen atoms omitted for clarity.[54,55]

Complexes of $WOCl_3$ have been equally extensively investigated despite $WOCl_3$ being more difficult to synthesise. $WOCl_3$ complexes with nitrile donors or ethers in both 1:2 and 1:1 ratios were isolated

initially.[48] There are two reported methods for isolating $[WOCl_3(2,2'\text{-bipy})]$; reaction of $[WOCl_3(THF)_2]$ and 2,2'-bipy in benzene or 2,2'-bipy and $WOCl_4$ in benzene/propionitrile, with both reports having concurring data.[48,56] Complexes of $[WOCl_3(L)_2]$ have been shown as some of the products from reactions of WCl_6 and ethers.[54] The complex, $[WOCl_3(OPPh_3)_2]$, has been reported from stoichiometric reaction of WCl_5 and $OPPh_3$ in MeCN, confirmed by a crystal structure and elemental analysis. However, it is unlikely that WCl_5 abstracted an oxygen from $OPPh_3$ and it more likely originates from adventitious oxygen in the atmosphere or partial hydrolysis.[55] Like $MoOCl_3$, $WOCl_3$ formed two different types of complex when reacting with $R_2P(S)(CH_2)_2P(S)R_2$ (R = Me or Et), $[WOCl_3(Et_2P(S)(CH_2)_2P(S)Et_2)]$ and $[(WOCl_3(dmpeS_2))_2(\mu\text{-}dmpeS_2)]$.[49]

Open chain thioethers have also been reacted with $WOCl_3$, when using $MoOCl_3$ a six-coordinate thioether bridged complex was reported, whereas $WOCl_3$ is reported as either a seven-coordinate tris-thioether mononuclear complex or a six-coordinate bis-thioether complex (Figure 6.8).[50] It was tentatively assigned as the seven-coordinate species based on the UV-Vis spectra and magnetic moment measurements.

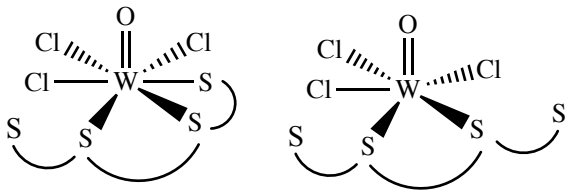

Figure 6.8: Proposition of the structure of $WOCl_3$ with $MeS(CH_2)_2S(CH_2)_2S(CH_2)_2SMe$.

An investigation into the reaction of $WOCl_4$ and a range of bidentate oxygen donor ligands ($RO(CH_2)_2OR$; R = Me, Et, ^{n}Pr or Ph; *o*-$C_6H_4(OMe_2)_2$) showed all reactions with a 1:1 ratio produced $[WOCl_3(O(CH_2)_2OR)]$ or $[WOCl_3(o\text{-}C_6H_4(OMe)(O))]$ by cleavage of one R-O link, except the phenyl substituted ligand, which formed $[(WOCl_4)_2(PhO(CH_2)_2OPh)]$.[57] Complexes of $WOCl_3$ with mono- and bi-dentate phosphine, arsine and stibine donors have also been reviewed in Chapter 3.[58]

6.2.2 Coordination Complexes of Transition Metal(V) Thiohalides

Investigations into metal(V) thiohalide coordination complexes are much less detailed; coordination complexes of $MSCl_3$ (M = Nb or Ta) with chalcogenoethers has been reviewed in Chapter 4. The complexes, $[NbSCl_3(L)_2]$ (L = $OPPh_3$, MeCN, $OP(NMe_2)_3$ or $OSPh_2$), have been shown to form from stoichiometric reaction of $NbSCl_3$ and ligand.[59,60]

Similar tantalum analogues, $[TaSCl_3(L)_2]$ (L = MeCN or $OPPh_3$), have been isolated as six-coordinate species. Bidentate ligands also formed stable complexes, $[TaSCl_3(L\text{-}L)]$ (L-L = 2,2'-bipy, 1,10-phen, $dppmO_2$, $dppeO_2$ or PPO_2).[43] Crystallographic investigations show mononuclear octahedral tantalum

with Ta=S *trans* to the neutral ligand, and many of the structures show S/Cl disorder *trans* ligand due to sulfur and chloride being difficult to distinguish *via* X-ray diffraction.[43] $MSCl_3$ (M = Nb or Ta) complexes with thioethers are reviewed in Chapter 4.

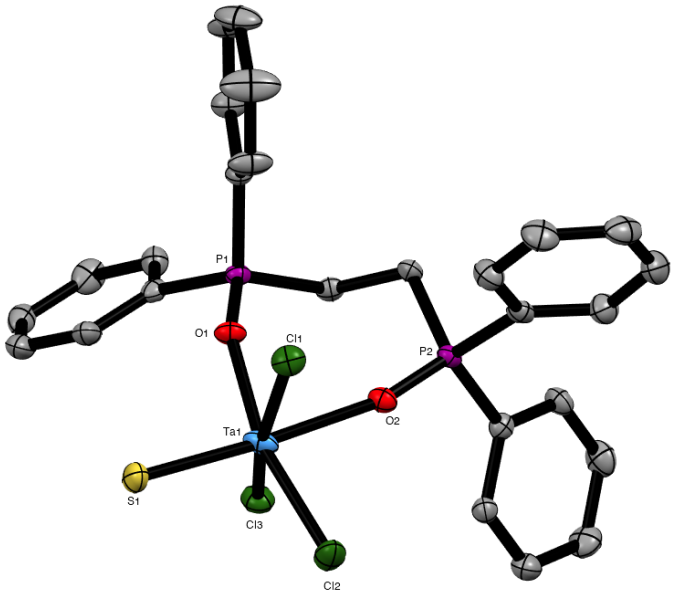

Figure 6.9: Crystal structure of [$TaSCl_3(dppeO_2)$]. Hydrogen atoms omitted for clarity.[43]

In contrast to $MoOCl_3$ (which is chloride bridged) $MoSCl_3$ contains S_2^{2-} units, which are difficult to cleave. This has resulted in no crystallographically-verified [$MoSCl_3(L)_2$] or [$MoSCl_3$(L-L)] complexes.[61] Prolonged refluxing of strongly coordinating solvents with $MoSCl_3$ is suggested to form either [$MoSCl_3(L)_2$] or [$MoSCl_3(L)$] (L = MeCN or py), but spectroscopic characterisation is extremely limited as there are not many spectroscopic handles.[62] The Mo(VI) species, $MoSCl_4$, is not known.

Reports of $WSCl_3$ complexes are more numerous than those of molybdenum analogues, but most form from the reduction of $WSCl_4$.[63,64] The complex [$WSCl_3(OPPh_3)_2$] was isolated from reaction of $WSCl_4$ and $OPPh_3$ from a MeCN/benzene solution.[65] There are no reports of direct synthesis of [$WSCl_3(L)_2$] from $WSCl_3$ and ligands, even with strongly coordinating ligands, as $WSCl_3$ is strongly polymeric and inert.[62]

6.2.3 Aims

The aim of this chapter is to develop a systematic series of $MoOCl_3$ complexes with a range of neutral donor ligands with a particular emphasis on thio-, seleno- and telluro-ether ligands, allowing comparisons to be drawn to the coordination complexes of $WECl_4$ (E = O or S) isolated in Chapters 2 to 4 and reported literature. The reaction of $MoOCl_4$ with various ligands will also be investigated and compared to $MoOCl_3$ complexes, although molybdenum(VI) will likely reduce to paramagnetic

molybdenum(V). Complexes will be characterised by IR spectroscopy, UV-Vis spectroscopy, elemental analysis, magnetic moments and X-ray crystal structures.

6.3 Results and Discussion

The six-coordinate complexes $[MoOCl_3(L\text{-}L)]$ or $[MoOCl_3(L)_2]$ have been isolated in moderate to good yields, 34-87 %, from direct stoichiometric reaction of either $[MoOCl_3(THF)_2]$ or $MoOCl_3$ (isolated from reaction of $MoCl_5$ and THF or $O(SiMe_3)_2$, respectively) and ligand in an appropriate non-coordinating solvent (CH_2Cl_2 or toluene).

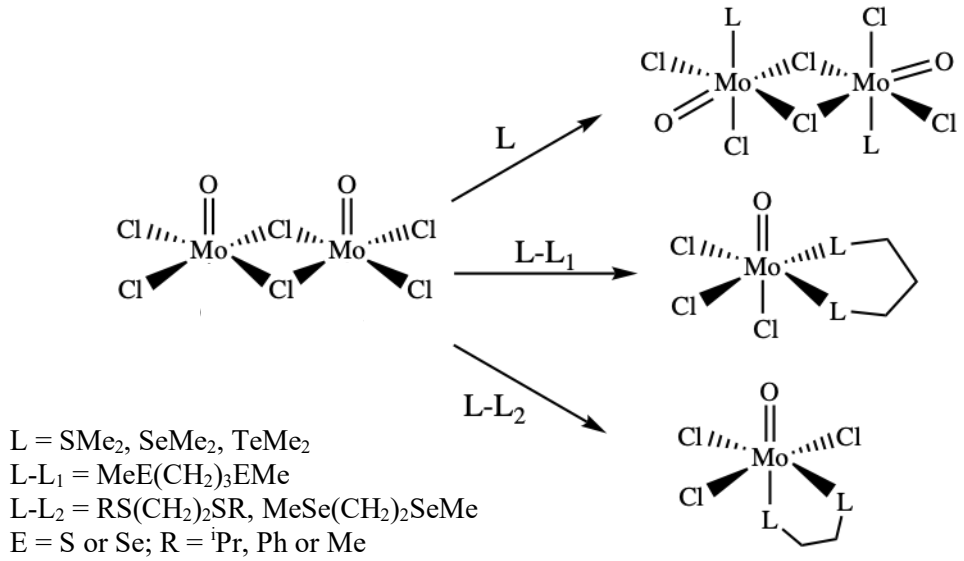

Figure 6.10: Reaction scheme of the synthesis of $[MoOCl_3(L\text{-}L)]$ and $[(MoOCl_2L)_2(\mu\text{-}Cl)_2]$ complexes from $MoOCl_3$.

Initially, $[MoOCl_3(THF)_2]$ was re-prepared and used as the parent precursor, and the spectroscopic data were consistent with literature reports.[66] A number of green crystals were isolated from a CH_2Cl_2 solution of $[MoOCl_3(THF)_2]$ (Figure 6.11); the unit cell and space group ($P2_12_12_1$) match the previously reported structure, but the new structure has slightly higher precision.[67]

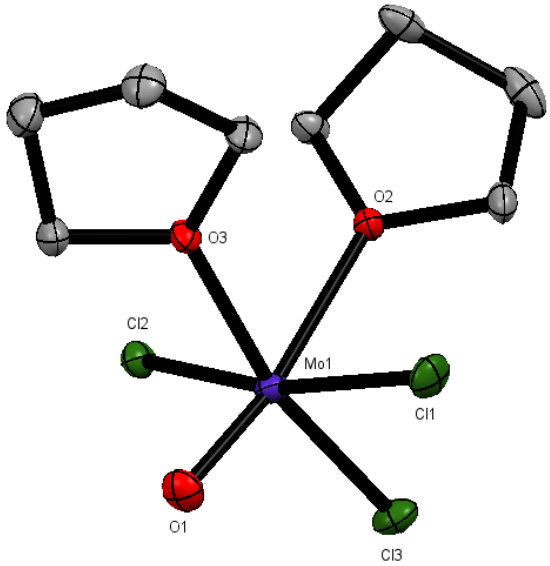

Figure 6.11: Crystal structure of [$MoOCl_3(THF)_2$] showing the atom numbering scheme. Ellipsoids shown at 50% probability, hydrogen atoms are omitted for clarity. Note that the O/Cl exhibited disorder which was modelled with split atom sites and refined to occupancies of 0.10:0.90. Only the major form is shown.

[$MoOCl_3(THF)_2$]			
Bond Lengths/ Å		**Bond Angles/ °**	
Mo1-Cl1	2.3541(6)	Cl1-Mo1-Cl3	89.08(4)
Mo1-Cl2	2.3746(6)	Cl1-Mo1-O1	99.4(4)
Mo1-Cl3	2.342(1)	Cl2-Mo1-Cl3	89.86(4)
Mo1-O1	1.79(2)	Cl2-Mo1-O2	89.03(4)
Mo1-O2	2.126(2)	Cl1–Mo1-O3	99.4(4)
Mo1-O3	2.294(2)		

Table 6.1: Selected bond lengths and angles for [$MoOCl_3(THF)_2$].

6.3.1 Complexes of $MoOCl_3$ and Chalcogenoethers

Reaction of [$MoOCl_3(THF)_2$] and $^{i}PrS(CH_2)_2S^{i}Pr$ in CH_2Cl_2 resulted in the formation of [$MoOCl_3(^{i}PrS(CH_2)_2S^{i}Pr)$], which was isolated as a moisture sensitive, yellow solid. Under the same conditions the complex [$MoOCl_3(MeS(CH_2)_3SMe)$] was isolated from [$MoOCl_3(THF)_2$] and $MeS(CH_2)_3SMe$. The IR spectra showed both thioether ligands had fully displaced the coordinated THF (determined by the lack of C-O stretches in the IR spectra). Crystals were obtained for both complexes from a saturated solution of CH_2Cl_2/hexane, both the structures revealed six-coordinate molybdenum(V) with a distorted octahedral geometry (Figure 6.12).

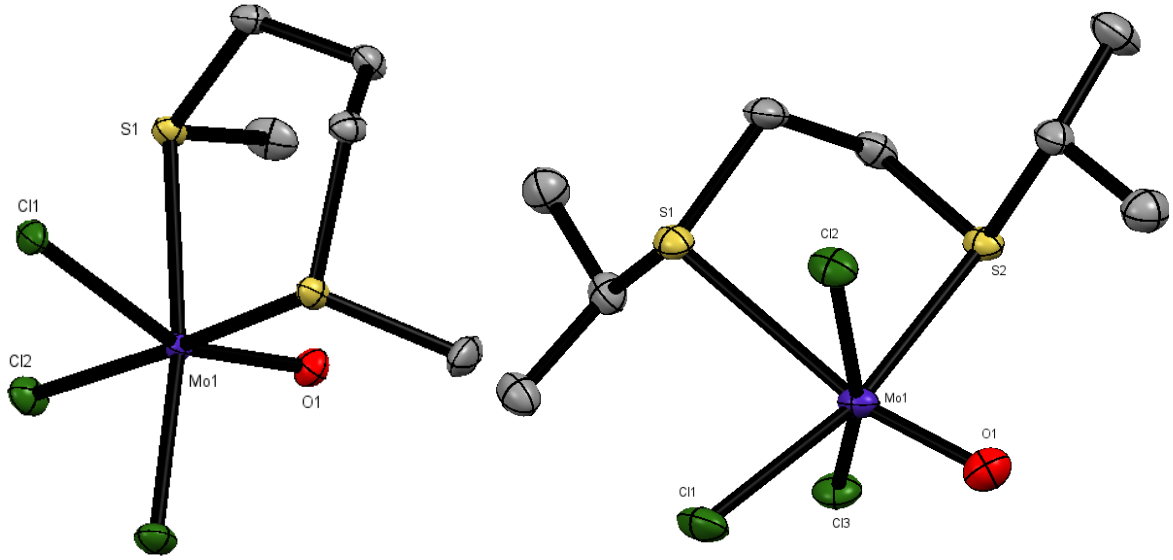

Figure 6.12: Crystal structures of [MoOCl$_3$(MeS(CH$_2$)$_3$SMe)] (left) and [MoOCl$_3$(^{i}PrS(CH$_2$)$_2$S^{i}Pr)] (right) showing the atom numbering scheme. Ellipsoids shown at 50% probability, hydrogen atoms omitted for clarity.

[MoOCl$_3$(MeS(CH$_2$)$_3$SMe)]			
Bond Lengths/ Å		**Bond Angles/ °**	
Mo1-Cl1	2.4541(2)	Cl1-Mo1-Cl2	94.52(2)
Mo1-Cl2	2.3451(2)	Cl2-Mo1-O1	101.87(4)
Mo1-Cl3	2.3451(4)	Cl2-Mo1-Cl3	92.55(3)
Mo1-O1	1.674(3)	Cl3-Mo1-O1	101.87(4)
Mo1-S1	2.5388(3)	S1-Mo1-S1	97.95(2)
Mo1-S2	2.5388(2)		
[MoOCl$_3$(^{i}PrS(CH$_2$)$_2$S^{i}Pr)]			
Bond Lengths/ Å		**Bond Angles/ °**	
Mo1-Cl1	2.3578(8)	Cl1-Mo1-Cl2	91.25(3)
Mo1-Cl2	2.3378(8)	Cl1-Mo1-O1	98.99(8)
Mo1-Cl3	2.3618(7)	Cl1-Mo1-Cl3	89.69(3)
Mo1-O1	1.671(2)	Cl2-Mo1-O1	98.99(8)
Mo1-S1	2.8298(8)	S1-Mo1-S2	78.83(2)
Mo1-S2	2.5665(8)		

Table 6.2: Selected bond lengths and angles for [MoOCl$_3$(MeS(CH$_2$)$_3$SMe)] and [MoOCl$_3$(^{i}PrS(CH$_2$)$_2$S^{i}Pr)].

The structure of [MoOCl$_3$(MeS(CH$_2$)$_3$SMe)] shows the Mo=O bond is *trans* to chlorine and *cis* to the thioether ligand, this is slightly unusual for these types of complex, however this geometric isomer is also seen for the structure [WOCl$_3$(MeS(CH$_2$)$_3$SMe)] (Chapter 4) which is isostructural. The structure of [MoOCl$_3$(^{i}PrS(CH$_2$)$_2$S^{i}Pr)] shows the thioether ligand lying *trans* to the Mo=O and one W-Cl bond with *mer* chlorines as is typical, this isomer is seen with most 5-membered ring chelate complexes.

There is no significant difference in Mo=O bond lengths between the two structures, indicating the different geometric isomers have little effect on the Mo=O bond lengths and the Mo-Cl and Mo-S bond lengths are also similar. Upon coordination of the thioethers, there is the possibility of the formation of a *meso* isomer and a pair of *DL* isomers. The structure of $[MoOCl_3(MeS(CH_2)_3SMe)]$ exhibits the optically inactive *meso* form, whereas $[MoOCl_3(^iPrS(CH_2)_2S^iPr)]$ has a pair of *DL* isomers.

Following the successful isolation of $[MoOCl_3(MeS(CH_2)_3SMe)]$ and $[MoOCl_3(^iPrS(CH_2)_2S^iPr)]$, the weaker σ-donor ligand $PhS(CH_2)_2SPh$ was reacted with $[MoOCl_3(THF)_2]$, however the thioether could not displace the THF, confirmed by the retention of THF in the IR spectroscopy, and crystals of unreacted $[MoOCl_3(THF)_2]$ were identified from the solution of the product. Subsequently, $MoOCl_3$ itself was reacted with $PhS(CH_2)_2SPh$ in CH_2Cl_2, producing the complex $[MoOCl_3(PhS(CH_2)_2SPh)]$ as a yellow/brown coloured solid. Although the ligand is a considerably weaker σ- donor than the methyl substituted ligands and therefore cannot displace the THF, steric crowding around the molybdenum centre may also play a part in its failure to displace the THF.

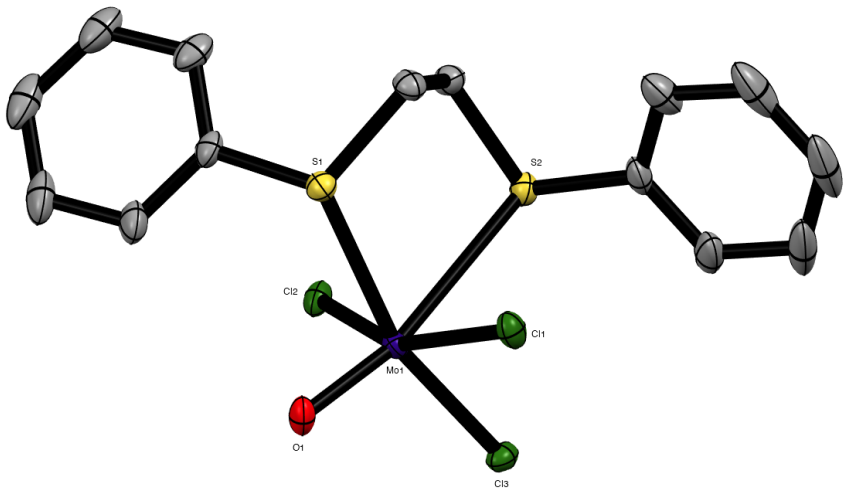

Figure 6.13: The structure of $[MoOCl_3(PhS(CH_2)_2SPh)]$, showing the atom numbering scheme. Ellipsoids shown at 50% probability, hydrogen atoms omitted for clarity. Note that the O/Cl exhibited disorder which was modelled with split atom sites and refined to occupancies of 0.53:0.43. Only the major form is shown.

$[MoOCl_3(PhS(CH_2)_2SPh)]$			
Bond Lengths/ Å		**Bond Angles/ °**	
Mo1-Cl1	2.324(1)	Cl1-Mo1-Cl3	89.93(7)
Mo1-Cl2	2.394(1)	Cl1-Mo1-O1	102.2(5)
Mo1-Cl3	2.312(3)	Cl2-Mo1-Cl3	91.28(7)
Mo1-O1	1.704(2)	Cl2-Mo1-S1	88.40(4)
Mo1-S1	2.532(1)	Cl1–Mo1–S2	81.49(4)
Mo1-S2	2.911(1)	S1-Mo1-S2	78.55(3)

Table 6.3: Selected bond lengths and angles for $[MoOCl_3(PhS(CH_2)_2SPh)]$.

Orange crystals of $[MoOCl_3(PhS(CH_2)_2SPh)]$ were isolated from a CH_2Cl_2 solution (Figure 6.13). The six-coordinate structure shows the same geometry as $[MoOCl_3(^iPrS(CH_2)_2S^iPr)]$ and $[WOCl_3(MeS(CH_2)_2SMe)]$. Strangely, the Mo-S bonds in $[MoOCl_3(PhS(CH_2)_2SPh)]$ are very different (2.532(2) Å, 2.911(1) Å). Although asymmetry is seen in similar complexes, it is not usually this extreme.

Prior to this work there is a single report of $MoOCl_3$ and a selenoether ligand, $[MoOCl_3(MeSe(CH_2)_3SeMe)]$,[52] but with limited spectroscopic data, similar complexes were attempted in this work. Reaction of $[MoOCl_3(THF)_2]$ and $MeSe(CH_2)_2SeMe$ formed $[MoOCl_3(MeSe(CH_2)_2SeMe)]$ which is surprising as selenoethers are considerably softer donors than thioethers so should be less competitive and struggle to displace the THF. However, using the *o*-phenylene backbone ligand *o*-$C_6H_4(SeMe)_2$ does not displace the THF under similar conditions. The IR spectrum reveals that the Mo=O stretch has shifted to a lower wavenumber but the C-O stretch from THF remains. Repeating the experiment with $MoOCl_3$ and *o*-$C_6H_4(SeMe)_2$ produced a pink/brown solid in the absence of THF, tentatively assigned $[MoOCl_3(o\text{-}C_6H_4(SeMe)_2)]$. The IR spectrum revealed a small coordination shift for Mo=O, while the UV-Vis spectrum confirms the molybdenum centre is still in the +V oxidation state, with two observed *d-d* bands.

The complex $[MoOCl_3(MeSe(CH_2)_3SeMe)]$ was obtained from direct reaction of $MoOCl_3$ and $MeSe(CH_2)_3SeMe$ and was isolated as a red/brown solid. The same reaction with $MeSeCH_2SeMe$ produced an unidentifiable black oil, the failure to produce a chelate complex is likely owing to the fact that the bite angle would be too strained due to the short ligand backbone.

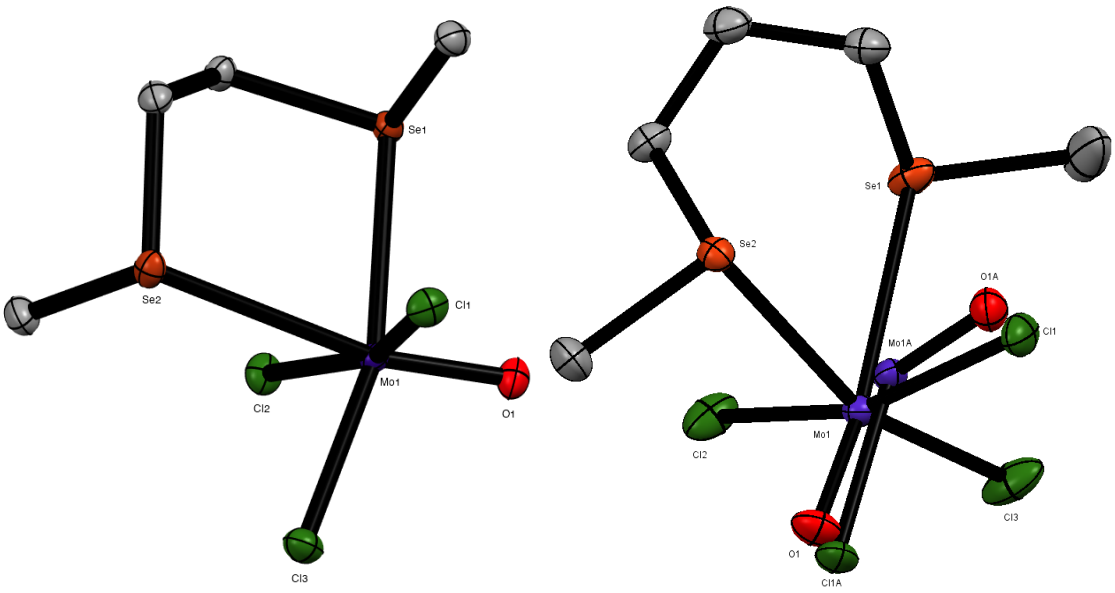

Figure 6.14: Crystal structures of $[MoOCl_3(MeSe(CH_2)_2SeMe)]$ (left) and $[MoOCl_3(MeSe(CH_2)_3SMe)]$ (right) showing the atom numbering scheme. Ellipsoids shown at 50% probability, hydrogen atoms omitted for clarity. Note that in $[MoOCl_3(MeSe(CH_2)_3SMe)]$ there are two geometric isomers present which was modelled with split atom sites and refined to occupancies of 0.60:0.40. Both forms are shown.

[$MoOCl_3(MeSe(CH_2)_2SeMe)$]			
Bond Lengths/ Å		**Bond Angles/ °**	
Mo1-Cl1	2.3553(5)	Cl1-Mo1-Cl3	90.35(2)
Mo1-Cl2	2.3517(5)	Cl1-Mo1-O1	98.98(5)
Mo1-Cl3	2.3453(5)	Cl2-Mo1-Cl3	90.65(2)
Mo1-O1	1.673(1)	Cl3-Mo1-O1	107.36(5)
Mo1-Se1	2.6564(2)	Se1-Mo1-Se2	79.76(1)
Mo1-Se2	2.8937(3)		
[$MoOCl_3(MeSe(CH_2)_3SeMe)$]			
Bond Lengths/ Å		**Bond Angles/ °**	
Mo1-Cl1	2.346(2)	Cl1-Mo1-Cl2	87.72(7)
Mo1-Cl2	2.312(1)	Cl1-Mo1-O1	98.5(4)
Mo1-Cl3	2.372(1)	Cl2-Mo1-Cl3	92.47(4)
Mo1-O1	1.66(1)	Cl2-Mo1-O1	100.9(4)
Mo1-Se1	2.9704(8)	Se1-Mo1-Se2	79.80(2)
Mo1-Se2	2.6768(8)		

Table 6.4: Selected bond lengths and angles for [$MoOCl_3(MeSe(CH_2)_2SeMe)$] and [$MoOCl_3(MeSe(CH_2)_3SeMe)$].

Dark green crystals of [$MoOCl_3(MeSe(CH_2)_2SeMe)$] were isolated, showing the molybdenum centre in a distorted octahedral geometry (Figure 6.14). The Mo=O bond is *trans* to selenoether ligand with *mer* chlorides and there is no evidence of O/Cl disorder *trans* to ligand. The structure has a R_1 = 1.98 % and all bond lengths are consistent with similar structures.

Dark orange crystals of [$MoOCl_3(MeSe(CH_2)_3SeMe)$] (Figure 6.14) were collected, it also shows the molybdenum centre in a distorted octahedral geometry. The structure has disorder in the {$MoOCl_3$} unit but there is no evidence of disorder in the ligand (Figure 6.14). Typically, these types of structure exhibit O/Cl disorder *trans* ligand, however this is not the case, instead the structure shows two different geometric isomers which have co-crystallised. It is highly unusual for geometric isomers to co-crystallise, although there are crystallographic examples of both geometric isomers occurring separately, see Figure 6.12 and Chapter 2.

In the first isomer (modelled at 40 % occupancy), the Mo=O bond is *cis* to the selenoether ligand with *fac* chlorines, the same geometric isomer as seen in [$MoOCl_3(MeS(CH_2)_3SMe)$] and [$WOCl_3(MeS(CH_2)_3SMe)$]. In the second isomer (modelled at 60 % occupancy) the Mo=O bond is *trans* to the selenoether ligand with *mer* chlorines. The modelled Mo=O bond lengths in both geometric isomers are similar (*trans*-Mo1-O1 = 1.66(1) and *cis*-Mo1A-O1A = 1.70(1) Å) and are consistent with non-disordered Mo=O bond lengths. The molybdenum atom is also spilt over two

sites as it would sit in slightly different positions in each geometric isomer. The structure was considered as a potential example of "bond length isomerism" where a small amount of $[MoCl_4(MeSe(CH_2)_3SeMe)]$ could have co-crystallised resulting in the disparity in bond lengths. An attempt to model one $\{MoCl_4\}$ unit and one $\{MoOCl_3\}$ unit as having co-crystallised was unsuccessful. Additionally, if it was "bond length isomerism" it is likely that there would only be a small amount of disorder, not the 40/60 atom occupancies modelled. Co-crystallisation of geometric isomers is highly unusual, but the structure has been satisfactorily modelled with a $R_1 = 2.09$ %. The reason for the co-crystallisation is unclear and may be a result of crystal packing or there being little energy difference between isomers. It is possible that in the solution state there is rapid exchange between isomers, unfortunately these compounds were paramagnetic, if the compounds were diamagnetic this could be probed by variable temperature NMR spectroscopy.

The synthesis of complexes of $MoOCl_3$ with monodentate chalcogenoethers, EMe_2 (E = S, Se or Te), proved challenging as the products were highly soluble in most organic solvents. Initial investigations with EMe_2 (E = S or Se) and $[MoOCl_3(THF)_2]$ showed that the EMe_2 ligands could not displace the THF. However, reaction with $MoOCl_3$ directly, led to the formation of the chloride-bridged dimers, $[(MoOCl_2(EMe_2))_2(\mu\text{-}Cl)_2]$. There was no evidence for the presence of mononuclear complexes, $[MoOCl_3(EMe_2)_2]$, in the spectroscopic data. The formation of dimers is not unusual for molybdenum(V) complexes or other transition metals, in the absence of any chelate effect, the six-coordinate monomer with two thioether ligands is likely to be less stable than the Cl-bridged dimer.[60,68,69]

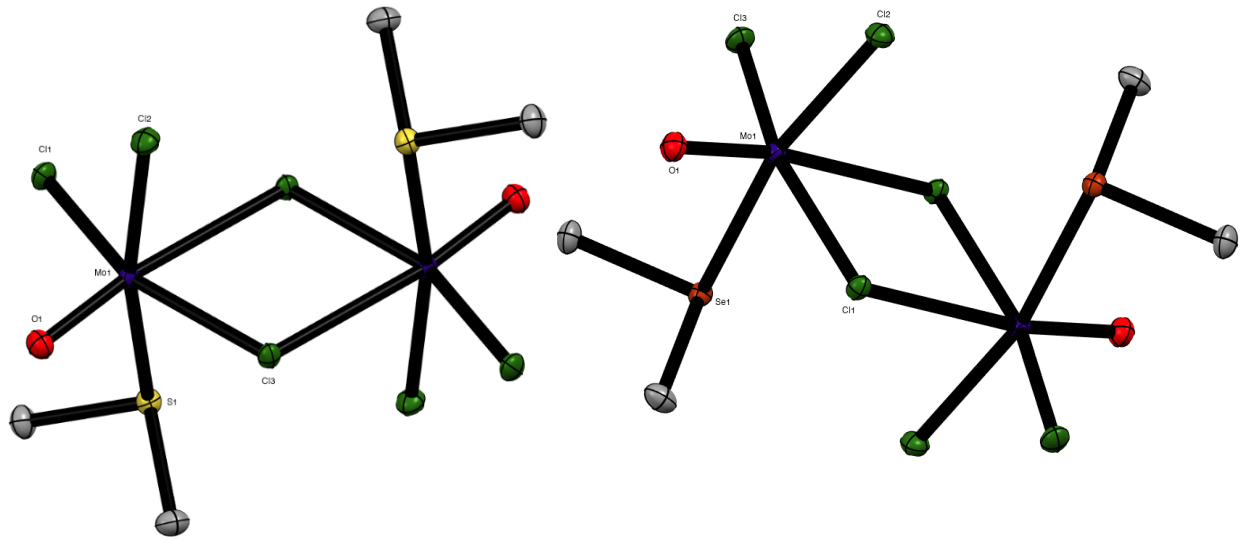

Figure 6.15: Crystal structures of $[(MoOCl_2(SMe_2))_2(\mu\text{-}Cl)_2]$ (left) and $[(MoOCl_2(SeMe_2))_2(\mu\text{-}Cl)_2]$ (right) showing the atom numbering scheme. Ellipsoids shown at 50% probability, hydrogen atoms omitted for clarity.

$[(MoOCl_2(SMe_2))_2(\mu\text{-}Cl)_2]$			
Bond Lengths/ Å		**Bond Angles/ °**	
Mo1-Cl1	2.3264(3)	Cl1-Mo1-O1	102.48(1)
Mo1-Cl2	2.3341(3)	Cl2-Mo1-O1	102.08(3)
Mo1-Cl3	2.3953(3)	Cl3-Mo1-O1	99.55(3)
Mo1-O1	1.6515(8)	Cl2-Mo1-Cl3	85.77(1)
Mo1-S1	2.5537(3)		
$[(MoOCl_2(SeMe_2))_2(\mu\text{-}Cl)_2]$			
Bond Lengths/ Å		**Bond Angles/ °**	
Mo1-Cl1	2.4024(4)	Cl1-Mo1-O1	98.89(4)
Mo1-Cl2	2.338(5)	Cl2-Mo1-O1	103.10(4)
Mo1-Cl3	2.3298(5)	Cl3-Mo1-O1	102.38(4)
Mo1-O1	1.653(1)	Cl2-Mo1-Cl3	92.32(2)
Mo1-Se1	2.6647(3)		

Table 6.5: Selected bond lengths and angles for $[(MoOCl_2(SMe_2))_2(\mu\text{-}Cl)_2]$ and $[(MoOCl_2(SeMe_2))_2(\mu\text{-}Cl)_2]$.

The chloride-bridged dimers (Figure 6.15) are isomorphous and adopt a distorted bioctahedral geometry, the Mo=O bonds are *trans* to the bridging chlorides, as is typical in dimers of this type.[70-72] The chloride bridges are asymmetric and the EMe_2 ligands lie *anti* to each other. Other than the Mo-E bond distances, there is little difference in the bond lengths between structures, suggesting the neutral ligand has little influence. The presence of molybdenum(V) in these species is confirmed in the bulk by UV-vis spectroscopy, with the presence of two *d-d* bands, while the magnetic moments are consistent with a single unpaired electron.

Following successful formation of the products from the reaction with EMe_2 (E = S or Se), $MoOCl_3$ was reacted with $TeMe_2$ using similar ambient conditions. The product was isolated as a fine brown powder. The IR spectrum showed a strong Mo=O stretch at 985 cm^{-1} consistent with the other chalcogenoether complexes in this series. In the solid state UV-vis spectrum two *d-d* bands are observed at 14,400 and 19,500 cm^{-1}, with the lowest LMCT band for Te→Mo(4*d*) assigned as 21,000 cm^{-1} (similar to the bands seen in thio- and seleno-ether complexes). It should be noted that the LMCT band for Te→Mo(4*d*) could be the band at 19,500 cm^{-1}, with the second *d-d* transition band hidden. In conjunction with the IR and UV-vis spectra, elemental analysis is also consistent with the formation of the complex, $[(MoOCl_2(TeMe_2))_2(\mu\text{-}Cl)_2]$. It is clear the monodentate ligands (and likely softer donors) are more stable as chloride-bridged dimers with a 1:1 metal to ligand ratio.

Following the successful isolation of $[(MoOCl_2(TeMe_2))_2(\mu\text{-}Cl)_2]$, the bidentate telluroethers, *o*-$C_6H_4(TeMe)_2$ and $MeTe(CH_2)_3TeMe$ were each reacted with $MoOCl_3$ in CH_2Cl_2 under similar

conditions, leading to the isolation of dark brown solids. Spectroscopic data for both products are consistent with the formation of molybdenum(V) complexes, shown by magnetic moments (Table 6.6). Both products show a Mo=O stretch in the IR spectra (992 and 988 cm^{-1}) and a number of Mo-Cl stretches. The UV-vis spectrum from the product isolated from $MoOCl_3$ and *o*-$C_6H_4(TeMe)_2$ shows two *d-d* bands (14,500 and 19,200 cm^{-1}) and a LMCT band for Te→Mo(4*d*) at 21,000 cm^{-1} (likely assignment of LMCT bands are presented in Table 6.16). Spectroscopic data reveals the expected functional groups (Mo=O and Mo-Cl), oxidation state (Mo^{V}) and Te→Mo(4*d*) transition band however the exact formulation is yet to be positively determined.

The product from $MoOCl_3$ and $MeTe(CH_2)_3TeMe$ seemed slightly less stable than the other telluroether complexes, turning black after a couple of days, even under inert conditions. The spectroscopic data is also consistent with similar thio- and seleno-ether complexes isolated in this work and the telluroether complex assigned as $[(MoOCl_2(TeMe_2))_2(\mu\text{-}Cl)_2]$. The product exhibits the expected functional groups (Mo=O and Mo-Cl), oxidation state (Mo^{V}) and Te→Mo(4*d*) transition band however the exact formulation is yet to be positively determined.

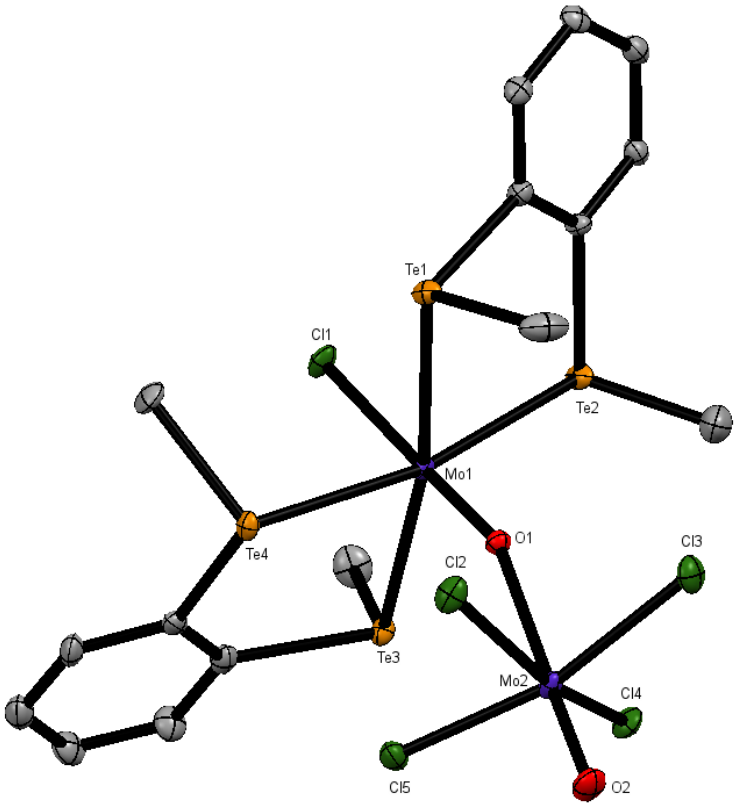

Figure 6.16: Crystal structure of $[(MoCl(o\text{-}C_6H_4(TeMe)_2)_2)(\mu\text{-}O)(MoOCl_4)]\bullet CH_2Cl_2$ showing the atom numbering scheme. Ellipsoids shown at 50% probability, hydrogen atoms and solvent omitted for clarity.

[(MoCl(o-$C_6H_4(TeMe)_2)_2$)(μ-O)($MoOCl_4$)]•CH_2Cl_2			
Bond Lengths/ Å		**Bond Angles/ °**	
Mo1-Cl1	2.449(1)	O2-Mo2-Cl	78.4(1)-82.2(1)
Mo2-Cl	2.363(2)-2.393(2)	Te-Mo1-Te	85.27(2)-86.18(2)
Mo1-Te	2.7440(6)-2.7836(6)	Te2-Mo1-Cl1	79.67(4)
Mo1-O1	1.705(4)	Te1-Mo1-Cl1	83.36(4)
Mo2-O1	2.368(4)		
Mo2-O2	1.659(5)		

Table 6.6: Selected bond lengths and angles for [(MoCl(o-$C_6H_4(TeMe)_2)_2$)(μ-O)($MoOCl_4$)]•CH_2Cl_2.

There is precedence of bidentate chalcogenoether ligands forming bridged species between transition metals when the alkyl backbone is long enough.[69,73-75] This type of system could form to stabilise the high valent molybdenum(V) as shown in *anti*-[($MoOCl_2(EMe_2)$)$_2$(μ-Cl)$_2$] (E = S or Se). A possible formulation could be *syn*-[($MoOCl_2$)$_2$(μ-Cl)$_2$(μ-MeTe(CH_2)$_3$MeTe)] which would be supported by the spectroscopic data but not conclusively proven. This potential formulation can be applied to *syn*-[($MoOCl_2$)$_2$(μ-Cl)$_2$(μ-*o*-$C_6H_4(TeMe)_2$)] as there are examples of bridging chalcogenoethers with C_2 backbones.

A number of crystallisation attempts were unsuccessful (but the product was very insoluble) but a small number of green crystals were isolated from the brown solution. The crystals were subsequently identified as [(Mo^{IV}Cl(o-$C_6H_4(TeMe)_2)_2$)(μ-O)($Mo^{V}OCl_4$)]•CH_2Cl_2, which is a mixed valent system. This is not the first example of this type of dimer, see Section 6.3.2, although this is the first crystallographically characterised example (along with another example Section 6.3.2) and the first and only telluroether coordinated to Mo(IV). Both molybdenum centres are in a distorted octahedral geometry, linked by an oxide bridge with asymmetrical Mo=O-Mo bonds. It is likely this structure originates from partial decomposition of [$MoOCl_3$(*o*-$C_6H_4(TeMe)_2$] as the spectroscopic data does not support this crystal structure as the bulk, and analogous bulk [(MoCl(L-L)$_2$)(μ-O)($MoOCl_4$)] complexes have been isolated from refluxing methanol with [$MoOCl_3$(L-L)].[53]

Compound	**IR Data**		**Magnetic Moment (μ_{eff})**
	ν(Mo=O)	*ν*(Mo-Cl)	
[$MoOCl_3(THF)_2$]	982 cm^{-1}	342, 315 cm^{-1}	1.71
[$MoOCl_3$(MeS(CH_2)$_3$SMe)]	955 cm^{-1}	348, 327, 306 cm^{-1}	1.71
[$MoOCl_3$(^{i}PrS(CH_2)$_2$S^{i}Pr)]	979 cm^{-1}	349, 312 cm^{-1}	1.69
[$MoOCl_3$(PhS(CH_2)$_2$SPh)]	966 cm^{-1}	354, 319 cm^{-1}	1.71
[$MoOCl_3$(MeSe(CH_2)$_2$SeMe)]	956 cm^{-1}	342, 310 cm^{-1}	1.70
[$MoOCl_3$(MeSe(CH_2)$_3$SeMe)]	954 cm^{-1}	346, 296 cm^{-1}	1.70

$[MoOCl_3(o\text{-}C_6H_4(SeMe)_2]$	999 cm^{-1}	351, 302, 292 cm^{-1}	1.69
$[MoOCl_3(o\text{-}C_6H_4(TeMe)_2]$	992 cm^{-1}	343, 328, 302 cm^{-1}	1.70
$[MoOCl_3(MeTe(CH_2)_3TeMe)]$	988 cm^{-1}	392, 303 cm^{-1}	1.68
$[(MoOCl_2(SMe_2))_2(\mu\text{-}Cl)_2]$	984 cm^{-1}	356, 319, 268 cm^{-1}	1.72
$[(MoOCl_2(SeMe_2))_2(\mu\text{-}Cl)_2$	956 cm^{-1}	367, 351, 313 cm^{-1}	1.68
$[(MoOCl_2(TeMe_2))_2(\mu\text{-}Cl)_2]$	985 cm^{-1}	327, 302, 292 cm^{-1}	1.68
$[MoOCl_3(2,2'\text{-bipy})]$	970 cm^{-1}	355, 348, 315 cm^{-1}	
$[MoOCl_3(1,10\text{-phen})]$	971 cm^{-1}	360, 348, 309 cm^{-1}	1.71
$[MoOCl_3(PMe_3)_2]$	957 cm^{-1}	352, 324, 305 cm^{-1}	
$[MoOCl_3(dppe)]$	954 cm^{-1}	337 cm^{-1}	1.70
$[MoOCl_3(dmpe)]$	951 cm^{-1}	362, 325, 306 cm^{-1}	1.72

Table 6.7: Selected IR stretches and magnetic moments for complexes in this chapter.

6.3.2 $MoOCl_3$ Complexes with Hard Donor Ligands

A small range of complexes, most previously known, were isolated to investigate the behaviour of $[MoOCl_3(THF)_2]$ and to use them as comparators for reactions of $MoOCl_4$. The six-coordinate complexes $[MoOCl_3(L\text{-}L)]$ (L-L = 2,2'-bipy or 1,10-phen) were isolated from a stoichiometric reaction of ligand and $[MoOCl_3(THF)_2]$. Both complexes have been previously reported and spectroscopic data are in good agreement with the literature.[46,76] Despite a number of reports of these complexes, no crystallographic data are available, possibly as they are poorly soluble in organic solvents.

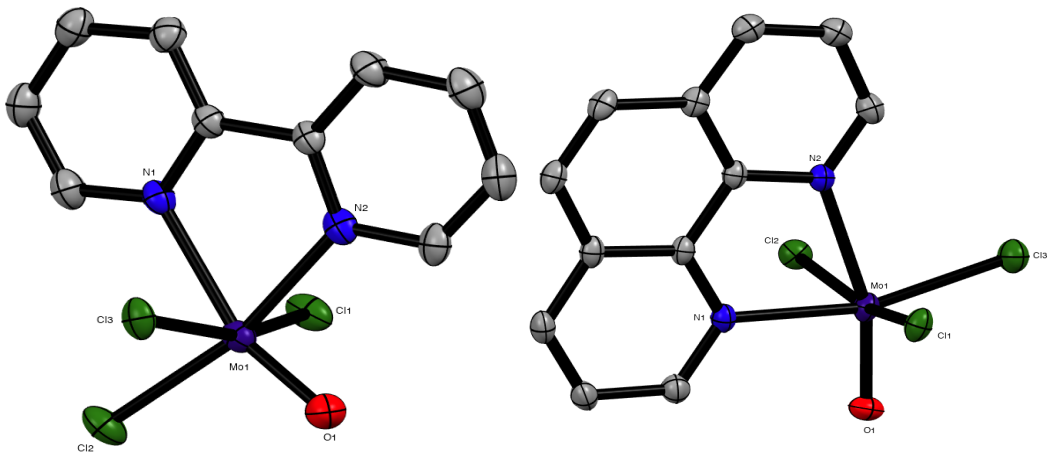

Figure 6.17: Crystal structures of $[MoOCl_3(2,2'\text{-bipy})]$ (left) and $[MoOCl_3(1,10\text{-phen})]$ (right) showing the atom numbering scheme. Ellipsoids shown at 50% probability, hydrogen atoms omitted for clarity. Note that in $[MoOCl_3(2,2'\text{-bipy})]$ there are three molecules in the asymmetric unit, two molecules exhibited whole molecule disorder which was modelled with split atom sites and refined to occupancies of 0.60:0.40 and 0.86:0.14. The non-disordered molecule is shown. $[MoOCl_3(1,10\text{-}$

phen)] exhibits O/Cl disorder which was modelled with split atom sites and refined to occupancies of 0.1:0.9 only the major form is shown.

[$MoOCl_3$(2,2'-bipy)]			
Bond Lengths/ Å		**Bond Angles/ °**	
Mo1-Cl1	2.346(2)	Cl1-Mo1-Cl2	90.61(6)
Mo1-Cl2	2.347(2)	Cl1-Mo1-O1	99.4(2)
Mo1-Cl3	2.358(1)	Cl2-Mo1-Cl3	89.17(6)
Mo1-O1	1.665(5)	Cl3-Mo1-O1	98.2(2)
Mo1-N1	2.325(5)		
Mo1-N2	2.191(6)		
[$MoOCl_3$(1,10-phen)]			
Bond Lengths/ Å		**Bond Angles/ °**	
Mo1-Cl1	2.3655(7)	Cl1-Mo1-Cl3	89.66(2)
Mo1-Cl2	2.3839(7)	Cl1-Mo1-O1	98.4(1)
Mo1-Cl3	2.3348(6)	Cl2-Mo1-Cl3	92.11(2)
Mo1-O1	1.629(3)	Cl2-Mo1-O1	97.30(6)
Mo1-N1	2.201(2)		
Mo1-N2	2.350(2)		

Table 6.8: Selected bond lengths and angles for [$MoOCl_3$ (2, 2' - bipy)] and [$MoOCl_3$ (1, 10 - phen)].

Dark pink crystals of [$MoOCl_3$(2,2'-bipy)] and [$MoOCl_3$(1,10-phen)] were each isolated from a diethyl ether solution (Figure 7.17); both structures show the expected distorted octahedral geometry with *mer* chlorines. [$MoOCl_3$(1,10-phen)] is isomorphous with [$TaOCl_3$(1,10-phen)], whereas [$MoOCl_3$(2,2'-bipy)] is not isomorphous with [$NbOCl_3$(2,2'-bipy)].[31,43] Both molybdenum structures have the Mo=O bond *trans* to the diimine ligand and both exhibit O/Cl disorder and asymmetric Mo-N bonds.

A small number of $MoOCl_3$ complexes with phosphine donor ligands were also prepared, including the six-coordinate [$MoOCl_3$(dppe)] whose spectroscopic data were in good agreement with reported literature.[53] Spectroscopic data for the new complex, [$MoOCl_3$(dmpe)], were consistent with similar complexes. The complexes yielded crystals (red, [$MoOCl_3$(dppe)] or yellow, [$MoOCl_3$(dmpe)]) from CH_2Cl_2 solution, the structure of [$MoOCl_3$(dppe)] has been reported previously (Figure 6.18).[77]

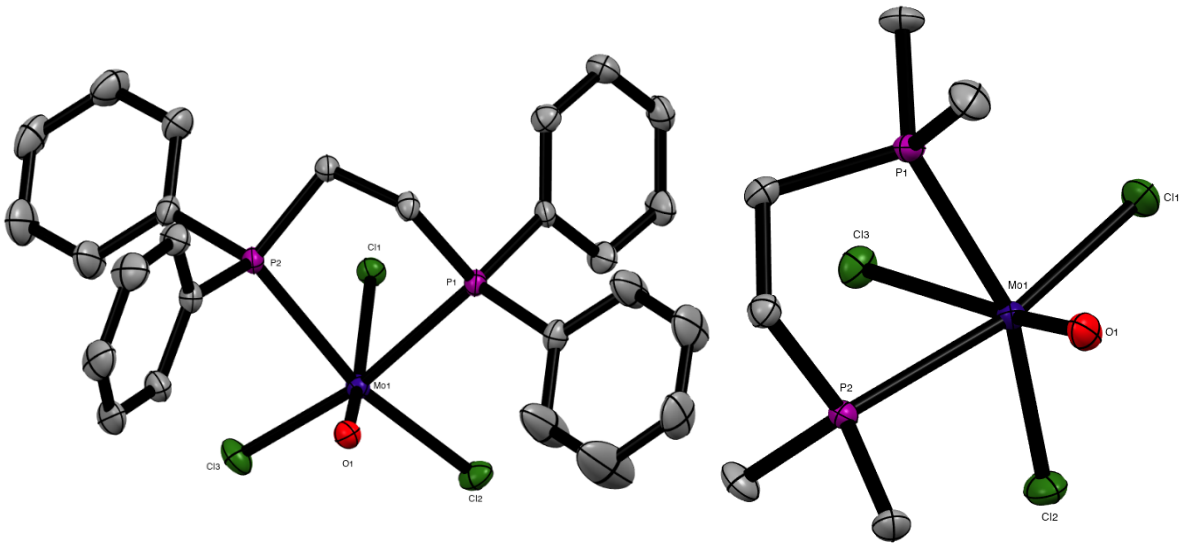

Figure 6.18: Crystal structures of [MoOCl₃(dppe)] (left) and [MoOCl₃(dmpe)] (right) showing the atom numbering scheme. Ellipsoids shown at 50% probability, hydrogen atom and solvent omitted for clarity.

[MoOCl₃(dppe)]			
Bond Lengths/ Å		**Bond Angles/ °**	
Mo1-Cl1	2.4638(7)	Cl1-Mo1-Cl2	92.25(3)
Mo1-Cl2	2.3655(6)	Cl2-Mo1-O1	100.91(8)
Mo1-Cl3	2.363(1)	Cl2-Mo1-Cl3	97.17(3)
Mo1-O1	1.691(2)	Cl3-Mo1-O1	100.98(8)
Mo1-P1	2.5726(8)	P1-Mo1-P2	80.27(2)
Mo1-P2	2.5649(6)		
[MoOCl₃(dmpe)]			
Bond Lengths/ Å		**Bond Angles/ °**	
Mo1-Cl1	2.3824(9)	Cl1-Mo1-Cl2	96.98(3)
Mo1-Cl2	2.383(1)	Cl1-Mo1-O1	100.19(8)
Mo1-Cl3	2.5011(8)	Cl2-Mo1-Cl3	88.76(3)
Mo1-O1	1.680(2)	Cl2-Mo1-O1	104.66(8)
Mo1-P1	2.5260(2)	P1-Mo1-P2	78.84(3)
Mo1-P2	2.5250(8)		

Table 6.9: Selected bond lengths and angles for [MoOCl₃(dppe)] and [MoOCl₃(dmpe)].

The structure of [MoOCl₃(dppe)] is in good agreement with the previously reported structure, interestingly both structures exhibit the Mo=O bond *cis* to the phosphine ligand, whereas in the majority of corresponding thio- and seleno-ether complexes discussed earlier, the Mo=O bond is *trans* to ligand.[77] The axial Mo-Cl bonds are longer than typical, due to being *trans* to the oxide.

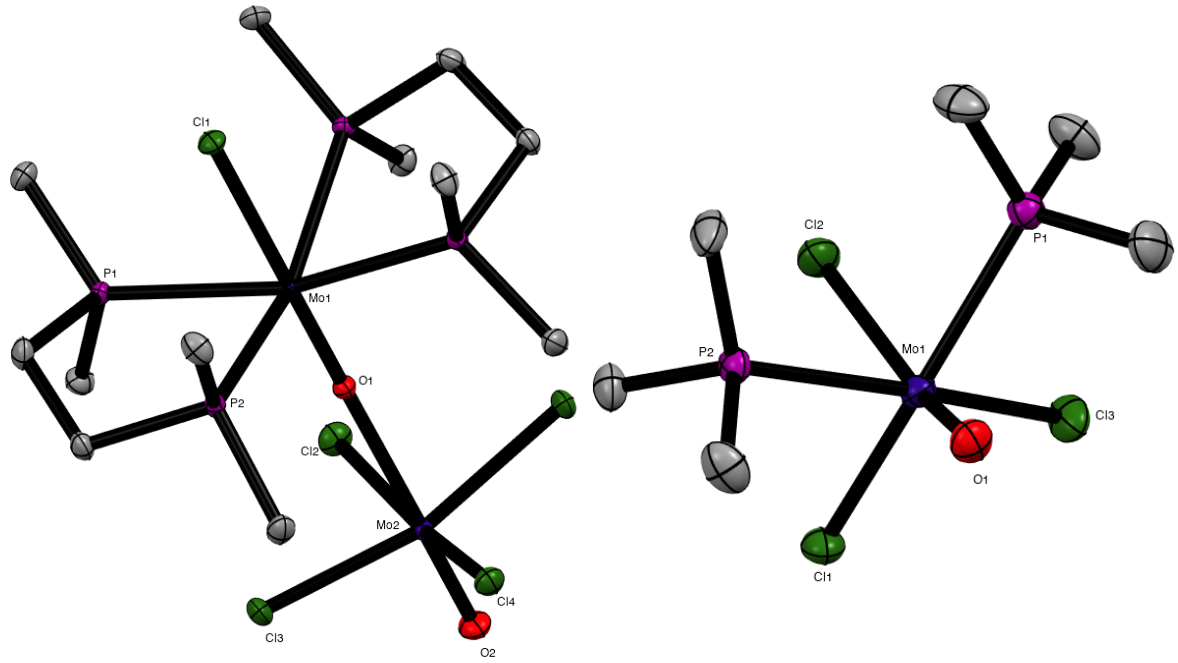

Figure 6.19: Crystal structures of [(MoOCl(dmpe)$_2$)(μ-O)(MoOCl$_4$)] (left) and [MoOCl$_3$(PMe$_3$)$_2$] (right) showing the atom numbering scheme. Ellipsoids shown at 50% probability, hydrogen atom and solvent omitted for clarity.

[(MoCl(dmpe)$_2$)(μ-O)(MoOCl$_4$)]			
Bond Lengths/ Å		**Bond Angles/ °**	
Mo1-Cl1	2.5186(2)	Cl1-Mo1-P1	78.92(2)
Mo2-Cl$_{cis}$	2.3573(4) – 2.3824(3)	Cl1-Mo1-P2	83.26(4)
Mo1-O1	1.703(4)	O2-Mo2-Cl	97.57(2) – 98.89(4)
Mo2-O1	2.394(2)	P1-Mo1-P2	80.16(4)
Mo2-O2	1.657(8)		
Mo1-P1	2.5131(2)		
Mo1-P2	2.5139(3)		
[MoOCl$_3$(PMe$_3$)$_2$]			
Bond Lengths/ Å		**Bond Angles/ °**	
Mo1-Cl1	2.367(1)	Cl1-Mo1-Cl2	91.99(3)
Mo1-Cl2	2.3507(1)	Cl1-Mo1-O1	103.81(9)
Mo1-Cl3	2.384(1)	Cl2-Mo1-Cl3	93.60(3)
Mo1-O1	1.689(3)	Cl3-Mo1-O1	102.39(9)
Mo1-P1	2.568(1)		
Mo1-P2	2.56339(9)		

Table 6.10: Selected bond lengths and angles for [(MoOCl(dmpe)$_2$)(μ-O)(MoOCl$_4$)] and [MoOCl$_3$(PMe$_3$)$_2$].

Attempts to grow crystals of $[MoOCl_3(dmpe)]$, resulted in a few separate purple crystals being isolated that were revealed to be $[(MoCl(dmpe)_2)(\mu\text{-}O)(MoOCl_4)]$ analogous to $[(MoCl(o\text{-}C_6H_4(TeMe)_2)_2)(\mu\text{-}O)(MoOCl_4)]\bullet CH_2Cl_2$ discussed earlier. Both molybdenum ions are in a distorted octahedral geometry and linked by an oxide bridge. The Mo=O-Mo bond lengths are asymmetric and the Mo-Cl_{axial} bonds are bent away from planarity by the terminally bonded oxygen.

A series of complexes with bidentate phosphine ligands of the form $[MoOCl(L\text{-}L)_2][MoOCl_4]$ have been reported as mauve solids. However, following the structural identification of $[(MoCl(dmpe)_2)(\mu\text{-}O)(MoOCl_4)]$, it is possible that the suggested formulation was incorrect in the solid state.[49] The complexes formulated as $[MoOCl(L\text{-}L)_2][MoOCl_4]$, the spectroscopic data reported would also be consistent with the crystal structure isolated. The complexes were reported to behave as 1:1 electrolytes in solution, so could dissociate in solution and be a dimer in the solid state. The crystal structure of $[MoOCl_3(PMe_3)_2]$ has been reported previously and is in good agreement with this structure.[78]

6.3.3 Reactions of $MoOCl_4$ with Neutral Donor Ligands

There are no reported coordination complexes that maintain the +VI oxidation state for $MoOCl_4$. This indicates that $MoOCl_4$ most likely reduces upon addition of ligand and will be investigated in this section.

Initially, $MoOCl_4$ was dissolved in MeCN to attempt to isolate $[MoOCl_4(MeCN)]$, however, a paramagnetic species was isolated instead. Crystallisation attempts produced two sets of crystals (yellow and green), which were identified as molybdenum(V) species, $[MoOCl_3(MeCN)_2]$ and $[(MoOCl_2(MeCN))_2(\mu\text{-}Cl)_2]$ (Figure 6.20). The IR spectrum for the bulk shows a single dominant peak at 986 cm^{-1}, assigned to Mo=O, but it is unclear which of the two structures identified below is the major product.

Both structures show distorted octahedral molybdenum(V), with the Mo=O bond *trans* to MeCN in $[MoOCl_3(MeCN)_2]$ and *trans* to chloride in $[(MoOCl_2(MeCN))_2(\mu\text{-}Cl)_2]$. In the dimer the MeCN ligands are *anti* to each other as is more commonly found in the literature (Figure 6.15), the structures are in good agreement with similar structures.

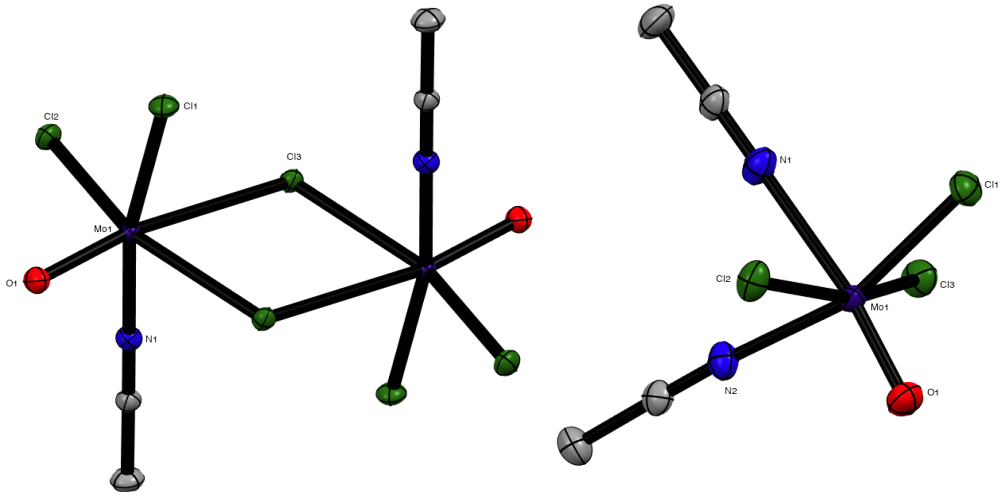

Figure 6.20: Crystal structures of $[(MoOCl_2(MeCN))_2(\mu\text{-}Cl)_2]$ (left) and $[MoOCl_3(MeCN)_2]$ (right) showing the atom numbering scheme. Ellipsoids shown at 50% probability, hydrogen atom for clarity. Note $[MoOCl_3(MeCN)_2]$ exhibits O/Cl disorder which was modelled with split atom sites and refined to occupancies of 0.30:0.70 only the major form is shown.

$[(MoOCl_2(MeCN))_2(\mu\text{-}Cl)_2]$			
Bond Lengths/ Å		**Bond Angles/ °**	
Mo1-Cl1	2.3082(4)	O1-Mo1-Cl1	100.82(4)
Mo1-Cl2	2.3199(3)	O1-Mo1-Cl2	102.70(3)
Mo1-Cl3	2.4142(3)	Cl1-Mo1-Cl3	88.38(1)
Mo1-O1	1.6502(9)	Cl2-Mo1-Cl3	81.19(1)
Mo1-N1	2.151(1)		
$[MoOCl_3(MeCN)_2]$			
Bond Lengths/ Å		**Bond Angles/ °**	
Mo1-Cl1	2.311(1)	Cl1-Mo1-Cl2	91.91(4)
Mo1-Cl2	2.3633(7)	Cl1-Mo1-O1	103.5(1)
Mo1-Cl3	2.3453(7)	Cl1-Mo1-Cl3	87.73(4)
Mo1-O1	1.653(4)	Cl3-Mo1-O1	100.1(1)
Mo1-N1	2.136(2)		
Mo1-N2	2.140(2)		

Table 6.11: Selected bond lengths and angles for $[(MoOCl_2(MeCN))_2(\mu\text{-}Cl)_2]$ and $[MoOCl_3(MeCN)_2]$.

Subsequently, $MoOCl_4$ was reacted with stoichiometric amounts of either 2,2'-bipy or 1,10-phen to compare with $[MoOCl_3(L\text{-}L)]$ complexes isolated above. It was clear that seven-coordinate molybdenum(VI) complexes did not form. In both reactions paramagnetic species were formed and the IR spectra were effectively identical to those of $[MoOCl_3(L\text{-}L)]$ (L-L = 2,2'-bipy or 1,10-phen).

IR Data	$MoOCl_4$ + 2,2'-bipy	$MoOCl_4$ + 1,10-phen
v(Mo=O)	968 cm^{-1}	971 cm^{-1}
v(Mo-Cl)	348 cm^{-1}	338 cm^{-1}
UV (*d-d* transitions)	13,800	13,400
	$[MoOCl_3$(2,2'-bipy)]	**$[MoOCl_3$(1,10-phen)]**
v(Mo=O)	970 cm^{-1}	971cm^{-1}
v(Mo-Cl)	348 cm^{-1}	342 cm^{-1}
UV (*d-d* transitions)	18,800, 13,800	18,700, 13,400

Table 6.12: Comparison of IR stretches obtained from reaction of $MoOCl_3$ or $MoOCl_4$ and 2,2'-bipy or 1,10-phen.

The solid-state UV-vis spectra for $[MoOCl_3$(L-L)] (L-L = 2,2'-bipy or 1,10-phen) shows two *d-d* transitions ($B_2 \rightarrow B_1$; $B_2 \rightarrow E$) and a number of ligand-to-metal charge transfer bands. The corresponding UV-vis spectra from the product isolated from the reaction of $MoOCl_4$ and the diimine also shows the lowest energy *d-d* band and additional LMCT bands; confirming reduction to molybdenum(V). Therefore, it is concluded that the ligands cause reduction of $MoOCl_4$ to $MoOCl_3$, which can then form stable complexes. Both products from $MoOCl_4$ and ligand (2,2'bipy and 1,10-phen) were isolated as green solids, whereas direct reactions between $MoOCl_3$ and ligand produced pink compounds. Both colours (green and pink) have been previously reported and shown to be spectroscopically identical and it was suggested the compounds could be isomers.[46,79,80] This work has shown two different geometric isomers in $[MoOCl_3$(L-L)] complexes (*fac* and *mer* chlorines) revealed by crystallography, so it could be possible this isomerism has caused the difference in colours. However, the colour difference could also stem from minor impurities but the colour difference is well documented so co-crystallisation is less likely.

Similar behaviour is observed when reacting $MoOCl_4$ and $OPPh_3$, where a light blue powder was isolated that exhibited a P=O stretch at 1159 cm^{-1} and a Mo=O stretch at 972 cm^{-1} in the IR spectrum, consistent with the molybdenum(V) species, $[MoOCl_3(OPPh_3)_2]$ (1157 cm^{-1}, 968 cm^{-1}).[47] This was also supported with the diffuse reflectance UV-vis spectrum, which exhibited two *d-d* transitions (22,300, 13,400 cm^{-1}), consistent with reported literature (22,300, 13,400 cm^{-1}), as well as a magnetic moment of 1.71 B.M.[81]

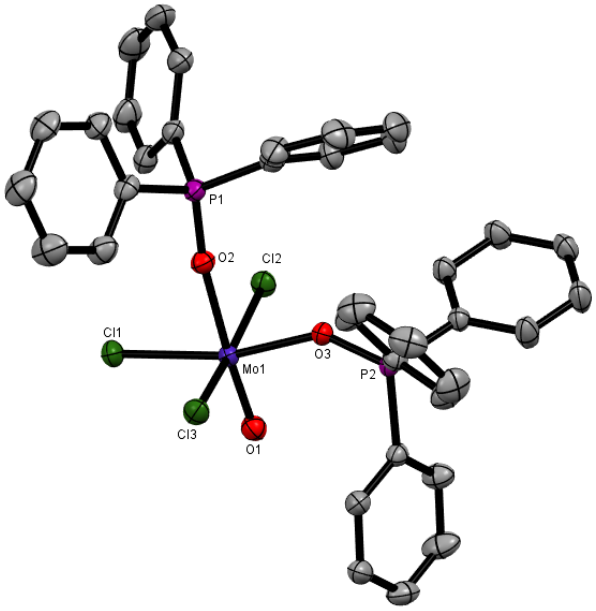

Figure 6.21: Crystal structure of [$MoOCl_3(OPPh_3)_2$] showing the atom numbering scheme. Ellipsoids shown at 50% probability, hydrogen atom for clarity.

[$MoOCl_3(OPPh_3)_2$]			
Bond Lengths/ Å		**Bond Angles/ °**	
Mo1-Cl1	2.3616(8)	Cl1-Mo1-Cl2	91.62(3)
Mo1-Cl2	2.3959(7)	Cl1-Mo1-O1	98.93(7)
Mo1-Cl3	2.3913(8)	Cl1-Mo1-Cl3	90.73.(3)
Mo1-O1	1.672(2)	Cl1-Mo1-O2	84.62(5)
Mo1-O3	2.145(2)		
Mo1-O3	2.063(2)		

Table 6.13: Selected bond lengths and angles for [$MoOCl_3(OPPh_3)_2$].

Blue crystals of [$MoOCl_3(OPPh_3)_2$] were isolated from CH_2Cl_2 solution and the structure was consistent with previous reports.[81,82]

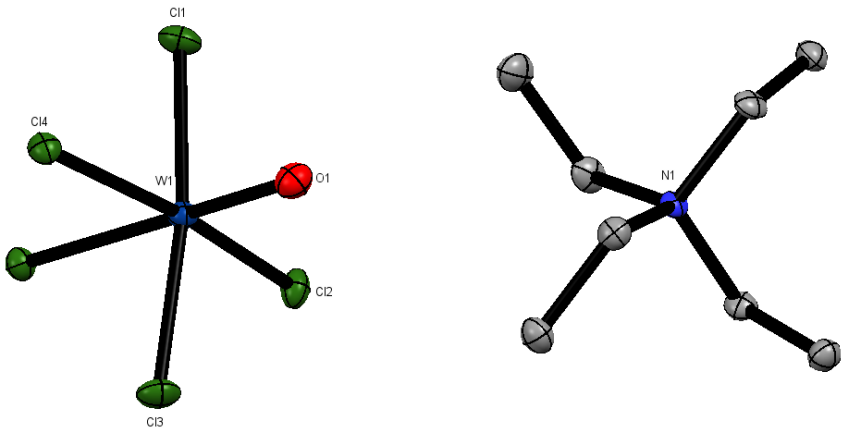

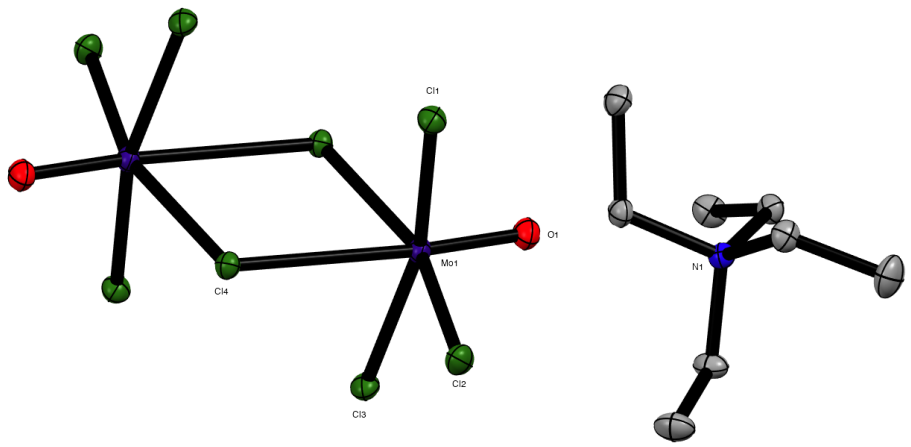

Figure 6.22: Crystal structures of $[Et_4N][WOCl_5]$ (top) and $[Et_4N]_2[(MoOCl_3)_2(\mu\text{-}Cl)_2]$ (bottom) showing the atom numbering scheme. Ellipsoids shown at 50% probability, hydrogen atom for clarity. Please note $[Et_4N][WOCl_5]$ exhibits O/Cl disorder which was modelled with split atom sites and refined to occupancies of 0.11:0.89 only the major form is shown.

$[Et_4N][WOCl_5]$			
Bond Lengths/ Å		**Bond Angles/ °**	
W1-Cl1	2.3266(9)	O1-Mo1-Cl1	94.51(9)
W1-Cl2	2.3054(8)	O1-Mo1-Cl2	95.18(9)
W1-Cl3	2.3145(9)	O1-Mo1-Cl3	94.04(9)
W1-Cl4	2.3439(8)	O1-Mo1-Cl4	93.65(9)
W1-Cl5	2.4848(8)		
W1-O1	1.729(2)		
$[Et_4N]_2[(MoOCl_3)_2(\mu\text{-}Cl)_2]$			
Bond Lengths/ Å		**Bond Angles/ °**	
Mo1-Cl1	2.3710(4)	O1-Mo1-Cl1	98.39(3)
Mo1-Cl2	2.3454(4)	O1-Mo1-Cl2	102.96(3)
Mo1-Cl3	2.3605(4)	O1-Mo1-Cl3	97.60(3)
Mo1-Cl4	2.4159(3)	O1-Mo1-Cl4	98.29(3)
Mo1-O1	1.6563(8)		

Table 6.14: Selected bond lengths and angles for $[Et_4N][WOCl_5]$ and $[EtN_4]_2[(MoOCl_3)(\mu\text{-}Cl)_2(MoOCl_3)]$.

It is clear that $MoOCl_4$ reduces readily upon addition of neutral ligands, producing a range of Mo(V) species, $[MoOCl_3(L\text{-}L)]$, $[MoOCl_3(L)_2]$ or $[(LMoOCl_2)_2(\mu\text{-}Cl)_2]$. A final reaction to attempt to isolate a salt which would be more stable was undertaken. The tungsten(VI) salt $[Et_4N][WOCl_5]$ can be isolated by reacting stoichiometric amounts of $WOCl_4$ and $[Et_4N]Cl$, and therefore the analogous reaction was performed to attempt to form $[Et_4N][MoOCl_5]$. However, the IR spectrum of the green product from $MoOCl_4$ and $[Et_4N]Cl$ is consistent with the formation of the dimeric anion,

$[(MoOCl_3)_2(\mu\text{-}Cl)_2]^{2-}$. It is clear that $MoOCl_4$ reduces readily at ambient conditions and it is highly unlikely that any molybdenum(VI) complexes can be formed.

$[Et_4N][WOCl_5]$ (Figure 6.22) shows tungsten in a distorted octahedral environment as is typical, the structure is very similar to $[C_5H_5NH][WOCl_5]$ described in Chapter 2. The molybdenum(V) dimer (Figure 6.22) also shows a distorted octahedral geometry, the Mo=O bonds are *trans* to the bridging chlorides resulting in asymmetric chloride bridges. The $[(MoOCl_3)_2(\mu\text{-}Cl)_2]^{2-}$ anion is known and has been crystallographically authenticated;[83,84] the new data are in good agreement with the literature report.

6.4 Conclusions

A systematic series of $MoOCl_3$ complexes with a range of neutral soft donor ligands (thio-, seleno- and teluro-ethers) has been developed and comparisons drawn to coordination complexes of $WECl_4$ (E = O or S) discussed in Chapters 2 to 4 and reported literature. Bidentate thio- and seleno-ether complexes, $[MoOCl_3(RE(CH_2)_nER)]$ (E = S or Se; R = Me, ^{i}Pr or Ph, n = 2 or 3) have been isolated and characterised. Monodentate thio-, seleno- and telluro-ether complexes were also isolated which formed chloride bridge dimers in the form $[(MoOCl_2)_2(\mu\text{-}Cl)_2(EMe)_2]$. The telluroether complexes are the first and only with molybdenum(V). Reactions of $MoOCl_3$ and (o-$C_6H_4(E'Me)_2$)] (E' = Se or Te) and $MeTe(CH_2)_3TeMe$ have been spectroscopically characterised but have yet to be have their actual formula confirmed. A single X-ray crystal structure of $[(MoCl(o\text{-}C_6H_4(TeMe)_2)_2)(\mu\text{-}O)(MoOCl_4)]\bullet CH_2Cl_2$ has been obtained, as the only example of a telluroether complex of molybdenum that is not Mo(0) as a partial reduction product. A number of $MoOCl_3$ complexes with nitrogen, phosphine and oxygen donor ligands were also isolated and characterised for comparison.

The stability of the Mo(V) seleno- and telluroether compounds compared to $WECl_4$ complexes (where only $[WSCl_4(SeMe_2)]$ was stable), clearly confirms that $MoOCl_3$ is a softer Lewis acid than $WECl_4$, as expected. The metal oxidation state in the bulk samples was confirmed as molybdenum(V) by both UV-vis spectroscopy and magnetic moment measurements.

The reaction of $MoOCl_4$ with various neutral ligands (N- and O-donors) was also investigated and confirmed that all ligands caused immediate reduction of the molybdenum(VI) to form molybdenum(V) species. IR spectra and UV-vis spectra for the products from the $MoOCl_4$ reactions and their comparative $MoOCl_3$ complexes were effectively identical. Attempts to isolate the anion $[MoOCl_5]^-$ were also unsuccessful, but the known chloride bridged Mo(V) anion, $[(MoOCl_3)(\mu\text{-}Cl))_2]^{2-}$, was identified. Results show $MoOCl_4$ is much less stable compared to $MoOF_4$ and MoO_2Cl_2 as both form relatively stable complexes.[85-87] Most of the products were identified by single crystal X-ray diffraction and compared to related compounds found in literature. Complexes were characterised by IR spectroscopy, UV-Vis spectroscopy, elemental analysis and X-ray crystal structures.

6.5 Experimental

Syntheses were performed by using standard Schlenk and glove-box techniques under a dry N_2 atmosphere. Solvents were dried by distillation from CaH_2 (CH_2Cl_2, MeCN) or Na/benzophenone ketyl (toluene, n-hexane, THF). Ligands (dppe, $OPPh_3$, 2,2'-bipy and 1,10-phen) were obtained from Sigma-Aldrich and dried by heating *in vacuo.* Dichalcogenoethers, $RE(CH_2)_nER$ (*n* = 2 or 3; E = S or Se; R = Me, Ph, ^iPr) and *o*-$C_6H_4(E'Me)_2$ (E' = Se or Te),[88-90] and $TeMe_2$ and $MeTe(CH_2)_3TeMe$ were prepared *via* literature methods.[91-93] Me_2S was purchased from Sigma-Aldrich and Me_2Se, $Me_2P(CH_2)_2PMe_2$ and PMe_3 from Strem and used as received. $MoOCl_3$ was prepared *via* literature methods.[94] For further details regarding the instrumentation see Appendix A.

6.5.1 $MoOCl_3$ Reactions

[$MoOCl_3(THF)_2$]

Following a reported literature method,[53] $MoCl_5$ (1.50 g, 5.5 mmol) was dissolved in CH_2Cl_2 (5 mL) and THF (5 mL) was slowly added. The solution was left to stir for 1h., the green solution was concentrated to ~3 mL *in vacuo* and filtered isolating a green solid and drying *in vacuo.* Yield: 1.77 g, 87%. Required for $C_8H_{16}Cl_3MoO_3 \bullet 0.25C_4H_8O$ (380.53): C: 28.41, H: 4.77 %. Found: C: 28.21, H: 4.45 %. IR spectrum (Nujol, ν / cm^{-1}): 982s Mo=O, 1117s, 833s br C-O, 342s, 315m Mo-Cl. UV/Vis spectrum (diffuse reflectance) ν / cm^{-1}: 32,550, 26,200, 22,000, 13,250. μ_{eff}: 1.71 B.M.

[$MoOCl_3$(2,2'-bipy)]

[$MoOCl_3(THF)_2$] (0.150 g, 0.41 mmol) was suspended in CH_2Cl_2 (3 mL) and a solution of 2,2'-bipy (0.065 g, 0.41 mmol) in CH_2Cl_2 (3 mL) was slowly added and the solution left to stir for 1h. The dark red solution was concentrated to 3 mL *in vacuo,* filtered then the solid dried *in vacuo* isolating a red solid. Yield: 0.087 g, 56%. Required for $C_{10}H_8Cl_3MoN_2O$ (374.48): C: 32.07, H: 2.15, N: 7.48 %. Found: C: 32.07, H: 2.28, N: 7.28 %. IR spectrum (Nujol, ν / cm^{-1}): 970s Mo=O, 365m, 348s, 316m Mo-Cl. UV/Vis spectrum (diffuse reflectance) ν / cm^{-1}: 30,900, 27,000, 25,100, 22,000, 18,800, 13,800.

[$MoOCl_3$(1,10-phen)]

[$MoOCl_3$(1,10-phen)] was prepared similarly to [$MoOCl_3$(2,2'-bipy)] isolated as a pink solid. Yield: 0.110 g, 66 %. Required for $C_{12}H_8Cl_3MoN_2O$ (398.50): C: 36.17, H: 2.02, N: 7.03 %. Found: C: 36.04, H: 1.85, N: 6.90 %. IR spectrum (Nujol, ν / cm^{-1}): 971s Mo=O, 360m, 342s, 309m Mo-Cl. UV/Vis spectrum (diffuse reflectance) ν / cm^{-1}: 31,100, 27,000, 25,800, 23,300, 18,700, 13,400. μ_{eff}: 1.69 B.M.

[$MoOCl_3$(dppe)]

Following reported literature method,[53] [$MoOCl_3(THF)_2$] (0.150 g, 0.41 mmol) was suspended in CH_2Cl_2 (3 mL) and a solution of dppe (0.165 g, 0.41 mmol) in CH_2Cl_2 (3 mL) was slowly added and the solution left to stir for 1h. The dark red solution was concentrated to 3 mL *in vacuo*, filtered then the solid dried *in vacuo* isolating a red solid. Yield: 0.206 g, 81 %. Required for $C_{26}H_{24}Cl_3MoOP_2$ (616.71): C: 50.64, H: 3.92 %. Found: C: 50.78, H: 3.77 %. IR spectrum (Nujol, ν / cm^{-1}): 954s Mo=O, 337s, 324m Mo-Cl. UV/Vis spectrum (diffuse reflectance) ν / cm^{-1}: 37,300, 31,000, 27,200, 26,200, 20,700, 19,400, 15,100. μ_{eff}: 1.70 B.M.

[$MoOCl_3(PMe_3)_2$]

[$MoOCl_3(THF)_2$] (0.150 g, 0.41 mmol) was suspended in CH_2Cl_2 (3 mL) and a solution of PMe_3 (0.063 g, 0.82 mmol) in CH_2Cl_2 (3 mL) was slowly added and the dark green solution left to stir for 1h. The red solution was concentrated to 3 mL *in vacuo* and filtered then the solid dried *in vacuo* isolating a red solid. Yield: 0.047 g, 31 %. Required for $C_6H_{18}Cl_3MoOP_2$ (370.45): C: 19.45, H: 4.90 %. Found: C: 19.28, H: 4.74 %. IR spectrum (Nujol, ν / cm^{-1}): 957s Mo=O, 352m, 324s, 305m Mo-Cl. UV/Vis spectrum (diffuse reflectance) ν / cm^{-1}: 29,400, 27,000sh, 22,500, 19,500, 14,200.

[$MoOCl_3$(dmpe)]

[$MoOCl_3$(dmpe)] was prepared similarly to [$MoOCl_3$(dppe)], isolated as a yellow solid. Yield: 0.131 g, 81 %. Required for $C_6H_{16}Cl_3MoOP_2$ (368.44): C: 19.56, H: 2.38 %. Found: C: 19.83, H: 4.26 %. IR spectrum (Nujol, ν / cm^{-1}): 951s Mo=O, 362m, 325s, 306s Mo-Cl. UV/Vis spectrum (diffuse reflectance) ν / cm^{-1}: 29,600, 27,000sh, 21,600, 20,000, 15,500. μ_{eff}: 1.72 B.M.

[$MoOCl_3(MeS(CH_2)_3SMe)$]

[$MoOCl_3(THF)_2$] (0.150 g, 0.41 mmol) was suspended in CH_2Cl_2 (3 mL) and a solution of $MeS(CH_2)_3SMe$ (0.056 g, 0.41 mmol) in CH_2Cl_2 (2 mL) was slowly added and the green solution left to stir for 1h. The brown solution was concentrated to 3 mL *in vacuo* and filtered then the solid dried *in vacuo* isolating a green solid. Yield: 0.070 g, 40 %. Required for $C_5H_{12}Cl_3MoOS_2$ (354.58): C: 16.94, H: 3.41 %. Found: C: 17.02, H: 3.39 %. IR spectrum (Nujol, ν / cm^{-1}): 955s Mo=O, 348s, 327s, 306m Mo-Cl. UV/Vis spectrum (diffuse reflectance) ν / cm^{-1}: 27,400, 26,000, 21,700, 20,000, 13,700. μ_{eff}: 1.71 B.M.

[$MoOCl_3(^iPrS(CH_2)_2S^iPr)$]

[$MoOCl_3(^iPrS(CH_2)_2S^iPr)$] was prepared similarly to [$MoOCl_3(MeS(CH_2)_3SMe)$] isolated as a green solid. Yield: 0.101 g, 62 %. Required for $C_8H_{18}Cl_3MoOS_2$ (396.66): C: 24.22, H: 4.57 %. Found: C:

24.45, H: 4.15 %. IR spectrum (Nujol, *v* / cm^{-1}): 979s Mo=O, 349s, 312m Mo-Cl. UV/Vis spectrum (diffuse reflectance) ν / cm^{-1}: 29,000sh, 27,000, 23,000sh, 21,500sh, 13,600. μ_{eff}: 1.69 B.M.

[$MoOCl_3(PhS(CH_2)_2SPh)$]

$MoOCl_3$ (0.150 g, 0.69 mmol) was suspended in CH_2Cl_2 (3 mL) and a solution of $PhS(CH_2)_2SPh$ (0.170 g, 0.69 mmol) in CH_2Cl_2 (2 mL) was slowly added and the green solution left to stir for 1h. The brown solution was concentrated to 3 mL *in vacuo* and filtered, then the solid dried *in vacuo* isolating a brown solid. Yield: 0.244 g, 76 %. Required for $C_{14}H_{14}Cl_3MoOS_2$ (464.69): C: 36.19, H: 3.04 %. Found: C: 35.97, H: 3.18 %. IR spectrum (Nujol, *v* / cm^{-1}): 966s Mo=O, 354s, 319m Mo-Cl. UV/Vis spectrum (diffuse reflectance) ν / cm^{-1}: 26,900, 22,600, 21,300, 13,000. μ_{eff}: 1.71 B.M.

[$(MoOCl_2)(\mu\text{-}Cl)_2(SMe_2)_2$]

$MoOCl_3$ (0.150 g, 0.69 mmol) was suspended in CH_2Cl_2 (3 mL) and a solution of SMe_2 (0.085 g, 1.38 mmol) in CH_2Cl_2 (2 mL) was slowly added and the green solution left to stir for 1h. The clear green solution was concentrated to 3 mL *in vacuo* and layered with hexane (3 mL) then green crystals were isolated *via* filtration and dried *in vacuo.* Yield: 0.73 g, 38 %. Required for $C_4H_{12}Cl_6Mo_2O_2S_2$ (560.86): C: 8.57, H: 2.16 %. Found: C: 8.98, H: 2.37 %. IR spectrum (Nujol, *v* / cm^{-1}): 969s Mo=O, 367sh, 351s, 312m Mo-Cl. UV/Vis spectrum (diffuse reflectance) ν / cm^{-1}: 21,600, 19,700, 13,000. μ_{eff}: 1.72 B.M.

[$(MoOCl_2)(\mu\text{-}Cl)_2(SeMe_2)_2$]

$MoOCl_3$ (0.150 g, 0.69 mmol) was suspended in CH_2Cl_2 (3 mL) and a solution of SMe_2 (0.150 g, 1.38 mmol) in CH_2Cl_2 (2 mL) was slowly added and the green solution left to stir for 1h. The red solution was concentrated to 3 mL *in vacuo* and layered with hexane (3 mL) then dark crystals were isolated *via* filtration, and dried *in vacuo.* Yield: 0.154 g, 68 %. Required for $C_4H_{12}Cl_6Mo_2O_2S_2$ (654.65): C: 7.34, H: 1.85 %. Found: C: 7.43, H: 1.93 %. IR spectrum (Nujol, *v* / cm^{-1}): 984s Mo=O, 368s, 356s, 319m Mo-Cl. UV/Vis spectrum (diffuse reflectance) ν / cm^{-1}: 26,500, 22,300, 20,700, 14,100. μ_{eff}: 1.68 B.M.

[$MoOCl_3(MeSe(CH_2)_2SeMe)$]

$[MoOCl_3(THF)_2]$ (0.150 g, 0.41 mmol) was suspended in CH_2Cl_2 (3 mL) and a solution of $MeSe(CH_2)_3SeMe$ (0.089 g, 0.41 mmol) in CH_2Cl_2 (2 mL) was slowly added and the green solution left to stir for 1h. The brown solution was concentrated to 3 mL *in vacuo* and filtered, then the solid dried *in vacuo* isolating a beige solid. Yield: 0.160 g, 90 %. Required for $C_4H_{10}Cl_3MoOSe_2$ (434.34): C: 11.06, H: 2.32 %. Found: C: 11.60, H: 2.50 %. IR spectrum (Nujol, *v* / cm^{-1}): 956s Mo=O, 342s,

310m Mo-Cl. UV/Vis spectrum (diffuse reflectance) ν / cm^{-1}: 27,600, 21,000, 19,300, 14,000. μ_{eff}: 1.71 B.M.

[$MoOCl_3(MeSe(CH_2)_3SeMe)$]•$CH_2Cl_2$

$MoOCl_3$ (0.150 g, 0.69 mmol) was suspended in CH_2Cl_2 (3 mL) and a solution of $MeSe(CH_2)_3SeMe$ (0.158 g, 0.69 mmol) in CH_2Cl_2 (2 mL) was slowly added and the red/brown solution left to stir for 1h. The brown solution was concentrated to 3 mL *in vacuo* and filtered and the solid dried *in vacuo* isolating a brown solid. Yield: 0.178 g, 58 %. Required for $C_5H_{12}Cl_3MoOSe_2$•CH_2Cl_2 (533.30): C: 13.51, H: 2.65 %. Found: C:13.96, H: 2.95 %. IR spectrum (Nujol *v* / cm^{-1}): 954s Mo=O, 346s br, 285m Mo-Cl. UV/Vis spectrum (diffuse reflectance) ν / cm^{-1}: 21,200, 19,500, 13,900. μ_{eff}: 1.70 B.M.

Attempted synthesis of [$MoOCl_3(o\text{-}C_6H_4(SeMe)_2)$] – see discussion (Section 6.3.1)

$MoOCl_3$ (0.150 g, 0.69 mmol) was suspended in dichloromethane (3 mL) and a solution of *o*-$C_6H_4(SeMe)_2$ (0.226 g, 0.69 mmol) in dichloromethane (2 mL) was slowly added and the dark red/brown solution left to stir for 1h. The brown solution was concentrated to 3 mL *in vacuo* producing a brown precipitate which was wash with OEt_2 (3 x 5 mL), then the solid dried *in vacuo* isolating a pink/brown solid. Required for $C_8H_{10}Cl_6Mo_2O_2Se_2$ (700.68): C: 13.71, H: 1.44 %. Found: C: 13.43, H: 1.53 %. IR spectrum (Nujol, *v* / cm^{-1}): 999s br Mo=O, 351w, 302s, 292sh, Mo-Cl. UV/Vis spectrum (diffuse reflectance) ν / cm^{-1}: 29,500sh, 24,900, 20,900, 14,300. μ_{eff}: 1.69 B.M.

[$(MoOCl_2)(\mu\text{-}Cl)_2(TeMe_2)_2$]

$MoOCl_3$ (0.150 g, 0.69 mmol) was suspended in toluene (3 mL) and a solution of $TeMe_2$ (0.217 g, 1.38 mmol) in toluene (2 mL) was slowly added and the purple solution left to stir for 1h. The deep purple solution was concentrated to 3 mL *in vacuo* and filtered, then the solid dried *in vacuo* isolating a dark brown solid. Yield: 0.203 g, 78 %. Required for $C_4H_{12}Cl_6Mo_2O_2Te_2$ (751.93): C: 6.39, H: 1.61%. Found: C: 6.76, H: 2.06 %. IR spectrum (Nujol, *v* / cm^{-1}): 985s br Mo=O, 327, 302s br, 256m Mo-Cl. UV/Vis spectrum (diffuse reflectance) ν / cm^{-1}: 34,500, 29,700sh, 26,100, 20,900, 19,400, 14,300. μ_{eff}: 1.68 B.M.

Attempted synthesis of [$MoOCl_3(MeTe(CH_2)_3TeMe)$] - see discussion (Section 6.3.1)

$MoOCl_3$ (0.150 g, 0.69 mmol) was suspended in dichloromethane (3 mL) and a solution of $MeTe(CH_2)_3TeMe$ (0.217 g, 0.69 mmol) in dichloromethane (2 mL) was slowly added and the brown solution left to stir for 1h. The brown solution was concentrated to 3 mL *in vacuo* producing a brown precipitate which was wash with OEt_2 (3 x 5 mL), then the solid dried *in vacuo* isolating a dark brown solid. Required for $C_5H_{12}Cl_6Mo_2O_2Te_2$ (763.95): C: 7.86, H: 1.58 %. Found: C: 7.20, H: 1.38 %. IR

spectrum (Nujol, *ν* / cm^{-1}): 988m Mo=O, 303s, 292m Mo-Cl. UV/Vis spectrum (diffuse reflectance) ν / cm^{-1}: 25,300, 20,800, 18,900. μ_{eff}: 1.68 B.M.

Attempted synthesis of [$MoOCl_3$(o-C_6H_4(TeMe)$_2$)] - see discussion (Section 6.3.1)

$MoOCl_3$ (0.150 g, 0.69 mmol) was suspended in dichloromethane (3 mL) and a solution of *o*-$C_6H_4(TeMe)_2$ (0.249 g, 0.69 mmol) in dichloromethane (2 mL) was slowly added and the dark brown solution left to stir for 1h. The brown solution was concentrated to 3 mL *in vacuo* producing a brown precipitate which was wash with OEt_2 (3 x 5 mL), then the solid dried *in vacuo* isolating a dark brown solid. Required for $C_8H_{10}Cl_6Mo_2O_2Te_2$ (797.96): C: 12.04, H: 1.26%. Found: C: 12.27, H: 1.43 %. IR spectrum (Nujol, *ν* / cm^{-1}): 992s br Mo=O, 343m, 328m, 302s Mo-Cl. UV/Vis spectrum (diffuse reflectance) ν / cm^{-1}: 32,500, 25,000sh, 21,000, 19,200, 14,500. μ_{eff}: 1.70 B.M.

6.5.2 $MoOCl_4$ Reactions

Reaction of $MoOCl_4$ and MeCN

$MoOCl_4$ (0.150 g, 0.59 mmol) was suspended in CH_2Cl_2 (5 mL) and MeCN (1 mL) was added slowly turning the red solution brown. The solution was left to stir for 1 h. then brought to dryness *in vacuo* isolated a green solid. IR spectrum (Nujol, *ν* / cm^{-1}): 987s Mo=O, 371m, 348s, 320m Mo-Cl. μ_{eff}: 1.71 B.M.

Reaction of $MoOCl_4$ and 2,2'-bipy

$MoOCl_4$ (0.150 g, 0.59 mmol) was suspended in CH_2Cl_2 (3 mL) and a solution of 2,2'-bipy (0.092 g, 0.59 mmol) in CH_2Cl_2 (3 mL) was slowly added and the solution left to stir for 1h. The dark green solution was concentrated to 3 mL *in vacuo* and filtered, then the solid dried *in vacuo* isolating a green solid. IR spectrum (Nujol, *ν* / cm^{-1}): 968s Mo=O, 364m, 348s, 315m Mo-Cl. UV/Vis spectrum (diffuse reflectance) ν / cm^{-1}: 31,000, 25,000, 13,800. μ_{eff}: 1.71 B.M.

[$MoOCl_3$(1,10-phen)]•0.5CH_2Cl_2

$MoOCl_4$ (0.150 g, 0.59 mmol) was suspended in CH_2Cl_2 (3 mL) and a solution of 1,10-phen (0.106 g, 0.59 mmol) in CH_2Cl_2 (3 mL) was slowly added and the solution left to stir for 1h. The dark green solution was concentrated to 3 mL *in vacuo* and filtered, then the solid dried *in vacuo* isolating a green solid. Yield: 0.87 g, 37 %. Required for $C_{12}H_8Cl_3MoN_2O$•0.5CH_2Cl_2 (440.95): C: 34.05, H: .06, N: 6.35. Found: C: 33.95, H: 1.77, N: 6.31. IR spectrum (Nujol, *ν* / cm^{-1}): 971s Mo=O, 360m, 338s, 309m Mo-Cl. UV/Vis spectrum (diffuse reflectance) ν / cm^{-1}: 30,500, 27,500sh, 13,400.

Reaction of $MoOCl_4$ and $OPPh_3$

$MoOCl_4$ (0.150 g, 0.59 mmol) was suspended in CH_2Cl_2 (3 mL) and a solution of $OPPh_3$ (0.328 g, 1.18 mmol) in CH_2Cl_2 (3 mL) was slowly added and the solution left to stir for 1h. The purple green solution was concentrated to 3 mL *in vacuo* and filtered, and the solid then dried *in vacuo* isolating a blue solid. IR spectrum (Nujol, ν / cm^{-1}): 1159s P=O, 972s Mo=O, 320s Mo-Cl. UV/Vis spectrum (diffuse reflectance) ν / cm^{-1}: 33,000, 28,200, 22,300, 13,400. μ_{eff}: 1.71 B.M.

Reaction of $MoOCl_4$ and Et_4NCl

$MoOCl_4$ (0.150 g, 0.59 mmol) was suspended in CH_2Cl_2 (3 mL) and a solution of $[Et_4N]Cl$ (0.097 g, 0.59 mmol) in CH_2Cl_2 (3 mL) was slowly added and the solution left to stir for 1h. The brown solution was concentrated to 3 mL *in vacuo* and filtered, and the solid then dried *in vacuo* isolating a brown solid. IR spectrum (Nujol, ν / cm^{-1}): 998s Mo=O, 383m, 352s, 334m Mo-Cl.

$[Et_4N][WOCl_5]$

$WOCl_4$ (0.150 g, 0.44 mmol) was suspended in CH_2Cl_2 (3 mL) and a solution of $[Et_4N]Cl$ (0.072 g, 0.44 mmol) in CH_2Cl_2 (2 mL) was slowly added and the orange solution left to stir for 1h. The orange solution was concentrated to 3 mL *in vacuo* and filtered then dried *in vacuo* isolating an orange solid. Yield: 0.117 g, 42%. Required for $C_8H_{20}Cl_5NOW$ (507.35): C: 18.94, H: 3.97, N: 2.76 %. Found: C: 17.19, H: 3.80, N: 2.44 %. IR spectrum (Nujol/ cm^{-1}): 955s W=O, 355sh, 339s, 345sh W-Cl. ^1H NMR (CD_2Cl_2): δ = 3.25 (q, J_{HH} 7.34 Hz, [2H], CH_2), 1.36 (tt, J_{HH} 7.24 Hz, [3H], CH_3).

6.5.3 Crystallography Tables

Compound	$[MoOCl_3(MeCN)_2]$	$[(MoOCl_2(MeCN))_2(\mu\text{-}Cl)_2]$	$[Et_4N]_2[(MoOCl_3)_2(\mu\text{-}Cl)_2]$	$[Et_4N][WOCl_5]$
Formula	$C_4H_6Cl_3MoN_2O$	$C_4H_6Cl_6Mo_2N_2O_2$	$C_8H_{40}C_{16}Mo_2N_2O_2$	$C_8H_{20}Cl_5NOW$
M	300.40	518.69	767.98	507.35
Crystal system	Monoclinic	Monoclinic	Monoclinic	Triclinic
Space group (no)	$P2_1/c$ (14)	$P2_1/c$ (14)	$P2_1/c$ (14)	$P\bar{1}$ (2)
a /Å	5.79300(10)	6.7943(1)	9.8073(2)	7.00730(10)
b /Å	13.3033(3)	8.9915(1)	11.2086(2)	14.5559(3)
c /Å	12.7461(3)	11.7775(1)	14.2779(3)	15.6183(3)
α /°	90	90	90	80.175(2)
β /°	90.889(2)	95.4310(1)	109.989(2)	89.868(2)
γ /°	90	90	90	89.9690(10)
U /Å^3	975.20(4)	716.269(2)	1474.96(5)	1569.66(5)
Z	4	2	2	4
μ(Mo-K$_\alpha$) /mm^{-1}	2.115	2.405	1.592	8.192
F(000)	580.0	492.0	772.0	968.0
Total number reflns	31937	22409	47926	33845
R_{int}	0.0225	0.0178	0.0256	0.0478
Unique reflns	3207	2372	4960	9585
No. of params, restraints	130/10	74/0	140/0	331/15
GOF	1.056	1.287	1.045	1.057
R_1, wR_2 [I > 2σ(I)][b]	0.0197, 0.0451	0.0138, 0.0317	0.0163, 0.0376	0.0299, 0.0776
R_1, wR_2 (all data)[b]	0.0241, 0.0466	0.0142, 0.0318	0.0189, 0.0385	0.0347, 0.0850

Table 6.15: X-ray crystallography table. a: common data: wavelength (Mo-K$_\alpha$) = 0.71073 Å; θ(max) = 27.5°; [b] $R_1 = \Sigma||Fo|-|Fc||/\Sigma|Fo|$; $wR_2=[\Sigma w(Fo^2-Fc^2)^2/\Sigma wFo^4]^{1/2}$

Compound	$[MoOCl_3(THF)_2]$	$[MoOCl_3(OPPh_3)_2]$	$[MoOCl_3(2,2'\text{-bipy})]$	$[MoOCl_3(1,10\text{-phen})]$
Formula	$C_8H_{16}Cl_3MoO_3$	$C_{36}H_{30}Cl_3MoO_3P_2$	$C_{10}H_8Cl_3MoN_2O$	$C_{12}H_8Cl_3MoN_2O$
M	362.50	774.83	374.47	398.49
Crystal system	Orthorhombic	Monoclinic	Monoclinic	Monoclinic
Space group (no)	$P2_12_12_1$ (19)	$P2_1/c$ (14)	Ia (9)	$P2_1/c$ (14)
a /Å	7.7693(1)	18.7734(1)	17.9139(5)	7.8218(2)
b /Å	12.1985(1)	16.7552(1)	12.4890(3)	17.8021(3)
c /Å	13.6748(1)	21.9336(1)	18.1127(5)	10.0811(2)
α /°	90	90	90	90
β /°	90	96.3960(1)	107.314(3)	106.197(2)
γ /°	90	90	90	90
U /Å^3	1296.01(2)	6856.32(6)	3868.68(19)	1348.02(5)
Z	4	8	12	4
μ(Mo-K_α) /mm^{-1}	1.615	0.745	1.621	1.557
F(000)	724.0	3144.0	2196.0	780.0
Total number reflns	23817	148617	40829	48679
R_{int}	0.0281	0.0470	0.0493	0.0522
Unique reflns	3933	20954	11794	4578
No. of params, restraints	145/0	839/15	558/110	182/15
GOF	1.074	1.183	1.066	1.068
R_1, wR_2 [I > 2σ(I)][b]	0.0174, 0.0408	0.0562, 0.1330	0.0430, 0.0967	0.0337, 0.0824
R_1, wR_2 (all data)[b]	0.0177, 0.0409	0.0664, 0.1401	0.052, 0.1048	0.0415, 0.0861

Table 6.15: Continued.

Compound	$[MoOCl_3(dmpe)]$	$[MoOCl_3(dppe)]\bullet 0.5CH_2Cl_2$	$[MoOCl_3(PMe_3)_2]$	$[(MoOCl)(dmpe)_2(\mu\text{-}O)(MoOCl_4)]$
Formula	$C_6H_{16}Cl_3MoOP_2$	$C_{26.5}Cl_4H_{25}MoOP_2$	$C_6H_{18}Cl_3MoOP_2$	$C_{12}H_{32}Cl_5Mo_2O_2P_4$
M	368.42	659.14	370.43	701.38
Crystal system	Monoclinic	Triclinic	Monoclinic	Orthorhombic
Space group (no)	$P2_1/n$ (14)	$P\bar{1}$ (2)	$P2_1/n$ (14)	$Cmc2_1$ (36)
a /Å	7.3716(1)	11.3059(2)	6.4676(1)	14.8497(1)
b /Å	29.8674(6)	14.3559(3)	12.6620(3)	12.54652(1)
c /Å	12.4489(2)	18.9775(4)	17.6653(4)	13.80599(1)
α /°	90	103.785(2)	90	90
β /°	93.989(2)	95.6440(1)	92.468(2)	90
γ /°	90	110.163(2)	90	90
U /Å^3	2734.24(8)	2752.54(1)	1445.32(5)	2572.22(4)
Z	8	4	4	4
μ(Mo-K$_\alpha$) /mm^{-1}	1.745	1.591	1.651	1.621
F(000)	1464.0	1328.0	740.0	2196.0
Total number reflns	24936	76598	31349	48483
R_{int}	0.0532	0.0401	0.0569	0.0221
Unique reflns	8018	17392	4654	4447
No. of params, restraints	253/15	632/25	170/39	128/1
GOF	1.035	1.025	1.037	1.122
R_1, wR_2 [$I > 2\sigma(I)$][b]	0.0399, 0.1024	0.0465, 0.1164	0.0458, 0.1120	0.0095, 0.0248
R_1, wR_2 (all data)[b]	0.0467, 0.1066	0.0568, 0.1221	0.0592, 0.1218	0.0103, 0.0256

Table 6.15: Continued.

Compound	$[MoOCl_3(MeS(CH_2)_3SMe)]$	$[MoOCl_3(^iPrS(CH_2)_2S^iPr)]$	$[MoOCl_3(PhS(CH_2)_2SPh)]$	$[(MoOCl_2(SMe_2))_2(\mu\text{-}Cl)_2]$
Formula	$C_5H_{12}Cl_3MoOS_2$	$C_8H_{18}Cl_3MoOS_2$	$C_{14}H_{14}Cl_3MoOS_2$	$C_4H_{12}Cl_3Mo_2O_2S_2$
M	354.56	396.63	464.66	560.84
Crystal system	Orthorhombic	Orthorhombic	Monoclinic	Monoclinic
Space group (no)	Pnma (62)	Pbca (62)	$P2_1/c$ (14)	$P2_1/c$ (14)
a /Å	12.2610(2)	12.4629(2)	19.6139(2)	7.81110(10)
b /Å	12.7705(2)	13.7536(2)	6.80640(10)	9.50630(10)
c /Å	7.6085(1)	17.5032(6)	12.9677(2)	11.2487(2)
α /°	90	90	90	90
β /°	90	90	96.1600(1)	105.1720(1)
γ /°	90	90	90	90
U /Å^3	1191.33(3)	3000.00(1)	1721.19(4)	806.15(2)
Z	4	8	4	2
μ(Mo-K$_\alpha$) /mm^{-1}	2.080	1.756	1.464	2.791
F(000)	700.0	1592.0	924.0	540.0
Total number reflns	18361	24043	64024	21532
R_{int}	0.0365	0.0587	0.0524	0.0175
Unique reflns	1948	4429	5833	2693
No. of params, restraints	62/0	140/0	217/2	75/0
GOF	1.105	1.072	0.795	1.208
R_1, wR_2 [$I > 2\sigma(I)$][b]	0.0399, 0.1024	0.0461, 0.1003	0.0542, 0.1252	0.0119 0.0276
R_1, wR_2 (all data)[b]	0.0184, 0.0428	0.0600, 0.1075	0.0580, 0.1271	0.0122, 0.0277

Table 6.15: Continued.

Compound	$[(MoOCl_2(SeMe_2))_2(\mu\text{-}Cl)_2]$	$[MoOCl_3(MeSe(CH_2)_2SeMe)]$	$[MoOCl_3(MeSe(CH_2)_3SeMe)]$	$[(MoOCl(o\text{-}C_6H_4(TeMe)_2)_2)(MoOCl_4)]\bullet CH_2Cl_2$
Formula	$C_4H_{12}Cl_3Mo_2O_2Se_2$	$C_4H_{10}Cl_3MoOSe_2$	$C_5H_{12}Cl_3MoOSe_2$	$C_{17}H_{22}Cl_7Mo_2O_2Te_4$
M	654.64	434.33	448.36	1208.77
Crystal system	Monoclinic	Monoclinic	Monoclinic	Monoclinic
Space group (no)	$P2_1/c$ (14)	$P2_1/n$ (14)	Pn (7)	$P2_1/n$ (14)
a /Å	7.8374(2)	7.45509(5)	6.5580(0)	13.4608(2)
b /Å	9.6744(2)	12.18741(7)	7.7672(0)	16.6232(2)
c /Å	11.2666(3)	12.5333(8)	12.1025(2)	14.2143(2)
α /°	90	90	90	90
β /°	105.647(3)	96.6596(6)	94.9310(1)	93.5460(1)
γ /°	90	90	90	90
U /Å^3	822.60(4)	1131.074(1)	614.187(2)	3174.53(8)
Z	2	4	2	4
μ(Mo-K$_\alpha$) /mm^{-1}	6.907	8.254	7.604	4.997
F(000)	612.0	812.0	422.0	2204.0
Total number reflns	11835	36105	15476	55806
R_{int}	0.0261	0.0585	0.0339	0.0534
Unique reflns	2616	3593	3630	9941
No. of params, restraints	75/0	102/0	138/2	320/23
GOF	1.035	1.162	1.049	1.218
R_1, wR_2 [I > 2σ(I)][b]	0.0167, 0.0348	0.0198, 0.0462	0.0209, 0.0531	0.0447, 0.0982
R_1, wR_2 (all data)[b]	0.0194, 0.0354	0.0209, 1.0466	0.0212, 0.0533	0.0479, 0.0992

Table 6.15: Continued.

Compound	(Ligand) → Mo(4d)	π-π* (rings)	π(Cl) → Mo(4d)	d-d Transitions ($B_2 \rightarrow B_1$, $B_2 \rightarrow E$)
$MoOCl_4$ +(2,2'-bipy)		31,056	25,000	13,812,
$MoOCl_4$ + 1,10-phen		30,488	27,475sh	13,404
$MoOCl_3(THF)_2$	32,500sh		25,300	19,600, 13,200
$MoOCl_3$(2,2'-bipy)	21,000	31,000	25,000	18,800, 13,800
$MoOCl_3$(1,10-phen)	23,300sh	30,700	26,300, 27,800	18,700, 13,400
$MoOCl_3(MeS(CH_2)_3SMe)$	21,700		26,000, 27,400	20,000, 13,700
$MoOCl_3({}^{i}PrS(CH_2)_2S{}^{i}Pr)$	23,000sh		27,700, 30,400sh	21,500sh, 13,600
$MoOCl_3(SMe_2)$	22,300		27,000	19,600, 13,800
$MoOCl_3(SeMe_2)$	22,300		26,500	20,700, 14,100
$MoOCl_3(PhS(CH_2)_2SPh)$	22,600		26,600, 27,000	21,300, 13,000
$MoOCl_3(MeSe(CH_2)_2SeMe)$	21,500		25,800	19,300, 14,600
$MoOCl_3(MeSe(CH_2)_3SeMe)$	21,400		26,000sh	19,500, 14,200
$MoOCl_3(o\text{-}C_6H_4(SeMe_2)_2$	20,900		24,900, 29,500sh	19,800sh, 14,300
$MoOCl_3(TeMe_2)$	21,000		27,150sh, 26,100	19,500, 14,400
$MoOCl_3(MeTe(CH_2)_3TeMe)$	20,600		25,300	18,600
$MoOCl_3(o\text{-}C_6H_4(TeMe_2)_2$	21,000	32,500sh	~25,000sh	19,200, 14,500
$MoOCl_3$(dppe)	20,100	32,000	27,200, 26,200	19,400, 15,100
$MoOCl_3(PMe_3)_2$	22,300		29,300, 27,000sh	19,600sh, 14,200
$MoOCl_3$(dmpe)	21,600		29,600, 26,500	20,500sh, 15,500
$MoOCl_3$+ $OPPh_3$		32,900	28,200	21,900, 13,500

Table 6.16: Showing the d-d and LMCT bands and their likely assignments for complexes in this work.

6.6 References

(1) Benjamin, S. L.; Levason, W.; Reid, G. *Chem. Soc. Rev.,* **2013,** *42*, 1460-99
(2) Levason, W.; Monzittu, F. M.; Reid, G.; Zhang, W. *Chem. Commun.,* **2018,** *54*, 11681-84
(3) El-Kurdi, S.; Al-Terkawi, A.-A.; Schmidt, B. M.; Dimitrov, A.; Seppelt, K. *Chem. Eur. J.,* **2010,** *16*, 595-99
(4) Turnbull, D.; Kostiuk, N.; Wetmore, S. D.; Gerken, M. *J. Fluorine. Chem.,* **2018,** *215*, 1-9
(5) Arnaudet, L.; Bougon, R.; Ban, B.; Lance, M.; Navaza, A.; Nierlich, M.; Vigner, J. *J. Fluorine. Chem.,* **1994,** *67*, 17-25
(6) Arnaudet, L.; Bougon, R.; Buu, B.; Lance, M.; Nierlich, M.; Thuéry, P.; Vigner, J. *J. Fluorine. Chem.,* **1995,** *71*, 123-29
(7) Levason, W.; Reid, G.; Zhang, W. *J. Fluorine. Chem.,* **2016,** *184*, 50-57
(8) Emsley, J. W.; Levason, W.; Reid, G.; Zhang, W.; De Luca, G. *J. Fluorine. Chem.,* **2017,** *197*, 74-79
(9) Davis, M. F.; Levason, W.; Ratnani, R.; Reid, G.; Rose, T.; Webster, M. *Eur. J. Inorg. Chem.,* **2007**, 306-13
(10) Arnaudet, L.; Bougon, R.; Ban, B.; Charpin, P.; Isabey, J.; Lance, M.; Nierlich, M.; Vigner, J. *Can. J. Chem.,* **1990,** *68*, 507-12
(11) Marchetti, F.; Pampaloni, G.; Zacchini, S. *Inorg. Chem.,* **2008,** *47*, 365-72
(12) Marchetti, F.; Pampaloni, G.; Zacchini, S. *Dalton Trans.,* **2009**, 6759-72
(13) Marchetti, F.; Pampaloni, G. *Inorg. Chim. Acta,* **2011,** *376*, 123-28
(14) Ignatov, M. E.; Grebeshkov, D. B.; Il'in, E. G. *Zh. Neorg. Khim.,* **1983,** *28*, 617-20
(15) Marchetti, F.; Pampaloni, G.; Zacchini, S. *J. Fluorine. Chem.,* **2010,** *131*, 21-28
(16) Fairbrother, F.; Grundy, K. H.; Thompson, A. *J. Less Common Met.,* **1966,** *10*, 38-41
(17) Buslayev, Y. A.; Ilyin, E. G.; Ignatov, M. E.; Butorina, L. S.; Mastryukova, T. A. *J. Fluorine. Chem.,* **1978,** *12*, 387-95
(18) Haiges, R.; Deokar, P.; Christe, K. O. *Z. anorg. allg. Chem.,* **2014,** *640*, 1568-75
(19) Levason, W.; Light, M. E.; Reid, G.; Zhang, W. *Dalton Trans.,* **2014,** *43*, 9557-66
(20) Levason, W.; Reid, G.; Zhang, W. *J. Fluorine. Chem.,* **2015,** *172*, 62-67
(21) Rahman, M. M.; Smith, M. D.; Amaya, J. A.; Makris, T. M.; Peryshkov, D. V. *Inorg. Chem.,* **2017,** *56*, 11798-803
(22) Marchetti, F.; Pampaloni, G.; Zacchini, S. *Eur. J. Inorg. Chem.,* **2008**, 453-62
(23) Stumpf, K.; Blachnik, R.; Roth, G.; Kastner, G. *Z. Kristallogr.,* **2000,** *215*, 589-90
(24) Brown, D.; Hill, J.; Rickard, C. E. F. *J. Less Common Met.,* **1970,** *20*, 57-65
(25) Benjamin, S. L.; Chang, Y. P.; Hector, A. L.; Jura, M.; Levason, W.; Reid, G.; Stenning, G. *Dalton Trans.,* **2016,** *45*, 8192-200
(26) Cotton, F. A.; Duraj, S. A.; Roth, W. J. *Inorg. Chem.,* **1984,** *23*, 3592-96
(27) Boyd, P. D. W.; Nielson, A. J.; Rickard, C. E. F. *J. Chem. Soc., Dalton Trans.,* **1987**, 307-14
(28) Cotton, F. A.; Roth, W. J. *Inorg. Chem.,* **1984,** *23*, 945-47
(29) Cotton, F. A.; Diebold, M. P.; Roth, W. J. *Polyhedron,* **1985,** *4*, 1103-08
(30) Cotton, F. A.; Diebold, M. P.; Roth, W. J. *Inorg. Chim. Acta,* **1985,** *105*, 41-49
(31) Levason, W.; Reid, G.; Trayer, J.; Zhang, W. *Dalton Trans.,* **2014,** *43*, 3649-59
(32) Gibson, V. C.; Kee, T. P.; Shaw, A. *Polyhedron,* **1988,** *7*, 2217-19
(33) Chavant, C.; Daran, J. C.; Jeannin, Y.; Constant, G.; Morancho, R. *Acta Cryst. B* **1975,** *31*, 1828-32
(34) Herrmann, W. A.; Thiel, W. R.; Herdtweck, E. *Chem. Ber.,* **1990,** *123*, 271-76
(35) Gibson, V. C.; Kee, T. P. *J. Chem. Soc., Dalton Trans.,* **1993**, 1657-59
(36) Gibson, V. C.; Kee, T. P.; Sorrell, R. M.; Bashall, A. P.; McPartlin, M. *Polyhedron,* **1988,** *7*, 2221-23
(37) Parkin, G. *Chem. Rev.,* **1993,** *93*, 887-911
(38) Bashall, A.; Gibson, V. C.; Kee, T. P.; McPartlin, M.; Robinson, O. B.; Shaw, A. *Angew. Chem. Int. Ed.,* **1991,** *30*, 980-82
(39) Fairbrother, F. *The Halides of Niobium and Tantalum*; Academic Press: New York, 1967.
(40) Hubert-Pfalzgraf, L. G.; Postel, M.; Reiss, J. G. *Comprehensive Coordination Chemistry I,* **1987,** *3*, 585-698

(41) Copley, D. B.; Fairbrother, F.; Thompson, A. *J. Less Common Met.,* **1965,** *8*, 256-61
(42) Benjamin, S. L.; Hyslop, A.; Levason, W.; Webster, M. *Acta Cryst. C,* **2011,** *67*, m221-m23
(43) Bannister, R. D.; Levason, W.; Light, M. E.; Reid, G.; Zhang, W. *Polyhedron,* **2019,** *167*, 1-10
(44) Walton, R. A. *Prog. Inorg. Chem.,* **1972,** *16*, 1 -194
(45) Feenan, K.; Fowles, G. W. A. *Inorg. Chem.,* **1965,** *4*, 310-13
(46) Edwards, D. A. *J. Inorg. Nucl. Chem.,* **1965,** *27*, 303-07
(47) Carmichael, W. M.; Edwards, D. A. *J. Inorg. Nucl. Chem.,* **1968,** *30*, 2641-46
(48) Crouch, P. C.; Fowles, G. W. A.; Marshall, P. R.; Walton, R. A. *J. Chem. Soc. A,* **1968**, 1634-838
(49) Levason, W.; McCullough, F. P.; McAuliffe, C. A. *Inorg. Nucl. Chem. Lett.,* **1976,** *12*, 843-47
(50) Levason, W.; McAuliffe, C. A.; McCullough, F. P.; Murray, S. G.; Rice, C. A. *Inorg. Chim. Acta,* **1977,** *22*, 227-31
(51) McAuliffe, C. A.; Sayle, B. J. *Inorg. Chim. Acta,* **1978,** *30*, 35-43
(52) McAuliffe, C. A.; Werfalli, A. *Inorg. Chim. Acta,* **1982,** *64*, L19-L20
(53) Levason, W.; McAuliffe, C. A.; Sayle, B. J. *J. Chem. Soc., Dalton Trans.,* **1976**, 1177-81
(54) Bortoluzzi, M.; Marchetti, F.; Pampaloni, G.; Zacchini, S. *Eur. J. Inorg. Chem.,* **2016**, 3169-77
(55) Hill, L. H.; Howlader, N. C.; Mabbs, F. E.; Hursthouse, M. B.; Malik, K. M. A. *J. Chem. Soc., Dalton Trans.,* **1980**, 1475-81
(56) Fowles, G. W. A.; Frost, J. L. *J. Chem. Soc. A,* **1967**, 671-75
(57) Fowles, G. A. W.; Rice, D. A.; Shanton, K. J. *J. Chem. Soc., Dalton Trans.,* **1978**, 1658-61
(58) Levason, W.; McAuliffe, C. A.; McCullough, F. P. *Inorg. Chem.,* **1977,** *16*, 2911-16
(59) Behzadi, K.; Baghlaf, A. O.; Thompson, A. *J. Less Common Met.,* **1978,** *57*, 103-10
(60) Chang, Y. P.; Hector, A. L.; Levason, W.; Reid, G. *Dalton Trans.,* **2017,** *46*, 9824-32
(61) Islam, S. M.; Subrahmanyam, K. S.; Malliakas, C. D.; Kanatzidis, M. G. *Chem. Mater.,* **2014,** *26*, 5151-60
(62) Britnell, D.; Fowles, G. W. A.; Rice, D. A. *J. Chem. Soc., Dalton Trans.,* **1974**, 2191-94
(63) Britnell, D.; Fowles, G. W. A.; Rice, D. A. *J. Chem. Soc., Dalton Trans.,* **1975**, 213-15
(64) Drew, M. G. B.; Griffin, G. F.; Rice, D. A. *Inorg. Chim. Acta,* **1979,** *34*, L192
(65) Baghlaf, A. O.; Thompson, A. *J. Less Common Met.,* **1977,** *53*, 291-93
(66) McAuliffe, C. A.; Werfali, A.; Hill, W. E.; Minahan, D. M. A. *Inorg. Chim. Acta,* **1982,** *60*, 87-91
(67) Vitzthumecker, C.; Robinson, F.; Pfitzner, A. *Monatsh. Chem.,* **2017,** *148*, 629-33
(68) Chang, Y. P.; Levason, W.; Light, M. E.; Reid, G. *Dalton Trans.,* **2016,** *45*, 16262-74
(69) Benjamin, S. L.; Chang, Y.-P.; Huggon, M.; Levason, W.; Reid, G. *Polyhedron,* **2015,** *99*, 230-37
(70) Dolci, S.; Marchetti, F.; Pampaloni, G.; Zacchini, S. *Eur. J. Inorg. Chem.,* **2013,** *2013*, 1371-80
(71) Favero, L.; Marchetti, F.; Pampaloni, G.; Zacchini, S. *Dalton Trans.,* **2014,** *43*, 495-504
(72) Marchetti, F.; Pampaloni, G.; Zacchini, S. *Dalton Trans.,* **2013,** *42*, 2477-87
(73) Kacholdt, H.; Berges, P.; Klar, G.; Hinrichs, W. *Transition Met. Chem.,* **1987,** *12*, 515-20
(74) Kemmitt, T.; Levason, W.; Spicer, M. D.; Webster, M. *Organomet.,* **1990,** *9*, 1181-84
(75) Poropudas, M. J.; Rautiainen, J. M.; Oilunkaniemi, R.; Laitinen, R. S. *Dalton Trans.,* **2016,** *45*, 17206-15
(76) Hull, C. G.; Stiddard, M. H. B. *J. Chem. Soc. A,* **1966,** *0*, 1633-35
(77) Isovitsch, R. A.; Fronczek, F. R.; Maverick, A. W. *Polyhedron,* **1998,** *17*, 1617-20
(78) Limberg, C.; Büchner, M.; Heinze, K.; Walter, O. *Inorg. Chem.,* **1997,** *36*, 872-79
(79) Taylor, R. D.; Todd, P. G.; Chasteen, N. D.; Spence, J. T. *Inorg. Chem.,* **1979,** *18*, 44-48
(80) Scullane, M. I.; Taylor, R. D.; Minelli, M.; Spence, J. T.; Yamanouchi, K.; Enemark, J. H.; Chasteen, N. D. *Inorg. Chem.,* **1979,** *18*, 3213-19
(81) Garner, C. D.; Howlader, N. C.; Mabbs, F. E.; McPhail, A. T.; Onan, K. D. *J. Chem. Soc., Dalton Trans.,* **1978**, 1848
(82) Jensen, L. M. R.; Abrahams, B. F.; Young, C. G. *J. Coord. Chem.,* **2013,** *66*, 1252-63

(83) Bartalucci, N.; Bortoluzzi, M.; Marchetti, F.; Pampaloni, G.; Schoch, S.; Zacchini, S. *New J. Chem.,* **2017,** *41*, 4329-40
(84) Marchetti, F.; Pampaloni, G.; Zacchini, S. *Polyhedron,* **2015,** *85*, 369-75
(85) Hursthouse, M. B.; Levason, W.; Ratnani, R.; Reid, G. *Polyhedron,* **2004,** *23*, 1915-21
(86) Brown, M. D.; Hursthouse, M. B.; Levason, W.; Ratnani, R.; Reid, G. *Dalton Trans.,* **2004**, 2487-91
(87) Levason, W.; Monzittu, F. M.; Reid, G.; Zhang, W.; Hope, E. G. *J. Fluorine. Chem.,* **2017,** *200*, 190-97
(88) Hartley, F. R.; Murray, S. G.; Levason, W.; Soutter, H. E.; McAuliffe, C. A. *Inorg. Chim. Acta,* **1979,** *35*, 265-77
(89) Gulliver, D. J.; Hope, E. G.; Levason, W.; Murray, S. G.; Potter, D. M.; Marshall, G. L. *J. Chem. Soc., Perkin Trans. II,* **1984,** *2*, 429-34
(90) Kemmitt, T.; Levason, W. *Organomet.,* **1989,** *8*, 1303-08
(91) Kuhn, N.; Faupel, P.; Zauder, E. *J. Organomet. Chem.,* **1986,** *302*, C4-C6
(92) Hope, E. G.; Kemmitt, T.; Levason, W. *Organomet.,* **1987,** *6*, 206-07
(93) Hope, E. G.; Kemmitt, T.; Levason, W. *Organomet.,* **1988,** *7*, 78-83
(94) Gibson, V. C.; Kee, T. P.; Shaw, A. *Polyhedron,* **1990,** *9*, 2293-98

Development of Precursors for Layered Transition Metal Dichalcogenides *via* Non-Aqueous Electrodeposition

7.1 Introduction

As discussed in Chapters 4 and 5, interest in early transition metal dichalcogenides has increased in recent years and having a variety of methods to produce ME_2 (M = Mo or W; E = S or Se) thin films is important for electronic devices. While CVD provides a cheap and versatile method to produce a range of thin film materials, electrodeposition allows control over where the material is deposited (only onto conducting surfaces) and offers a greater amount of control over the film's properties; including thickness. This section of work focuses on the development of a series of potential single source precursors suitable for the electrodeposition of ME_2 thin films using non-aqueous solvents. This chapter is split into two sections covering the synthesis of precursors and subsequent electrodeposition of MoS_2 and WS_2, respectively.

7.2 Transition Metal and *p* Block Metals *via* Non-Aqueous Electrodeposition

The use of non-aqueous solvents in electrodeposition has advanced significantly and it has been shown to facilitate the deposition of a large variety of *d* and *p* block metals.[1-3] Traditionally, electrodeposition used aqueous baths, which allows fast deposition rates, but can pose a problem of hydrolysis of metal reagents, subsequently incorporating undesirable metal oxides into the deposited materials. In addition, aqueous baths can have quite narrow electrochemical windows and promote hydrogen evolution from the competing reduction of water, which is usually undesirable.[1] Conventional organic solvents such as MeCN, dmso and ethers are also common electrodeposition media which provide sufficient electrochemical windows and diffusivity of electrolytes. This allows depositions that are easy to control, are cost effective and have been proven to effectively deposit metals and materials such as Lu-Ni alloys from dmso, for example.[4,5] The lower temperatures required compared to vapour deposition methods, and the ability to control the potential of the system (and therefore the growth rate), in principle allows greater control of the films. Since electrodeposition is a 'bottom-up' technique it allows a high-density material to be formed and offers efficient volume filling with fewer defects. Electrodeposition has many potential applications and is used in industry for integrated copper circuits, known as the dual Damascene process,[6] and for the read-write heads in magnetic recording devices.[7] Compared to other methods such as CVD, transition metal dichalcogenide fabrication *via* electrodeposition is much less developed.

7.2.1 Electrodeposition of *p* Block Metals and Metalloids

Electrodeposition, like CVD, has certain desirable properties from a successful precursor and it is common for precursors to be ionic salts to increase solubility in the electrolyte solutions. A range of chlorometallate salts, $[^nBu_4N][MCl_3]$ (M = Ge or Sn), $[^nBu_4N][MCl_4]$ (M = Ga, In, Sb or Bi) and $[^nBu_4N]_2[MCl_6]$ (M = Se or Te) have been shown to deposit pure elemental metals onto TiN electrodes from either CH_2F_2 or CH_2Cl_2.[2,8,9] The chlorometallate salts were shown to form stable, reproducible electrochemical systems from which the elemental metals can be deposited. The haloplumbate salts $[PPh_4][PbCl_3]$ or $[^nBu_4N][PbCl_3]$ were shown to deposit elemental Pb and combining $[^nBu_4N][SnCl_3]$ and $[^nBu_4N][BiCl_4]$ allows deposition of Sn-Bi alloys with the ratio directly controlled by potential.[10,11] Using $[^nBu_4N][BiCl_4]$ and $[^nBu_4N]_2[TeCl_6]$ in CH_2Cl_2 produces the thermoelectric material Bi_2Te_3, with evidence of preferred orientation in the <110> plane.[12] A similar example using $[^nBu_4N]_2[TeCl_6]$ and $[^nBu_4N]_2[HgCl_4]$ in CH_2Cl_2 also deposits the crystalline HgTe onto Pt substrates, with no evidence of elemental tellurium.[13] Using dual precursors to deliver the required materials is typical, but finding suitable reagents for early transition metals can prove challenging and most are hydrolytically unstable.

The use of chlorometallate salts can be expanded to introduce the ability to deposit ternary systems such as germanium antimony telluride, leading to functional and switchable phase change memory nanocells.[14-16] Thus, by using $[^nBu_4N]_2[TeCl_6]$, $[^nBu_4N][SbCl_4]$ and $[^nBu_4N][GeCl_5]$, the phase change memory material, $Ge_2Sb_2Te_5$, can be deposited. Varying either the concentration of the precursors in the electrochemical bath or the deposition potential can directly alter the material composition.[14-16]

The use of $[^nBu_4N]^+$ salts increases the solubility of the metal anions in weakly coordinating solvents such as CH_2Cl_2. The cations are electrochemically inert and contain the same cation as the supporting electrolyte used, $[^nBu_4N]Cl$. It is also demonstrated that chlorometallate salts can be synthesised with suitable purity and are stable in solution.

7.2.2 Electrodeposition of Transition Metal Dichalcogenides

There are very few reports of electrodepositing transition dichalcogenides from either aqueous or non-aqueous baths. Using aqueous baths also limits the range of suitable reagents. Hexagonal $ZrSe_2$ films have been electrochemically deposited from an aqueous bath using $ZrO(NO_3)_2 \bullet H_2O$ or $Zr(SO_4)_2$ and SeO_2 onto stainless steel or fluorine doped tin oxide glass (FTO) substrates.[17,18] The deposition of $ZrSe_2$ is one of the few examples of transition metal dichalcogenides electrochemically deposited.

MoS_2 films are by far the most studied transition metal dichalcogenide. MoS_2 is a diamagnetic semiconductor with an indirect band gap similar to that of silicon, 1.7 eV, making it a possible alternative to silicon in solar cells. MoS_2 has also been studied for electrochemical applications and

microelectronics.[19] Due to the two dimensional stacking (layered structure), it shows a diverse range of optical and electronic properties that differ from bulk. The bulk material has an indirect band gap of 1.2 eV, whereas the two dimensional monolayer has a direct band gap of 1.8 eV making it suitable for switchable transistors and typically exhibits *n*-type semiconducting behaviour.[19,20] As the thickness of films decreases this causes strong photoluminescence in 2H-MoS_2, which is not present in the bulk, allowing the possibility of using MoS_2 for visible light photocatalytic reactions.[20,21]

Amorphous MoS_2 films have been shown to deposit from $[NH_4]_2[MoS_4]$ in ethylene glycol at 165 ºC. Subsequent annealing at 550 ºC formed polycrystalline 2H-MoS_2 films ~150 nm thick.[22,23] From an aqueous electrolyte bath MoS_2 has deposited onto indium tin oxide coated glass (ITO) using H_2MoO_4 and $Na_2S_2O_3$•$5H_2O$,[24] $[NH_4]_2[MoS_4]$ has also been used in an aqueous bath to deposit MoS_2.[25]

Following this, MoS_2 has been deposited onto glassy carbon substrates from a room-temperature ionic liquid (RTIL), $[PP_{13}][TFSI]$ with the dual source precursors, molybdenum glycolate and $HS(CH_2)_4SH$.[26]

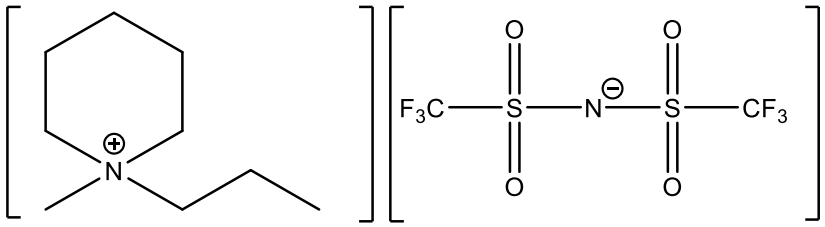

Figure 7.1: Illustration of the ionic liquid PP_{13}-TFSI.

Another report of the electrodeposition of amorphous MoS_x using a RTIL ([EMIM][TFSI]) electrolyte bath used the single source precursor $[PPh_4]_2[MoS_4]$, but film characterisation is limited.[27] XPS analysis showed the presence of Mo and S but O is also incorporated into the amorphous films. As the films have not been annealed the material characterisation is not conclusive and the Mo : S ratio is suggested to be 1 : >2.[27]

$MoSe_2$ is homologous to MoS_2 and has potential properties for photochemical applications and energy storage, it shows higher electrical conductivity than MoS_2 due to selenium's more metallic nature, which improves its performance in photoelectrochemical devices.[28,29] Similar to MoS_2, $MoSe_2$ has 2 phases, 2H and 1T, but the 1T phase is thermodynamically unstable and degrades into the 2H phase over time, making it unsuitable for many applications.[30] There are a few reports of $MoSe_2$ being deposited from dual source aqueous chemical baths using H_2MoO_4 and SeO_2[31] or Na_2MoO_4 and H_2SeO_3 with mixed success, due to MoO_3 incorporation.[32] The $MoSe_2$ films deposited from H_2MoO_4 and SeO_2 were annealed at 150 ºC and shown to be polycrystalline with preferred orientation in the <102> plane.[31] Also, there is a report of $MoSe_2$ being deposited using electrochemical atomic layer deposition (E-ALD) using $[HMoO_4]^-$ and SeO_2 using $[NH_4]Cl$ as a supporting electrolyte.[33] The amorphous $MoSe_2$ films were then annealed at 300 ºC to produce

polycrystalline films and to remove unreacted MoO_2. There is one report of single source deposition of amorphous $MoSe_x$ from $[PPh_4]_2[MoSe_4]$ in [EMIM][TFSI], although the characterisation of the deposited film is limited to XPS and Raman spectroscopy.[27]

There are fewer reports of the electrodeposition of tungsten dichalcogenides than molybdenum dichalcogenides. WS_2 has a slightly larger indirect bandgap than the molybdenum analogue.[34] There are some reports of hydrogen evolution reactions occurring when depositing WS_2 from $[WS_4]^{2-}$ in aqueous solutions as the deposit potential can overlap with the hydrogen evolution reaction.[35] WS_2 films were reported using H_2WO_4 and Na_2SO_3 in aqueous solution from galvanostatic methods.[36] Single source electrodeposition of WS_2 thin films onto ITO substrates from an acetonitrile bath using $[NH_4]_2[WS_4]$ and $LiClO_4$ has been reported.[37] They describe the annealed film as the polycrystalline 2H-phase of WS_2, however evidence of WO_3 incorporation is not clear. A similar report using $[NH_4]_2[WS_4]$ in aqueous KCl solution is shown to deposit WS_2 onto glassy carbon electrodes and it is suggested that the as-deposited films have the ratio W : S (1:2.64) consistent with other reports of depositing WS_x (x = 2-3) films.[38]

Again there is very little reported literature for the electrodeposition of WSe_2, but there are a few reports using galvanostatic methods from aqueous baths with H_2WO_4 and SeO_2.[39,40] There is one other report using an aqueous bath of Na_2WO_4, tartaric acid and Na_2SSeO_3.[17]

The majority of electrochemical depositions of transition metal dichalcogenides are from aqueous baths, however, the water stable precursors (commonly metal oxides) can cause the inclusion of oxide. The aqueous baths also promotes hydrogen evolution, the release of hydrogen gas can result in films having a rough morphology with pinholes, which is not suitable for device quality materials.[41] The hydrogen evolution can also interfere with the electrochemistry of solutions making it difficult to assess the suitability of precursors; this can be minimised by using non-aqueous solvents with wider potential windows.

7.2.3 Thiometallates

Thiometallates have been of interest since studies in the 19th century due to their strong colours and more recently have been building blocks for the formation of metal chalcogen-clusters.[42,43] Tetrathio- and tetraseleno-metallates are extensively studied for a range of metals and all metals are in their highest oxidation state.[42,44]

Known tetrathio- and tetraseleno-metallates		
$[VS_4]^{3-}$	$[MoS_4]^{2-}$	$[ReS_4]^{-}$
$[VSe_4]^{3-}$	$[MoSe_4]^{2-}$	
$[NbS_4]^{3-}$	$[WS_4]^{2-}$	
$[TaS_4]^{3-}$	$[WSe_4]^{2-}$	

Table 7.1: Table showing known tetrathio- and tetraseleno-metallates.

The most common way to synthesise $[MoS_4]^{2-}$ salts is to pass H_2S through a $[NH_4]_x[MO_4]^{x-}$ solution, however many ammonium thiometallate salts are now commercially available.[45] The alkylammonium and phosphonium salts can be readily prepared from aqueous solutions of the ammonium salts *via* metathesis of the cation.[46,47] The tetraselenometallates are more complicated to synthesise but are commonly prepared from Na_2Se_3 or K_2Se_3 and $M(CO)_x$.

Thiometallates can act as ligands forming sulfide bridges with up to four other metal centres, forming simple chains or more complex cubane structures.[42] These clusters can exhibit redox behaviour which has become important in biological systems including removing copper from the blood stream.[42] More recently, they have been identified as potential single source precursors for the electrodeposition of transition metal dichalcogenide thin films due to suitable solubility, stability and the incorporation of both metal and chalcogen in the anion.

7.2.4 Aims

This chapter focuses on the development and synthesis of a series of potential precursors suitable for the electrodeposition of ME_2 (M = Mo or W; E = S or Se) thin films using non-aqueous solvents. The chapter is split into two parts covering the synthesis of precursors for the electrodeposition of MoS_2 and WS_2 and their respective electrochemical studies. The precursors will be fully characterised by IR, ^{1}H NMR, ^{77}Se{^{1}H} NMR, ^{95}Mo NMR spectroscopy where possible, elemental analysis and X-ray crystal structures. Deposited thin films of ME_2 will be characterised by Raman spectroscopy, grazing incidence X-ray diffraction, SEM and EDX/WDX.

7.3 Results and Discussion

7.3.1 Synthesis of Precursors for MoE_2 Films

The compound, $[^nBu_4N]_2[MoS_4]$ was prepared from stoichiometric reaction of $[NH_4]_2[MoS_4]$ and $[^nBu_4N]Cl$ in deionised water in good yields. The IR spectrum shows a strong T_2 stretch at 468 cm^{-1} which can be assigned to a Mo=S stretch. The ^{95}Mo NMR spectrum shows a sharp singlet at +2234 ppm, which corresponds with the reported literature.[48]

Additional ^{95}Mo NMR experiments were also carried out in acetonitrile and dichloromethane with added electrochemical electrolytes (tetrabutylammonium chloride and tetrabutylammonium tetrafluoroborate), causing no significant shift. This shows that these supporting electrolytes do not interact with the $[MoS_4]^{2-}$ anion in solution and could be suitable for electrodeposition in organic solvents.

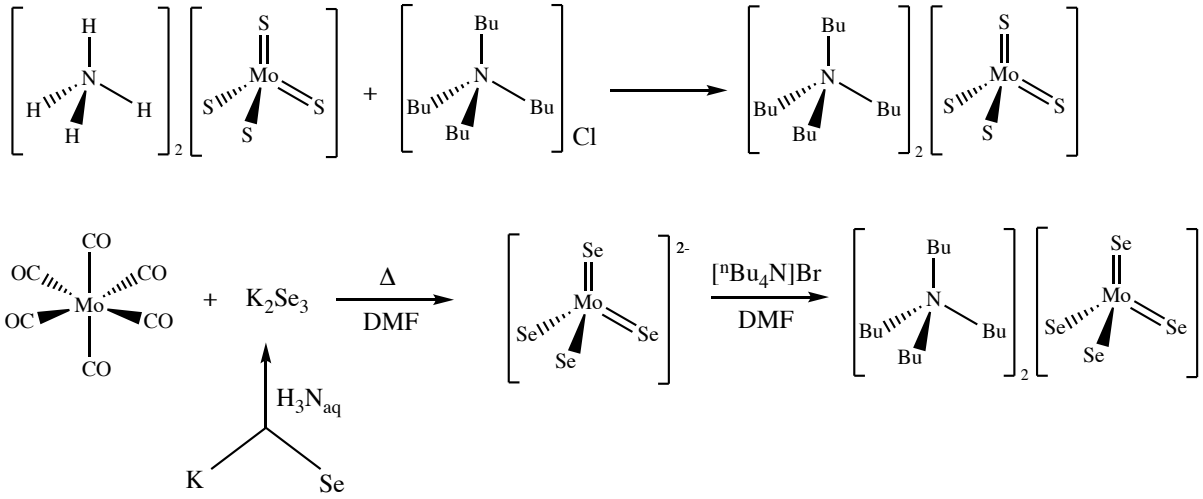

Figure 7.2: Reaction scheme for $[^nBu_4N]_2[ME_4]$ (E = S or Se).

The selenium analogues $[MoSe_4]^{2-}$ were more complex to syntheses as $[NH_4]_2[MoSe_4]$ is not commercially available, therefore $[MoSe_4]^{2-}$ has to be prepared in house. Fresh K_2Se_3 was prepared in liquid ammonia and then heated to reflux with $Mo(CO)_6$ in DMF to form $K_2[MoSe_4]$, before the appropriate alkylammonium or phosphonium salt is then added. Two salts were isolated, $[PPh_4]_2[MoSe_4]$ and $[^nBu_4N]_2[MoSe_4]$, which exhibit different solubilites in organic solvents. The highly soluble $[^nBu_4N]_2[MoSe_4]$ proved challenging to isolate in a pure form. The IR spectra for both $[PPh_4]_2[MoSe_4]$ and $[^nBu_4N]_2[MoSe_4]$ show a single T_2 stretch at 340 and 341 cm^{-1}, respectively, showing that the cation has no effect on the Mo=Se bond and the data are consistent with reported literature.[49] Both compounds show a single peak in both the $^{77}Se\{^1H\}$ and ^{95}Mo NMR spectra. The ^{95}Mo NMR spectrum for $[^nBu_4N]_2[MoSe_4]$ also shows ^{77}Se satellites (13 Hz) consistent with the $[MoSe_4]^{2-}$ ion. Attempts to find the ^{77}Se satellites in the ^{95}Mo NMR spectrum for $[PPh_4]_2[MoSe_4]$ were unsuccessful. Possible due to its poorer solubility in CH_2Cl_2, however the main resonance is 120 Hz wide at the base, so it is likely to obscure the coupling, as the ^1J coupling is only 13 Hz.[50]

Compound	^{95}Mo NMR Shifts	$^{77}Se\{^1H\}$ NMR Shifts
$[^nBu_4N]_2[MoSe_4]$	+3088 ppm	+ 1652 ppm
$[PPh_4]_2[MoSe_4]$	+3094 ppm	+ 1656 ppm

Table 7.2: $^{77}Se\{^1H\}$ and ^{95}Mo NMR data for the $[MoSe_4]^{2-}$ salts.

7.3.2 Electrochemistry of Precursors for MoS_2 Films

The electrochemical studies of the precursors have been undertaken by Dr S. Thomas at the University of Southampton, along with the EDX/WDX and Raman spectroscopic analysis of the deposited films. Cyclic voltammetry was first performed on the precursors in CH_2Cl_2 to evaluate their electrochemical behaviour, thus providing a quick screening process. The supporting electrolyte used was either $[^nBu_4N]Cl$ or $[NH_4]Cl$ in order minimise additional ions in the system to

reduce potential complications with speciation and ensuring both the supporting electrolyte and precursors were completely dissolved.

Initially, experiments to replicate the results from Albu-Yaron and co-workers using ethylene glycol and $[NH_4]_2[MoS_4]$ were attempted.[22] A solution containing 5 mM $[NH_4]_2[MoS_4]$ with 0.57 M $[NH_4]Cl$ as the proton source and 100 mM KCl as supporting electrolyte in ethylene glycol was prepared and a CV conducted.

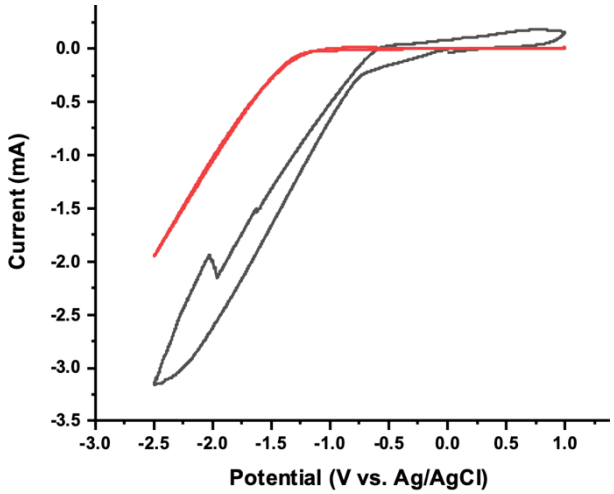

Figure 7.3: CV of 5 mM $[NH_4]_2[MoS_4]$ (black) in ethylene glycol and background (red).

As shown in Figure 7.3, the cathodic scan shows a reduction at increasing negative potential with the cathodic peak potential (E_{pa}) at ~-2.5 V. The deposition onset peak, peak deposition current and stripping onset occur at -1.0 V, -2.5 V and -0.5 V, respectively. Subsequent deposition experiments showed the deposition of MoS_x (x = 2-3) and post-annealing MoS_2.

Cyclic voltammetry was also performed in CH_2Cl_2 solution containing 5 mM $[^nBu_4N]_2[MoS_4]$ with 100 mM $[^nBu_4N]Cl$ as the supporting electrolyte and 200 mM $[Me_3HN]Cl$ as a proton source. Previous voltammetric studies of CH_2Cl_2 have demonstrated that $[^nBu_4N]Cl$ provides a good potential window and conductivity (σ = ~1 mS cm^{-1} for 100 mM $[^nBu_4N]Cl$), comparable to 10 mM KCl solution.[2] The electrochemical window for 100 mM $[^nBu_4N]Cl$ in CH_2Cl_2 was found to be between –1.85 V and +1 V. A proton source is required for deposition of MoS_2 as without it the deposition current does not exceed -0.6 mA and there is very little deposition, whereas with a proton source the deposition current is ~-8.2 mA.

The reasoning behind such a low current without a proton source is that four protons are required for the reduction of $[MoS_4]^{2-}$.

$$[MoS_4]^{2-} + 4H^+ + 2e^- \rightarrow MoS_2 + 2H_2S$$

Equation 7.1: Suggest electrochemical reaction for the deposition of MoS_2 from $[^nBu_4N]_2[MoS_4]$.

Without sufficient protons the reduction cannot be completed, resulting in an extremely small current which is not strong enough to allow deposition to proceed. MoS_3 has been shown to deposit

on the anodic scan on the counter electrode and is then subsequently stripped as the potential is swept more negative, reproducing the $[MoS_4]^{2-}$ ion back into the electrochemical solution.[51]

To investigate the anodic deposition, the experiment was completed with an EQCM (Figure 7.4). This allows changes in mass at the electrode to be observed, without the proton source there is no mass change on the cathodic scan confirming that the current is too low to produce deposition. There is anodic deposition at ~0.4 V, which is then stripped and $[MoS_4]^{2-}$ is returned to the solution; with the proton source added, the EQCM characteristics are very different. Once again, during the anodic scan there is deposition of MoS_3, which is then stripped away, reducing the relative mass. During the cathodic scan there is deposition of MoS_2, which increases the relative mass. The deposited MoS_2 does not get stripped away during the anodic scan, therefore increasing the effective mass with each sweep.

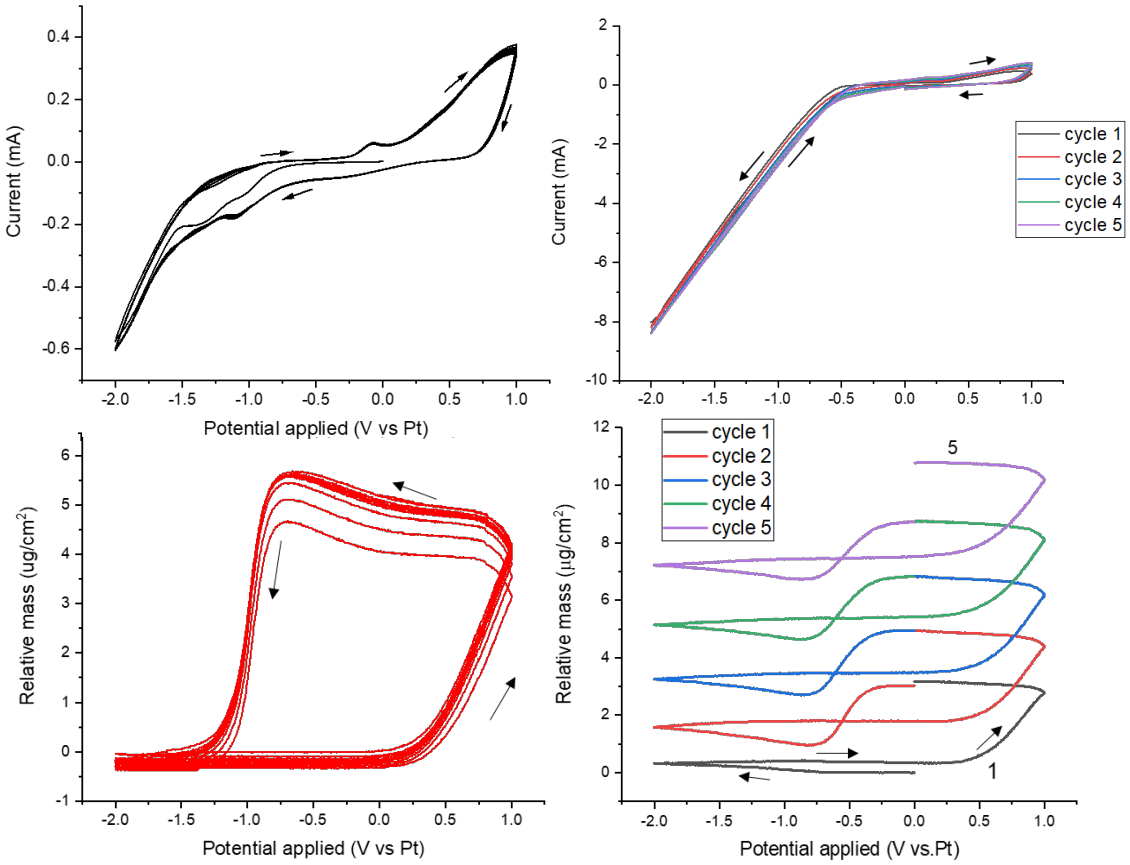

Figure 7.4: CV of 5 mM of $[^nBu_4N]_2[MoS_4]$ in CH_2Cl_2 without a proton source (top left) with 200 mM $[Me_3NH]Cl$ (top right). EQCM of 5 mM of $[^nBu_4N]_2[MoS_4]$ in CH_2Cl_2 without a proton source (bottom left) with 200 mM $[Me_3NH]Cl$ (bottom right).

From the CV experiments a potential of -0.8 V was identified as a suitable deposition potential, when using CH_2Cl_2, after the onset of the reduction peak, but well before the solvent breakdown, to reduce contamination in the films.

MoS_2 was deposited potentiostatically on to a planar TiN electrode using $[^nBu_4N]_2[MoS_4]$ containing $[^nBu_4N]Cl$ and $[Me_3NH]Cl$ as the supporting electrolyte and proton source, respectively, in CH_2Cl_2. The electrodes were held at constant potential, -0.8 V for CH_2Cl_2, *vs* Ag/AgCl which

provided enough overpotential to obtain films of suitable thickness, whilst falling within the available electrochemical window and minimising the effects of the electrolyte. After the deposition had finished, the films were gently washed in fresh CH_2Cl_2 to dissolve any residual salts. In order to crystallise the films, they were annealed at 100ºC for 10 minutes under vacuum then 500 ºC for 2 hours with sulfur under N_2.

As-deposited films gave none of the expected peaks of MoS_2 in grazing incidence XRD due to the films being amorphous. Subsequent acquisitions on the annealed films showed a very broad single peak at 14.4º attributed to the <002> plane from 2H-MoS_2 suggesting crystallites parallel to the crystallographic plane. The SEM image (Figure 7.5) shows a very flat and continuous layered deposit with few cracks. It is likely the cracks occur from internal stress due to long deposition times to obtain bulk films, the flat structure indicates a laminar like structure typical of these types of layered materials.

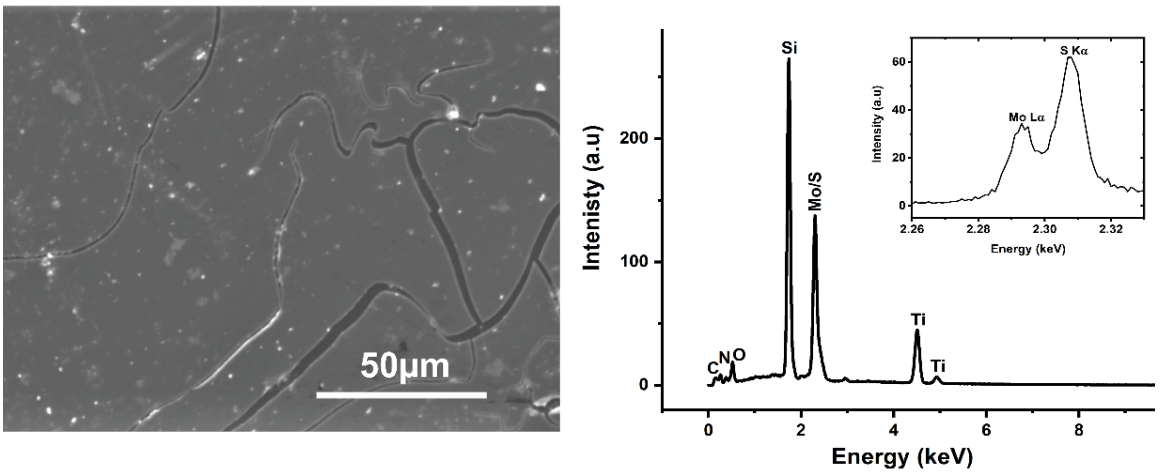

Figure 7.5: Top-view of an annealed deposit obtained after potentiostatic deposition at -0.8 V for 1 hour from CH_2Cl_2 containing 5 mM $[^nBu_4N]_2[MoS_4]$. 0.2 M $[Me_3HN]Cl$ with 0.1 M $[^nBu_4N]Cl$ as the supporting electrolyte (left). EDX spectrum of an annealed film, insert shows WDX spectrum for Mo L_α and S K_α lines (right).

The EDX spectrum of the annealed film confirmed the presence of molybdenum and/or sulfur (2.3 keV), but their respective emission peaks overlap (Mo $L_{\alpha1}$: 2.29 keV and S $K_{\alpha1}$: 2.31 keV) so a ratio cannot be quantified.[52] WDX data was obtained which has better resolution and shows two clearly separate peaks and quantification of the ratio confirmed Mo : S (1 : 1.9-2.1) against a standard commercial MoS_2 sample.

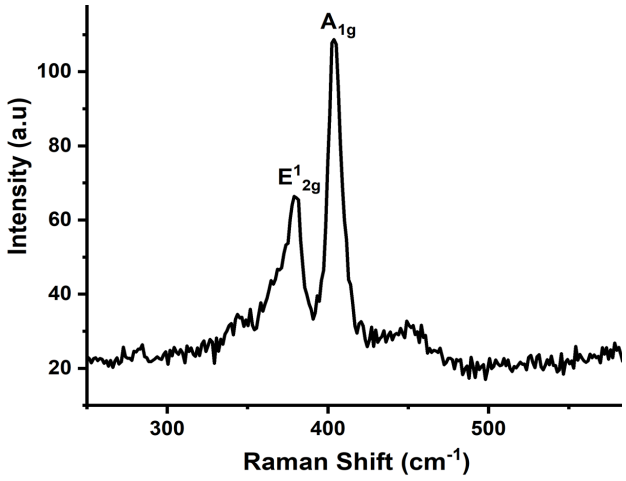

Figure 7.6: Raman spectra for an annealed MoS_2 film deposit.

Raman spectra were collected using a 532 nm excitation laser and the spectra show the two main peaks at 380 cm^{-1} and 404 cm^{-1}, which were assigned to the E_{2g} (in-plane) and A_{1g} (out of plane) vibrational modes of MoS_2, respectively.[53]

7.3.3 Electrochemistry of Precursors for $MoSe_2$ Films

Cyclic voltammetry was completed on a CH_2Cl_2 solution containing 5 mM $[^nBu_4N]_2[MoSe_4]$ with 200 mM $[^nBu_3HN]Cl$ as the proton source and 100 mM $[^nBu_4N]Cl$ as supporting electrolyte. The cyclic voltammogram is similar to $[^nBu_4N]_2[MoS_4]$, suggesting similar electrochemical properties. The cyclic voltammogram shows that reduction is occurring in the cathodic scan, with the deposition onset peak, peak deposition and stripping onset occurring at -0.8 V, -2.0 V and -1.1 V respectively.

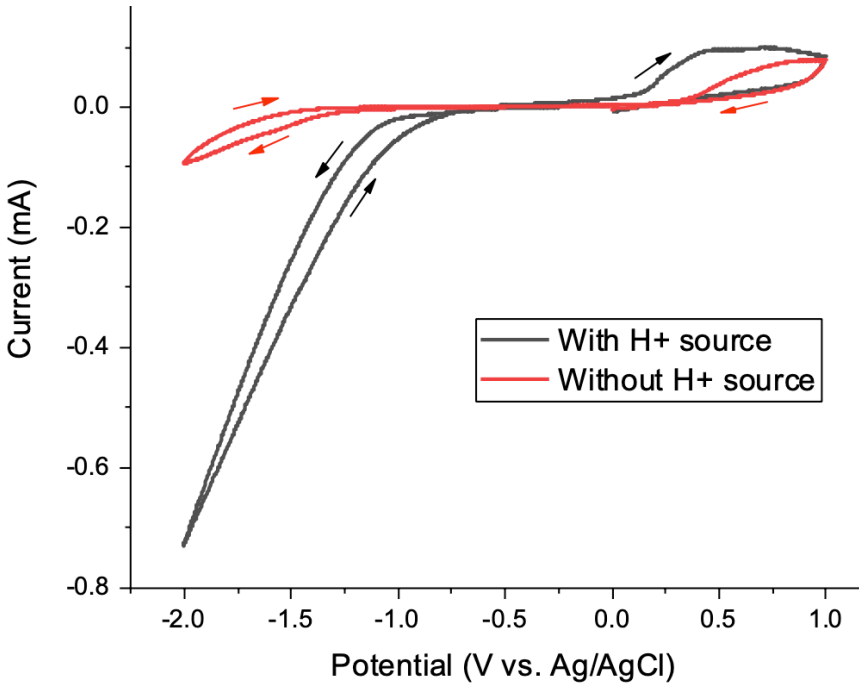

Figure 7.7: CV of 5mM $[Bu_4N]_2[MoSe_4]$ in CH_2Cl_2.

As with MoS_2, a proton source is required for deposition, as without it the deposition current does not exceed -0.1 mA which is not sufficient for deposition, whereas with a proton source the deposition current is ~-7.5 mA. Again it is suggested that $[MoSe_4]^{2-}$ undergoes similar chemistry to $[MoS_4]^{2-}$ that upon sweeping to positive potentials the reaction below occurs.[27]

$$[MoSe_4]^{2-} + 4H^+ + 2e^- \rightarrow MoSe_2 + 2H_2Se$$

Equation 7.2: Suggest electrochemical reaction for the deposition of MoS_2 from $[^nBu_4N]_2[MoSe_4]$.

Films were deposited potentiostatically on to planar TiN slide electrodes using $[^nBu_4N]_2[MoSe_4]$ containing $[^nBu_4N]Cl$ as the supporting electrolyte in CH_2Cl_2. The electrodes were held at constant potential, -1.2 V *vs* Ag/AgCl which provided enough overpotential to obtain films of suitable thickness, whilst falling within the available electrochemical window. After the deposition had finished, the films were gently washed in fresh CH_2Cl_2 to dissolve any residual salts.

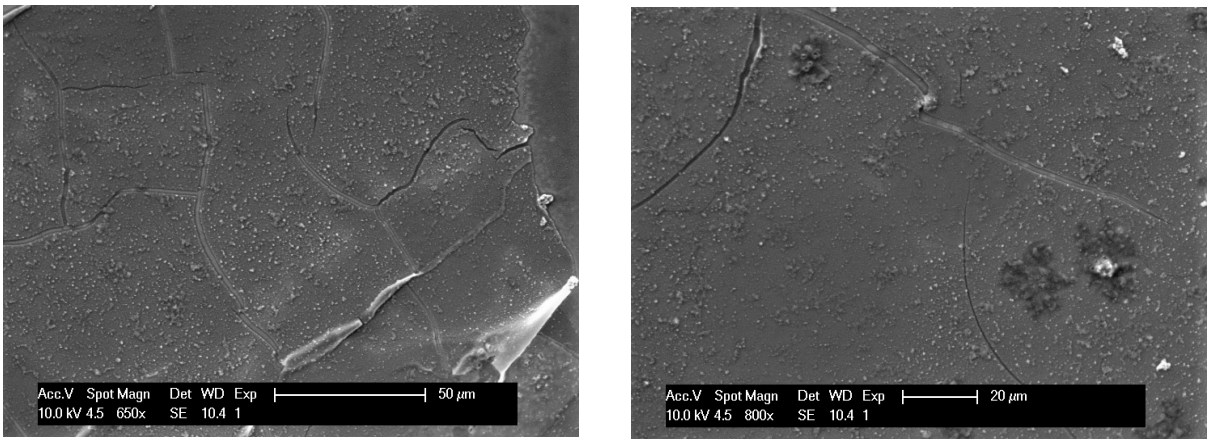

Figure 7.8: SEM for electrodeposited film on planar TiN from $[^nBu_4N]_2[MoSe_4]$.

The SEM images (Figure 7.8) of the deposited films show relatively uniform morphology across the surface of the electrode. EDX analysis of the deposited film shows both Mo and Se but significantly more Se than Mo, suggesting the possibility of elemental Se being co-deposited. There is also C and Cl present, most likely from the electrochemical breakdown of the electrolyte salts, also observed are emission peaks from Ti, Si and N from the electrode. Raman spectroscopy shows a broad peak at 259 cm^{-1} which is close to the A_{1g} vibrational mode of crystalline $MoSe_2$ (~242 cm^{-1}), however it can also be assigned to ν(Se-Se) common in amorphous Se.[54,55] An attempt to anneal the films was unsuccessful, it was attempted at 550 ^oC under N_2 but the selenium appears to have distilled off, confirmed by EDX. Further annealing attempts will be tried at lower temperatures, possibly with an additional selenium source in the annealing tube as well.

7.3.4 Synthesis of Precursors for WE_2 Films

Synthesis of $[WE_4]^{2-}$ salts (E = S or Se) were analogous to the $[MoE_4]^{2-}$ salts described above. The IR spectrum for $[^nBu_4N]_2[WS_4]$ shows a strong T_2 absorption at 449 cm^{-1} which corresponds with a W=S stretch and the ^1H NMR data shows 4 peaks corresponding to the tetrabutylammonium

cation. An attempt to obtain ^{183}W NMR spectroscopic data was tried but due to the tungsten nucleus' insensitivity, the compound degrades before a spectrum could be obtained (only stable for a few hours), so no spectrum could be recorded despite the high symmetry of the anion and possible instrumental problems with low resonance probes.

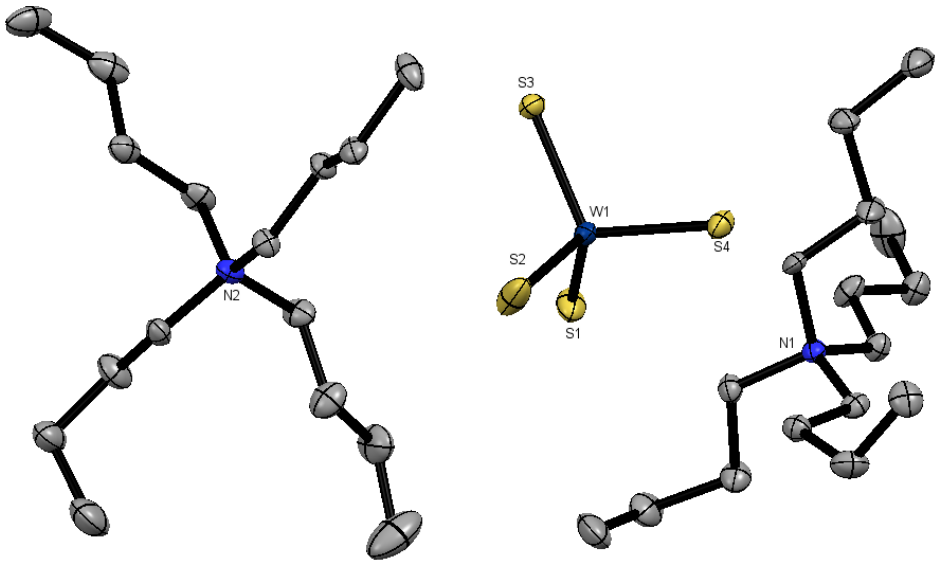

Figure 7.9: Crystal structure of [^{n}Bu$_4$N]$_2$[WS$_4$] showing the atom numbering scheme. Ellipsoids shown at 50% probability, hydrogen atoms omitted for clarity.

[^{n}Bu$_4$N]$_2$[WS$_4$]			
Bond Lengths/ Å		**Bond Angles/ °**	
W1-S1	2.200(2)	S1-W1-S2	110.09(9)
W1-S2	2.192(2)	S1-W1-S3	110.52(9)
W1-S3	2.182(2)	S1-W1-S4	110.19(9)
W1-S4	2.193(3)		

Table 7.3: Selected bond lengths and angles for [^{n}Bu$_4$N]$_2$[WS$_4$].

The yellow crystals obtained from slow evaporation from water showed [^{n}Bu$_4$N]$_2$[WS$_4$], the [WS$_4$]$^{2-}$ anion is in tetrahedral geometry which is what is expected based on to the single T_2 peak observed in the IR spectrum. The compound has crystallised in the orthorhombic space group, Fdd2, and the structure is relatively simple.

The [WSe$_4$]$^{2-}$ salts show a single T_2 stretch from W=Se in the IR spectra and both compounds exhibit a single peak in ^{77}Se{^{1}H} NMR spectra which had ^{183}W satellites, +1239 ppm and +1238 ppm for [^{n}Bu$_4$N]$_2$[WSe$_4$] (J_{WSe} 53 Hz) and [PPh$_4$]$_2$[WSe$_4$] (J_{WSe} 50 Hz), respectively.

Compound	W=Se	^{77}Se NMR Shifts
[^{n}Bu$_4$N]$_2$[WSe$_4$]	305 cm^{-1}	+1238 ppm
[PPh$_4$]$_2$[WSe$_4$]	304 cm^{-1}	+1239 ppm

Table 7.4: ^{77}Se{^{1}H} NMR data and IR data for the [WSe$_4$]$^{2-}$ salts.

Both salts yielded dark red crystals from saturated MeCN/THF solutions, the structure of [PPh$_4$]$_2$[WSe$_4$] has been previously reported but [^{n}Bu$_4$N]$_2$[WSe$_4$] is not currently known.[49]

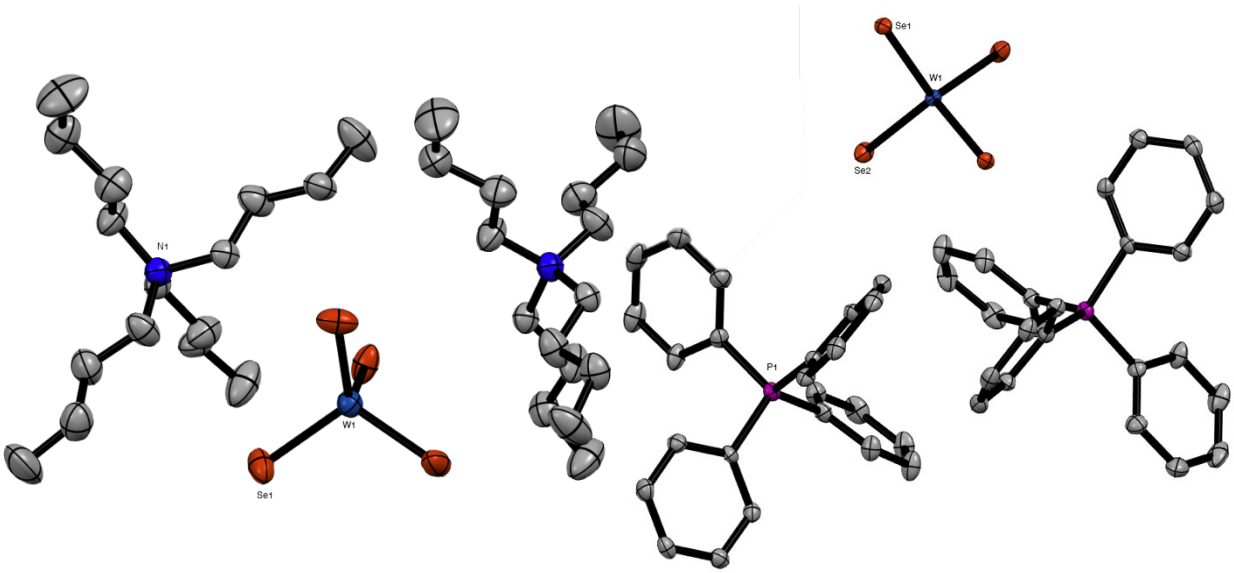

Figure 7.10: Crystal structures of [^{n}Bu$_4$N]$_2$[WSe$_4$] (left) and [PPh$_4$]$_2$[WSe$_4$] (right) showing the atom numbering scheme. Ellipsoids shown at 50% probability, hydrogen atoms omitted for clarity.

[^{n}Bu$_4$N]$_2$[WSe$_4$]			
Bond Lengths/ Å		**Bond Angles/ °**	
W1-Se1	2.3106(2)	Se1-W1-Se1	109.35(4)
[PPh$_4$]$_2$[WSe$_4$]			
Bond Lengths/ Å		**Bond Angles/ °**	
W1-Se1	2.369(2)	Se1-W1-Se1	109.21(2)
W1-Se2	2.360(4)	Se1-W1-Se2	108.40(2)

Table 7.5: Selected bond lengths and angles for [^{n}Bu$_4$N]$_2$[WSe$_4$] and [PPh$_4$]$_2$][WSe$_4$].

The complex [^{n}Bu$_4$N]$_2$[WSe$_4$] has crystallised in the highly symmetrical tetragonal space group $I\bar{4}2d$ (Figure 7.11), its W=Se bond lengths are not significantly different to those in [PPh$_4$]$_2$[WSe$_4$]. The crystals of [PPh$_4$]$_2$[WSe$_4$] were grown from MeCN/THF and the structure is previously known. It has the space group C2/c; the W=Se bonds are 2.369(2) and 2.360(4) Å, which are comparable to the reported bond lengths, 2.314(1), 2.316(1) Å.[49]

Following work on WSCl$_4$ coordination chemistry, tungsten(VI) thiohalide salt derivatives were synthesised to attempt to isolate a precursor with the correct stoichiometric ratio of tungsten and sulfur so that a proton source would not be required, simplifying the electrochemistry. Reaction of pre-made WSCl$_4$ and one equivalent of [^{n}Bu$_4$N]Cl or [PPh$_4$]Cl in CH$_2$Cl$_2$ led to the isolation of green solids of [^{n}Bu$_4$N][WSCl$_5$] or [PPh$_4$][WSCl$_5$], respectively. The compound [^{n}Bu$_4$N][WSCl$_5$] exhibits a W=S stretch at 508 cm^{-1} in the IR spectrum, consistent with the range of WSCl$_4$ coordination complexes isolated in previous chapters (albeit lower in wavenumber). These compounds have not been previously characterised, but there are examples of other salts with the same anion, [PPh$_3$(CH$_2$Ph)][WSCl$_5$][56] and [AsPh$_4$][WSCl$_5$], which have been structurally chacterised.[57]

After the successful isolation of $[WSCl_5]^-$ salts, an attempt to prepare $[WS_2Cl_4]^{2-}$ following a reported method failed.[58] Pre-made $WSCl_4$ was reacted with $S(SiMe_3)_2$ to form isolated WS_2Cl_2, which was subsequently reacted with two equivalents of $[PPh_4]Cl$. However WS_2Cl_2 showed no evidence of reacting as it is highly polymeric and inert. A new method was therefore developed, in which pre-made $WSCl_4$ was reacted with two equivalents of $[PPh_4]Cl$ to form $[PPh_4][WSCl_5]$ as an intermediate *in situ*, and then treated with an equivalent of $S(SiMe_3)_2$, allowing isolation of the target $[PPh_4]_2[WS_2Cl_4]$. Attempts to make the analogous compound $[^nBu_4N]_2[WS_2Cl_4]$ proved challenging as it was a very sticky red oil that was difficult to purify. Since the cation $[PPh_4]^+$ is not electrochemically inert, the compound $[Et_4N]_2[WS_2Cl_4]$ was prepared, as the $[NEt_4]^+$ cation provided enough solubility in CH_2Cl_2, was electrochemically inert and this salt easier to purify than the $[N^nBu_4]^+$ analogue.

7.3.5 Electrochemistry of Precursors for WS_2 Films

Attempts to deposit WS_2 and WSe_2 from $[WE_4]^{2-}$ salts have been unsuccessful as the potential required to bring about reduction of the $[ME_4]^{2-}$ salt does not appear to be in the available electrochemical window and is in the same range as the solvent/electrolyte breakdown.

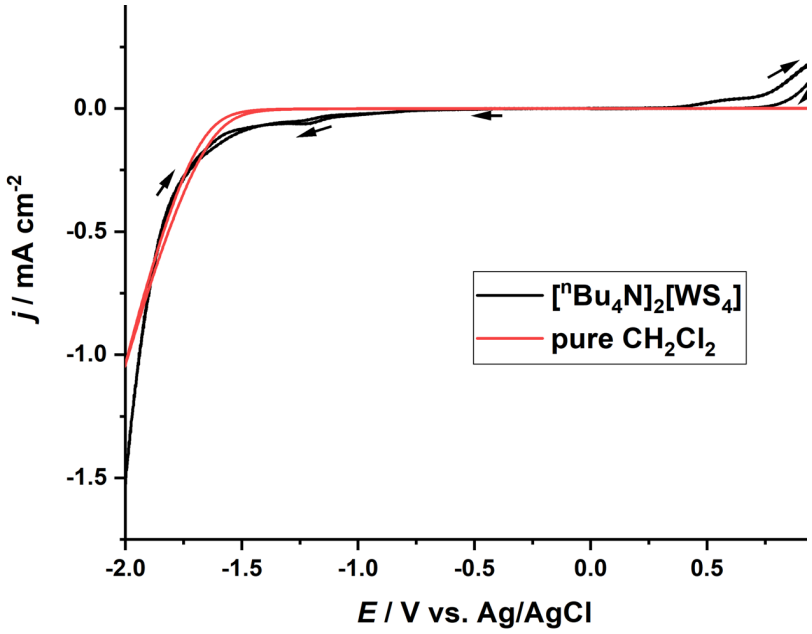

Figure 7.11: Cyclic voltammogram of 5 mM $[^nBu_4N]_2[WS_4]$ on TiN, $[^nBu_4N]Cl$ was the supporting electrolyte.

Figure 7.12 shows the cyclic voltammogram of $[^nBu_4N]_2[WS_4]$ in CH_2Cl_2 (with a proton source), it is clear there is no reduction of $[^nBu_4N]_2[WS_4]$ before the solvent breakdown. Therefore $[^nBu_4N]_2[WS_4]$ is not a suitable precursor, it can be expected that tungsten(VI) would be harder to reduce than molybdenum(VI), hence the reduction potential is more negative. Following the unsuccessful electrodeposition from $[^nBu_4N]_2[WS_4]$, $[Et_4N]_2[WS_2Cl_4]$ was isolated as a potential precursor (see Section 7.3.4).

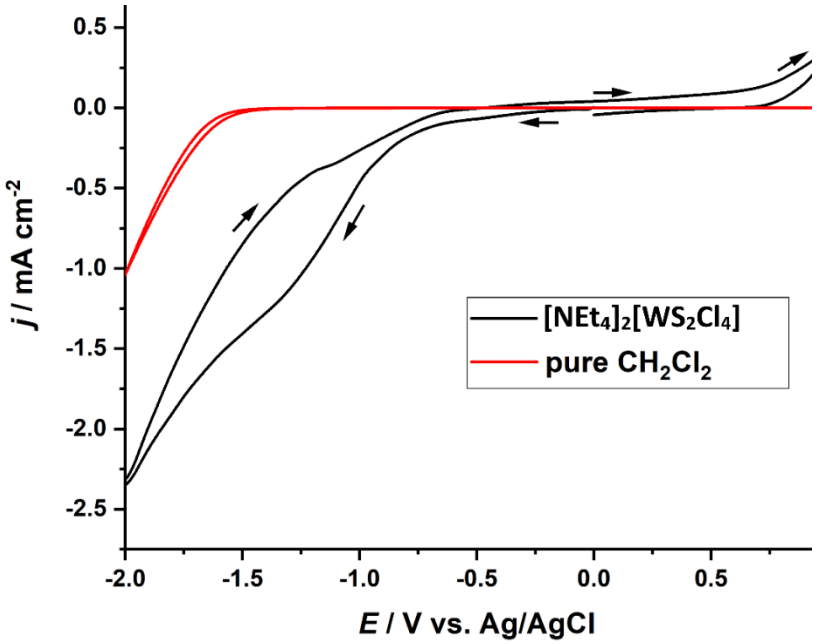

Figure 7.12: Cyclic voltammogram of 5mM $[Et_4N]_2[WS_2Cl_4]$ on TiN, in CH_2Cl_2, $[^nBu_4N]Cl$ was the supporting electrolyte.

The cyclic voltammogram of $[Et_4N]_2[WS_2Cl_4]$ in CH_2Cl_2 with $[^nBu_4N]Cl$ as the supporting electrolyte, without the addition of any proton source, shows a reduction starting at -0.7 V on the forward scan with a shoulder around -1.3 V. Compared to the CV of $[^nBu_4N]_2[WS_4]$ the reduction current was much larger and corresponds to the reduction of $[WS_2Cl_4]^{2-}$ ions.

$$[WS_2Cl_4]^{2-} + 2e^- \rightarrow WS_2 + 2Cl_2$$

Equation 7.3: Suggested electrochemical mechanism from the deposition of WS_2 from $[Et_4N]_2[WS_2Cl_4]$.

Equation 7.3 is the suggested mechanism for the deposition of WS_2 from $[WS_2Cl_4]^{2-}$ ions and it is clear there is no need for a proton source due to the stoichiometric ratio of W : S (1:2). There is no requirement for a proton source with this precursor as the protons were there to react with the excess sulfur in the system from $[MS_4]^{2-}$, this resulted in the films being slightly sulfur rich. Potentiostatic deposition at 1.2 V for 1 hour deposited amorphous WS_2 onto TiN, the films were then annealed under N_2 with S_8 as a source of sulfur at 500 ºC for 2 hours. The polycrystalline films were shown to be 4H-WS_2 *via* grazing incidence XRD.

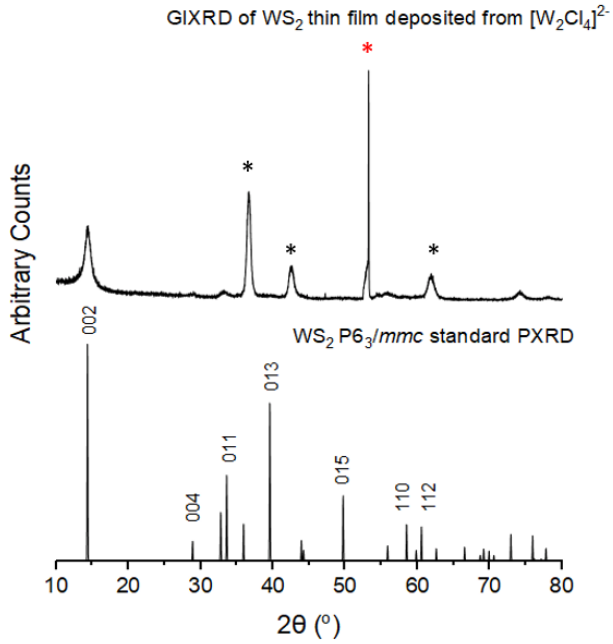

*Figure 7.13: Grazing incidence XRD pattern (top) from WS_2 electrodeposited from $[Et_4N]_2[WS_2Cl_4]$ in CH_2Cl_2. XRD pattern for bulk WS_2 (bottom).[59] * peaks from TiN and *(red) from crystalline Si.*

Analysis of the films deposited from $[Et_4N]_2[WS_2Cl_4]$ are consistent with polycrystalline 4H-WS_2 in the space group $P6_3/mmc$ and the lattice parameters were refined as a = 3.133(7), c = 12.41(4) Å (R_{wp} = 29.24%, literature: a = 3.1532(4), c = 12.323(5) Å).[59] The grazing incidence XRD pattern is dominated by the <002> reflection, suggesting highly preferred orientation in the <00*l*> direction. This is not unusual in 2D layered materials as they typically grow perpendicular to the substrate, resulting in flat platelets;[60,61] although this preferred orientation is commonly suppressed as the films get thicker. The sharp peak at ~55º can be assigned to crystalline Si and peaks at ~37º, 42º and ~60º are from the TiN electrode.

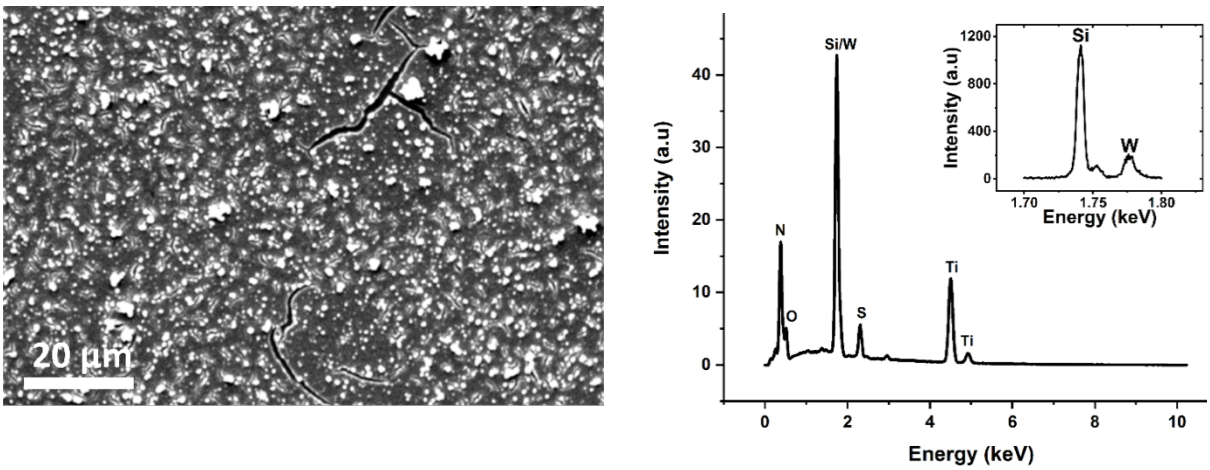

Figure 7.14: SEM image of continuous WS_2 film electrodeposited from $[Et_4N]_2[WS_2Cl_4]$ (left) and EDX spectrum of an annealed film, insert shows WDX spectrum for W M_α and Si K_α lines (right) onto TiN substrates.

Scanning electron microscopy (SEM) shows a continuous and reasonably flat deposit with evenly distributed particulates across the surface. The film is homogenously covering the electrode with few cracks. Accurate determination of composition was attempted using EDX analysis, however

due to the overlap of emission peaks from tungsten and silicon within the substrate (W $M\alpha_1$: 1.775 keV and Si $K\alpha_1$: 1.740 keV)[52] this was not possible. A subsequent attempt using WDX (which has higher resolution) confirmed the presence of both tungsten and sulfur (Figure 7.15). The peaks in the EDX spectrum from O, N and Ti originate from the electrode. Unfortunately, an accurate W : S ratio has yet to be obtained *via* XPS which is a surface technique and should provide more accurate results as there will be no interference from the substrate.

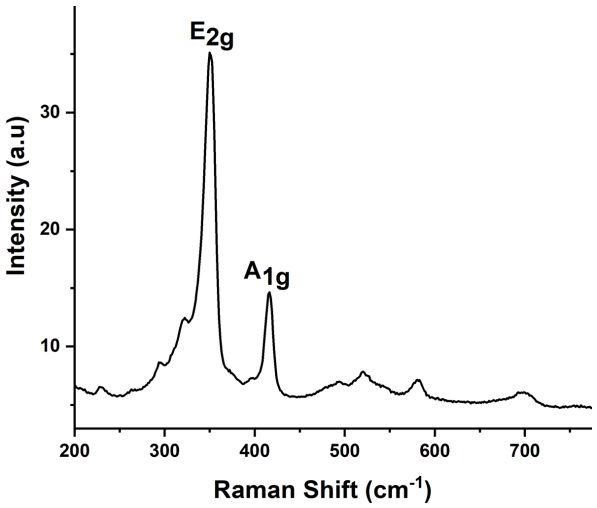

Figure 7.15: Raman spectrum recorded from an annealed WS_2 deposit using 532 nm laser excitation.

Raman spectra were collected using a 532 nm excitation laser and the spectra show the two main peaks at 352 and 419 cm^{-1}, which are assigned to the E_{2g} and A_{1g} vibrational modes of WS_2, respectively; the weaker features present in the spectra are also consistent with WS_2 peaks.[62]

7.4 Conclusions

This chapter focused on the development and synthesis of a series of potential precursors suitable for the electrodeposition of ME_2 thin films using non-aqueous solvents. A series of molybdenum(VI) and tungsten(VI) salts in the form $[ME_4]^{2-}$ (M = Mo or W; E = S or Se) were isolated and their suitability for electrodeposition of ME_2 thin films evaluated. Successful deposition of 2H-MoS_2 films from $[^nBu_4N]_2[MoS_4]$ in CH_2Cl_2 was shown and deposits were shown to be very smooth and uniform, as confirmed by SEM. The deposition of $MoSe_2$ films from $[^nBu_4N]_2[MoSe_4]$ is unclear, material is deposited onto the electrode, but characterisations suggest co-deposition of amorphous selenium and so a further detailed investigation is required.

The tungsten salts $[WE_4]^{2-}$ did not lead to deposition of any material as the reduction potential was too negative and occurred after the solvent breakdown. Following this, the successful electrodeposition of $[Et_4N]_2[WS_2Cl_4]$ did allow the electrodeposition of 4H-WS_2 thin films without the aid of a proton source. This is first example for truly single-source electrodeposition of WS_2 thin films from a tailored precursor.

All precursors were fully characterised by IR, ^{1}H NMR, ^{77}Se{^{1}H} NMR, ^{95}Mo NMR spectroscopy where possible, elemental analysis and X-ray crystal structures. All deposited thin films of ME_2 were characterised by Raman spectroscopy, X-ray diffraction, SEM and EDX/WDX.

7.5 Experimental

Syntheses were performed using standard Schlenk and glove-box techniques under a dry N_2 atmosphere. Solvents were dried by distillation from CaH_2 (CH_2Cl_2, MeCN) or Na/benzophenone (*n*-hexane, THF, toluene), DMF was dried by molecular sieve. Compounds $[PPh_4]Cl$, $[Et_4N]Cl$, $[^nBu_4N]Cl$, $[PPh_4]Br$, $[^nBu_4N]Br$, $Mo(CO)_6$ and $W(CO)_6$ were obtained from Sigma-Aldrich and dried by heating *in vacuo*. $[NH_4]_2[MoS_4]$ was obtained from Arcos Organics, $[NH_4]_2[WS_4]$ was obtained from Alfa Aesear, $S(SiMe_3)_2$ was obtained from Sigma Aldrich and used as received. $WSCl_4$ and K_2Se_3 were made by literature methods.[49,63] For further details regarding instrumentation see Appendix A.

$[^nBu_4N]_2[MoS_4]$

Following reported literature,[46] ammonium tetrathiomolybdate (0.367 g, 1.41 mmol) was dissolved in deionised water (10 mL) to form a red solution. A solution of tetrabutylammonium chloride (0.784 g, 2.82 mmol) was slowly added dropwise; a red solid immediately precipitated. The solution was filtered, and the red solid washed with water (1x 2 mL) and ^{i}PrOH (1 x 2 mL) and dried *in vacuo*. Yield: 0.728 g, 90 %. Required for $C_{32}H_{72}N_2MoS_4$ (709.12): C: 54.20, N: 3.95, H: 10.23 %. Found: C: 53.92, N: 4.05, H: 10.14 %. IR spectrum (Nujol, ν / cm^{-1}): 468s Mo=S. ^{1}H NMR ($CDCl_3$): δ = 0.99 (t, [3H], J_{HH} 7.3 Hz, CH_3), 1.46 (sxt, [2H], J_{HH} 1.0 Hz, CH_2), 1.6 - 1.7 (m, [2H], CH_2), 3.34 (m, [2H], CH_2). ^{95}Mo NMR (CD_2Cl_2): δ = +2213 (s).

$[^nBu_4N]_2[WS_4]$

Following reported literature method,[64] ammonium tetrathiotungstate (0.490 g, 1.41 mmol) was dissolved in deionised water (10 mL) to form a yellow solution. A solution of tetrabutylammonium hydroxide (40% wt., 1.83 g, 2.82 mmol) in water (10 mL) was slowly added dropwise, a yellow solid immediately precipitated. The solution was filtered and the solid washed with water (1 x 2 mL) and cold ^{i}PrOH (1 x 2 mL) and dried *in vacuo*. Yield: 0.513 g, 45 %. Required for $C_{32}H_{72}N_2WS_4$ (797.02): C: 48.22, N: 3.51, H: 9.11 %. Found: C: 48.17, N: 3.55, H: 9.18 %. IR spectrum (Nujol, ν / cm^{-1}): 448s W=S. ^{1}H NMR ($CDCl_3$): δ = 1.0 (t, [3H], J_{HH} = 7.34 Hz, CH_3), 1.44 (sxt, [2H], J_{HH} = 7.38 Hz, CH_2), 1.6 - 1.7 (m, [2H], CH_2), 3.2 - 3.4 (m, [2H], CH_2).

$[PPh_4][WSCl_5]$

Tetraphenylphosphonium chloride (0.105 g, 0.28 mmol) in dichloromethane (5 mL) was slowly added to a red solution of $WSCl_4$ (0.100 g, 0.28 mmol) in dichloromethane (5 mL). The green solution was stirred for 1 h., concentrated to a half and filtered to isolate a green solid which was dried *in vacuo*. Yield: 0.106 g, 52 %. Required for $C_{24}H_{20}Cl_5PSW$ (732.56): C: 39.35, H: 2.75 %. Found: C: 39.13, H: 2.74 %. IR spectrum (Nujol, ν / cm^{-1}): 332s, W-Cl. ^{1}H NMR (CD_2Cl_2): δ = 7.63 (m, [2H], aromatic CH), 7.71 - 7.82 (m, [H], aromatic CH), 7.82 - 8.04 (m, [2H], aromatic CH).

[$^{n}Bu_4N$][$WSCl_5$]

Tetrabutylammonium chloride (0.078 g, 0.28 mmol) in dichloromethane (5 mL) was slowly added to a red solution of $WSCl_4$ (0.100 g, 0.28 mmol) in dichloromethane (5 mL). The green solution was stirred for 1 h., concentrated to a half and filtered to isolate a green solid which was dried *in vacuo*. Yield: 0.090 g, 51 %. Required for $C_{16}H_{36}Cl_5NSW$ (635.63): C: 30.23, H: 5.04, N: 2.20 %. Found: C: 30.54, H: 5.33, N: 2.34 %. IR spectrum (Nujol, ν / cm^{-1}): 508s W=S, 320s W-Cl. ^{1}H NMR (CD_2Cl_2): δ = 1.04 (br s, [3H], CH_3), 1.46 (br s, [2H], CH_2), 1.81 (m, [2H], CH_2), 3.10 (br s, [2H], CH_2).

[Et_4N]$_2$[WS_2Cl_4]

A solution of tetraethylammonium chloride (0.185 g, 1.12 mmol) was dissolved in dichloromethane (3 mL) and slowly added to a solution of $WSCl_4$ (0.200 g, 0.56 mmol) in dichloromethane (5 mL). The green solution was stirred for 30 minutes, then a solution of hexamethyldisilathiane (0.100 g, 0.56 mmol) in dichloromethane (1 mL) was slowly added and the reaction was left to stir for 1 h. A brown precipitate was observed and supernatant filtered and the beige solid isolated and dried *in vacuo*. Yield: 0.250 g, 68 %. Required for $C_{16}H_{40}Cl_4N_2S_2W$ (650.28): C: 29.55, H: 6.20, N: 4.31 %. Found: C: 29.19, H: 6.06, N: 4.33 %. IR spectrum (Nujol, ν / cm^{-1}): 498s W=S, 289s W-Cl. ^{1}H NMR (CD_2Cl_2): δ = 1.30 (br s, [3H], Me), 3.23 (br s, [2H], CH_2). UV/Vis (diffuse reflectance)/cm^{-1}: 27,770, 24,630, 20,000sh.

[PPh_4]$_2$[$MoSe_4$]

K_2Se_3 (0.578 g, 1.83 mmol) and $Mo(CO)_6$ (242 mg, 0.92 mmol) were suspended in DMF (15 mL) the green solution turned purple after being heated to 90°C for 2 h. A solution [PPh_4]Br (0.769 g, 1.83 mmol) in DMF (3 mL) was added and the solution stirred for 15 mins. The solution was then filtered and was placed at 4°C overnight to produce a precipitate; this was filtered off and the solid dried *in vacuo.* Then the solid was dissolved in MeCN, the purple solution filtered and brought to dryness *in vacuo*. Yield: 0.110 g, 11 %. IR spectrum (Nujol, ν / cm^{-1}): 340s Mo=Se. ^{95}Mo NMR (CD_3CN): δ = +3094. $^{77}Se\{^{1}H\}$ NMR (CD_3CN): δ = +1656.

[PPh_4]$_2$[WSe_4]

K_2Se_3 (0.578 g, 1.83 mmol) and $W(CO)_6$ (322 mg, 0.92 mmol) were suspended in DMF (15 mL) the green solution turned red after being heated to 90°C for 2 h. A solution [PPh_4]Br (0.769 g, 1.83 mmol) in DMF (3 mL) was added and the solution stirred for 15 mins. The solution was then filtered, an equal volume of THF was added and was placed at 4°C overnight to produce a precipitate; this was filtered and the solid dried *in vacuo.* Then the solid was dissolved in MeCN, the red solution filtered and brought to dryness *in vacuo*. Yield: 0.111 g, 11 %. Required for $C_{48}H_{40}P_2Se_4W$ (1090.56): C: 48.92, H: 3.42 %. Found: C: 48.86, H: 3.56 %. IR spectrum (Nujol, ν / cm^{-1}): 304s W=Se. $^{77}Se\{^{1}H\}$ NMR (CD_3CN): δ = +1239 (J_{SW}, 53 Hz.).

[$^{n}Bu_4N]_2[MoSe_4]$

K_2Se_3 (2.500 g, 19.90 mmol) and $Mo(CO)_6$ (1.18 mg, 5.46 mmol) were suspended in DMF (20 mL) the green solution turned purple solution after being heated to 90°C for 2 h. A solution [$^{n}Bu_4N$]Br (2.500 g, 10.90 mmol) in DMF (6 mL) was added and the solution stirred for 15 mins. The DMF was removed *in vacuo*, then the solid was dissolved in MeCN, filtered, the filtrate layered with toluene and placed at 4°C overnight. The dark precipitate was filtered and the solid dried *in vacuo.* Yield: 1.765 g, 36 %. Required for $C_{32}H_{72}MoN_2Se_4 \bullet 0.5C_7H_8$ (942.77): C: 42.23, H: 8.12, N: 2.97 %. Found: C: 45.50, H: 6.98, N: 2.85 %. IR spectrum (Nujol, ν / cm^{-1}): 341s Mo=Se. ^{95}Mo NMR (CD_3CN): δ = +3088, (J_{MoSe} 13 Hz). $^{77}Se\{^1H\}$ NMR (CD_3CN): δ = +1652.

[$^{n}Bu_4N]_2[WSe_4]$

K_2Se_3 (1.28g, 4.06 mmol) and $W(CO)_6$ (0.715 g, 2.03 mmol) were suspended in DMF (10 mL) the green solution turned red solution after being heated to 90°C for 2 h. A solution [$^{n}Bu_4N$]Br (1.25 g, 4.06 mmol) in DMF (4 mL) was added and the solution stirred for 15 mins. The DMF was removed *in vacuo*, then the solid was dissolved in MeCN, filtered, the solution layered in toluene and placed at 4°C overnight. The red precipitate was filtered and the solid dried *in vacuo*. Yield: 0.606 g, 29 %. Required for $C_{32}H_{72}N_2Se_4W$ (1032.65): C: 41.87, H: 7.03 %. Found: C: 40.70, H: 7.44 %. IR spectrum (Nujol, ν / cm^{-1}): 305s W=Se. $^{77}Se\{^1H\}$ NMR (CD_3CN): δ = +1238 (J_{SW} 50 Hz.).

7.5.1 Electrochemical Experiments

All electrochemical experiments were performed by Dr Shibin Thomas, and carried in a N_2 filled glove box including supporting electrolyte and precursor preparation, using freshly dried CH_2Cl_2 (distilled from CaH_2) or ethylene glycol (distilled from Na) to ensure exclusion of air and moisture. The experiments in CH_2Cl_2 were performed at room temperature using a three electrode system in a one compartment electrochemical cell. A Pt electrode was used as the counter electrode and Ag/AgCl electrode (in 0.1M [$^{n}Bu_4N$]Cl in CH_2Cl_2) was used as the reference electrode. A freshly polished Pt electrode was used as working electrode for cyclic voltammetry experiments. In ethylene glycol, [NH_4]Cl was used as the supporting electrolyte due to insolubility of the tetrabutylammonium salt, films of MoS_2 were deposited potentiostatically onto TiN or Pt slide electrodes.

7.5.2 Crystallographic Tables

Compound	$[^nBu_4N]_2[WS_4]$	$[PPh_4]_2[WSe_4]$	$[^nBu_4N]_2[WSe_4]$
Formula	$C_{32}H_{72}N_2S_4W$	$C_{48}H_{40}P_2Se_4W$	$C_{32}H_{72}N_2Se_4W$
M	797.00	1178.43	993.46
Crystal system	Orthorhombic	Monoclinic	Tetragonal
Space group (no)	Fdd2 (43)	C2/c (15)	$I\bar{4}2d$ (122)
a /Å	35.5582(6)	11.1576(2)	14.2137(1)
b /Å	28.7216(5)	19.5668(4)	14.2137(1)
c /Å	15.5658(4)	20.2404(3)	24.2056(3)
α /°	90	90	90
β /°	90	91.4470(10)	90
γ /°	90	90	90
U /Å^3	15897.2(6)	4417.45(14)	4890.24(9)
Z	16	4	4
μ(Mo-$K_α$) /mm^{-1}	3.138	6.016	5.371
F(000)	6656.0	2272.0	1969.0
Total number reflns	24116	24315	51338
R_{int}	0.0402	0.0601	0.0538
Unique reflns	10952	6249	3860
No. of params, restraints	355/1	249/0	91/0
GOF	1.054	1.095	1.084
R_1, wR_2 $[I > 2σ(I)]^b$	0.0572, 0.1407	0.0435, 0.1076	0.0444, 0.1258
R_1, wR_2 (all data)^b	0.0623, 0.1446	0.0515, 0.1118	0.0503, 0.1318

Table 7.6: X-ray crystallography table.a: common data: wavelength (Mo-$K_α$) = 0.71073 Å; θ(max) = 27.5°; ^{b} $R_1 = Σ||Fo|-|Fc||/Σ|Fo|$; $wR_2=[Σw(Fo^2-Fc^2)^2/ΣwFo^4]^{1/2}$

7.6 References

(1) Simka, W.; Puszczyk, D.; Nawrat, G. *Electrochim. Acta,* **2009,** *54*, 5307-19
(2) Bartlett, P. N.; Cook, D.; de Groot, C. H.; Hector, A. L.; Huang, R.; Jolleys, A.; Kissling, G. P.; Levason, W.; Pearce, S. J.; Reid, G. *RSC Adv.,* **2013,** *3*, 15645-54
(3) Zhang, Q.; Wang, Q.; Zhang, S.; Lu, X.; Zhang, X. *ChemPhysChem,* **2016,** *17*, 335-51
(4) Li, G.; Tong, Y.; Liu, G. *J. Electroanal. Chem.,* **2004,** *562*, 223-29
(5) Li, G.; Tong, Y.; Wang, Y.; Liu, G. *Electrochim. Acta,* **2003,** *48*, 4061-67
(6) Andricacos, P. C.; Uzoh, C.; Dukovic, J. O.; Horkans, J.; Deligianni, H. *IBM J. Res. Dev.,* **1998,** *42*, 567-74
(7) Andricacos, P. C.; Romankiw, L. T. *Adv. Electrochem. Sci. Eng.,* **1993**, 227-321
(8) Cummings, C. Y.; Bartlett, P. N.; Pugh, D.; Reid, G.; Levason, W.; Hasan, M. M.; Hector, A. L.; Spencer, J.; Smith, D. C. *J. Electrochem. Soc.,* **2015,** *162*, D619-D24
(9) Bartlett, P. N.; Burt, J.; Cook, D. A.; Cummings, C. Y.; George, M. W.; Hector, A. L.; Hasan, M. M.; Ke, J.; Levason, W.; Pugh, D.; Reid, G.; Richardson, P. W.; Smith, D. C.; Spencer, J.; Suleiman, N.; Zhang, W. *Chem. Eur. J.,* **2016,** *22*, 302-09
(10) Bartlett, P. N.; Burt, J.; Hasan, M. M.; Hector, A. L.; Levason, W.; Reid, G.; Richardson, P. W. *RSC Adv.,* **2016,** *6*, 73323-30
(11) Vieira, L.; Burt, J.; Richardson, P. W.; Schloffer, D.; Fuchs, D.; Moser, A.; Bartlett, P. N.; Reid, G.; Gollas, B. *Chem. Open,* **2017,** *6*, 393-401
(12) Meng, L.; Cicvarić, K.; Hector, A. L.; de Groot, C. H.; Bartlett, P. N. *J. Electroanal. Chem.,* **2019,** *839*, 134-40
(13) Kissling, G. P.; Aziz, M.; Lodge, A. W.; Zhang, W.; Alibouri, M.; Huang, R.; Hector, A. L.; Reid, G.; de Groot, Cornelis H.; Beanland, R.; Bartlett, P. N.; Smith, D. C. *J. Electrochem. Soc.,* **2018,** *165*, D802-D07
(14) Huang, R.; Kissling, G. P.; Kashtiban, R.; Noori, Y. J.; Cicvaric, K.; Zhang, W.; Hector, A. L.; Beanland, R.; Smith, D. C.; Reid, G.; Bartlett, P. N.; de Groot, C. H. K. *Faraday Discuss.,* **2019,** *213*, 339-55
(15) Kissling, G. P.; Huang, R.; Jolleys, A.; Benjamin, S. L.; Hector, A. L.; Reid, G.; Levason, W.; de Groot, C. H.; Bartlett, P. N. *J. Electrochem. Soc.,* **2018,** *165*, D557-D67
(16) Bartlett, P. N.; Benjamin, S. L.; de Groot, C. H.; Hector, A. L.; Huang, R.; Jolleys, A.; Kissling, G. P.; Levason, W.; Pearce, S. J.; Reid, G.; Wang, Y. *Mater. Horiz.,* **2015,** *2*, 420-26
(17) Hankare, P. P.; Manikshete, A. H.; Sathe, D. J.; Chate, P. A.; Rathod, K. C. *Mater. Chem. Phys.,* **2009,** *113*, 183-86
(18) Rakkini, A. P. V.; Mohanraj, K. *Ionics,* **2017,** *24*, 1243-52
(19) Radisavljevic, B.; Radenovic, A.; Brivio, J.; Giacometti, V.; Kis, A. *Nat. Nanotechnol.,* **2011,** *6*, 147-50
(20) Splendiani, A.; Sun, L.; Zhang, Y.; Li, T.; Kim, J.; Chim, C. Y.; Galli, G.; Wang, F. *Nano Lett.,* **2010,** *10*, 1271-75
(21) Liu, C.; Kong, D.; Hsu, P.-C.; Yuan, H.; Lee, H.-W.; Liu, Y.; Wang, H.; Wang, S.; Yan, K.; Lin, D.; Maraccini, P. A.; Parker, K. M.; Boehm, A. B.; Cui, Y. *Nat. Nanotechnol.,* **2016,** *11*, 1098-104
(22) Albu-Yaron, A. *Electrochem. Solid-State Lett.,* **1999,** *2*, 627-30
(23) Ponomarev, E. A. *J. Electrochem. Soc.,* **1997,** *144*, L277-L79
(24) Shariza, S.; Anand, T. J. S. *Chalcogenide Lett.,* **2011,** *8*, 529-39
(25) Albu-Yaron, A.; Lévy-Clément, C.; Katty, A.; Bastide, S.; Tenne, R. *Thin Solid Films,* **2000,** *361-362*, 223-28
(26) Murugesan, S.; Akkineni, A.; Chou, B. P.; Glaz, M. S.; Vanden Bout, D. A.; Stevenson, K. J. *ACS Nano,* **2013,** *7*, 8199-205
(27) Redman, D. W.; Rose, M. J.; Stevenson, K. J. *Langmuir,* **2017,** *33*, 9354-60
(28) Pathak, V. M.; Patel, K. D.; Pathak, R. J.; Srivastava, R. *Sol. Energy Mater. Sol. Cells,* **2002,** *73*, 117-23
(29) Kautek, W.; Gerischer, H. *Electrochim. Acta,* **1981,** *26*, 1771-78
(30) Eftekhari, A. *Appl. Mater. Today,* **2017,** *8*, 1-17
(31) Delphine, S. M.; Jayachandran, M.; Sanjeeviraja, C. *Mater. Res. Bull.,* **2005,** *40*, 135-47
(32) Dukstiene, N.; Kazancev, K.; Prosicevas, I.; Guobiene, A. *J. Solid State Electrochem.,* **2004,** *8*, 330-36
(33) Tsang, C. F.; Ledina, M. A.; Stickney, J. L. *J. Electroanal. Chem.,* **2017,** *793*, 242-49

(34) Delphine, S. M.; Jayachandran, M.; Sanjeeviraja, C. *Crystallogr. Rev.,* **2011,** *17*, 281-301
(35) Pu, Z.; Liu, Q.; Asiri, A. M.; Obaid, A. Y.; Sun, X. *Electrochim. Acta,* **2014,** *134*, 8-12
(36) Devadasan, J. J.; Sanjeeviraja, C.; Jayachandran, M. *J. Cryst. Growth,* **2001,** *226*, 67-72
(37) Fan, L.; Suni, I. I. *J. Electrochem. Soc.,* **2017,** *164*, D681-D86
(38) Tan, S. M.; Pumera, M. *ACS Appl. Mater. Interfaces,* **2016,** *8*, 3948-57
(39) Delphine, S. M.; Jayachandran, M.; Sanjeeviraja, C. *Mater. Chem. Phys.,* **2003,** *81*, 78-83
(40) Devadasan, J. J.; Sanjeeviraja, C.; Jayachandran, M. *Mater. Chem. Phys.,* **2003,** *77*, 397-401
(41) Aliyev, A. S.; Elrouby, M.; Cafarova, S. F. *Mater. Sci. Semicond. Process.,* **2015,** *32*, 31-39
(42) Laurie, S. H. *Eur. J. Inorg. Chem.,* **2000**, 2443-50
(43) Zhang, Q.; Hong, M.; Su, W.; Cao, R.; Liu, H. *Polyhedron,* **1997,** *16*, 1433-37
(44) Dori, Z. *Comprehensive Coordination Chemistry I,* **1987,** *3*, 973-1022
(45) Mellor, J. W. *A comprehensive treatise on inorganic and theoretical chemistry,* **1943,** *11*, 650
(46) Alonso, G.; Aguirre, G.; Rivero, I. A.; Fuentes, S. *Inorg. Chim. Acta,* **1998,** *274*, 108-10
(47) Alonso, G.; Berhault, G.; Chianelli, R. R. *Inorg. Chim. Acta,* **2001,** *316*, 105-09
(48) Kroneck, P.; Lutz, O.; Nolle, A. *Z. Naturforsch. A,* **1980,** *35*, 226-29
(49) O'Neal, S.; Kolis, J. W. *J. Am. Chem. Soc.,* **1988,** *110*, 1971-73
(50) Hong, M.; Zhang, Q.; Cao, R.; Wu, D.; Chen, J.; Zhang, W.; Liu, H.; Lu, J. *Inorg.Chem.,* **1997,** *36*, 6251-60
(51) Bélanger, D.; Laperriére, G.; Marsan, B. *J. Electroanal. Chem.,* **1993,** *347*, 165-83
(52) Thompson, A. C.; Vaughan, D. *X-ray data booklet*; Lawrence Berkeley National Laboratory, University of California: Berkely, CA, 2001.
(53) Li, H.; Zhang, Q.; Yap, C. C. R.; Tay, B. K.; Edwin, T. H. T.; Olivier, A.; Baillargeat, D. *Adv. Funct. Mater.,* **2012,** *22*, 1385-90
(54) Redman, D. W.; Murugesan, S.; Stevenson, K. J. *Langmuir,* **2014,** *30*, 418-25
(55) Tonndorf, P.; Schmidt, R.; Bottger, P.; Zhang, X.; Borner, J.; Liebig, A.; Albrecht, M.; Kloc, C.; Gordan, O.; Zahn, D. R.; Michaelis de Vasconcellos, S.; Bratschitsch, R. *Opt. Express,* **2013,** *21*, 4908-16
(56) Drew, M. G. B.; Fowles, G. W. A.; Page, E. M.; Rice, D. A. *J. Chem. Soc., Dalton Trans.,* **1981**, 2409-13
(57) Weller, F.; Ruschke, P.; Dehnicke, K. *Z. anorg. allg. Chem.,* **1980,** *467*, 89-94
(58) Klingelhöfer, P.; Müller, U. *Z. anorg. allg. Chem.,* **1988,** *556*, 70-78
(59) Schutte, W. J.; De Boer, J. L.; Jellinek, F. *J. Solid State Chem.,* **1987,** *70*, 207-09
(60) Chang, Y. P.; Hector, A. L.; Levason, W.; Reid, G. *Dalton Trans.,* **2017,** *46*, 9824-32
(61) Chang, Y. P.; Hector, A. L.; Levason, W.; Reid, G.; Whittam, J. *Dalton Trans.,* **2018,** *47*, 2406-14
(62) Berkdemir, A.; Gutiérrez, H. R.; Botello-Méndez, A. R.; Perea-López, N.; Elías, A. L.; Chia, C.-I.; Wang, B.; Crespi, V. H.; López-Urías, F.; Charlier, J.-C.; Terrones, H.; Terrones, M. *Sci. Rep.,* **2013,** *3*, 1755
(63) Gulliver, D. J.; Hope, E. G.; Levason, W.; Murray, S. G.; Potter, D. M.; Marshall, G. L. *J. Chem. Soc., Perkin Trans. II,* **1984,** *2*, 429-34
(64) Hanewald, K.; Gattow, G. *Z. anorg. allg. Chem.,* **1981,** *476*, 159-70

Summary and Outlook

The work described in this thesis has considerably advanced the coordination of tungsten(VI) oxo- and thio-halides and molybdenum(V) oxohalides. This advancement has led to the development of new synthetic routes to produce 2D metal dichalcogenides.

The successful synthesis of a range of neutral complexes of $WOCl_4$ and $WSCl_4$ with phosphine oxides and N-heterocycles under mild reaction conditions has been completed. Excluding the 2,2'-bipy complexes, which are seven-coordinate, all other complexes are six-coordinate. The bidentate phosphine oxides formed six-coordinate bridged dimers in the form $[(WSCl_4)_2(\mu\text{-}Ph_2(O)P(CH_2)_nP(O)Ph_2)]$, the bridge dimers more favourable than the seven-coordinate systems. Comparison of all the data collected suggests that the sulfide chlorides are slightly less Lewis acidic than the oxide chlorides.

A short investigation into complexes of WCl_6 analogous to complexes of WF_6 proved unsuccessful, with data indicating reduction to tungsten(V) complexes (and potentially others). The complex $[WCl_5(2,2'\text{-bipy})]$ was isolated and characterised, but 1,10-phen analogues could not be isolated. Therefore, it can be assumed that complexes of WCl_6 are significantly less stable than their WF_6 analogues and cannot be formed under mild conditions, no further work required.

Further studies to continue the chemistry of tungsten(VI) oxo- and thio-tetrachlorides were completed to develop a short series of neutral phosphine and arsine complexes under mild and ambient conditions. Four examples of rare seven-coordinate complexes have been isolated, $[WECl_4(o\text{-}C_6H_4(E'Me_2)_2)]$ (E = O or S; E' = P or As); two have been structurally characterised revealing pentagonal bipyramidal geometries. A number of W(V) reduction products have also been structurally characterised, including cationic salts and compared to the products of the failed attempt to isolate $[WOCl_4(o\text{-}C_6H_4(PPh_2)_2)]$ and known $[WF_4(o\text{-}C_6H_4(EMe_2)_2)_2]^{n+}$ species.

A small number of other complexes with the ligands PMe_3, dmpe and $AsEt_3$ were also attempted, but proved unsuccessful, with some side products shown to be chlorinated ligand and potentially some tungsten(V) reduction species. The reaction with $WOCl_4$ and PMe_3 showed that the complex $[WOCl_4(PMe_3)_2]$ could potentially be formed under the right conditions but is likely to be extremely sensitive to trace moisture.

This investigation was continued to probe the boundaries of tungsten(VI) coordination chemistry. A systematic series of $WSCl_4$ complexes with monodentate and bidentate thioethers has been established and comparative analogues of $WOCl_4$ have also been isolated. Complexes with softer selenoether donor ligands were attempted, but $[WSCl_4(SeMe_2)]$ was the only stable complex that could be isolated. All the complexes isolated were six-coordinate and controlling the W : ligand stoichiometry is paramount for the isolation of tungsten(VI) species, as excess ligand reduces the

metal centre. A number of reduced tungsten (V) decomposition products have also been identified by X-ray crystallography.

Thioether complexes with terminal substituents bearing β-hydrogens have the possibility to be single-source precursors for the production of WS_2 thin films *via* LPCVD providing the potential of a low energy decomposition pathway. Complexes of $[(WSCl_4)_2(^iPrS(CH_2)_2S^iPr)]$, $[WSCl_3(^iPrS(CH_2)_2S^iPr)]$ and $[WSCl_4(S^nBu_2)]$ were tested as single source low pressure chemical vapour deposition precursors at 550-700 ºC. The complex $[WSCl_3(^iPrS(CH_2)_2S^iPr)]$ was found to be unsuitable for LPCVD and did not deposit any material onto the substrates. $[(WSCl_4)_2(^iPrS(CH_2)_2S^iPr)]$ and $[WSCl_4(S^nBu_2)]$ were found to deposit 4H-WS_2 thin films successfully between 650 ºC and 700 ºC. The two novel single source precursors deposited continuous uniform coverage of the substrate and the films have been shown to have a W:S ratio of 1:2.2 consistent with WS_2.

These are the first examples of single source LPCVD precursors to deposit WS_2 thin films and the films have been characterised by Raman spectroscopy, grazing incidence XRD and in-plane XRD, EDX, WDX, XPS and SEM. The films have preferred orientation in <00*l*> direction with SEM confirming the crystallites parallel to the substrate surface. These precursors potentially provide a viable route for the growth of thin films of this important semiconducting material if conditions and optimisation of reagent can be achieved.

Surprisingly, the two precursors produce films with different electrical behaviour with $[(WSCl_4)_2(^iPrS(CH_2)_2S^iPr)]$ behaving as a typical semiconductor and $[WSCl_4(S^nBu_2)]$ behaving as a semi-metal/conductor. The difference probably stems from defects, likely sulfur deficiency which is not due to temperature. Following the successful deposition of WS_2 thin films *via* LPCVD from $[WSCl_4(S^nBu_2)]$ and the successful isolation of $[WSCl_4(SeMe_2)]$, it is highly likely that $[WSCl_4(Se^nBu_2)]$ would also be stable. Potentially it would be a suitable precursor to deposit the mixed chalcogen thin films WSSe.

A systematic series of $MoOCl_3$ complexes with a range of neutral donor ligands (sulfur, selenium, tellurium donors) has been developed. Bidentate thio- and seleno-ether complexes have been isolated and characterised as well as monodentate thio-, seleno- and telluro-ether complexes which formed chloride bridge dimers; the telluroether complex $[(MoOCl_2(TeMe_2))_2(\mu\text{-}Cl)_2]$ is the first telluroether complex with high valent molybdenum. A number of $MoOCl_3$ complexes with nitrogen, phosphine and oxygen donors was isolated for comparison.

The reaction of $MoOCl_4$ with various neutral ligands (N- and O- donors) was also investigated and all reactions reduced the molybdenum(VI) centre to form molybdenum(V) species. Attempts to isolate the anion $[MoOCl_5]^-$ were also unsuccessful but the chloride bridged anion $[(MoOCl_3)(\mu\text{-}Cl))_2]^{2-}$ was identified. Results show $MoOCl_4$ is much less stable compared to $MoOF_4$ and MoO_2Cl_2 as both form relatively stable complexes.

The initial development and synthesis of a series of potential precursors suitable for the electrodeposition of ME_2 thin films using non-aqueous solvents has been completed. A series of molybdenum(VI) and tungsten(VI) salts in the form $[ME_4]^{2-}$ (M = Mo or W; E = S or Se) were isolated and suitability for electrodeposition evaluated. Successful deposition of 2H-MoS_2 films from $[^nBu_4N]_2[MoS_4]$ in CH_2Cl_2 was shown and deposits were shown to be very smooth and uniform confirmed by SEM. The deposition of $MoSe_2$ films from $[^nBu_4N]_2[MoSe_4]$ is unclear, material is deposited onto the electrode, but characterisations suggest co-deposition of amorphous selenium and further investigation is required.

The tungsten salts which contained the $[WE_4]^{2-}$ anions did not deposit material as the reduction potential was too negative and occurred after the solvent breakdown. Following this, the successful isolation of $[WSCl_5]^-$ and $[WS_2Cl_4]^{2-}$ salts and $[Et_4N]_2[WS_2Cl_4]$ proved successful at depositing 4H-WS_2 thin films without the aid of a proton source. This is first example for truly single-source electrodeposition of WS_2 thin films from a tailored precursor. There is potential for $[Et_4N]_2[WSSeCl_4]$ to be isolated as a future precursor for the electrodeposition of WSSe thin films.

Appendix A General Experimental Techniques

Syntheses were performed by using standard Schlenk and glove-box techniques under a dry N_2 atmosphere (where required). Solvents were dried by distillation from CaH_2 (CH_2Cl_2, MeCN, $CHCl_3$) or Na/benzophenone ketyl (toluene, n-hexane, THF, OEt_2), DMF dried *via* molecular sieve.

Complexes Characterisation: Infrared spectra were recorded on a Perkin-Elmer Spectrum 100 spectrometer in the range 4000–200 cm^{-1}, with samples prepared as Nujol mulls between CsI plates. Raman spectra were collected by a Renishaw InVia Raman Microscope with a 100 mW He-Ne 785 nm Laser. UV-Vis spectra were recorded from sealed PTFE cells with a silica window on neat samples or diluted with $BaSO_4$, using the diffuse reflectance attachment, in Perkin Elmer 750S spectrometer. Magnetic measurements were made on a Johnson Matthey magnetic balance. ^1H NMR spectra were recorded using a Bruker AV 400 or Bruker DPX400 spectrometer and referenced to the residual protio-resonance of the solvent. $^{31}P\{^1H\}$, ^{95}Mo, $^{77}Se\{^1H\}$, $^{125}Te\{^1H\}$ NMR spectra were obtained from CD_2Cl_2 solutions using a Bruker AV 400 spectrometer see Table A.1 for reference. Spectra were recorded at 295 K unless indicated otherwise. Microanalyses on new compounds were undertaken by London Metropolitan University or Medac Ltd.

NMR Nucleus	Resonance Frequency (at 9.4 T)	Reference Standard
^1H	400.0	Residual solvent protons
^{31}P	162.0	H_3PO_4, 85% aq
^{77}Se	76.4	Me_2Se
^{95}Mo	26.8	2M Na_2MoO_4 aq
^{125}Te	126.0	Me_2Te
^{183}W	16.8	1M Na_2WO_2 aq

Table A.1: Showing resonance frequency of NMR active nuclei studied in the work and their reference standards.

X-ray single crystal experimental: Data collections used a Rigaku AFC12 goniometer equipped with an enhanced sensitivity (HG) Saturn724+ detector mounted at the window of an FR-E+ SuperBright molybdenum ($\lambda = 0.71073$) rotating anode generator with VHF Varimax optics (70 micron focus) with the crystal held at 100 K (N_2 cryostream). Structure solution was performed using SHELX(T)-2018/2 (heavy atom methods), and refinement SHELX-2018/3 through Olex$_2$[1-3] and were mostly straightforward, H atoms were added and refined with a riding model. Where additional restraints were required, details are provided in the cif file for each structure, or are discussed in the text. Many of the structures showed significant residual electron peaks near to the heavy metals (tungsten/molybdenum), which are attributed to absorption correction problems.

Appendix A

Film characterisation: X-ray diffraction (XRD) patterns were collected in grazing incidence mode ($\theta 1 = 1°$) or in-plane mode ($\theta 1 = 0.5°$, $2\theta\chi$ scan with the detector scanning in the film plane) using a Rigaku SmartLab diffractometer (Cu-Kα, $\lambda = 1.5418$ Å) with parallel X-ray beam and a DTex Ultra 250 1D detector. Phase matching, lattice parameter calculations used the PDXL2 software package27 and diffraction patterns from ICSD. Scanning electron microscopy (SEM) was performed on samples at an accelerating voltage of 10 or 15 kV using a Philips XL30 ESEM. Energy dispersive X-ray spectroscopy (EDX) spectra were obtained coupled to SEM, using a Thermo Scientific NORAN System 7 X-ray Microanalysis System. Raman spectra were obtained using Horiba Xplora System equipped with a 532nm laser excitation. WDX were collected using Thermo Magnaray WDX spectrometer. XPS spectra were collected using Theta probe PARXPS system.

References

(1) Sheldrick, G. M. *Acta Cryst. C,* **2015,** *71*, 3-8
(2) Sheldrick, G. M. *Acta Cryst. A,* **2008,** *64*, 112-22
(3) Dolomanov, O. V.; Bourhis, L. J.; Gildea, R. J.; Howard, J. A. K.; Puschmann, H. *J. Appl. Crystallogr.,* **2009,** *42*, 339-41

Appendix B Crystallographic Information Files

Cif files located on CD attached to back of the thesis

The filenames correspond to the complexes as follows

Chapter 2

$[WOCl_4(OPPh_3)]$	LHS WOCl4-OPPh3
$[WOCl_4(OPMe_3)]$	LHS-WOCl4-OPR3
$[W_3O_3(\mu\text{-}O)_3Cl_6(OPMe_3)_3]\bullet 2CH_2Cl_2$	WOCl4-Trimer
$[(WOCl_4)_2(dppmO_2)]$	DES WOCl4 dppmO2
$[(WOCl_2(dppmO_2))(\mu\text{-}O)(WOCl_4)]$	DES WOCl4 dppmO2-Bridge
$[C_5H_5NH][WOCl_5]$	EX DS WOCl4 py
$[(WSCl_4)_2(dppeO_2)]$	DS EX77
$[(WOCl_4)_2(dppeO_2)]$	WOCl4(dppeO2)
$[WSCl_4(OPPh_3)]$	WOCl4(OPPh3)
$[WOCl_3(dppmO_2)]\bullet CH_2Cl_2$	WOCl3-dppmo2
$[WSCl_3(dppmO_2)]\bullet CH_2Cl_2$	WSCl3(dppmO2)
$[(WSCl_4)_2(dppmO_2)]$	(WSCl4)2(dppmO2)
$[WSCl_4(C_5H_5N)]$	WSCl4(py)
$[WSCl_3(2,2'\text{-bipy})]$	DS EX74
$[(WOCl_2(phen))(\mu\text{-}O)(WOCl_4)]$	DES WCl5-Phen

Chapter 3

$[WOCl_4(o\text{-}C_6H_4(AsMe_2)_2)]$	WOCl4(diarsine)
$[WSCl_4(o\text{-}C_6H_4(PMe_2)_2)]$	WSCl4(diphos)
$[WOCl_3(o\text{-}C_6H_4(PMe_2)_2)]$	WOCl3(diphos)
$[WOCl_3(o\text{-}C_6H_4(PMe_2)(P(O)Me_2))]\bullet 0.5CH_2Cl_2$	WOCl3(diphos)-Blue
$[WCl_4(o\text{-}C_6H_4(PPh_2)_2)_2][WCl_6]\bullet 2.5(C_7H_8)$	WOCl4 dppBz
$[WCl_4(o\text{-}C_6H_4(PMe_2)_2)_2][WS_{0.5}O_{0.5}]$	[WSCl4][WCl4(diphos)2]

Chapter 4

$[(WSCl_4)_2(MeS(CH_2)_2SMe)]$	(WSCl4)2(mte)
$[WSCl_3(MeS(CH_2)_2SMe)]$	(WSCl3)(MeS(CH2)2SMe)
$[WOCl_3(MeS(CH_2)_2SMe)]$	WOCl3(MeS(CH2)2SMe)
$[WOCl_3(MeS(CH_2)_3SMe)]$	WOCl3-MeS(CH2)3SMe
$[(WSCl_4)_2(MeS(CH_2)_3SMe)]$	(WSCl4)2-Heptane-2
$[(WSCl_4)_2(PhS(CH_2)_2SPh)]$	(WSCl4)2PhS(CH2)2Ph)
$[(WSCl_4)_2(^iPrS(CH_2)_2S^iPr)]$	(WSCl4)2(PrS(CH2)2SPr)
$[(WCl_3)_2(\mu\text{-}S_2)(\mu\text{-}S)(SPPh_3)_2]\bullet 2CH_2Cl_2$	WSCl4(SPPh3)-1
$[(WCl_3)_2(\mu\text{-}S_2)(\mu\text{-}S)(SeMe_2)_2]$	WSCl4(SeMe2)
$[(WCl_2)_2(\mu\text{-}S)_2(^iPrS(CH_2)_2S^iPr)_2][WSCl_5]\bullet CH_2Cl_2$	WSCl3(PrS(CH2)2SPr

Chapter 6

$[MoOCl_3(MeCN)_2]$	MoOCl4(MeCN) - Yellow
$[(MoOCl_2(MeCN))_2(\mu\text{-}Cl)_2]$	MoOCl4+MeCN (green)
$[Et_4N]_2[(MoOCl_3)_2(\mu\text{-}Cl)_2]$	(Et4N)(MoOCl5)
$[Et_4N][WOCl_5]$	$[Et_4N][WOCl_5]$
$[MoOCl_3(THF)_2]$	MoOCl3(THF)2
$[MoOCl_3(OPPh_3)_2]$	MoOCl4(OPPh3)
[MoOCl3(2,2'-bipy)]	MoOCl3bipy-1
[MoOCl3(1,10-phen)]	MoOCl3(phen)
[MoOCl3(dmpe)]	MoOCl3dmpe
$[MoOCl_3(dppe)]\bullet 0.5CH_2Cl_2$	MoOCl3dppe
$[MoOCl(PMe_3)_2]$	MoOCl3 PMe3 - Red
$[(MoOCl)(dmpe)_2(\mu\text{-}O)(MoOCl_4)]$	MoOCl3dmpe-purple
$[MoOCl_3(MeS(CH_2)_3SMe)]$	JP20
$[MoOCl_3(^iPrS(CH_2)_2S^iPr)]$	MoOCl3(PrS(CH2)2SPr)

$[MoOCl_3(PhS(CH_2)_2SPh)]$	MoOCl3(PhS(CH2)2SPh)
$[(MoOCl_2(SMe_2))_2(\mu\text{-}Cl)_2]$	MoOCl3(SMe2)2
$[(MoOCl_2(SeMe_2))_2(\mu\text{-}Cl)_2]$	MoOCl3(SeMe2)2
$[MoOCl_3(MeSe(CH_2)_2SeMe)]$	MoOCl3(MeSe(CH2)2SeMe)
$[MoOCl_3(MeSe(CH_2)_3SeMe)]$	MoOCl3(MeSe(CH2)3SeMe)
$[(MoOCl(o\text{-}C_6H_4(TeMe)_2)_2)(MoOCl_4)]\bullet CH_2Cl_2$	MoOCl3(o-C6H4(TeMe)2-bridge

Chapter 7

$[^nBu_4N]_2[WS_4]$	TBA WS4
$[PPh_4]_2[WSe_4]$	(PPh4)2WSe4
$[^nBu_4N]_2[WSe_4]$	DS EX79